**DOCTORAL THESIS**

# New micro and mesoporous materials for the reaction of methanol to olefins

PhD Thesis submitted by

**Zhibin Li**

Advisor:

**Prof. Avelino Corma Canós**
**Dr. Joaquín Martínez Triguero**

Valencia, October 2014

UNIVERSITAT POLITECNICA DE VALENCIA

INSTITUTO UNIVERSITARIO MIXTO DE TECNOLOGIA QUIMICA(UPV-CSIC)

# New micro and mesoporous materials for the reaction of methanol to olefins

**DOCTORAL THESIS**

PhD Thesis submitted by

**Zhibin Li**

Advisor:

**Prof. Avelino Corma Canós**
**Dr. Joaquín Martínez Triguero**

Valencia, October 2014

# Resumen

La transformación de metanol en olefinas empleando catalizadores ha atraído el interés de la comunidad científica debido a las amplias reservas de gas natural. El metanol se obtiene a partir del gas natural a través del gas de síntesis y también a partir de biomasa mediante gasificación, por lo que representa una alternativa frente a otras fuentes fósiles de energía como el petróleo y el carbón. En esta tesis se han estudiado nuevos materiales catalíticos para la reacción de metanol en olefinas optimizando las propiedades de los que actualmente se emplean de manera comercial y proponiendo nuevos materiales alternativos. Los catalizadores empleados actualmente están basados en zeolitas que son materiales microporosos de alta área específica pero presentan como limitaciones una vida corta antes de la desactivación por coque, o una baja estabilidad frente a la presencia de agua en el medio de reacción. El aumento del área específica a través de la disminución del tamaño de cristal o de la mesoporosidad mejorará las propiedades de difusión del catalizador.

El silicoaluminofosfato SAPO-34 es empleado comercialmente en la actualidad. En esta tesis se ha optimizado la síntesis de este material disminuyendo drásticamente el tamaño de cristal y mejorando la estabilidad frente a la humedad ambiente. La disminución del tamaño de cristal ha aumentado la vida del catalizador frente a la deposición de coque y ha permitido relacionar la selectividad a productos con la distribución de silicio en la partícula, distribución que es variable al contacto con la humedad ambiente. La estabilidad frente a la humedad ha sido mejorada mediante el tratamiento con vapor post-síntesis y también se ha estudiado el efecto de la eliminación del agente orgánico director de estructura en atmósfera reductora de hidrógeno y agua. De esta manera se han sintetizado muestras con mayor tiempo de vida en la reacción de metanol. El efecto de la reducción del tamaño de cristal se ha estudiado también para la zeolita SSZ-13, isomorfa con SAPO-34, mediante la adición de agentes surfactantes durante la síntesis y también se ha probado cómo esta reducción de tamaño produce el aumento el tiempo de vida del catalizador.

Por último se ha optimizado el tiempo de vida y la estabilidad hidrotérmica de la zeolita ZSM-5, también usada comercialmente como componente activo del catalizador del proceso de metanol a propileno. Se ha estudiado el efecto del aumento de la mesoporosidad mediante tratamientos básicos/ácidos en las propiedades catalíticas y se ha comprobado cómo la mesoporosidad aumenta el tiempo de vida pero afecta a la estabilidad hidrotérmica del catalizador. En la parte final se ha optimizado la estabilidad hidrotérmica de ZSM-5 mesoporosa mediante la adición de fósforo. El estudio ha permitido comprobar que la actividad del catalizador basado el ZSM-5 mesoporosa se puede preservar mediante la mejora de la estabilidad hidrotérmica, incluyendo fósforo en la composición del catalizador.

# Resum

La transformació de metanol en olefines emprant catalitzadors ha atret l'interès de la comunitat científica a causa de les àmplies reserves de gas natural. El metanol s'obté a partir del gas natural a través del gas de síntesi i també a partir de biomassa mitjançant gasificació, per la qual cosa representa una alternativa enfront d'altres fonts fòssils d'energia com el petroli i el carbó. En aquesta tesi s'han estudiat nous materials catalítics per a la reacció de metanol en olefines optimitzant les propietats dels quals actualment s'empren de manera comercial i proposant nous materials alternatius. Els catalitzadors emprats actualment estan basats en zeolites que són materials microporosos d'alta àrea específica però presenten com a limitacions una vida curta abans de la desactivació per coc, o una baixa estabilitat enfront de la presència d'aigua en el mitjà de reacció. L'augment de l'àrea específica a través de la disminució de la grandària de cristall o de la mesoporositat millorarà les propietats de difusió del catalitzador.

El silicoaluminofosfat SAPO-34 és emprat comercialment en l'actualitat. En aquesta tesi s'ha optimitzat la síntesi d'aquest material disminuint dràsticament la grandària de cristall i millorant l'estabilitat enfront de la humitat ambient. La disminució de la grandària de cristall ha augmentat la vida del catalitzador enfront de la deposició de coc i ha permès relacionar la selectivitat a productes amb la distribució de silici en la partícula, distribució que és variable al contacte amb la humitat ambient. L'estabilitat enfront de la humitat ha sigut millorada mitjançant el tractament amb vapor post-síntesi i també s'ha estudiat l'efecte de l'eliminació de l'agent orgànic director d'estructura en atmosfera reductora d'hidrogen i aigua. D'aquesta manera s'han sintetitzat mostres amb major temps de vida en la reacció de metanol. L'efecte de la reducció de la grandària de cristall s'ha estudiat també per a la zeolita SSZ-13, isomorfa amb SAPO-34, mitjançant l'addició d'agents surfactants durant la síntesi i també s'ha provat com aquesta reducció de grandària produeix l'augment el temps de vida del catalitzador.

Finalment s'ha optimitzat el temps de vida i l'estabilitat hidrotérmica de la zeolita ZSM-5, també usada comercialment com a component actiu del catalitzador del procés de metanol a propilè. S'ha estudiat l'efecte de l'augment de la mesoporositat mitjançant tractaments bàsics/àcids en les propietats catalítiques i s'ha comprovat

com la mesoporositat augmenta el temps de vida però afecta a l'estabilitat hidrotérmica del catalitzador. En la part final s'ha optimitzat l'estabilitat hidrotérmica de ZSM-5 mesoporosa mitjançant l'addició de fòsfor. L'estudi ha permès comprovar que l'activitat del catalitzador basat en ZSM-5 mesoporosa es pot preservar mitjançant la millora de l'estabilitat hidrotérmica, incloent fòsfor en la composició del catalitzador.

# Abstract

The conversion of methanol to olefins by catalysts has attracted the interest of the scientific community due to the vast reserves of natural gas. Methanol is produced from natural gas via synthesis gas and biomass via gasification, which represents an alternative to other fossil energy sources like oil and coal. In this work, we have studied new catalytic materials for the reaction of methanol to olefins optimizing the properties of these currently used commercially and proposing new alternative materials. The catalysts currently used are based on zeolites which are microporous materials of high specific area but present as drawbacks a short lifetime before deactivation by coking, or a low stability when water is present in the reaction medium. Increasing the specific area by decreasing the size of crystal or increasing mesoporosity will improve the diffusion properties of the catalyst.

The silicoaluminophosphate SAPO-34 is currently the material commercially used. In this thesis, the synthesis of this material has been drastically optimized by decreasing the crystal size and improving the stability against humidity. Decreasing the size of the crystal has increased catalyst life against coke deposition and has made possible to relate product selectivity to the distribution of silicon in the particle of the catalyst which varies upon contact with ambient moisture. The stability to humidity has been improved by post-synthesis treatment with steam. Thus, we have synthesized samples with longer lifetime in the reaction of methanol. The effect of crystal size reduction has also been studied for zeolite SSZ-13 that is isomorphous with SAPO-34, by addition of surfactant agents during the synthesis and it has also been tested how this size reduction produces an increased lifetime of the catalyst.

Finally, lifetime and hydrothermal stability of zeolite ZSM-5, current catalyst component of the methanol to propylene process, have been optimized. We have studied the effect of increased mesoporosity by base / acid treatments on the catalytic properties and it has been proved that mesoporosity increases lifetime while, conversely, hydrothermal stability is affected. In the final part, the hydrothermal stability of mesoporous ZSM-5 has been improved by addition of phosphorus. The study has shown that the activity of the catalyst based on mesoporous ZSM-5 can be preserved by improving the hydrothermal stability including phosphorus into the catalyst composition.

# Index

# 1.Introduction

# 1.1.Zeolites

Zeolites are porous crystalline materials formed by $TO_4$ tetrahedra (T=Si, Al,) which are connected by the sharing oxygen atom in a three-dimensional array. The different ways of the $TO_4$ tetrahedral connections, result in different zeolitic structures with distinct channels and cages, where water and alkali or alkali-earth cations are situated. In addition, due to the trivalent Al in the tetrahedral units, the framework presents negative charges, which are balanced by the non-framework cations and can be removed by ion exchange[1], one of the important properties of zeolitic materials.

Table 1.1 Evolution of molecular sieve materials [1].

| Time of initial discovery | Composition |
| --- | --- |
| Late 1940s to early 1950s | Low Si/Al ratio zeolites |
| Mid-1950s to late 1960s | High Si/Al ratio zeolites |
| Early 1970s | $SiO_2$ molecular sieves |
| Late 1970 | $AlPO_4$ molecular sieves |
| Late 1970s to early 1980s | SAPO and MeAPO molecular sieves |
| Late 1970s | Metallo-silicates, aluminosilicates |
| Early to mid-1980s | $AlPO_4$-based molecular sieves |
| Early to mid-1990s | Metallophosphates |
| | Mesoporous molecular sieves |
| | Octahedral-tetrahedral frameworks |
| Late 1990s | Metal organic framework |
| 2000s | UZM aluminosilicate zeolites, Si/Al=2-30 |
| | Germanosilicate zeolites |
| | $SiO_2$ molecular sieves in fluoride media |

The research on zeolites has a long story since they were first found by the Swedish mineralogist Cronsted in 1756[2]. Since then many efforts have been applied on the synthesis and uses of zeolites. Richard M. Barrer did pioneering work on the synthesis of zeolites and adsorption since 1930s. He reported the first definitive synthesis of zeolites as the analog to the mineral mordenite zeolite and the new zeolites with KFI structure identified later [3]. In 1950s, Robert M. Milton and coworker Donald W Breck, discovered series of important commercial synthetic materials even today such as zeolites A, X and Y, which improved more and more the study on the zeolites. And only since then zeolites became an important catalyst instead of the former used amorphous aluminosilicates, and started the new era of

the application in the catalytic industrial processes[4]. The introduction of organic molecules in the synthesis of zeolites, which are used as the structure directing agent (or called template)  sparked the preparation of new structure types zeolites in 1970s, especially on the synthesis of high-silica or all-silica zeolites[5, 6], for instance the zeolites ZSM-5 and Beta[5, 7].  ZSM-5 zeolite is widely used in the industry as we will mention in detail later. Templates play an important role in the synthesis of zeolites such as to stabilize the structure, balance the negative charge of the structure and fill the space of the channels[8]. The aluminophosphate zeolites were discovered by Flanigen and Wilson from Union Carbide Corp in 1982[9], and sooner the aluminophosphates (MeAlPOs) and silicoaluminophosphates zeolites (SAPO) were described due to the isomorphous  substitution of aluminum and phosphorus by other metals(Mn, Mg, Co, Ni,  and Fe) and silicon respectively[10, 11]. And later ordered mesoporous silicate and aluminosilicate materials with the amorphous framework walls such as M41S and FSM-16 were prepared in 1990s by Kresge et al. and Beck et al. from Mobil [12, 13]. It also opened a new field of research and applications on micro-mesoporous molecular sieve materials[14]. In the beginning of the new century, the development of the zeolites preparation turns to new situations such as (i) the application of microwave heating, multiple templates and fluoride media (ii) the synthesis of small particle sizes zeolites such as nano zeolites [1] (iii) Ge containing zeolites obtained by Corma's group from Spain which have smaller structural units and more open framework in which Ge used as co-structural directing agent and form the smaller Ge-O-Ge angles[11, 15-18].

According to definition from the IUPAC, the porosity of zeolites can be classified in three types according the pore sizes: micropores: (a) (2.0 nm ≥ dp) (b) mesopores: 2.0nm< dp ≤ 50 nm (c) macropores: dp > 50 nm. Also, zeolites can be categorized as below according to the member rings [1]: small pore zeolites with 8-membered ring pores (e.g., SAPO-34, SSZ-13), medium pore zeolites with 10 – membered ring pores, (ZSM – 5), large pore zeolites with 12 – membered ring (e.g., zeolites X, Y) and extra - large pore zeolites with 14 - membered ring pores (e.g., UTD-1, ITQ-43,44[19]). And also by its dimensionality: mono, bi and tridimensional.  Right now more than 200 kinds of different zeolitic framework materials have been prepared [20].

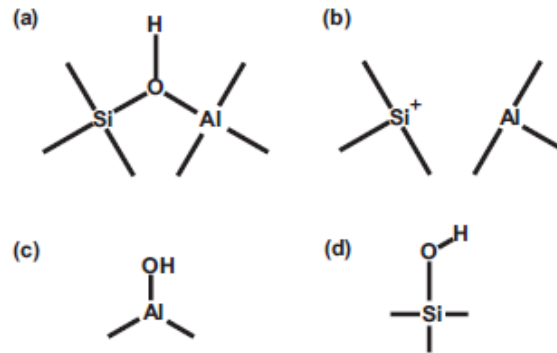# 1.1.1. The acidity and shape selectivity of zeolites



Fig 1.1 Types of acid sited in zeolites—bridging OH group—Brønsted acid site (a), structural defect—Lewis acid site (b), extra-framework aluminum species—Lewis acid site (c),and silanol group (d)[8].

Zeolites are widely used as an important kind of catalysts, due to their remarkable properties such as high surface area, controllable adsorption capacity, tailored acidity strength and concentration, selectivity to molecules, high thermal and hydrothermal stability[21, 22].

For example, one of most important properties of zeolites for catalysts is their acidity. The framework of zeolites presents negative charges due to the appearance of trivalent Al. When they are compensated by protons, zeolites serve as solid Brønsted acids and are used for acid catalyzed reactions[23]. Other sites as shown in Fig.1.1 act as Lewis acids and can be found when Al behaves as electron-acceptor due to the presence of extra-framework aluminum atoms or unsaturated aluminum atoms in the framework [24].

Another unique property of zeolites is the selectivity in the chemistry reactions and can be described as below [25]:

1) Reactant-Shape Selectivity: When there are more than two reactants in the reactions, only the one whose size is smaller than zeolites pores can be allowed to enter the molecular channels. This kind of selectivity is called reactant-shape selectivity, as shown in Fig 1.2 [25].

2) Product-Shape Selectivity: When the reactions start, there may be different thermodynamically feasible products, but the potential products whose size is too large cannot diffuse through the molecular-dimmension pores. This kind of selectivity is called Product-Shape Selectivity, as show in Figure 1.2.
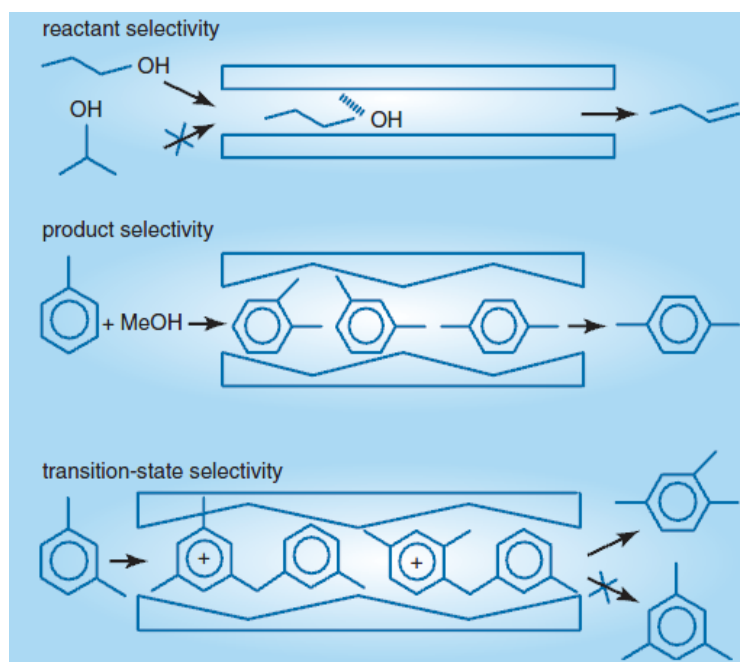


Fig 1.2 Three types of shape-selective catalytic reactions with representative examples: reactant-shape selectivity in the alcohol dehydration reactions; product shape selectivity in toluene methylation reactions; transition-state-shape selectivity in m-xylene disproportionation (transmethylation) reactions[25].

3) Transition-State Selectivity: When the channels act as confined reactors, they can impose steric geometrical restrictions on the transitions states. This kind of selectivity is called Product-Shape Selectivity, as shown in Figure 1.2, whose selectivity mostly depends not on crystal size or activity but on zeolite structure and pore diameter. Some new studies show that electronic factor may play an important affection in shape-selective products, and they proposed a new concept named restricted-electronic transition-state selectivity [26, 27].

The effect of shape selectivity on catalysis is very clear in directing the selectivity of the catalytic reaction to the desired products as for example: p-xylene in the isomerization of xylenes on ZSM-5, light olefins in the reaction of methanol to olefins on 8MR zeolites and others [18]. However, there are drawbacks that limit the

full applicability of shape selectivity as the processing of molecules larger than the size of the channels and also the presence of internal diffusion control inside the crystals of zeolites. The latter is especially important for 8MR zeolites with cages as SSZ-13 and SAPO-34, in which only the part of the crystals close to the surface is active and coking presents high deactivation effect.

## 1.1.2. Application of zeolites

Table 1.2 The main applications of zeolitic catalysts in the important industrial processes [8].

| Structural type (zeolite or zeotype) | Catalytic process |
| --- | --- |
| FAU (Y) | Fluid catalytic cracking, Hydrocracking, Aromatic alkylation and transalkylation, Olefin/paraffin alkylation, $NO_x$ reduction, Acylation |
| BEA (Beta) | Benzene alkylation, Acylation, Baeyer-Villiger reaction |
| MOR (Mordenite) | Light alkanes hydroisomerization, Dewaxing(cracking), Aromatic alkylation and transalkylation, Olefin oligomerization |
| LTL (KL) | Alkane aromatization |
| MTW (ZSM-12) | Aromatic alkylation |
| MFI (ZSM-5,TS-1,Silicalite) | Fluid catalytic cracking, Dewaxing(cracking), MTG/MTO gasoline/olefins, Olefin cracking and oligomerization, Benzene alkylation, Xylene isomerization, Toluene disproportionation and alkylation, Aromatization, $NO_x$ reduction, Ammoxidation, Beckman rearrangement |
| MWW(MCM-22) | Benzene alkylation |
| FER (Ferrierite) | n-Butene skeletal isomerization |
| TON (Theta-1, ZSM-22) | Dewaxing (long chain alkane hydroisomerisation), Olefin skeletal isomerization |
| AEL (SAPO-11) | Dewaing (long chain alkane hydroisomerization) |
| ERI (Erionite) | Selectoforming |
| CHA (SAPO-34) | MTO |

Since 1962, faujasites (zeolites X and Y) were introduced to industry as the catalyst for fluid catalytic cracking (FCC) of heavy petroleum distillates, which showed more activity and yield comparing with the catalyst used before in this process. This remarkable result attended more and more attention to the synthesis of zeolites and their application in catalytic reactions[28]. Nowadays zeolitic catalysts have been wildly used in fields of fine chemistry, agriculture, ion-exchange, and oil cracking, some of them are very important processes for our daily life [14]. The

applications of zeolites in the most important industrial processes are shown in the Table.1.2 [8].

Here, because of the space, we will focus just on zeolites SAPO-34 and ZSM-5 and their application in the methanol to olefins and methanol to hydrocarbons reactions.

## 1.2. SAPO-34 and ZSM-5

SAPO-34 is a silicoaluminophosphate with chabazite (CHA) structure three-directional formed by 8-ring channels (0.38 X 0.38nm) connecting large cavities, while ZSM-5 is a 10-ring silicoaluminate with the MFI structure and consists of a sinusoidal (0.55 X 0.51nm) and a straight(0.56X 0.53) channels forming also a three-directional pore system. Due to the different structure of both samples, they show different performance in the methanol to olefins reaction, offering a good example of product shape selectivity in which SAPO-34 exhibit high selectivities of ethylene and propylene while ZSM-5 presents a broader product distribution including olefins, aromatics, paraffins, naphthenes and so on[29-31].

As it was shown in Fig.1.3 reproduced from Haw et al. [32], different structures of catalysts were tested in MTO reaction and the corresponding products were obtained. For SAPO-34, only small hydrocarbons can diffuse and benzene is too large to go out of the cage while for ZSM-5 it can be seen that the main products are methylbenzenes and light alkanes especially isobutane and isopentane and also olefins. Although zeolite Ferrierite with the FER structure has a similar acid strength with ZSM-5 and different structures, the main products of FER are almost entirely olefins, especially butenes andpentenes also due to the smaller dimensions of its channels in which aromatics cannot be formed.
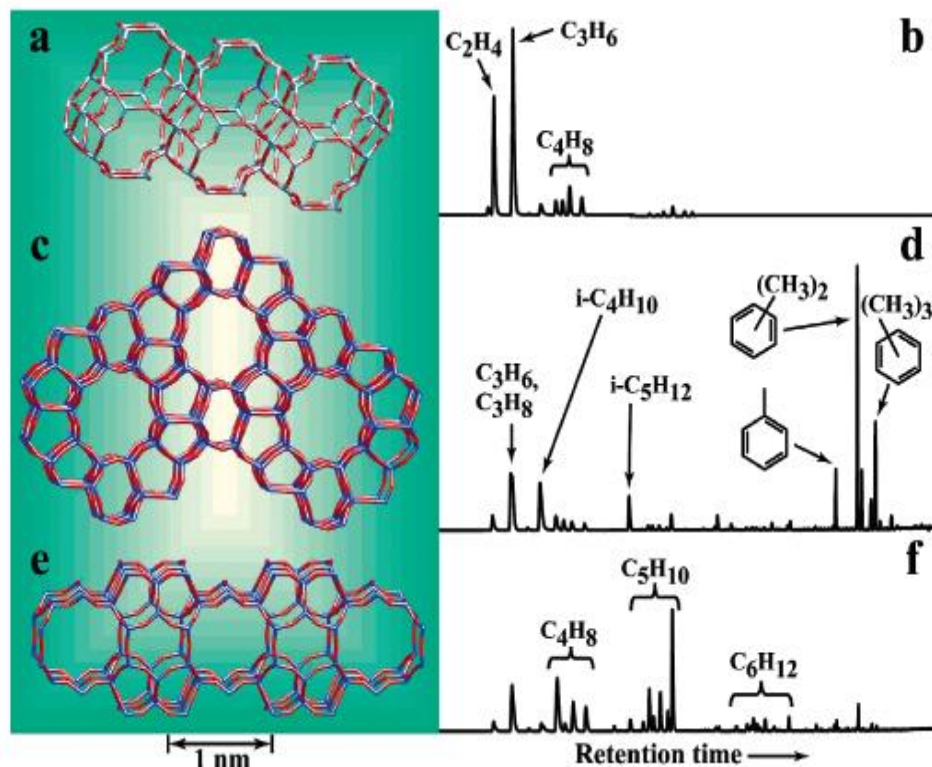
Fig 1.3 The methanol conversion of different materials (a) The CHA topology of the silico-aluminophosphate catalyst H-SAPO-34. (c) The MFI structure of the aluminosilicate zeolite HZSM-5. (e) The FER topology of H-Ferrierite. (b) (d) (f) are the products of methanol conversion on MTO catalysis corresponding to the materials. Each experiment used 300 mg of catalyst operated at 723 K, and products were sampled 1.5 s following pulsed introduction of 10.2μL of methanol [32].

# 1.3.MTO

Methanol to olefins is an important process in industry for obtaining ethylene and propylene. It was discovered by Chang and Silvestri from Mobil Central Research when they tried to find new ways to get more gasoline from methanol and isobutene in 1970s [33]. Since then, a lot of researchers in the world put their attention on the MTO studies. Compared with the current ethylene and propylene production process such as steaming cracking or Fluid Catalytic Cracking, MTO may offer a wider yield of ethylene and propylene to supply market needs [34, 35].
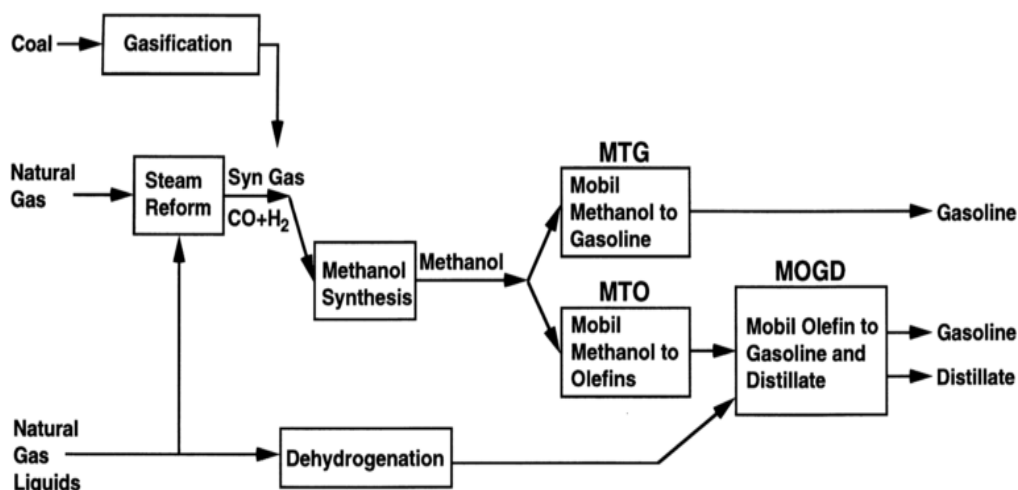
Fig 1.4 Gasoline and distillate production via methanol and Mobil's ZSM-5 technology [36].

The first commercial MTG (methanol to gasoline as shown in Fig.1.4) plant using ZSM-5 as the catalyst was built in New Zealand, but was shut down later due to negative fluctuations of the oil price [37]. Later, Haldor Topsøe developed the Topsøe Integrated Gasoline Synthesis (TIGAS) process [38], which also applied ZSM-5 as the catalyst. This process integrates the synthesis of methanol from synthesis gas and its conversion to aromatics. The variant of the methanol to gasoline reaction called methanol to olefins in which mainly product are ethylene and propylene was developed by Norsk Hydro and UOP joint, based on the application of H-SAPO-34 as the catalyst. By now they have projected four MTO process plants in China [27].  A similar process named DMTO, which also uses H-SAPO-34 as catalyst has been developed by scientists from Dalian Institute of Chemical Physics[39], and  several plants have been already built since the first commercial one in Baotou, China  in 2010[40]. Other currently commercial process is Lurgi's MTP (methanol to propylene), in which by using a small high Si/Al ZSM-5-based catalyst manufactured by Süd-Chemie (now Clariant) the yield of aromatics is decreased increasing therefore the yield to propylene. Two plants are working in China [40].

Currently, due to the increasing demand of ethylene and propylene, along with the technologies which obtain methanol from natural gas, biomass, and other

carbon-rich feedstocks, the conversion of methanol, has attracted a lot of interest both in industry and academia [41-44].

# 1.4.Mechanism of MTO

The mechanism of MTO has been studied by plenty of scientists for more than 30 years, but there is still of debate about the initial formation of C-C bonds from methanol. To answer this question, more than 20 distinct mechanisms have been proposed in these almost 40 years, such as the mechanism of carbenes, free radicals, oxonium ylides, and carbocations which are featured the intermediates [24]. However, none of these can be certified by the experiment results or theoretical studies [25]. Dessau and coworkers addressed that after the product formation in the induction period, ethylene and higher alkenes could be formed by sequence of reaction of methylations , oligomerizaition and cracking in the steady period[26, 27]. Almost at the same time, Mole et al. reported the important role in improvement of methanol conversion by the addition of traces of aromatics to MTH reaction, which was called aromatic co-catalysis later[28, 29]. On the base of results from Mole and Langner[30], Dahl and Kolboe proposed that olefins were formed from methanol reacting with a hydrocarbon pool of intermediates [31-33]as shown in Figure 1.5.

.
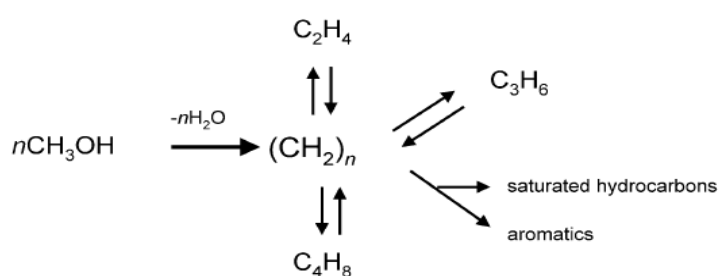


Fig 1.5 Mechanism of hydrocarbon pool from Dahl and Kolboe [50-52].

The latter study on the SAPO-34 by Kolboe and Arstad demonstrated the important role of methylbenzenes in the HP (hydrocarbon pool) mechanism [53, 54], which was also proved by Haw and co-workers [32, 55-57]. These results confirmed the importance of the protonated HP species intermediates. Two distinct hypotheses have been proposed to answer how the alkenes are formed from the aromatic

intermediates in HP mechanisms: one is called paring type mechanism first proposed by Sullivan et al. [58] in which olefins results from the elimination of methyl groups by ring-contraction and methyl shifts. Other is the side- chain methylation model addressed by Mole et al [47, 48], and further developed by Haw and coworkers [59, 60], in which olefins are formed by the deprotonation, methylations and elimination processes. The paring and side-chain models were shown in Fig.1.6.
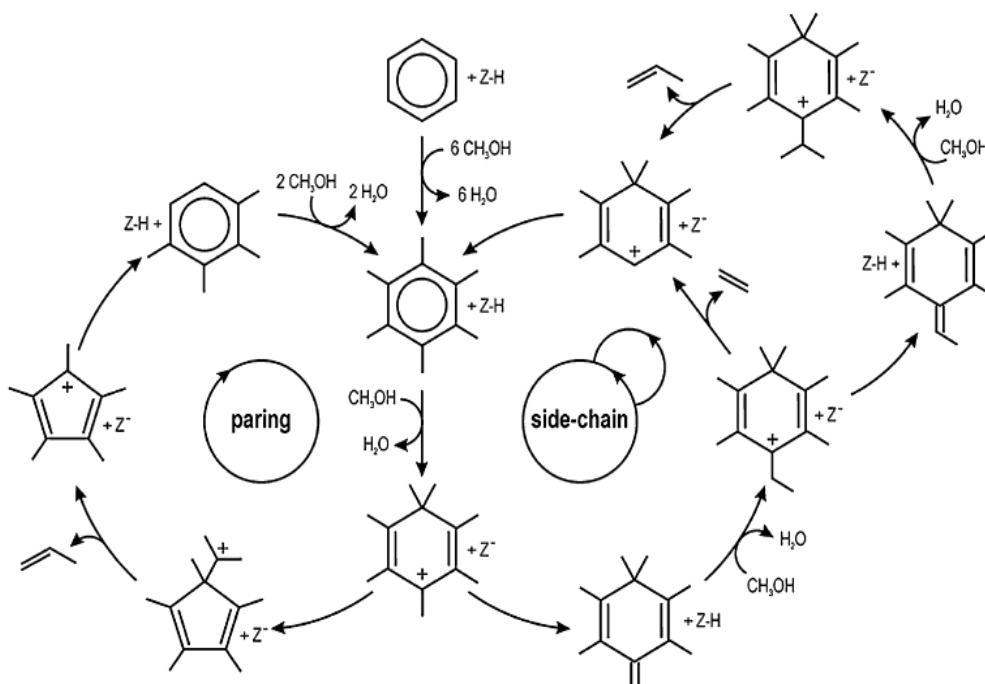
Fig 1.6 Paring and side-chain schemes for MTO conversion based on aromatic HP species [61].
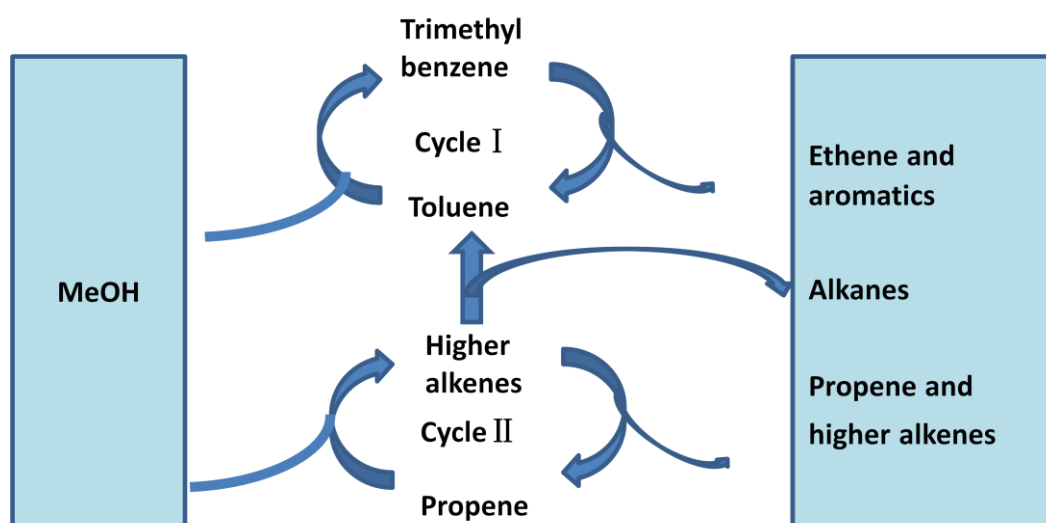
Fig 1.7 Dual cycle concept for the conversion of methanol on ZSM-5 (from ref [62]).

However, the HP mechanism were only applied in the research of SAPO-34 and Beta zeolites catalysts, and it can't explain the experimental observations when ZSM-5 of low acidity and ferrierite or ZSM-22 are used as catalysts in which aromatics are not formed [62, 63].   Then, a dual cycle mechanism for MTO conversion in ZSM-5 (Fig.1.7) have been proposed which reveals that the ethylene comes mainly from the aromatic routes and propylene and other higher alkenes from the alkenes route by methylation and interconversion process [62-64].   So in this cycle mechanism, ethylene and propylene are formed by different mechanisms, which offer a possibility to control the ethylene/propylene ratios in the methanol conversion by the modification of the ZSM-5 catalyst [65]. These two cycles can interact with each other. For instance, propylene traces derived from the polymethylbenzene cycle can play as a co-catalyst in the alkenes route. In the meantime, the alkenes formed by oligomerization and cyclization may lead to additional polymethylbenzene species [42, 66].
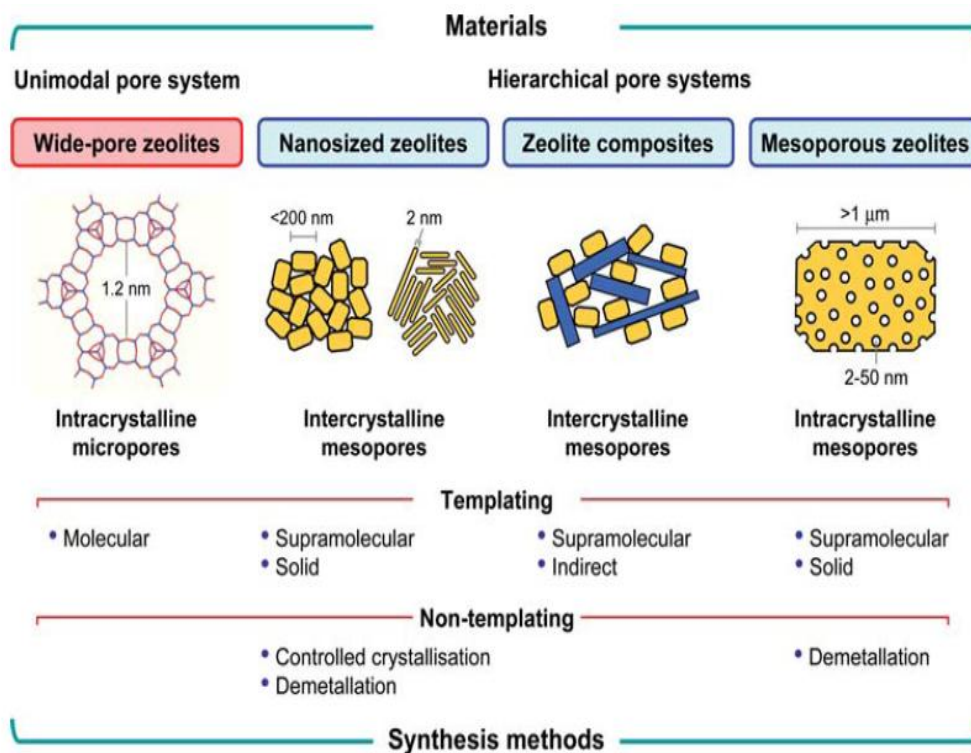
# 1.5. Modification of zeolites



Fig 1.8 Different ways to obtain zeolitic materials with enhanced improved transport characteristics [68].

As we have mentioned zeolite catalysts are widely used in oiling refining, petrochemistry, adsorption and separation due to their unique properties of channels and cavities[14]. However, only 5% of these more than 200 zeolites structures have been used in industrial processes, such as FAU, MOR, MFI,FER, LTA Bea and CHA types zeolites[67]. Even these widely used zeolites still can't match the increasing need for the fast diffusion and high conversion demand for the bulk molecule reagents, intermediates and product. The efficiency in the use of the microporous materials can be strongly improved if intracrystalline diffusion limitations in the small channels and cavities are lowered [68, 69]. To overcome the diffusion limitations which may cause the loss of activity and lifetime, even the loss of selectivity [68], many approaches (Fig.1.8) have been proposed such as the synthesis of ultra-large pore crystallines structure, zeolite delamination, nanosized zeolites and the preparation of hierarchical materials.

## 1.5.1.Extra-large zeolites

The synthesis of extra-large micropore zeolites (more than 12 member-rings) may be other choices which could enlarge the diffusion limitation, such as the VPI-5[34], ITQ-21[35], ITQ-40[19] and other extra-large zeolites [36]. Unfortunately, the undesirable stability of these materials and expensive price of the organic templates applied for the synthesis limits yet the application of these zeolite materials[37].

## 1.5.2.Nano particle zeolites

Reducing the crystal size of the zeolites may offer another way to overcome the diffusion limitations. Catalytic performance has been improved by decreasing the size of the crystals which has been demonstrated for ZSM-5[73, 74], zeolite beta[75], zeolite Y[76], mordenite[77] and SAPO-34 [39, 78]. Microwaves are widely applied in the synthesis of the nano particle zeolites which could offer efficient way to enhance crystalline process in a short time, and high control in the morphology and crystal size, besides this, it also plays an important effect on the yield and phase purity[79]. The comparison with conventional hydrothermal synthesis is summarized in Fig.1.9

**Advantages of microwave synthesis approach:**
1. Efficient control of size, yield, phase purity, morphology
2. Accelerates the nucleation via rapid/uniform heating
3. High conversion of amorphous precursors into zeolites
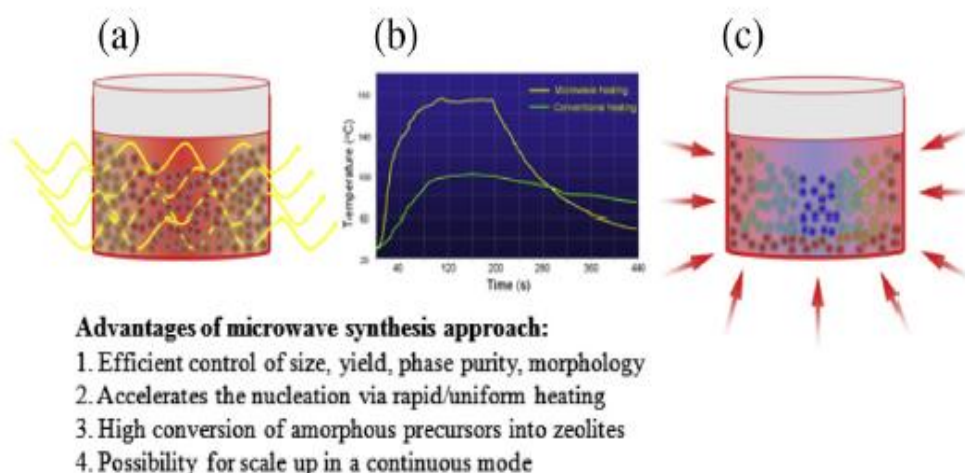4. Possibility for scale up in a continuous mode

Fig 1.9 The comparison of different methods to synthesize zeolites (a) microwave oven, (b) temperature profile in microwave and conventional heating reactors, and (c) conventional oven[79].

The nano particle catalysts present higher external surface and shorter diffusion ways to enhance accessibility of the channel and the diffusion rate of products(Fig 1.10), which is more important for the reaction of bulky molecules[69]. Recently, the nano SAPO-34 synthesized by microwave method and their application in methanol to olefins has been reported [40, 80].



Fig 1.10 Properties of nanosized zeolites [79].

# 1.5.3.Hierarchical zeolites

Table 1.3 The methods summary of preparation of hierarchical zeolites [69].

| Method | Template/support | Structure/morphology | Framework/composition of porous materials |
|---|---|---|---|
| Solid templating | Nanocarbon | Cave-like mesoporosity | ZSM-5,MTW, MEL, TS-1 |
| | Carbon nanotubes/nanofibers | | Silicalite-1, ZSM-5 |
| | CMK-3 | | ZSM-5 |
| | Large pore mesoporous carbons | | Silicalite-1 |
| | Carbon aerogels | | ZSM-5, Y |
| | Organic aerogels | | Silicalite-1,NaA |
| | $CaCO_3$ | | Silicalite-1 |
| | Starch-derived bread | | ZSM-5 |
| | 3Dom carbon | 3D ordered mesopores | Silicalite-1, BEA, LAT, FAU,LTL |
| Soft templating | Hydrophilic cationic polymers(PDADMAC) | | Beta, ZSM-5, NaX |
| | Amphiphilic organosilane | Tunable mesoporosity | MFI, LTA,AlPO4-n,SOD |
| | Silylated polyethylenimine polymer | | MFI |
| | Polyvinyl butyral(PVB) | | Beta, ZSM-11 |
| | CTAB | | MFI, Y, SOD |
| | Diquatemary ammonium-type surfactant | Lamellar single-unit-cell nanosheets | MFI |
| | Dual-porogenic surfactant | Hexagonally ordered mesopores | MFI |
| Post treatments | Steaming | | ZSM-5, TUD-1, TS-1 |
| | Leaching with acid treatment | | Zeolite-Y |
| | Leching with alkali treatment | | ZSM-5 |

Another effective route proposed to overcome diffusion limitations is the combination of micropores with meso/macroporous in one material (hierarchical materials Table 1.3), which contains properties of the catalytic zeolite micropores with high accessibility and meso/macropores with higher diffusion rate [69, 77]. Following this, a vast amount of hierarchical zeolites has been obtained by desilication treatments such as ZSM-5[81] or by soft or hard template[69, 82, 83] and

other surfactant[82, 84, 85]. Recently, the silicogermanate ITQ-43 with interconnecting pores have been reported by Corma et al. which is the first truly hierarchical zeolites [17]. To date, the approaches to prepare hierarchical zeolites can be classified into one indirect synthesis by the using of soft or hard templates or the addition of surfactant in the synthesis system way [69, 85], and the post-synthesis ways such as acid and base etching, steaming, dealumination, desilication or steaming [67, 69, 85].
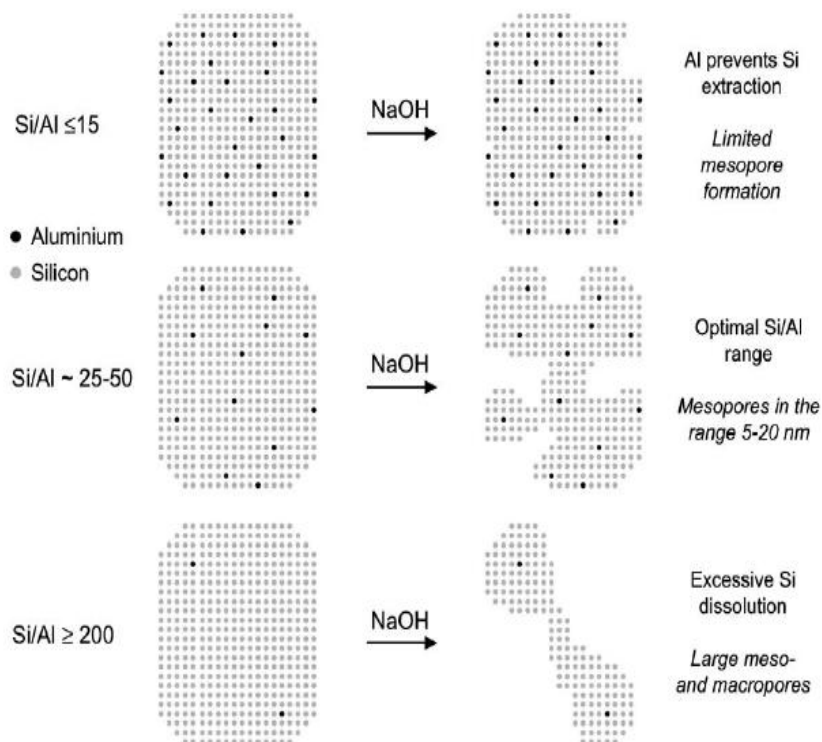


Fig 1.11 The influence of the amount of Al in desilication process of MFI zeolites when they are treated by NaOH solution and the associated mechanism of pore formation from Groen et al. [99].

Here, we will give a short introduction to the preparation of hierarchical zeolites by soft template method and desilication process treated by alkali solution. The use of dual templates which contains small organic structure directing agent for formation of micropores and large organic surfactant molecular for fabrication of mesopores respectively as a strategy to prepare meso-MFI has been proposed by the earlier researchers [86-91]. The large molecular surfactant hexadecyl trimethyl ammonium bromide (CTAB) firstly used to prepare MCM-41 has been employed to the synthesis of hierarchical zeolites[92-95] in the dual templates method. It has been proved that

the zeolite precursor contains primary units of zeolite seeds, nanocyrstals, nanoparticles and subnanocrystals that assembly and grow to zeolite crystals by feeding later in the crystallization. With the addition of CTAB, the process of zeolite crystallization is delayed and the formation of the mesoporous phase is accelerated and controlled by kinetic priority [92, 93]. Hensen et al. have applied a co-templates way in the synthesis of SSZ-13 zeolites, which have shown increased mesoporosity and longer lifetime when tested in reaction of methanol to olefins [91].

As it has been reported, mesopores are formed when different zeolites are treated in alkaline solutions such as NaOH, $Na_2CO_3$, TPAOH, TBAOH [96] that selectively removes Si from the crystals. The desilication of H-ZSM-5 and the effect of the mesoporosity developed have been investigated in the reaction of MTH, and also the influence of the Si/Al ratio in the formation of mesopores (Fig.1.11) have been discussed [97-99]. It is generally accepted that the optimal ratios of ZSM-5 for the desilication process is 25-50. At lower ratios aluminum protects against the treatment while at higher ratios the desilication process remove excessive amount of Si atoms out of the framework leading to non-selective extractions happened and formation of macropores [99]. The addition of TPAOH or TBAOH to NaOH solution protects the framework of high Silica ZSM-5 against excessive desilication. The role of amines is to bind to the silica surface controlling the extension of the desilication and also the size of mesopores [68, 96, 99-102].

# 1.6. Phosphorus modified ZSM-5

The introduction of phosphorus to modify ZSM-5 is one of the ways to improve the propylene selectivity and reduce the aromatics product in the expense of the decrease of acidity[103-106], and with the washing of hot water, additional Brønsted acidity can be recovered[107, 108]. Since it was firstly reported, the phosphorus modification of ZSM-5 has been applied to different reactions such as fluid catalytic cracking, toluene alkylation, and also methanol to hydrocarbons [108]. The introduction of phosphorus also play an important role in enhancement the hydrothermal stability of the ZSM-5, as it was first reported by Lischke et al[107], and confirmed by other researchers[109-113]. This is especially important for the application of ZSM-5 in the MTH reaction, since water is present in the reaction

media and causes progressive dealumination and therefore irreversible deactivation of the catalyst.
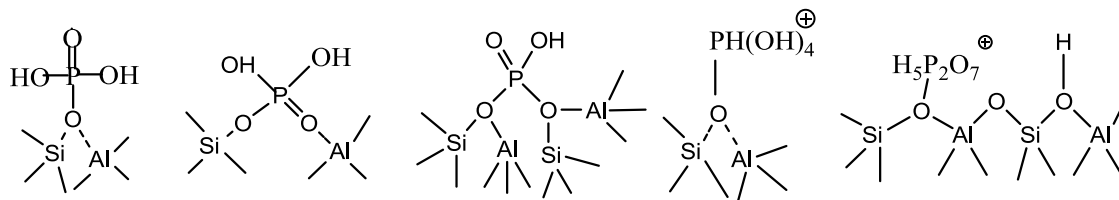


Scheme 1.1 Different model on the interaction between the phosphorus and the ZSM-5 framework [108].

However, there is still controversy about the mechanism of the introduction phosphorus, along with the disagreement about the interaction of phosphorus with the zeolitic structure and the origin of the stabilization against dealumination. Many mechanisms have been proposed such as the direct connection of phosphorus and the zeolites framework, no framework interactions or the formation of tetrahydroxyphosphonium ions [107, 109, 110, 114-119], which have been summarized by Lercher and shown in Scheme 1.1[108].

# References

[1] E.M. Flanigen, R.W. Broach, S.T. Wilson, Introduction, in: Zeolites in Industrial Separation and Catalysis, Wiley-VCH Verlag GmbH & Co. KGaA, 2010, pp. 1-26.

[2] A.F. Cronstedt Ron och beskriting om en obekant b ä rg ant, som kallas zeolites, Akad. Handl. Stockholm, 18 (1756) 120 – 130.

[3] R.M. Barrer, 435. Syntheses and reactions of mordenite, Journal of the Chemical Society, (1948) 2158-2163.

[4] J. Biswas, I.E. Maxwell, Recent process- and catalyst-related developments in fluid catalytic cracking, Applied Catalysis, 63 (1990) 197-258.

[5] R.J. Argauer, G.R. Landolt, Crystalline zeolite zsm-5 and method of preparing the same, in, Google Patents, 1972.

[6] E.M. Flanigen, J.M. Bennett, R.W. Grose, J.P. Cohen, R.L. Patton, R.M. Kirchner, J.V. Smith, Silicalite, a new hydrophobic crystalline silica molecular sieve, Nature, 271 (1978) 512-516.

[7] R.L. Wadlinger, G.T. Kerr, E.J. Rosinski, Catalytic composition of a crystalline zeolite, in, Google Patents, 1967.

[8] J. Čejka, D. Kubička, Zeolites and Other Micro- and Mesoporous Molecular Sieves, in: Kirk-Othmer Encyclopedia of Chemical Technology, John Wiley & Sons, Inc., 2000.

[9] S.T. Wilson, B.M. Lok, C.A. Messina, T.R. Cannan, E.M. Flanigen, Aluminophosphate molecular sieves: a new class of microporous crystalline inorganic solids, Journal of the American Chemical Society, 104 (1982) 1146-1147.

[10] E.M. Flanigen, R.L. Patton, S.T. Wilson, Structural, Synthetic and Physicochemical Concepts in Aluminophosphate-Based Molecular Sieves, Studies in Surface Science and Catalysis, Elsevier, 1988, pp. 13-27.

[11] M. Moliner, Direct Synthesis of Functional Zeolitic Materials, ISRN Materials Science, 2012 (2012) 1-24.

[12] C.T. Kresge, M.E. Leonowicz, W.J. Roth, J.C. Vartuli, J.S. Beck, Ordered mesoporous molecular sieves synthesized by a liquid-crystal template mechanism, Nature, 359 (1992) 710-712.

[13] J.S. Beck, J.C. Vartuli, W.J. Roth, M.E. Leonowicz, C.T. Kresge, K.D. Schmitt, C.T.W. Chu, D.H. Olson, E.W. Sheppard, A new family of mesoporous molecular sieves prepared with liquid crystal templates, Journal of the American Chemical Society, 114 (1992) 10834-10843.

[14] A. Corma, From Microporous to Mesoporous Molecular Sieve Materials and Their Use in Catalysis, Chemical Reviews, 97 (1997) 2373-2420.

[15] J. Sun, C. Bonneau, A. Cantin, A. Corma, M.J. Diaz-Cabanas, M. Moliner, D. Zhang, M. Li, X. Zou, The ITQ-37 mesoporous chiral zeolite, Nature, 458 (2009) 1154-1157.

[16] J. Jiang, J. Yu, A. Corma, Extra-large-pore zeolites: bridging the gap between micro and mesoporous structures, Angewandte Chemie, 49 (2010) 3120-3145.

[17] J. Jiang, J.L. Jorda, J. Yu, L.A. Baumes, E. Mugnaioli, M.J. Diaz-Cabanas, U. Kolb, A. Corma, Synthesis and Structure Determination of the Hierarchical Meso-Microporous Zeolite ITQ-43, Science, 333 (2011) 1131-1134.

[18] C. Martínez, A. Corma, Inorganic molecular sieves: Preparation, modification and industrial application in catalytic processes, Coordination Chemistry Reviews, 255 (2011) 1558-1580.

[19] A. Corma, M.J. Díaz-Cabañas, J. Jiang, M. Afeworki, D.L. Dorset, S.L. Soled, K.G. Strohmaier, Extra-large pore zeolite (ITQ-40) with the lowest framework density containing double four- and double three-rings, Proceedings of the National Academy of Sciences, 107 (2010) 13997-14002.

[20] http://www.iza-structure.org.

[21] A. Corma, Inorganic Solid Acids and Their Use in Acid-Catalyzed Hydrocarbon Reactions, Chemical Reviews, 95 (1995) 559-614.

[22] G.J.d.A.A. Soler-Illia, C. Sanchez, B. Lebeau, J. Patarin, Chemical Strategies To Design Textured Materials: from Microporous and Mesoporous Oxides to Nanonetworks and Hierarchical Structures, Chemical Reviews, 102 (2002) 4093-4138.

[23] S. Svelle, M. Visur, U. Olsbye, Saepurahman, M. Bjørgen, Mechanistic Aspects of the Zeolite Catalyzed Methylation of Alkenes and Aromatics with Methanol: A Review, Topics in Catalysis, 54 (2011) 897-906.

[24] P.A. PJacobs, Carboniogenic Activity of Zeolites, (1977) 105

[25] C. Song, Selective Conversion of Polycyclic Hydrocarbons to Specialty Chemicals over Zeolite Catalysts, CATTECH, 6 (2002) 64-77.

[26] C. Song, X. Ma, A.D. Schmitz, H.H. Schobert, Shape-selective isopropylation of naphthalene over mordenite catalysts: Computational analysis using MOPAC, Applied Catalysis A: General, 182 (1999) 175-181.

[27] C. Song, X. Ma and H. H. Schobert, Chemicals Synthesis and Hydrocarbon Processing (ACS Symposium Series 738), American Chemical Society, Washington, DC, (1999) 381–390 (Chapter 27)

[28] M. Boudart, B. H. Davis, H. Heinemann, Introduction, Handbook of Heterogeneous Catalysis, Wiley-VCH Verlag GmbH, (2008) 1-48.

[29] P.L. Benito, A.G. Gayubo, A.T. Aguayo, M. Olazar, J. Bilbao, Effect of Si/Al ratio and of acidity of H-ZSM5 zeolites on the primary products of methanol to gasoline conversion, Journal of Chemical Technology & Biotechnology, 66 (1996) 183-191.

[30] A.T. Aguayo, A.G. Gayubo, M. Castilla, J.M. Arandes, M. Olazar, J. Bilbao, MTG Process in a Fixed-Bed Reactor. Operation and Simulation of a Pseudoadiabatic Experimental Unit, Industrial & Engineering Chemistry Research, 40 (2001) 6087-6098.

[31] H.A. Zaidi, K.K. Pant, Catalytic conversion of methanol to gasoline range hydrocarbons, Catalysis Today, 96 (2004) 155-160.

[32] J.F. Haw, W. Song, D.M. Marcus, J.B. Nicholas, The Mechanism of Methanol to Hydrocarbon Catalysis, Accounts of Chemical Research, 36 (2003) 317-326.

[33] C.D. Chang, A.J. Silvestri, The conversion of methanol and other O-compounds to hydrocarbons over zeolite catalysts, Journal of Catalysis, 47 (1977) 249-259.

[34] E.C.A. C.N. Eng, B.V. Vora, Integration of the UOP/HYDRO MTO process into ethylene plants, Presented at the 1998 AIChE Spring National Meeting, Session 16, Fundamental Topics in Ethlyene Production, Paper 16g, New Orleans, Louisiana, (1998).

[35] B.V. Vora, T.L. Marker, P.T. Barger, H.R. Nilsen, S. Kvisle, T. Fuglerud, Economic route for natural gas conversion to ethylene and propylene, Studies in Surface Science and Catalysis, Elsevier, (1997), 87-98.

[36] M. Stöcker, Methanol-to-hydrocarbons: catalytic materials and their behavior, Microporous and Mesoporous Materials, 29 (1999) 3-48.

[37] J. Cobb, New Zealand Synfuel: The Story of the World's First Natural Gas to Gasoline Plant, New Zealand Synthetic Fuels Corporation, (1985).

[38] J. Topp-Jørgensen, Topsøe Integrated Gasoline Synthesis – The Tigas Process, Studies in Surface Science and Catalysis, Elsevier, (1988), 293-305.

[39] J. Liang, H. Li, S. Zhao, W. Guo, R. Wang, M. Ying, Characteristics and performance of SAPO-34 catalyst for methanol-to-olefin conversion, Applied Catalysis, 64 (1990) 31-40.

[40] Z. Li, J. Martinez-Triguero, P. Concepcion, J. Yu, A. Corma, Methanol to olefins: activity and stability of nanosized SAPO-34 molecular sieves and control of selectivity by silicon distribution, Physical Chemistry Chemical Physics, 15 (2013) 14670-14680.

[41] Y.-K. Park, C. Lee, N. Kang, W. Choi, S. Choi, S. Oh, D. Park, Catalytic Cracking of Lower-Valued Hydrocarbons for Producing Light Olefins, Catal Surv Asia, 14 (2010) 75-84.

[42] U. Olsbye, S. Svelle, M. Bjorgen, P. Beato, T.V. Janssens, F. Joensen, S. Bordiga, K.P. Lillerud, Conversion of methanol to hydrocarbons: how zeolite cavity and pore size controls product selectivity, Angewandte Chemie, 51 (2012) 5810-5831.

[43] S. Ilias, A. Bhan, Mechanism of the Catalytic Conversion of Methanol to Hydrocarbons, ACS Catalysis, 3 (2013) 18-31.

[44] D. Chen, K. Moljord, A. Holmen, A methanol to olefins review: Diffusion, coke formation and deactivation on SAPO type catalysts, Microporous and Mesoporous Materials, 164 (2012) 239-250.

[45] R.M. Dessau, R.B. LaPierre, On the mechanism of methanol conversion to hydrocarbons over HZSM-5, Journal of Catalysis, 78 (1982) 136-141.

[46] R.M. Dessau, On the H-ZSM-5 catalyzed formation of ethylene from methanol or higher olefins, Journal of Catalysis, 99 (1986) 111-116.

[47] T. Mole, G. Bett, D. Seddon, Conversion of methanol to hydrocarbons over ZSM-5 zeolite: An examination of the role of aromatic hydrocarbons using 13-carbon- and deuterium-labeled feeds, Journal of Catalysis, 84 (1983) 435-445.

[48] T. Mole, J.A. Whiteside, D. Seddon, Aromatic co-catalysis of methanol conversion over zeolite catalysts, Journal of Catalysis, 82 (1983) 261-266.

[49] B.E. Langner, Reactions of methanol on zeolites with different pore structures, Applied Catalysis, 2 (1982) 289-302.

[50] I.M. Dahl, S. Kolboe, On the reaction mechanism for propene formation in the MTO reaction over SAPO-34, Catalysis Letters, 20 (1993) 329-336.

[51] I.M. Dahl, S. Kolboe, On the Reaction Mechanism for Hydrocarbon Formation from Methanol over SAPO-34: I. Isotopic Labeling Studies of the Co-Reaction of Ethene and Methanol, Journal of Catalysis, 149 (1994) 458-464.

[52] I.M. Dahl, S. Kolboe, On the Reaction Mechanism for Hydrocarbon Formation from Methanol over SAPO-34: 2. Isotopic Labeling Studies of the Co-reaction of Propene and Methanol, Journal of Catalysis, 161 (1996) 304-309.

[53] B. Arstad, S. Kolboe, The Reactivity of Molecules Trapped within the SAPO-34 Cavities in the Methanol-to-Hydrocarbons Reaction, Journal of the American Chemical Society, 123 (2001) 8137-8138.

[54] B. Arstad, S. Kolboe, Methanol-to-hydrocarbons reaction over SAPO-34. Molecules confined in the catalyst cavities at short time on stream, Catalysis Letters, 71 (2001) 209-212.

[55] H. Fu, W. Song, J. Haw, Polycyclic Aromatics Formation in HSAPO-34 During Methanol-to-Olefin Catalysis: Ex Situ Characterization After Cryogenic Grinding, Catalysis Letters, 76 (2001) 89-94.

[56] W. Song, H. Fu, J.F. Haw, Supramolecular Origins of Product Selectivity for Methanol-to-Olefin Catalysis on HSAPO-34, Journal of the American Chemical Society, 123 (2001) 4749-4754.

[57] W. Song, J.F. Haw, J.B. Nicholas, C.S. Heneghan, Methylbenzenes Are the Organic Reaction Centers for Methanol-to-Olefin Catalysis on HSAPO-34, Journal of the American Chemical Society, 122 (2000) 10726-10727.

[58] R.F. Sullivan, C.J. Egan, G.E. Langlois, R.P. Sieg, A New Reaction That Occurs in the Hydrocracking of Certain Aromatic Hydrocarbons, Journal of the American Chemical Society, 83 (1961) 1156-1160.

[59] A. Sassi, M.A. Wildman, H.J. Ahn, P. Prasad, J.B. Nicholas, J.F. Haw, Methylbenzene Chemistry on Zeolite HBeta: Multiple Insights into Methanol-to-Olefin Catalysis, The Journal of Physical Chemistry B, 106 (2002) 2294-2303.

[60] A. Sassi, M.A. Wildman, J.F. Haw, Reactions of Butylbenzene Isomers on Zeolite HBeta: Methanol-to-Olefins Hydrocarbon Pool Chemistry and Secondary Reactions of Olefins, The Journal of Physical Chemistry B, 106 (2002) 8768-8773.

[61] D. Lesthaeghe, A. Horré, M. Waroquier, G.B. Marin, V. Van Speybroeck, Theoretical Insights on Methylbenzene Side-Chain Growth in ZSM-5 Zeolites for Methanol-to-Olefin Conversion, Chemistry – A European Journal, 15 (2009) 10803-10808.

[62] M. Bjørgen, S. Svelle, F. Joensen, J. Nerlov, S. Kolboe, F. Bonino, L. Palumbo, S. Bordiga, U. Olsbye, Conversion of methanol to hydrocarbons over zeolite H-ZSM-5: On the origin of the olefinic species, Journal of Catalysis, 249 (2007) 195-207.

[63] S. Svelle, F. Joensen, J. Nerlov, U. Olsbye, K.P. Lillerud, S. Kolboe, M. Bjørgen, Conversion of methanol into hydrocarbons over zeolite H-ZSM-5: Ethene formation is mechanistically separated from the formation of higher alkenes, Journal of the American Chemical Society, 128 (2006) 14770-14771.

[64] W. Wu, W. Guo, W. Xiao, M. Luo, Dominant reaction pathway for methanol conversion to propene over high silicon H-ZSM-5, Chemical Engineering Science, 66 (2011) 4722-4732.

[65] S. Svelle, U. Olsbye, F. Joensen, M. Bjørgen, Conversion of Methanol to Alkenes over Medium- and Large-Pore Acidic Zeolites: Steric Manipulation of the Reaction Intermediates Governs the Ethene/Propene Product Selectivity, The Journal of Physical Chemistry C, 111 (2007) 17981-17984.

[66] K. Hemelsoet, J. Van der Mynsbrugge, K. De Wispelaere, M. Waroquier, V. Van Speybroeck, Unraveling the Reaction Mechanisms Governing Methanol-to-Olefins Catalysis by Theory and Experiment, ChemPhysChem, 14 (2013) 1526-1545.

[67] V. Valtchev, G. Majano, S. Mintova, J. Perez-Ramirez, Tailored crystalline microporous materials by post-synthesis modification, Chemical Society Reviews, 42 (2013) 263-290.

[68] J. Perez-Ramirez, C.H. Christensen, K. Egeblad, C.H. Christensen, J.C. Groen, Hierarchical zeolites: enhanced utilisation of microporous crystals in catalysis by advances in materials design, Chemical Society Reviews, 37 (2008) 2530-2542.

[69] L.H. Chen, X.-Y. Li, J.C. Rooke, Y.-H. Zhang, X.-Y. Yang, Y. Tang, F.-S. Xiao, B.-L. Su, Hierarchically structured zeolites: synthesis, mass transport properties and applications, Journal of Materials Chemistry, 22 (2012) 17381.

[70] M.E. Davis, C. Saldarriaga, C. Montes, J. Garces, C. Crowdert, A molecular sieve with eighteen-membered rings, Nature, 331 (1988) 698-699.

[71] A. Corma, M.J. Diaz-Cabanas, J. Martinez-Triguero, F. Rey, J. Rius, A large-cavity zeolite with wide pore windows and potential as an oil refining catalyst, Nature, 418 (2002) 514-517.

[72] F.S. Xiao, L. Wang, C. Yin, K. Lin, Y. Di, J. Li, R. Xu, D.S. Su, R. Schlogl, T. Yokoi, T. Tatsumi, Catalytic properties of hierarchical mesoporous zeolites templated with a mixture of small organic ammonium salts and mesoscale cationic polymers, Angewandte Chemie, 45 (2006) 3090-3093.

[73] M. Firoozi, M. Baghalha, M. Asadi, The effect of micro and nano particle sizes of H-ZSM-5 on the selectivity of MTP reaction, Catalysis Communications, 10 (2009) 1582-1585.

[74] K. Na, M. Choi, R. Ryoo, Recent advances in the synthesis of hierarchically nanoporous zeolites, Microporous and Mesoporous Materials, 166 (2013) 3-19.

[75] G. Bellussi, G. Pazzuconi, C. Perego, G. Girotti, G. Terzoni, Liquid-Phase Alkylation of Benzene with Light Olefins Catalyzed by β-Zeolites, Journal of Catalysis, 157 (1995) 227-234.

[76] G. Tonetto, J. Atias, H. de Lasa, FCC catalysts with different zeolite crystallite sizes: acidity, structural properties and reactivity, Applied Catalysis A: General, 270 (2004) 9-25.

[77] S. van Donk, A.H. Janssen, J.H. Bitter, K.P. de Jong, Generation, Characterization, and Impact of Mesopores in Zeolite Catalysts, Catalysis Reviews, 45 (2003) 297-319.

[78] S. Lin, J. Li, R.P. Sharma, J. Yu, R. Xu, Fabrication of SAPO-34 crystals with different morphologies by microwave heating, Topics in Catalysis, 53 (2010) 1304-1310.

[79] M. Zaarour, B. Dong, I. Naydenova, R. Retoux, S. Mintova, Progress in zeolite synthesis promotes advanced applications, Microporous and Mesoporous Materials, 189 (2014) 11-21.

[80] S. Lin, J. Li, R. Sharma, J. Yu, R. Xu, Fabrication of SAPO-34 Crystals with Different Morphologies by Microwave Heating, Topics in Catalysis, 53 (2010) 1304-1310.

[81] J.C. Groen, W. Zhu, S. Brouwer, S.J. Huynink, F. Kapteijn, J.A. Moulijn, J. Pérez-Ramírez, Direct Demonstration of Enhanced Diffusion in Mesoporous ZSM-5 Zeolite Obtained via Controlled Desilication, Journal of the American Chemical Society, 129 (2006) 355-360.

[82] V.N. Shetti, J. Kim, R. Srivastava, M. Choi, R. Ryoo, Assessment of the mesopore wall catalytic activities of MFI zeolite with mesoporous/microporous hierarchical structures, Journal of Catalysis, 254 (2008) 296-303.

[83] M. Choi, K. Na, J. Kim, Y. Sakamoto, O. Terasaki, R. Ryoo, Stable single-unit-cell nanosheets of zeolite MFI as active and long-lived catalysts, Nature, 461 (2009) 246-249.

[84] K. Egeblad, C.H. Christensen, M. Kustova, C.H. Christensen, Templating Mesoporous Zeolites, Chemistry of Materials, 20 (2008) 946-960.

[85] K. Moller, T. Bein, Mesoporosity--a new dimension for zeolites, Chemical Society reviews, 42 (2013) 3689-3707.

[86] L. Emdadi, Y. Wu, G. Zhu, C.-C. Chang, W. Fan, T. Pham, R.F. Lobo, D. Liu, Dual Template Synthesis of Meso- and Microporous MFI Zeolite Nanosheet Assemblies with Tailored Activity in Catalytic Reactions, Chemistry of Materials, 26 (2014) 1345-1355.

[87] A. Karlsson, M. Stöcker, R. Schmidt, Composites of micro- and mesoporous materials: simultaneous syntheses of MFI/MCM-41 like phases by a mixed template approach, Microporous and Mesoporous Materials, 27 (1999) 181-192.

[88] J. Pérez-Pariente, R. García, L. Gómez-Hortigüela, A.B. Pinar, Co-Templates in Synthesis of Zeolites, in: Zeolites and Catalysis, Wiley-VCH Verlag GmbH & Co. KGaA, 2010, pp. 107-129.

[89] S.J. Weigel, J.-C. Gabriel, E.G. Puebla, A.M. Bravo, N.J. Henson, L.M. Bull, A.K. Cheetham, Structure-Directing Effects in Zeolite Synthesis: A Single-Crystal X-ray Diffraction, 29Si MAS NMR, and Computational Study of the Competitive Formation of Siliceous Ferrierite and Dodecasil-3C (ZSM-39), Journal of the American Chemical Society, 118 (1996) 2427-2435.

[90] R. García, L. Gómez-Hortigüela, I. Díaz, E. Sastre, J. Pérez-Pariente, Synthesis of Materials Containing Ferrierite Layers Using Quinuclidine and 1-Benzyl-1-methylpyrrolidine as Structure-Directing Agents. An Experimental and Computational Study, Chemistry of Materials, 20 (2008) 1099-1107.

[91] L. Wu, V. Degirmenci, P.C.M.M. Magusin, B.M. Szyja, E.J.M. Hensen, Dual template synthesis of a highly mesoporous SSZ-13 zeolite with improved stability in the methanol-to-olefins reaction, Chemical Communications, 48 (2012) 9492-9494.

[92] Y. Liu, W. Zhang, T.J. Pinnavaia, Steam-Stable MSU-S Aluminosilicate Mesostructures Assembled from Zeolite ZSM-5 and Zeolite Beta Seeds, Angewandte Chemie International Edition, 40 (2001) 1255-1258.

[93] K.S. Triantafyllidis, E.F. Iliopoulou, E.V. Antonakou, A.A. Lappas, H. Wang, T.J. Pinnavaia, Hydrothermally stable mesoporous aluminosilicates (MSU-S) assembled from zeolite seeds as catalysts for biomass pyrolysis, Microporous and Mesoporous Materials, 99 (2007) 132-139.

[94] D. Pan, P. Yuan, L. Zhao, N. Liu, L. Zhou, G. Wei, J. Zhang, Y. Ling, Y. Fan, B. Wei, H. Liu, C. Yu, X. Bao, New Understanding and Simple Approach to Synthesize Highly Hydrothermally Stable and Ordered Mesoporous Materials, Chemistry of Materials, 21 (2009) 5413-5425.

[95] Y. Zhu, Z. Hua, J. Zhou, L. Wang, J. Zhao, Y. Gong, W. Wu, M. Ruan, J. Shi, Hierarchical mesoporous zeolites: direct self-assembly synthesis in a conventional surfactant solution by kinetic control over the zeolite seed formation, Chemistry, 17 (2011) 14618-14627.

[96] K. Sadowska, A. Wach, Z. Olejniczak, P. Kuśtrowski, J. Datka, Hierarchic zeolites: Zeolite ZSM-5 desilicated with NaOH and NaOH/tetrabutylamine hydroxide, Microporous and Mesoporous Materials, 167 (2013) 82-88.

[97] M. Bjørgen, F. Joensen, M. Spangsberg Holm, U. Olsbye, K.-P. Lillerud, S. Svelle, Methanol to gasoline over zeolite H-ZSM-5: Improved catalyst performance by treatment with NaOH, Applied Catalysis A: General, 345 (2008) 43-50.

[98] S. Fathi, M. Sohrabi, C. Falamaki, Improvement of HZSM-5 performance by alkaline treatments: Comparative catalytic study in the MTG reactions, Fuel, 116 (2014) 529-537.

[99] J.C. Groen, J.C. Jansen, J.A. Moulijn, J. Pérez-Ramírez, Optimal Aluminum-Assisted Mesoporosity Development in MFI Zeolites by Desilication, The Journal of Physical Chemistry B, 108 (2004) 13062-13065.

[100] D. Verboekend, J. Perez-Ramirez, Desilication mechanism revisited: highly mesoporous all-silica zeolites enabled through pore-directing agents, Chemistry, 17 (2011) 1137-1147.

[101] K. Mlekodaj, K. Tarach, J. Datka, K. Góra-Marek, W. Makowski, Porosity and accessibility of acid sites in desilicated ZSM-5 zeolites studied using adsorption of probe molecules, Microporous and Mesoporous Materials, 183 (2014) 54-61.

[102] K. Sadowska, K. Góra-Marek, M. Drozdek, P. Kuśtrowski, J. Datka, J. Martinez Triguero, F. Rey, Desilication of highly siliceous zeolite ZSM-5 with NaOH and NaOH/tetrabutylamine hydroxide, Microporous and Mesoporous Materials, 168 (2013) 195-205.

[103] H.E. van der Bij, B.M. Weckhuysen, Local silico-aluminophosphate interfaces within phosphated H-ZSM-5 zeolites, Physical Chemistry Chemical Physics , 16 (2014) 9892-9903.

[104] J. Liu, C. Zhang, Z. Shen, W. Hua, Y. Tang, W. Shen, Y. Yue, H. Xu, Methanol to propylene: Effect of phosphorus on a high silica HZSM-5 catalyst, Catalysis Communications, 10 (2009) 1506-1509.

[105] P. Li, W. Zhang, X. Han, X. Bao, Conversion of Methanol to Hydrocarbons over Phosphorus-modified ZSM-5/ZSM-11 Intergrowth Zeolites, Catalysis Letters, 134 (2010) 124-130.

[106] J.C. Védrine, A. Auroux, P. Dejaifve, V. Ducarme, H. Hoser, S. Zhou, Catalytic and physical properties of phosphorus-modified ZSM-5 zeolite, Journal of Catalysis, 73 (1982) 147-160.

[107] G. Lischke, R. Eckelt, H.G. Jerschkewitz, B. Parlitz, E. Schreier, W. Storek, B. Zibrowius, G. Öhlmann, Spectroscopic and physicochemical characterization of P-Modified H-ZSM-5, Journal of Catalysis, 132 (1991) 229-243.

[108] M. Derewinski, P. Sarv, X. Sun, S. Müller, A.C. van Veen, J.A. Lercher, Reversibility of the Modification of HZSM-5 with Phosphate Anions, The Journal of Physical Chemistry C, 118 (2014) 6122-6131.

[109] J. Zhuang, D. Ma, G. Yang, Z. Yan, X. Liu, X. Liu, X. Han, X. Bao, P. Xie, Z. Liu, Solid-state MAS NMR studies on the hydrothermal stability of the zeolite catalysts for residual oil selective catalytic cracking, Journal of Catalysis, 228 (2004) 234-242.

[110] T. Blasco, A. Corma, J. Martineztriguero, Hydrothermal stabilization of ZSM-5 catalytic-cracking additives by phosphorus addition, Journal of Catalysis, 237 (2006) 267-277.

[111] G. Zhao, J. Teng, Z. Xie, W. Jin, W. Yang, Q. Chen, Y. Tang, Effect of phosphorus on HZSM-5 catalyst for C4-olefin cracking reactions to produce propylene, Journal of Catalysis, 248 (2007) 29-37.

[112] D. Liu, W.C. Choi, C.W. Lee, N.Y. Kang, Y.J. Lee, C.-H. Shin, Y.K. Park, Steaming and washing effect of P/HZSM-5 in catalytic cracking of naphtha, Catalysis Today, 164 (2011) 154-157.

[113] H.E. van der Bij, L.R. Aramburo, B. Arstad, J.J. Dynes, J. Wang, B.M. Weckhuysen, Phosphatation of Zeolite H-ZSM-5: A Combined Microscopy and Spectroscopy Study, ChemPhysChem, 15 (2014) 283-292.

[114] J.A. Lercher, G. Rumplmayr, Controlled decrease of acid strength by orthophosphoric acid on ZSM5, Applied Catalysis, 25 (1986) 215-222.

[115] W.W. Kaeding, S.A. Butter, Production of chemicals from methanol: I. Low molecular weight olefins, Journal of Catalysis, 61 (1980) 155-164.

[116] M. Göhlich, W. Reschetilowski, S. Paasch, Spectroscopic study of phosphorus modified H-ZSM-5, Microporous and Mesoporous Materials, 142 (2011) 178-183.

[117] N. Xue, X. Chen, L. Nie, X. Guo, W. Ding, Y. Chen, M. Gu, Z. Xie, Understanding the enhancement of catalytic performance for olefin cracking: Hydrothermally stable acids in P/HZSM-5, Journal of Catalysis, 248 (2007) 20-28.

[118] G. Seo, R. Ryoo, 31P, 27Al, and 129Xe NMR study of phosphorus-impregnated HZSM-5 zeolite catalysts, Journal of Catalysis, 124 (1990) 224-230.

[119] K. Damodaran, J.W. Wiench, S.M. Cabral de Menezes, Y.L. Lam, J. Trebosc, J.P. Amoureux, M. Pruski, Modification of H-ZSM-5 zeolites with phosphorus. 2. Interaction between phosphorus and aluminum studied by solid-state NMR spectroscopy, Microporous and Mesoporous Materials, 95 (2006) 296-305

# 2. The objective of this thesis

The methanol to olefins (hydrocarbons) reaction is one of the promising routes to obtain light olefins (mainly ethylene and propylene) and other chemical products such as aromatics, gasoline-range hydrocarbons, and branched alkanes, which has attracted more and more attention especially with new technologies development in the production of methanol by syngas from biomass and natural gas transformation. SAPO-34 and ZSM-5 are the two mainly applied catalysts in these methanol conversion reactions. How to improve the selectivity to products and the lifetime of the catalysts is still a hot topic in this research area. The objective of this thesis is to prepare new micro and mesoporous materials for methanol to olefins, which could improve lifetime, hydrothermal stability of the catalyst and control the selectivities to different products.

Chapter 3. The short lifetime of SAPO-34 after deactivation by coke is a drawback comparing the much longer lifetime of ZSM-5. In this chapter we will study how to extend lifetime of SAPO-34 by synthesizing nanocrystals by means of microwaves. The catalytic performance and stability of nanoSAPO-34 will be compared with other samples of SAPO-34 synthesized by conventional hydrothermal methods using a mixture of morpholine and TEAOH as structure directing agents. In addition, we will show how the selective hydrolysis of nanoSAPO-34 changes the distribution of silicon species after exposure of to moisture, and its effect on the activity, selectivity and deactivation behavior of nano-SAPO-34. We will discuss whether the selectivity of the MTO reaction on SAPO-34 is affected by product or transition-state selectivity and clearly separate the effects of crystal size, silicon distribution, hydrocarbon pool and equilibrium of olefins in the overall selectivity.

Chapter 4. Our objective has been to stabilize nano and standard SAPO-34 against hydrolysis in the presence of moisture at room conditions. We will show how by an appropriate steaming temperature, nano SAPO-34 becomes stabilized towards moisture. In addition, we will show that hydrothermal stability tests for SAPO-34, which are normally performed at very high temperatures (800°C) should also include stability tests at reaction temperatures close to the reaction temperature used for MTO (400°C), to better ascertain the viability of hierarchical SAPO-34 catalysts for the mentioned catalytic process.

Chapter 5. Nano-SSZ-13 will be tried to obtain by a one-pot method synthesis procedure with the addition of surfactant to the synthesis precursor solution. We will

characterize the obtained materials and compare with the standard one. We will reveal the catalytic performance in methanol to olefins of obtained materials, and illustrate the reason for the performance.

Chapter 6. In the chapter the objective is to investigate the effect of different desilication methods on the high silica ZSM-5 (40 and 140) samples and catalytic behavior in the reaction of methanol to olefins. The treatments will be carried out in NaOH or NaOH/TPAOH solutions respectively. In addition, the use of TPAOH mix NaOH solution will be used to treat the ZSM-5 samples and the mesopore size and their interconnection to the micropores will be compared with the mesoporosity obtained with the samples desilicated in NaOH alone.

In the final Chapter 7, we will study the hydrothermal stability of mesoporous ZSM-5 obtained by desilication and its performance in the reaction of methanol to olefins. Different amounts of phosphorus will be introduced to the high Si/Al ratio (140) ZSM-5. It will be shown that how the desilicated samples present in hydrothermal stability and the maximum amount of phosphorus that could be introduced to the parent samples. The role of phosphorus on mesoporous ZSM-5 and its influence on activity, selectivity and lifetime will be discussed.

# 3. Methanol to olefins: activity and stability of nanosized SAPO-34 molecular sieve and control of selectivity by silicon distribution

# 3.1. Introduction

The development of shale gas has decreased the price of natural gas and has renewed the interest in transforming methane into alcohols and olefins that can be used for the production of clean fuels and chemicals [1]. Alcohols can be converted to gasoline range hydrocarbons or short olefins depending mainly on the nature of the catalyst used and, among the short olefins, propylene has shown a growing demand in the past years mainly for the polypropylene industry. Catalyst based on zeolites ZSM-5 and the silicoaluminophosphate molecular sieve SAPO-34 are being industrially used for the conversion of methanol into olefins and more specifically into propylene and ethylene [2].

While the selectivity of SAPO-34 when reacting methanol can be tuned to increase propylene by changing catalyst composition and process variables, extending lifetime as much as possible has still to be improved since it will greatly increase the profitability of the process. Following this, effort has been done in the case of ZSM-5 to decrease the rate of deactivation and its lifetime has been extended by increasing mesoporosity while preserving the micropore of the zeolites. This has been achieved by several procedures such as desilication[3-5], nanosheets of ZSM-5[6] or by co-templating with carbon black or other organics [7,8]. Some methods have been shown more efficient than others since besides active site accessibility and enhanced diffusion of product, the formation of internal defects should be minimized. In summary it was shown that when diffusion of reactants and products is facilitated by generating mesopores, coking is slowed down and lifetime increases. A similar result was obtained when small crystallites or nanosized particles of ZSM-5 have been used [9, 10].

When similar methods for developing mesoporosity have been translated to SAPO-34 and other 8MR zeolites, the expected increase in lifetime was not always attained. Sommer et al, could not improve the lifetime of SSZ-13(CHA) by basic treatments [11]. On the contrary, the addition of co-templates like silanes or surfactants did obtain an increase in mesoporosity and lifetime for SSZ-13 [12, 13] and recently the addition of carbon nanotubes to the synthesis gel also succeeded [14]. An increase in rate of diffusion can be achieved by preparing CHA type materials with smaller crystalline size. For doing that, a dry gel synthesis method

[15], the use of a combination of different SDA [16-19], as well as the use of microwaves [20,21] has been applied to the synthesis of SAPO-34 with the objective of enhancing lifetime of the catalyst for the reaction of methanol to olefins It has been found that a combination of TEAOH and morpholine in the synthesis results in a decrease of the size of the crystals with the corresponding increase in lifetime[17]. Wang [18] also studied the combination of TEA and TEAOH with an improvement in lifetime, and very recently Alvaro-Muñoz et al.[19] compared different SDA and remarked the importance that high external surface, smaller crystal size and high acidity have for the lifetime of SAPO-34. Hirota et al. [15] obtained nanocrystals of SAPO-34 of around 75nm by a dry gel synthesis method extending lifetime in the reaction of methanol. Yang et al. [22] also demonstrated nanosize-enhanced lifetime of SAPO-34 in MTO reactions by investigating the SAPO-34's with different crystallite sizes varying from 80 nm to 8 $\mu$m synthesized from the gel with the same composition using TEAOH as SDA.

Since it is clear the benefit of a higher external surface on the lifetime of SAPO-34 for the MTO reaction that can be easily achieved by synthesizing nanosized SAPO-34 samples for which the contribution of the external to the total surface is very important. In this work we have synthesized nanosized samples of SAPO-34 following the microwave method reported by Lin et al.[20] and have studied the activity, lifetime and selectivity in the reaction of methanol to olefins. The catalytic performance and stability of nanoSAPO-34 has been compared with other samples of SAPO-34 synthesized by conventional hydrothermal methods using a mixture of morpholine and TEAOH as structure directing agents, which has been reported to also give small crystal size[17]. We have observed that the selective hydrolysis changes the distribution of silicon species after continuous exposure of calcined SAPO-34 samples to moisture, and it affects the activity, selectivity and deactivation behavior of nanosized and conventional samples. We will discuss whether the selectivity of the MTO reaction is affected by product or transition-state selectivity and we will clearly separate the effects of crystal size, silicon distribution, hydrocarbon pool and equilibrium of olefins in the overall selectivity.

# 3.2.Experimental

## 3.2.1.Synthesis of materials

SAPO-34 was synthesized by microwave heating as reported by Lin et al.[20]. The composition of the synthesis gel was 1 $Al(OPri)_3$ : 2 $H_3PO_4$ : 0.3 $SiO_2$ : 2 TEAOH: 30 $H_2O$. Aluminum isopropoxide $Al(OPri)_3$ was firstly mixed with TEAOH solution (35 wt%, Aldrich) and deionized water at room temperature until it was dissolved completely. Tetraethylorthosilicate was then added as the silica source and stirred for 2h. Finally, phosphoric acid (85 wt% in water, Aldrich) was dispersed slowly into the above solution. The reaction mixture was further stirred for 1h and then transferred into a Teflon autoclave. The crystallization was conducted in a microwave oven (Milestone ETHOS-D) with a moving 100mL Teflon-lined autoclave and was heated from room temperature to 180°C in 2 minutes with pre-programmed heating profiles and kept at 180°C for 1h. The product was separated by high speed centrifugation, washed thoroughly with deionized water and ethanol, and then dried overnight at 50°C. The as-synthesized crystals were calcined at 550°C in air for 6h to remove the template molecules. This sample will be called nano-SAPO-34. For comparison purposes, a second sample of SAPO-34 was synthesized following a hydrothermal method, with a mixture of morpholine and TEAOH 1:1 mol/mol as SDA with a gel composition of 1 $Al_2O_3$ : 2.12 $H_3PO_4$ : 1.08 $SiO_2$ : 2.09SDA : 66 $H_2O$. First, distilled water was mixed with phosphoric acid and then pseudoboehmite (Merck 85%) was added slowly, while stirring, and it was further stirred for 7 hours. This resultant solution is named solution A. Fumed silica (Degussa Aerosil-200 99% $SiO_2$) and morpholine (Aldrich 99% $C_4H_9O$) were mixed thoroughly with water, and formed solution B. Solution B was added dropwise to solution A while stirring and then maintained for 7 hours. The resultant product was introduced into a 150 mL Teflon-lined autoclave and heated at 200°C under autogenous pressure for 24 hours. This sample will be called standard-SAPO-34.

## 3.2.2. Characterization

The crystallinity of the samples was followed by X-ray powder diffraction (XRD) with a Panalytical CUBIX diffract meter with monochromatic CuKα1,2 radiation (λ=1.5406, 1.5444 Å; Kα2 / Kα1 intensity ratio=0.5). The morphology and particle size of the zeolite were characterized by Scanning Electron Microscope (SEM, JEOL JSM-6300) and Transmission Electron Microscopy. The MAS NMR spectra were recorded with a Bruker AV400 spectrometer. $^{29}$Si MAS NMR spectra were at 79.459 MHz with a 60⁰ pulse length of 4µs and 60s repetition time, spinning the sample at 5kHz. Deconvolution of $^{29}$Si NMR bands corresponding to different Si environments was performed with Origin Pro 9.0 software with Gaussian shapes of constant width. $^{27}$Al MAS NMR spectra were recorded at 104.218 MHz with a spinning rate of 10 kHz at a 90⁰ pulse length of 0.5 µs with 1 s repetition time. $^{31}$P MAS NMR spectra were recorded at 161.9 MHz with a spinning rate of 10 kHz and at a 90⁰ pulse length of 5 µs with 20s repetition time. $^{29}$Si, $^{27}$Al and $^{31}$P chemical shifts are reported relative to tetramethylsilane, Al(H$_2$O)$_6$, and H$_3$PO$_4$ respectively. Elemental composition was determined by inductively coupled plasma atomic absorption spectroscopy (ICP-OES) using a Varian 715-ES. The BET surface area, micropore volume and pore volume distribution were measured by N$_2$ adsorption and desorption in a Micromeritics ASAP2000. Low-temperature infrared spectroscopic (FTIR) experiments were performed in a Bio-Rad FTS-40A spectrometer using, respectively, a homemade stainless steel cell and a quartz cell fitted with KRS-5 windows, both connected to a vacuum dosing system. Before each experiment, the catalysts were pressed into self-supported wafers (5–10 mg/cm$^2$) degassed under vacuum (ca. 10−5 mbar) at 673 K and then cooled down to RT under vacuum. For low-temperature CO adsorption experiments, the samples were cooled to 77 K followed by CO dosing at increasing pressure (0.4–8.5 mbar) and recording the IR spectrum after each dosage. After CO dosing, the samples were evacuated and the spectra collected. NH$_3$-TPD experiments were carried out in a Micromeritics 2900 apparatus. A calcined sample (100 mg) was activated by heating to 400°C for 2 h in an oxygen flow and for 2 h in argon flow. Subsequently, the samples were cooled to 176°C, and NH$_3$ was adsorbed. The NH$_3$ desorption was monitored with a quadrupole mass spectrometer (Balzers, Thermo Star GSD 300T) while the temperature of the sample

was ramped at 10°C min$^{-1}$ in helium flow. Total ammonia adsorption was measured by repeated injection of calibrated amounts of ammonia at 176°C until saturation. Ammonia desorption was recorded by means of the mass 15, since this mass is less affected by the water desorbed.

## 3.2.3. Catalytic experiments

The catalyst was pelletized, crushed and sieved into 0.2-0.4 mm particle size. 50mg of sample were mixed with 2 g quartz (Fluka) before being introduced into the fix-bed reactor (the diameter is about 7mm)(Scheme 3.1). Flowing of $N_2$ (19mL/min) was bubbled in methanol at 25°C, giving a WHSV=7 h$^{-1}$. The catalyst was first activated with a nitrogen flow of 80 mL/min for 1 h at 540°C, and then the temperature was decreased to reaction conditions (400°C). Each experiment was analyzed every 5 minutes with an online gas chromatograph (BRUKER 450GC, with PONA and $Al_2O_3$-Plot capillary columns, and two FID detectors). After reaction, the catalyst was regenerated at 540°C in 80ml of air for 3h and the reaction was repeated again. Preliminary experiments were carried out at constant WHSV, different amount of catalyst and increasing flow rates, and later with catalyst with in different particle sizes, to check that, at the selected reaction conditions the process is not controlled by either external or intraparticle diffusion. Conversion and selectivities were considered in carbon basis and methanol and dimethylether were lumped together for calculation of conversion.
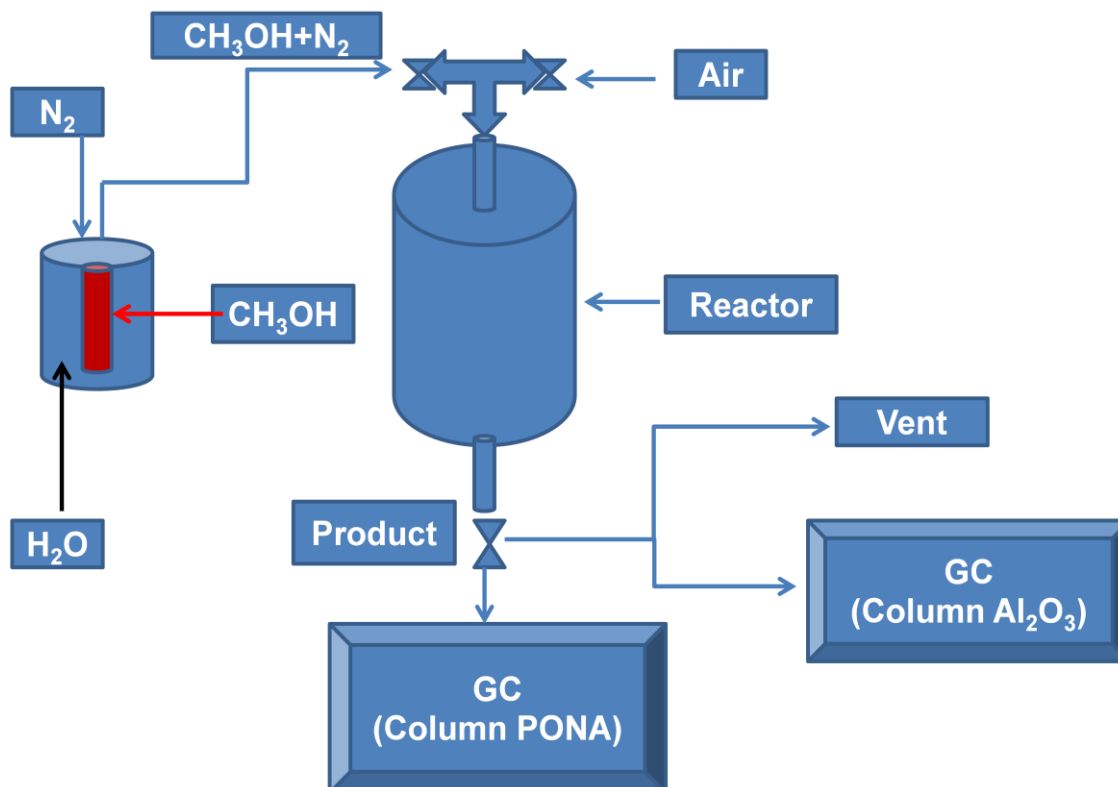
Scheme 3.1 The scheme of methanol to olefins reactions.

Table 3.1 The conditions of Gas Chromatographs in the product of methanol to olefins reaction.

|  | GC (Column PONA) | GC (Column $Al_2O_3$) |
|---|---|---|
| Oven | 35 °C | 60 °C |
| Rate of heating | 0°C | 20 °C /min |
| Final temperature | 35 °C | 220°C |
| Detector | 250°C | 250°C |

# 3.3.Results and discussion

## 3.3.1.Catalyst characterization
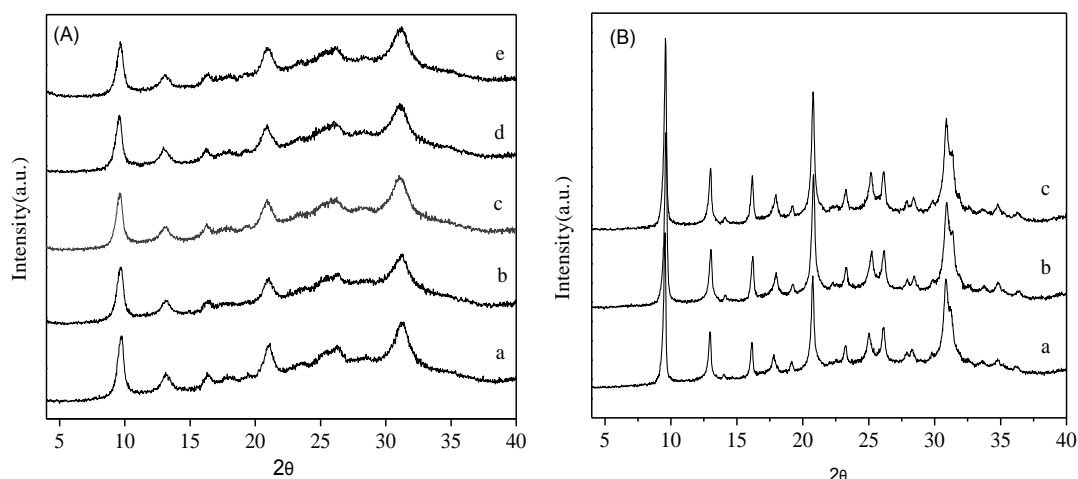


Fig 3.1 XRD patterns of calcined nano-SAPO-34 (A) after exposure to moisture for a) 1 day, b) 7 days, c) 14days, d) 21days, e) 42days; and standard-SAPO-34 (B) for a) 1 day, b) 21 days, c) 42 days.

XRD of nano and standard SAPO-34 samples are shown in Fig 3.1 after exposure to room conditions for 1 to 42 days, being therefore in contact with air with 40-60% moisture. The nano-SAPO-34 sample presents as expected, a diffraction pattern with very low resolution due to the small size of the crystals and there is no indication of any decrease in intensity after exposition at room conditions during the period of exposure. The standard-SAPO-34 shows a diffraction pattern more intense and also there is no modification after the same period of exposure to moisture. ICP analysis of calcined samples determined a bulk molar composition of Al:Si:P=1:0.31:0.73 and 1:0.91:0.66 for nano-SAPO-34 and standard-SAPO-34 respectively.
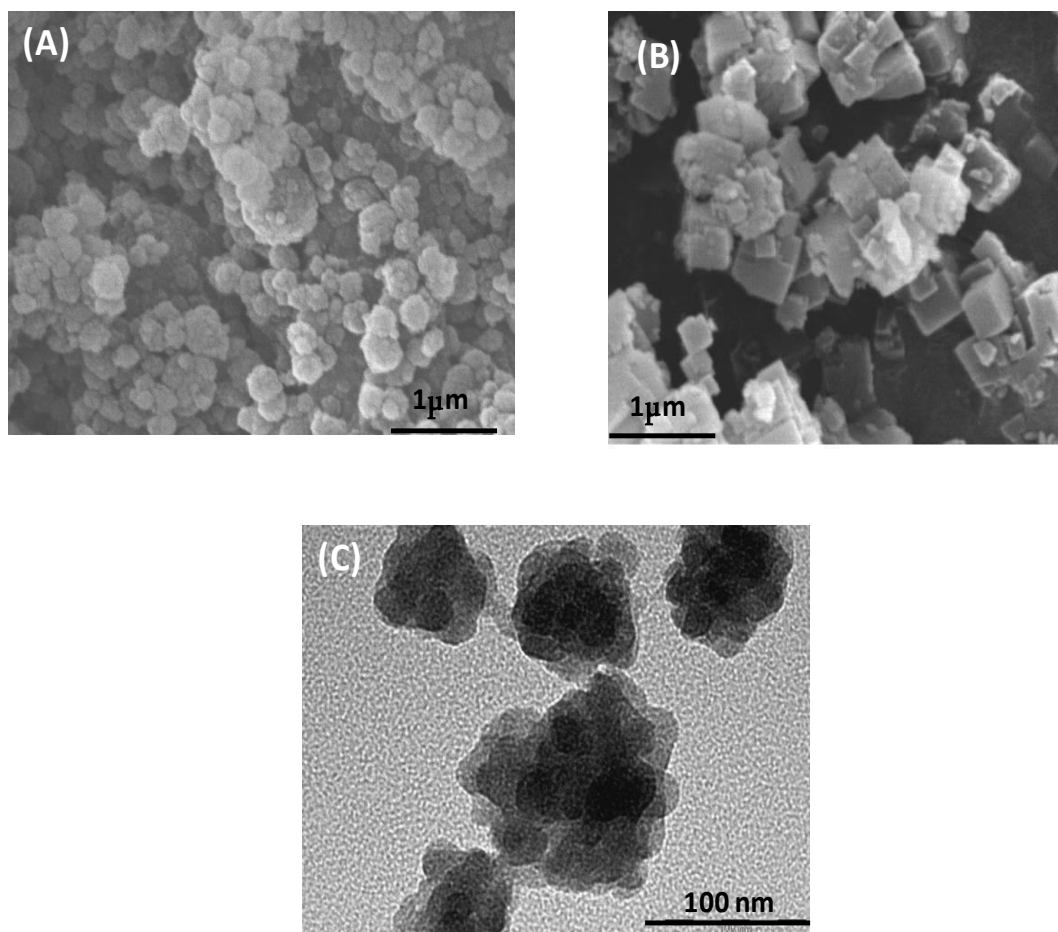
Fig 3.2 SEM pictures of (A) nano-SAPO-34, (B) standard-SAPO-34, and (C) TEM of nano-SAPO-34.

Fig 3.2 shows the SEM and TEM images of nano-SAPO-34 prepared by microwave heating and the standard-SAPO-34. The nano-SAPO-34 sample shows spherical aggregates of 150-300 nm formed by smaller crystals of around 20-50 nm, while standard SAPO-34 presents cubic crystals of ~ 300-600 nm. The smaller dimensions of the crystals of nanoSAPO-34 are consistent with the broad XRD peaks shown in Figure 1, and the size of standard-SAPO-34 is in agreement with the examples reported by Lee et al[17], in which SAPO-34 synthesized with the same mixture 1:1 of morpholine and TEAOH also presented crystal size in sub-micrometer range.

Table 3.2 Textural properties of nano and standard-SAPO-34 samples after days of exposure to moisture.

| Sample | BET (m$^2$/g) | t-plot S$_{ext}$ ( m$^2$/g) | V$_{micro}$ (cm$^3$/g) | V$_{meso}$ (cm$^3$/g) |
|---|---|---|---|---|
| Nano-SAPO-34-1day | 646 | 231 | 0.20 | 0.21 |
| Nano-SAPO-34-7days | 639 | 226 | 0.20 | 0.21 |
| Nano-SAPO-34-14days | 616 | 224 | 0.19 | 0.20 |
| Nano-SAPO-34-28days | 613 | 224 | 0.19 | 0.20 |
| Nano-SAPO-34-42days | 561 | 223 | 0.18 | 0.20 |
| Nano-SAPO-34-107days | 536 | 223 | 0.15 | 0.20 |
| Standard-SAPO-34-5days | 460 | 63 | 0.19 | 0.11 |
| Standard-SAPO-34-29days | 463 | 62 | 0.19 | 0.11 |
| Standard SAPO-34-44days | 463 | 64 | 0.19 | 0.11 |

The textural properties measured by adsorption of nitrogen of the two SAPO-34 samples are shown in Table 3.2. Nano-SAPO-34 shows very high external surface 231 m$^2$/g area as a consequence of the small size of the crystals. In fact the adsorption-desorption isotherm for nano-SAPO-34 (Fig 3.3) shows a strong increase in adsorption with hysteresis at high relative pressures due to the intercrystalline porosity typical of nanocrystalline materials. After contact with ambient moisture for up to 107 days, the micropore volume steadily decreases while external surface area seems not to be affected Fig 3.4). On the contrary, standard-SAPO-34 presents a lower external and BET surface area which does not seem to be affected after 2 months of exposure to moisture (Fig 3.4 b).
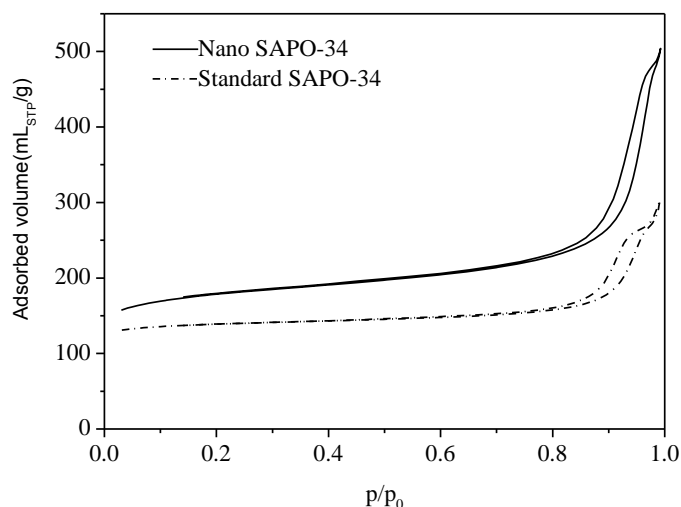


Fig 3.3 N$_2$ adsorption-desorption isotherms of nano and standard-SAPO-34.
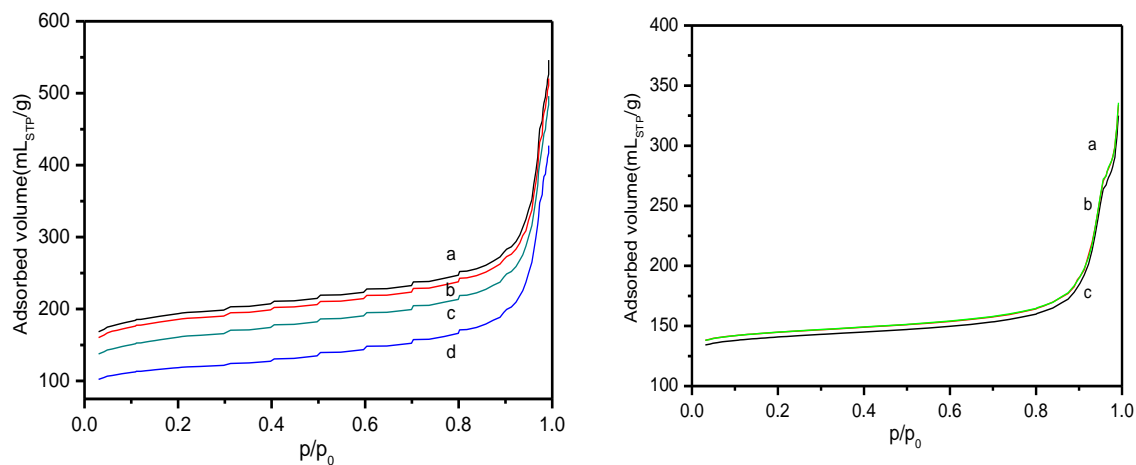
Fig 3.4 Nitrogen desorption isotherms of nano-SAPO-34 after a) 7, b) 28, c) 42 and d) 107 days of exposition to moisture. Fig 3.4 b. Nitrogen desorption isotherms of standard-SAPO-34 after a) 5, b) 29 and c) 44 days of exposition to moisture.
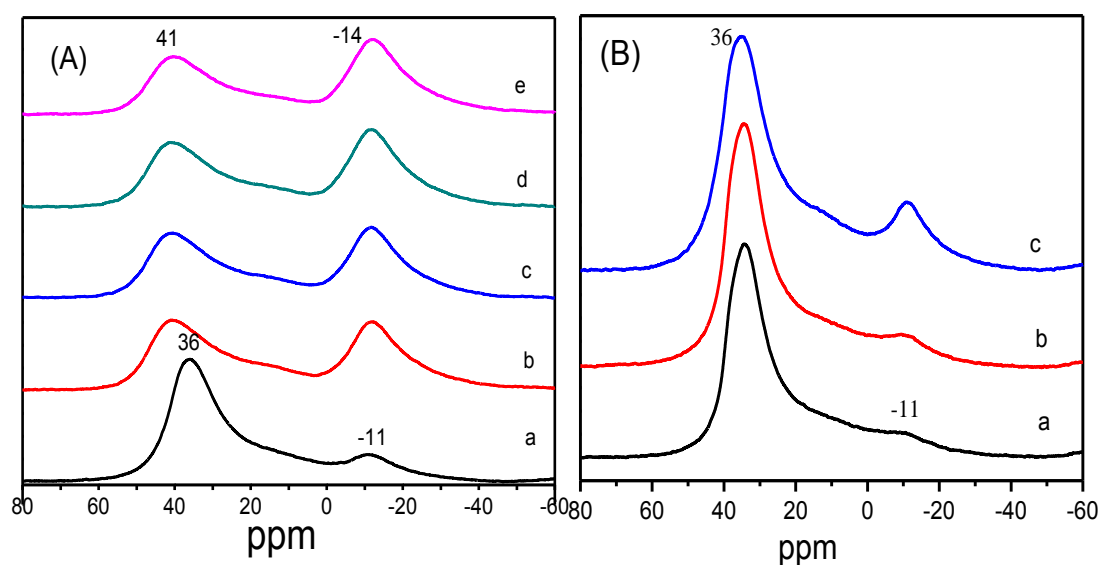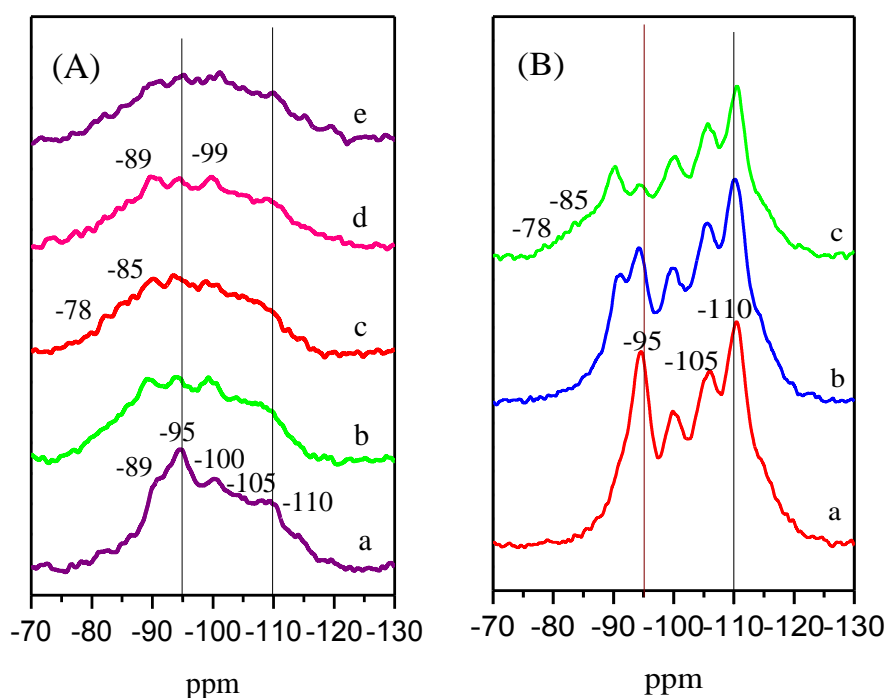


Fig 3.5 $^{27}$Al MAS NMR after exposure to moisture of (A) nano-SAPO-34 a) 1 day, b) 7 days, c) 14 days, d) 21 days e) 42days,  (B) standard-SAPO-34 a) 21 day  b) 32 days c) 40 days.

The coordination of Al, P and Si atoms in SAPO-34 was studied by $^{27}$Al, $^{31}$P and $^{28}$Si MAS NMR. The $^{27}$Al MAS NMR spectra are given in Fig 3.5. Calcined nano-SAPO-34 shows an intense peak at 36 ppm followed by other signals at -11 and 14 ppm, that corresponds to tetrahedrally coordinated aluminum in local structures of $Al(PO)_4$, and octa and pentacoordinated aluminum, respectively[23]. After 7 days of storage, the signal at 14ppm continuously increased indicating hydration of $Al(PO)_4$

species[23,24], while the signal of tetracoordinate aluminum is shifted to 41 ppm. The shifting of the tetrahedral signal could be attributed to a distortion of the framework due to the hydration of the structure [25]. The standard-SAPO-34 sample shows the same signals, with a lower intensity of octahedral aluminum, possibly due to a lower effect of hydration that is accompanied with a lower shifting of the tetrahedral signal at 36ppm. When both hydrated samples were dehydrated in vacuum at 200ºC, the initial $^{27}$Al MAS NMR spectra was recovered only for standard SAPO-34, indicating the irreversibility of the hydration process of nano-SAPO-34.
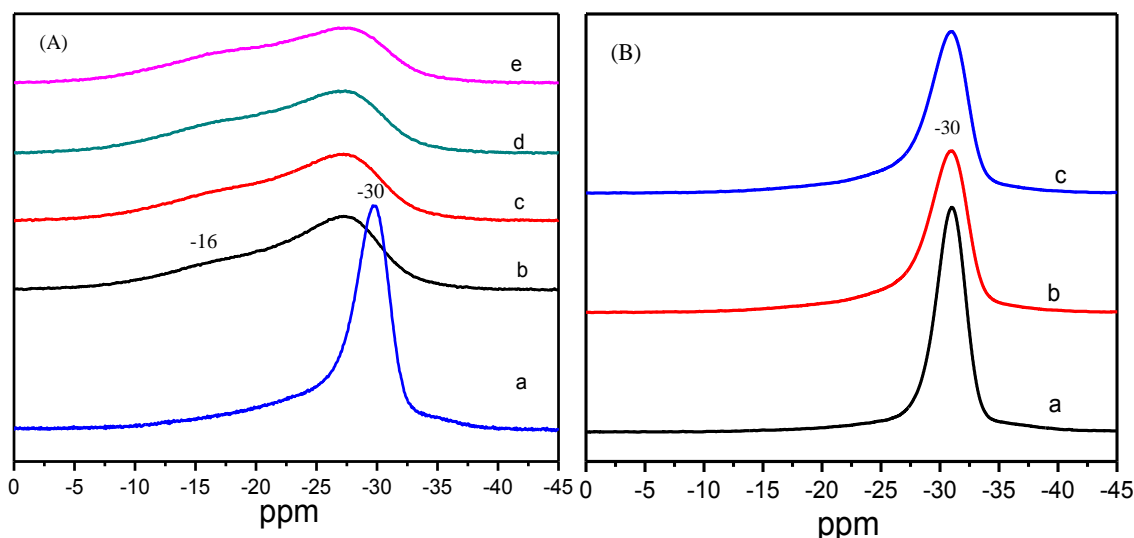


Fig 3.6 $^{29}$Si MAS NMR after exposure to moisture of (A) nano-SAPO-34 a) 1 day, b) 7 days, c) 14 days, d) 21 days e) 42days,  (B) standard-SAPO-34 a) 21 day  b) 32 days c) 40 days.

Table 3.3 Distribution of silicon species by deconvolution of different $^{29}$Si MAS NMR signal of samples of Standard and nano-SAPO-34 after exposure to moisture.

| Sample | Silicon species | 1 day | 7 days | 14 days | 21 days | 42 days |
|---|---|---|---|---|---|---|
| Standard SAPO-34 | Defects | 1 | | | 3 | 5 |
| Nano SAPO-34 | Defects | 7.4 | 16.4 | 19.6 | 16.7 | 15.6 |
| | Si4Al | 16.6 | 17.5 | 16.6 | 17.5 | 15.6 |
| | Si3Al1Si | 23.6 | 18.3 | 17.8 | 16.6 | 17.7 |
| | Si2Al2Si | 18.2 | 18.3 | 16.9 | 17.8 | 18.4 |
| | Si1Al3Si | 13.9 | 12.8 | 13.3 | 13.5 | 13.8 |
| | Si4Si | 20.3 | 16.5 | 15.6 | 17.6 | 18.7 |

The ^{29}Si MAS NMR spectra of nano and standard-SAPO-34 is shown in Fig 3.6. This technique is useful to study the mechanism of silicon incorporation in the framework of AlPO$_4$. In silicoaluminophosphates, silicon is incorporated following two different mechanisms, SM2 in which a single Si substitutes a single P atom, or SM3 in which two Si atoms substitute two neighbours Al and P atoms[26,27]. Nano-SAPO-34 shows a broad signal formed by components at -89, -95, -100, -105 and -110 ppm, that correspond to Si(4Al), Si(3Al), Si(2Al), Si(1Al) and Si(0Al) respectively[25,27-29]. The incorporation of silicon through SM2 generates Si4Al groups while mechanism SM3 generates the others. It appears then that in the nano-SAPO-34 sample there is an important contribution of the SM3 substitution mechanism. By performing the deconvolution of the different silicon signals (Table 3.3) it can be observed that after 7 days of hydration, the signal at -95 ppm corresponding to Si(3Al) and also the signal at -110 (Si0Al) decrease while a broad small band around -78 to -85 appears. This broad band has been assigned to $Q^1$ , $Q^2$ , and $Q^3$ Si species (Si(OT)$_n$)OH)$_{4-n}$) due to hydration at room temperature and breaking of Si-OH-Al bonds[30], disordered Si(4Al)[23] or partially hydrated Si species located at the edge of a Si domain[31]. We have seen that the intensity of this band is enhanced by H cross-polarization[30,31], suggesting that it corresponds to Si3AlOH or defect Si sites. Therefore, it appears that Si(3Al) species are first affected by hydrolysis creating groups Si(OAl)$_{(3-x)}$(SiOH)$_x$. It is important to note that silicon species incorporated by SM3 mechanism are first affected by hydrolysis, because their associated Brönsted acid sites are stronger than those generated by single Si incorporation (SM2). In fact, recently Katada et al. [32] studied different SAPO-34 and determined that samples with less isolated Si presented weaker Brönsted acidity and attributed the stronger acidity to the presence of distorted structure including SiO2 islands or defects. Other authors[28,33,34], assign the higher acidity of some SAPOs to the presence of silicon islands in which acid sites are generated at the borders, and correspond to (Si3Si1Al), which would be the strongest acid sites. Consequently, in our case for nano-SAPO-34 the silicon species first affected by hydrolysis are those that generate stronger acid sites and then, the overall acidity should be decreased by hydrolysis and the acid strength will be shifted to milder acidities. The standard-SAPO-34 sample shows sharper signals of [29]Si

MAS NMR at the same positions that nano-SAPO-34, with higher intensity of the signals at -105 and -110 corresponding to Si(1Al) and Si(0Al) due to its higher silicon content. However, the changes after several days of hydration are slower. After 32 days of hydration the signal at -95 ppm corresponding to Si(3Al) starts to decrease, and only after 40 days, the signal of defects from the signals at -78 to -85 ppm are visible. Again, the standard-SAPO-34 is shown less sensitive to hydrolysis than nano-SAPO-34.



Fig 3.7 $^{31}$P MAS NMR after exposure to moisture of (A) nano-SAPO-34 a) 1 day, b) 7 days, c) 14 days, d) 21 days e) 42days, (B) standard-SAPO-34 a) 21 day  b) 32 days c) 40 days.

The $^{31}$P NMR spectra (Fig 3.7) for fresh nano-SAPO-34 shows an asymmetrical signal at -30 ppm corresponding to tetrahedral P(OAl)$_4$. After 7 days of hydration another signal at -16 ppm appears corresponding to P atoms coordinated with water molecules in form of species P(OAl)x(H2O)y[23,35,36]. The relative intensity of the signal at -16ppm increased continuously even up to 42 days of hydration and correlates well with the increase in the octahedral signal of $^{27}$Al NMR at -12ppm which was assigned to the hydration of the Al(PO)$_4$ species. In the case of the standard SAPO-34 sample, the only signal that appears is the one corresponding to tetrahedral phosphorus at -30 ppm up to 40 days of hydration.
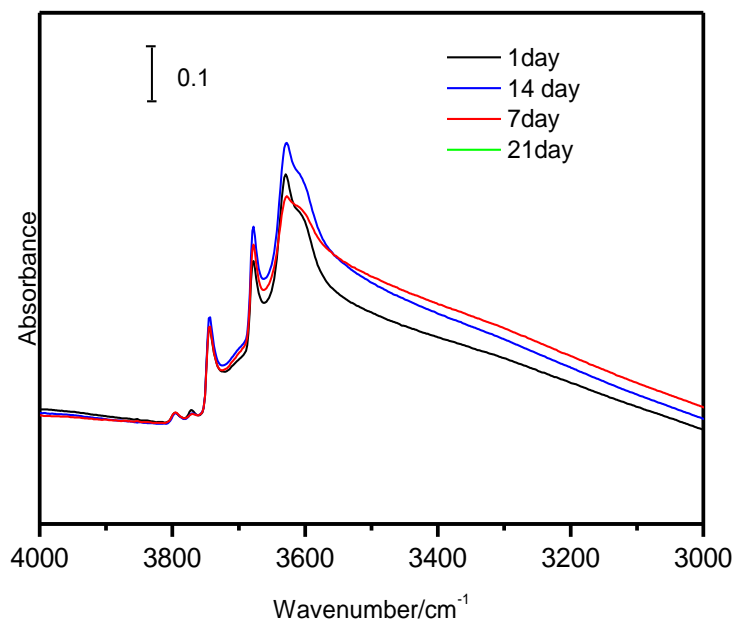
Fig 3.8  FTIR in the OH range of nano-SAPO-34 after exposure to moisture.
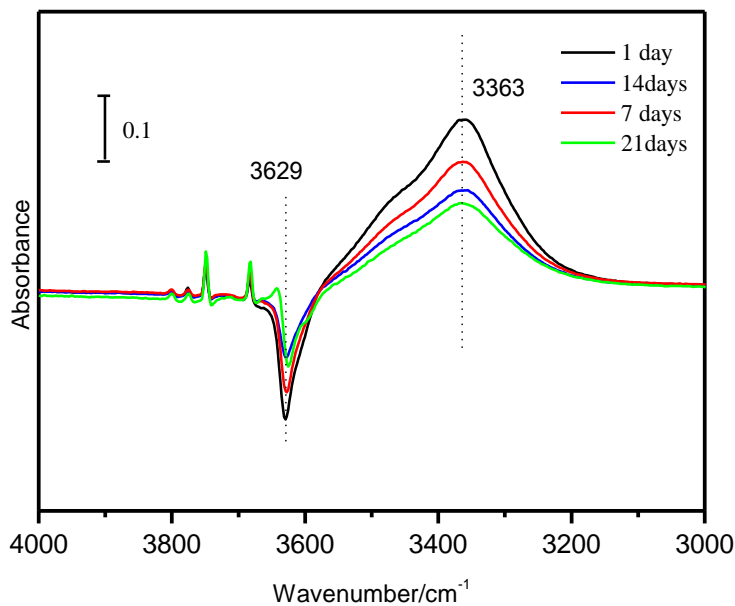


Fig 3.9 FTIR in the OH stretching range of fresh nano-SAPO-34 after adsorption of 8.5 mb of CO. Spectra subtracted from the parent sample free of CO.

The FTIR spectrum of nanoSAPO-34 in the hydroxyl region is shown in Fig 3.8 . The sample nano-SAPO-34 shows characteristic signals at 3600 and 3630 cm$^{-1}$ assigned to low and high-frequency Brönsted OH groups, 3745 and 3678 cm$^{-1}$ which

correspond to external Si-OH and P-OH groups respectively. Two more signals are visible at 3796 and 3770 cm^{-1} which are assigned to OH groups linked to tetrahedral Al[37,38]. The relatively high intensity of these latter two bands must be assigned to the high external surface of the sample. In addition, there is a broad band centered around 3400-3500 cm^{-1} which probably corresponds to Si-OH and P-OH groups in different interacting through H-bonds, as reported for high silica CHA zeolites [39] and mesoporous AlPO [40]. After several days of hydration this broad band increases in intensity indicating that defects are being formed. In addition, the band at 3678 cm-1 corresponding to P-OH groups also increases due to the irreversible hydrolysis of some Al-O-P bonds.

The adsorption of CO at low temperatures has been used to characterize the strength of the acid sites of SAPO-34. In the case of nano-SAPO-34 (Fig 3.9 ), the bands corresponding to HF and LF Brönsted acid sites are shifted after adsorption and interaction of bridging hydroxyl groups with CO to a broad band around 3200-3500 cm^{-1} which is in agreement with that reported in the literature[28,41]. The broad band around 3200-3500 cm^{-1} is composed of a main signal at 3364 cm-1 and a shoulder at 3474 cm^{-1}. These signals have been assigned to CO interacting with HF and LF hydroxyls and, in agreement with the work of Martins et al [28]. By deconvolution of the broad IR band, other band at at 3280 cm^{-1} is required. Due to its larger shift and according to ref. data [28], this band at 3280 cm^{-1} has been assigned to CO interacting with acid sites corresponding to Si in the borders of the silicon islands, and which have a stronger acidity. As shown above in the analysis of Si-NMR spectra, after days of hydration of nano-SAPO-34 it was expected to see a decrease of those sites of higher strength as shown by CO adsorption if they are related to Si(3Si1Al). However, the fitting process for deconvolution of the overlapped bands showed a contribution of the 3280cm^{-1} band of around 10% of the overall area of the broad band, being almost impossible to distinguish if there is a decrease in the concentration of these sites due to hydrolysis and transformation in defects. In the CO stretching vibration region a band at 2171 cm^{-1} appears after CO adsorption (Fig 3.10 ), corresponding to CO interacting with Brönsted acid sites [42]. The position of this band is the same for the different nano-SAPO-34 hydrated samples. Therefore, by adsorption of CO we could not found any evidence of different acid strength of the nano-SAPO-34 samples after hydration.
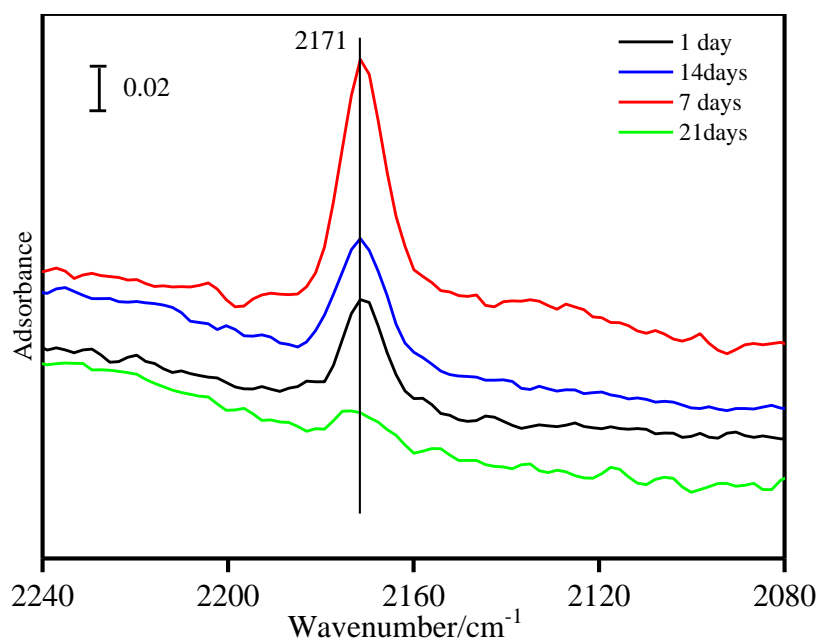
Fig 3.10 FTIR in the CO stretching range after adsorption of 0.4 mb of CO on nano-SAPO-34 samples exposed to moisture for 1, 7, 14 and 21 days. Spectra subtracted from the parent sample free of CO.

In summary from the characterization results, it has been shown that nano-SAPO-34 presents much lower crystal size and therefore more external surface area than standard-SAPO-34. As a consequence, the structure of nano-SAPO-34 has been shown very sensitive to moisture, with a change in the distribution of silicon species, in which at short range of time, a clear decrease in the $^{29}$Si MAS NMR assigned to Si on the edge of the Si islands indicates a selective hydrolysis of these Si-O-Al bonds. From these results, it is expected that nano-SAPO-34 presents higher lifetime in the reaction of methanol in which selectivity to products should depend on the different distribution of silicon species.

## 3.3.2. **Catalytic experiments**

### 3.3.2.1. Activity and kinetic analysis
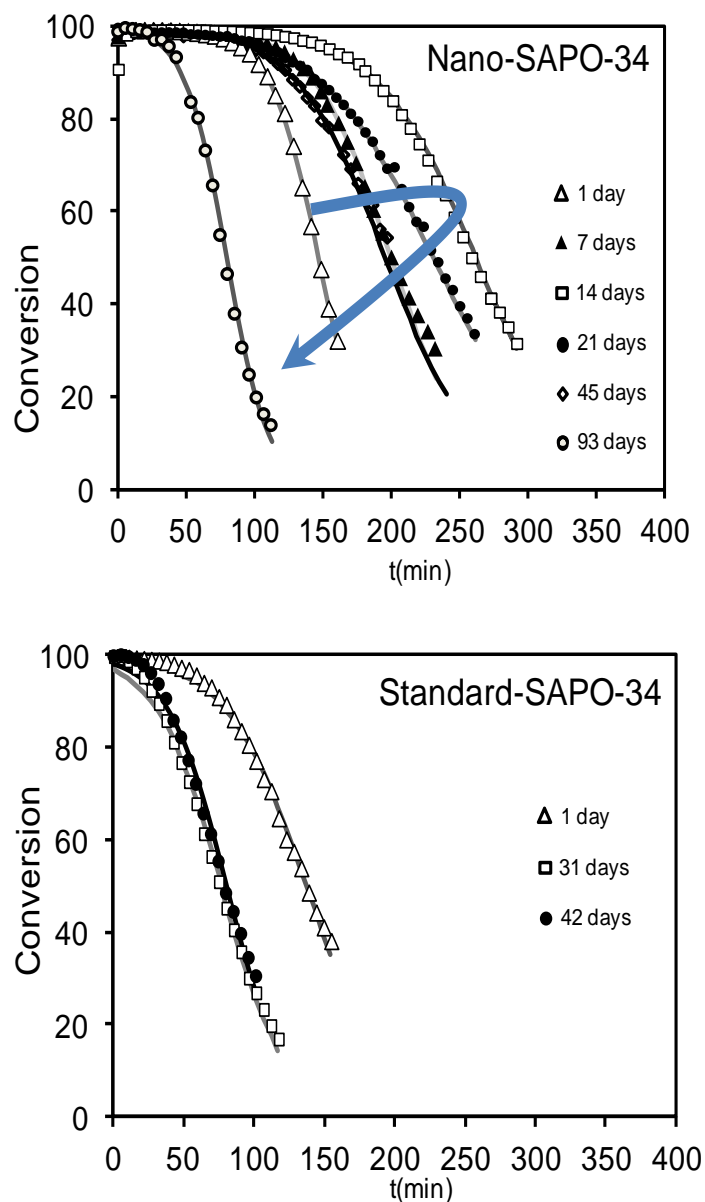


Fig 3.11 Conversion of Methanol at 400ºC and WHSV=7h$^{-1}$ on nano-SAPO-34 and standard-SAPO-34 samples after exposure to moisture. Lines correspond to the fitting following the Jannssens's kinetic model.

The activity of nano and standard SAPO-34 is shown in Fig 3.11 at WHSV=7h$^{-1}$. It is important to note that lifetime of nano-SAPO-34 and standard-SAPO-34 are very similar when the samples are freshly calcined. However, in the case of nano-SAPO-

34, lifetime changes with time of storage and exposure to moisture at room temperature. First, the activity increases up to 14 days of storage and then decreases continuously. Standard-SAPO-34 showed always lower lifetime changes than of nano-SAPO-34, and activity seems to stabilize after 42 days of storage. In order to rationalize the different behavior of activity for the of SAPO-34 samples, we have performed a kinetic analysis following the model proposed by Janssens[43] for the deactivation of ZSM-5 during conversion of methanol to gasoline. Jannsens proposes that conversion of methanol to hydrocarbons on zeolites can be modeled with a kinetic equation that includes only two parameters, the rate constant and the deactivation coefficient, assuming a first order of reaction and a deactivation rate proportional to the conversion. Also by following this methodology, half lifetime and conversion capacity of methanol, that is the amount of methanol that can be converted before full deactivation, can easily be estimated (Table 3.4). The model proposed by Janssens considers deactivation as an effective decrease of contact time, and agrees with a "non selective deactivation" of the reaction, in which the successive steps from reactants to products are affected by deactivation at the same rate and can be modeled by a single parameter. The model reproduces quite well the oligomerization of olefins, as well as the reaction of methanol to gasoline in ZSM-5[44,45]. However, the reaction of methanol to olefins on SAPO-34 was shown by Chen et al[46,47] to follow a "selective deactivation". In our case, the fitting of the conversion of methanol+dimethylether lumped for both SAPO-34 samples is surprisingly as good as the fitting reported with ZSM-5 suggesting that a "single event kinetics model" can also be used with SAPO-34 as in the case of ZSM-5. In addition, the selectivity at three different spatial times were compared in Fig 3.12, and it was shown that the selectivities are very similar at constant conversion and do not depend on spatial time. So, also in SAPO-34 as it occurs when the catalyst was ZSM-5, deactivation can be considered as "a decrease of contact time", that at the end is equivalent to say a decrease in the amount of active catalyst during time on stream. Then, by fitting the following model in where: X=conversion, tau=spatial time $g_{cat}$ per $mol^{-1}$ $h^{-1}$, a is the deactivation constant, K is the kinetic rate constant, the values of the kinetic rates and deactivation constants are given in Table 3.5
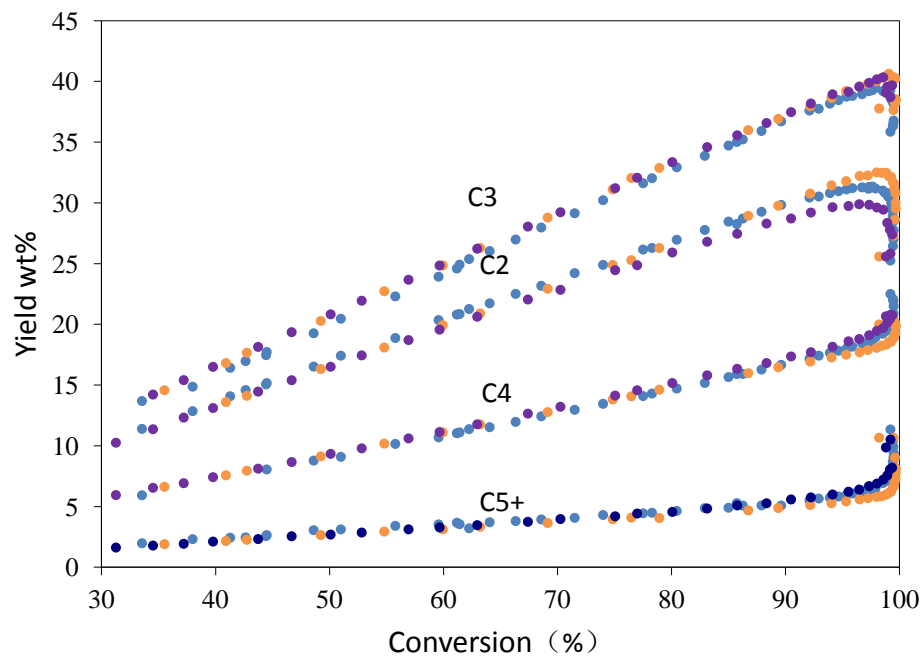
Fig 3.12 Yields to C2, C3, C4 and C5+ hydrocarbons in the conversion of methanol on nano-SAPO-34 (21 days exposed to moisture) at different WHSV (•7, •11, •15 h$^{-1}$) at 400°C.

$$\frac{dX}{dt} = k(1 - X)$$

$$\frac{d\tau}{dt} = -aX$$

$$X = \frac{(\exp(k\tau_0) - 1)\exp(-kat)}{1 + (\exp(k\tau_0) - 1)\exp(-kat)}$$

Table 3.4 Kinetic parameters, half lifetime ($t_{0.5}$), breakthrough time ($t_{0.98}$), and methanol conversion capacity of nano and standard-SAPO-34 samples obtained by fitting of Janssen's kinetic model.

| Sample | Days of exposure to moisture | k (mol/gh) | a (g/mmol) | $t_{0.5}$ (min) | $t_{0.98}$ (min) | Methanol conversion capacity ($g_{metanol}/g_{catalyst}$) |
|---|---|---|---|---|---|---|
| Nano-SAPO-34 | 1 | 9.98 | 5.59 | 146 | 77 | 15.9 |
| | 7 | 8.60 | 4.10 | 200 | 89 | 21.7 |
| | 14 | 8.84 | 3.13 | 262 | 121 | 28.4 |
| | 28 | 6.82 | 3.55 | 231 | 70 | 25.1 |
| | 45 | 7.33 | 4.18 | 196 | 69 | 21.3 |
| | 93 | 6.33 | 10.4 | 79 | 20 | 8.59 |
| Standard-SAPO-34 | 1 | 5.92 | 5.97 | 137 | 27 | 14.9 |
| | 32 | 4.17 | 10.6 | 78 | <0 | 8.4 |
| | 41 | 4.72 | 10.1 | 81 | <0 | 8.8 |

Table 3.5 Initial and steady-state distribution of olefins in the conversion of Methanol to Olefins at 400ºC, WHSV=7h-1 on Standard-SAPO-34 (1day) and Nano-SAPO-34 (14days). Thermodynamic equilibrium of C2-C5 olefins calculated at P=0.04bar of methanol and T=400ºC by minimization of the total Gibbs energy of the system, method of the undetermined Lagrange's multipliers[39]. Free Gibbs standard formation energy of different olefins were taken from Alberty et al.[40].

| | Thermodynamic equilibrium | | Standard-SAPO-34 | | Nano-SAPO-34 | |
|---|---|---|---|---|---|---|
| | Linear olefins | Linear+Branched olefins | Initial olefin distribution | Steady-state | Initial olefin distribution | Steady-state |
| C2 | 17.8 | 15 | 30 | 36.1 | 25 | 31 |
| C3 | 47.8 | 38.3 | 43.3 | 43.3 | 36.2 | 37.2 |
| C4 | 28.2 | 26.8 | 19.5 | 15.5 | 25.1 | 21.1 |
| C5+ | 6.2 | 19.9 | 7.2 | 5.2 | 13.7 | 10.8 |

Table 3.6 Total acidity measured by $NH_3$ Temperature Programmed Desorption after days of exposure to moisture

| Days | Nano-SAPO-34 ($mmol_{NH3} g^{-1}$ zeolite) | Days | Standard-SAPO-34 ($mmol_{NH3} g^{-1}$ zeolite) |
|---|---|---|---|
| 1 | 1.03 | 1 | 1.01 |
| 30 | 0.86 | 28 | 0.97 |
| 43 | 0.72 | 40 | 0.95 |

It can be seen there that the initial kinetic rate constant is much higher for nano-SAPO-34 than for the standard sample. This would agree with the smaller size of the crystals of nano-SAPO-34, since methanol reaction on eight member ring zeolites is controlled by diffusion within the micropore and a catalyst with a higher external surface should increase initial activity. Moreover, taking into account that both samples presented similar acidity measured by ammonia-TPD (Table 3.6), the kinetic rate constant obtained must be directly related to the number of accessible sites close to the surface of the catalyst. After exposure to moisture at room temperature the kinetic rate constant steadily decreases in both nano and standard SAPO-34. The initial deactivation constant is similar for both catalysts. However its behavior after exposure to moisture at room atmosphere is different. In the case of nano-sapo-34, the deactivation constant strongly decreases up to 14 days and then increases, while for standard-SAPO-34 it continuously increases. The long-term increase in the deactivation constant could be due to the presence of defects created by the irreversible hydrolysis of the structure, as shown above by FTIR and NMR that could accelerate deactivation by adsorption of coke precursors. In fact, a higher deactivation and shorter lifetime was reported in the case of zeolite ZSM-5, in which the creation of internal silanol nests by carbon templating induced higher deactivation in the MTH reaction[41, 42]. On the other hand, the short-term decrease in the deactivation constant until the 14th day of exposure for nano-SAPO-34 could be attributed to the hydrolysis of the Si-O-Al groups at the border of the silicon islands shown before by NMR. These acid sites are believed to present strong acidity and which will promote coking faster than single silicon sites in SAPO-34. The disappearance by hydrolysis of the very strong acid sites would enhance lifetime. Therefore by selective hydrolysis of Si-O-Al bonds corresponding to the strongest

acid sites, the remaining acidity makes a catalyst with lower deactivation rate and longer lifetime.

## 3.3.2.2.Shape-selectivity and thermodymanic equilibrium of olefins
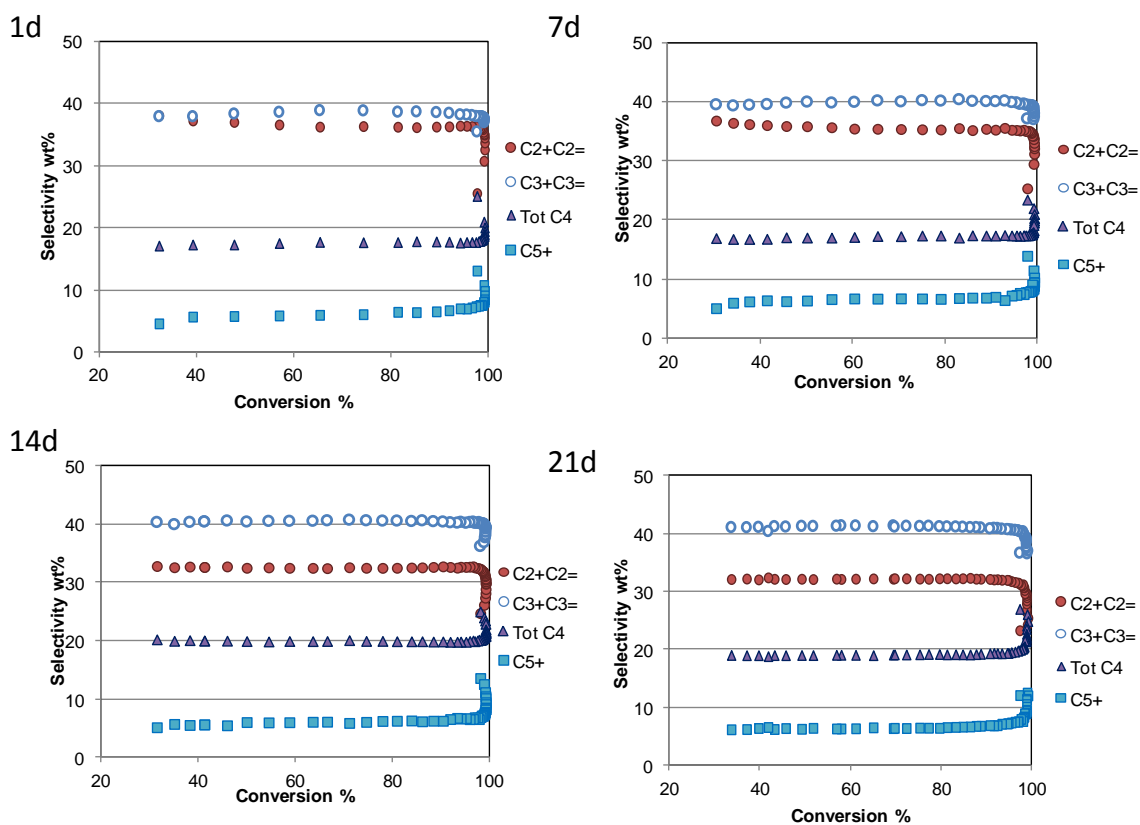


Fig 3.13 Selectivities to C2, C3, C4 and C5+ hydrocarbons in the conversion of methanol on nano-SAPO-34 after exposure to moisture for 1, 7, 14 and 21 days.

1d



32d



41d
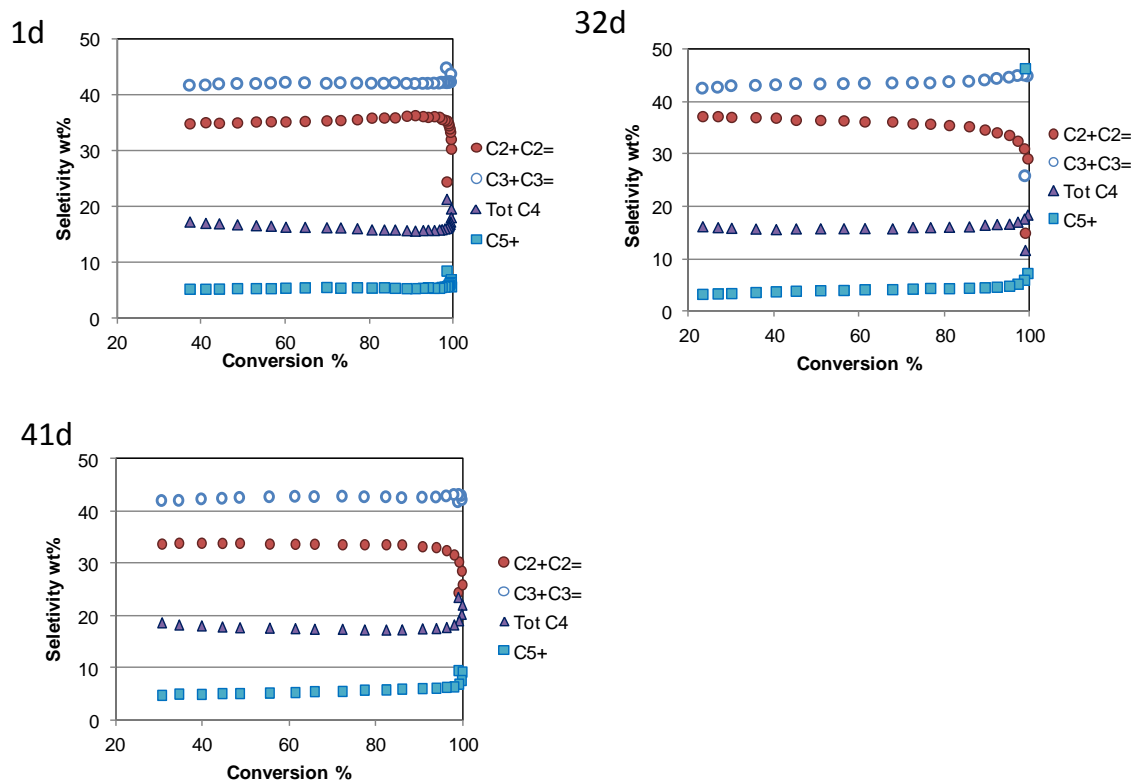


Fig 3.14 Selectivities to C2, C3, C4 and C5+ hydrocarbons in the conversion of methanol on standard-SAPO-34 after exposure to moisture for 1, 31 and 44 days

.
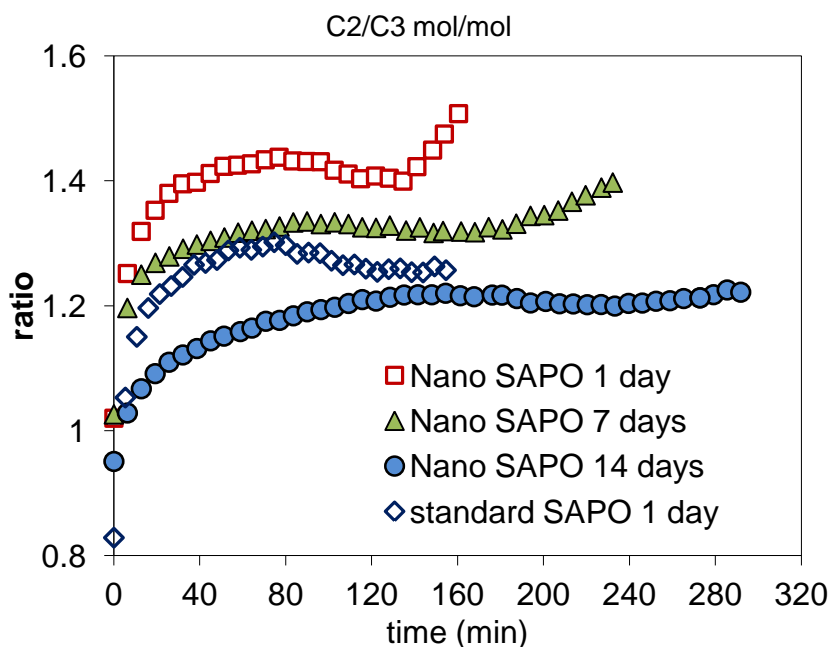


Fig 3.15 C2/C3 ratio for nano and standard-SAPO-34 at 400°C and WHSV=7h$^{-1}$.

When selectivities to olefins are plotted vs. conversion (Fig 3.13, Fig 3.14), in general, selectivity is constant when conversion is not complete, and changes with

time on stream when regarded at full conversion. As a consequence, the C2/C3 ratio tends to increase with time on stream (Fig 3.15). This was already described by several authors and Chen et al.[43] showed that ethylene selectivity increases when increasing coke and proposed that coke has an effect for the effective reduction of void volume of the cavities modifying the transition-shape selectivity by favoring the formation of smaller molecules. On the other hand Dahl[44] and Barger[45] have proposed that it is a product shape selectivity effect the one that controls product distribution and that higher ethylene selectivity is due to a faster diffusion of the shorter ethylene vs. the longer propylene through 8MR windows. The latter proposition was supported by Hereijgers et al.[46] who, by means of isotopic experiments with $^{13}$C-marked methanol, claimed hexamethylbenzene as the most active intermediate for the MTO reaction, being this independent of the amount of coke formed. However, if an easier diffusion of ethylene was the main factor affecting the ratio C2/C3 with time on stream, this ratio should be greatly affected by the size of the crystal of SAPO-34 and higher C2/C3 value would be expected with larger zeolite crystals. When looking into the C2/C3 ratio of nano and standard-SAPO-34, one can observe that the trend is the opposite, i.e. C2/C3 is higher for nano-SAPO-34 and increases with TOS. Moreover, when the samples are aged at room condition the C2/C3 ratio decreases. Taking into account the effect of zeolite crystallite size and the effect of moisture on the C2/C3 ratio in the present work, we cannot support the hypothesis that a higher C2 selectivity is due to differences in diffusion between C2 and C3 through the 8-ring pores. We believe that the results obtained could be better explained on the bases of acid strength than on the bases of diffusion. In fact Song et al.[47] have reported that the selectivity of ethylene was favoured by methylbenzenes trapped in the cages with lower number methyl groups, while propylene is favoured when the number of methyl groups is higher. Also Arstad et al.[48] showed that the formation of ethylene from either hexa or tetramethylbenzene reaction center is energetically less favoured than propylene. So, it can be deduced that stronger acidities should induce higher C2/C3 ratios. In the case of fresh nanoSAPO-34, the presence of strong acid sites related to Si located at the border of silicon islands, could then be the reason of the higher C2/C3 ratio observed with this sample. Then, when the number of these sites is reduced by hydrolysis at room atmosphere, the C2/C3 ratio drops sensibly.

The variation of the C2/C3 ratio with Time on Stream is restricted to the analysis in which conversion is close to 100% and it seems logical to think that thermodynamic equilibrium between olefins should be approached with the corresponding effect on selectivity. In Table 3.5, initial and "steady-state selectivity" are compared with thermodynamic values calculated including or not branched C4 and C5 olefins. It is important to notice that the branched olefins obtained in the case of nano-SAPO-34 must be attributed to reactions occurring at the external surface area which, in this case is much larger. When branched olefins were included in the thermodynamic calculations a distribution of C2/C3 a different of equilibrium, with lower amounts of C2-C3 olefins were observed. In fact, the initial distribution of olefin in both SAPO-34 correlates with the different equilibrium distribution, with the exception of ethylene. This is not surprising taking into account that in the transformation of different olefins, ethylene is very difficult to activate or protonate comparing with longer olefins. Similar results were obtained by Zhou et al.[49] showing that the rate of conversion of ethylene on SAPO-34 is much lower than propylene and butene. In summary, at the start of the reaction, after the induction period, the olefins formed at the top of the bed are transformed along the catalytic bed with the fresh catalyst towards the equilibrium distribution. Then, in the case of nano-SAPO-34 with higher external surface, olefins can further isomerize, and branched C4 and C5 products appear as products. As the deactivation front moves through the catalyst bed, less fresh catalyst remains until breakthrough of conversion below 100wt%, from where the selectivity reaches a steady-state, less affected by interconversion of olefins and approaching the original selectivity of the hydrocarbon pool (Fig 3.16).
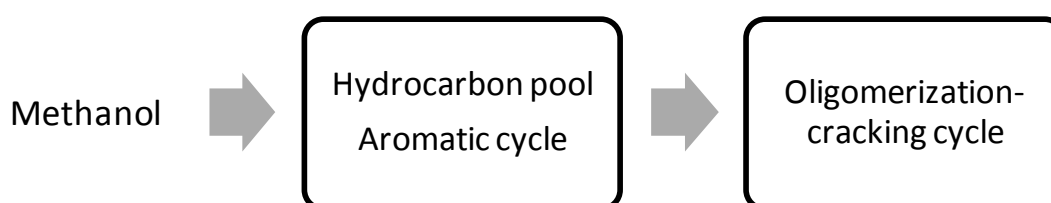


Fig 3.16 Proposed consecutive mechanism in the conversion of Methanol on SAPO-34 taking into account secondary equilibration of olefins.

Very recently Chen et al.[50] proposed that at the beginning of the reaction, when low coke is formed in the cavities and not any methylated benzyl cation has

been formed yet, the olefinic part of the "dual cycle mechanism" in which olefins follows a methylation-cracking mechanism is already working, resulting in low selectivity to ethylene. In our case, it is hard to think that for more than two hours the selectivity in nano SAPO-34 is mainly governed by the olefin cycle. This would assume that the rate of cyclization and hydrogen transfer of olefins to aromatics in the cages is very much slower than the rate of methylation-cracking. In addition, the presence of branched C4 and C5 in the reaction on nano-SAPO-34 indicates that thermodynamic equilibrium of olefin is greatly affecting selectivity at high conversion values.

Therefore, while conversion during MTO reaction on SAPO-34 is close to 100%, which is the working parameter for the industrial unit, the selectivity to olefins is strongly affected by thermodynamic distribution. In addition, the differences in C2/C3 ratio after exposition to moisture, and also the comparison with the values obtained with the larger-sized Standard-SAPO-34 do not correlate with an easier diffusion of ethylene vs. propylene. Moreover, this result is more in agreement with "transition selectivity effect" in which distribution of products is affected by different silicon distribution or different acid properties of the catalyst and not to a "product shape selectivity" in which coking reduces the size of the cages and hinders diffusion of products. Recently, Wang et al.[51] have proposed by DFT calculations that olefins themselves are likely the dominating hydrocarbon pool species on SAPO-34, and that ethene and propene are produced through the cracking of C5+ and C6+ ions. Our experimental results cannot support this. If the olefin cycle were so predominant and only the cracking of carbenium ions influences selectivity, the distribution of products would be governed by thermodynamic distribution. However, as we showed above, in the presence of methanol and DME, the selectivity to ethylene among the olefins is constant and always above thermodynamic equilibrium. Therefore, taking into account the experimental results obtained and assuming that the paring scheme of the hydrocarbon pool is expected to be less predominant in SAPO-34[52], olefins selectivity should be produced through aromatic intermediates by the side-chain methylation mechanism[53]. These aromatic and positively charged transition states could lead to different selectivities depending on differences in acid strength, as suggested recently by Westgard et al.[54]. In addition, the potential participation of aromatic radical cations, already detected as reaction intermediates[55], could

contribute to lower energy barriers for ethene production than those calculated by previous DFT calculations.

# 3.4. Conclusions

We have shown that nano sized samples of SAPO-34 synthesized by microwave heating presents much higher better performance than standard-SAPO-34 synthesized by conventional hydrothermal method for the reaction of methanol to olefins. However the stability of nano-SAPO-34 when exposed to moisture at room conditions is lower than that of the standard-SAPO-34. Firstly, hydrolysis of Si-O-Al bonds of silicon in the border of silicon islands occurs and since the acid sites corresponding to these Si species are believed to present higher acidity and favor coking and deactivation of the catalyst a decrease in the rate of deactivation of nano-SAPO-34 by coking is observed with sample exposed to moisture up to 14 days. Then, after 14 days, lifetime decreases continuously due to hydrolysis of both Si-O-Al and Al-O-P bonds.

The selectivity to different olefins in the reaction strongly changes for samples of nano-SAPO-34 exposed to moisture during a different number of days. The C2/C3 ratio decreases after exposure of the samples to moisture. A higher C2/C3 ratio is related to a higher population of Si in the border of the Si islands, with acid sites of higher strength. This is in agreement with a "transition-state selectivity effect" in which higher amount distribution of products is affected by different acid properties of the catalyst and not by an "easier diffusion" of ethylene vs. propylene. In addition, the initial olefin distribution is strongly affected by thermodynamic distribution among the two olefins, decreasing the yield of ethylene, which is produced above the equilibrium by the aromatics-based hydrocarbon pool mechanism.

# References

[1] Annual Energy Outlook 2012 with Projections to 2035, in, U.S. Energy Information Administration, 2012.

[2] M. Stöcker, Methanol to Olefins (MTO) and Methanol to Gasoline (MTG), in: Zeolites and Catalysis, Wiley-VCH Verlag GmbH & Co. KGaA, 2010, pp. 687-711.

[3] M. Bjørgen, F. Joensen, M. Spangsberg Holm, U. Olsbye, K.P. Lillerud, S. Svelle, Methanol to gasoline over zeolite H-ZSM-5: Improved catalyst performance by treatment with NaOH, Applied Catalysis A: General, 345 (2008) 43-50.

[4] P.N.R. Vennestrøm, M. Grill, M. Kustova, K. Egeblad, L.F. Lundegaard, F. Joensen, C.H. Christensen, P. Beato, Hierarchical ZSM-5 prepared by guanidinium base treatment: Understanding microstructural characteristics and impact on MTG and NH 3-SCR catalytic reactions, Catalysis. Today, 168 (2011) 71-79.

[5] K. Barbera, F. Bonino, S. Bordiga, T.V.W. Janssens, P. Beato, Structure-deactivation relationship for ZSM-5 catalysts governed by framework defects, Journal of Catalysis, 280 (2011) 196-205.

[6] K. Na, M. Choi, R. Ryoo, Recent advances in the synthesis of hierarchically nanoporous zeolites, Microporous Mesoporous Materials., 166 (2013) 3-19.

[7] C.J.H. Jacobsen, C. Madsen, J. Houzvicka, I. Schmidt, A. Carlsson, Mesoporous zeolite single crystals [2], Journal of American Chemical Society., 122 (2000) 7116-7117.

[8] J. Kim, M. Choi, R. Ryoo, Effect of mesoporosity against the deactivation of MFI zeolite catalyst during the methanol-to-hydrocarbon conversion process, Journal Catalysis, 269 (2010) 219-228.

[9] M. Firoozi, M. Baghalha, M. Asadi, The effect of micro and nano particle sizes of H-ZSM-5 on the selectivity of MTP reaction, Catalysis Communication, 10 (2009) 1582-1585.

[10] A.A. Rownaghi, J. Hedlund, Methanol to gasoline-range hydrocarbons: Influence of nanocrystal size and mesoporosity on catalytic performance and product distribution of ZSM-5, Industrial & Engineering Chemistry Research, 50 (2011) 11872-11878.

[11] L. Sommer, D. Mores, S. Svelle, M. Stöcker, B.M. Weckhuysen, U. Olsbye, Mesopore formation in zeolite H-SSZ-13 by desilication with NaOH, Microporous Mesoporous Materials, 132 (2010) 384-394.

[12] L. Wu, V. Degirmenci, P.C.M.M. Magusin, B.M. Szyja, E.J.M. Hensen, Dual template synthesis of a highly mesoporous SSZ-13 zeolite with improved stability in the methanol-to-olefins reaction, Chemical Communication, 48 (2012) 9492-9494.

[13] L. Wu, V. Degirmenci, P.C.M.M. Magusin, N.J.H.G.M. Lousberg, E.J.M. Hensen, Mesoporous SSZ-13 zeolite prepared by a dual-template method with improved

performance in the methanol-to-olefins reaction, Journal of Catalysis, 298 (2013) 27-40.

[14] F. Schmidt, S. Paasch, E. Brunner, S. Kaskel, Carbon templated SAPO-34 with improved adsorption kinetics and catalytic performance in the MTO-reaction, Microporous Mesoporous Materials, 164 (2012) 214-221.

[15] Y. Hirota, K. Murata, S. Tanaka, N. Nishiyama, Y. Egashira, K. Ueyama, Dry gel conversion synthesis of SAPO-34 nanocrystals, Materials Chemistry and Physics, 123 (2010) 507-509.

[16] K.Y. Lee, H.J. Chae, S.Y. Jeong, G. Seo, Effect of crystallite size of SAPO-34 catalysts on their induction period and deactivation in methanol-to-olefin reactions, Applied Catalysis A: General, 369 (2009) 60-66.

[17] Y.J. Lee, S.C. Baek, K.W. Jun, Methanol conversion on SAPO-34 catalysts prepared by mixed template method, Applied Catalysis A: General, 329 (2007) 130-136.

[18] P. Wang, A. Lv, J. Hu, J. Xu, G. Lu, The synthesis of SAPO-34 with mixed template and its catalytic performance for methanol to olefins reaction, Microporous Mesoporous Materials, 152 (2012) 178-184.

[19] T. Álvaro-Muñoz, C. Márquez-Álvarez, E. Sastre, Use of different templates on SAPO-34 synthesis: Effect on the acidity and catalytic activity in the MTO reaction, Catalysis Today, 179 (2012) 27-34.

[20] S. Lin, J. Li, R.P. Sharma, J. Yu, R. Xu, Fabrication of SAPO-34 crystals with different morphologies by microwave heating, Topics in Catalysis, 53 (2010) 1304-1310.

[21] F.M. Shalmani, R. Halladj, S. Askari, Effect of contributing factors on microwave-assisted hydrothermal synthesis of nanosized SAPO-34 molecular sieves, Powder Technology, 221 (2012) 395-402.

[22] G. Yang, Y. Wei, S. Xu, J. Chen, J. Li, Z. Liu, J. Yu, R. Xu, Nanosize-Enhanced Lifetime of SAPO-34 Catalysts in Methanol-to-Olefin Reactions, The Journal of Physical Chemistry C, 117 (2013) 8214-8222.

[23] A. Buchholz, W. Wang, A. Arnold, M. Hunger, Successive steps of hydration and dehydration of silicoaluminophosphates H-SAPO-34 and H-SAPO-37 investigated by in situ CF MAS NMR spectroscopy, Microporous Mesoporous Materials, 57 (2003) 157-168.

[24] A. Buchholz, W. Wang, M. Xu, A. Arnold, M. Hunger, Thermal stability and dehydroxylation of brønsted acid sites in silicoaluminophosphates H-SAPO-11, H-SAPO-18, H-SAPO-31, and H-SAPO-34 investigated by multi-nuclear solid-state NMR spectroscopy, Microporous Mesoporous Materials, 56 (2002) 267-278.

[25] C.S. Blackwell, R.L. Patton, Solid-state NMR of silicoaluminophosphate molecular sieves and aluminophosphate materials, The Journal of Physical Chemistry, 92 (1988) 3965-3970.

[26] B.M. Lok, C.A. Messina, R.L. Patton, R.T. Gajek, T.R. Cannan, E.M. Flanigen, Silicoaluminophosphate molecular sieves: Another new class of microporous crystalline inorganic solids, Journal of American Chemical Society, 106 (1984) 6092-6093.

[27] R. Vomscheid, M. Briend, M.J. Peltre, P.P. Man, D. Barthomeuf, The Role of the Template in Directing the Si Distribution in SAPO Zeolites, Journal of Physical Chemistry, 98 (1994) 9614-9618.

[28] G.A.V. Martins, G. Berlier, S. Coluccia, H.O. Pastore, G.B. Superti, G. Gatti, L. Marchese, Revisiting the nature of the acidity in chabazite-related silicoaluminophosphates: Combined FTIR and29Si MAS NMR study, Journal of Physical Chemistry C, 111 (2007) 330-339.

[29] Y. Wei, D. Zhang, L. Xu, F. Chang, Y. He, S. Meng, B.-l. Su, Z. Liu, Synthesis, characterization and catalytic performance of metal-incorporated SAPO-34 for chloromethane transformation to light olefins, Catalysis Today, 131 (2008) 262-269.

[30] M. Briend, R. Vomscheid, M.J. Peltre, P.P. Man, D. Barthomeuf, Influence of the Choice of the Template on the Short- and Long-Term Stability of SAPO-34 Zeolite, Journal of Physical Chemistry, 99 (1995) 8270-8276.

[31] K. Suzuki, T. Nishio, N. Katada, G. Sastre, M. Niwa, Ammonia IRMS-TPD measurements on Brønsted acidity of proton-formed SAPO-34, Physical Chemistry Chemical Physics, 13 (2011) 3311-3318.

[32] N. Katada, K. Nouno, J.K. Lee, J. Shin, S.B. Hong, M. Niwa, Acidic properties of cage-based, small-pore zeolites with different framework topologies and their silicoaluminophosphate analogues, Journal of Physical Chemistry C, 115 (2011) 22505-22513.

[33] G. Sastre, D.W. Lewis, C. Richard, A. Catlow, Modeling of silicon substitution in SAPO-5 and SAPO-34 molecular sieves, J. Phys. Chem. B, 101 (1997) 5249-5262.

[34] D. Barthomeuf, Topological model for the compared acidity of SAPOs and SiAl zeolites, Zeolites, 14 (1994) 394-401.

[35] A. Buchholz, W. Wang, M. Xu, A. Arnold, M. Hunger, Sequential Steps of Ammoniation of the Microporous Silicoaluminophosphates H-SAPO-34 and H-SAPO-37 Investigated by In Situ CF MAS NMR Spectroscopy, Journal of Physical Chemistry B, 108 (2004) 3107-3113.

[36] Y. Watanabe, A. Koiwai, H. Takeuchi, S.A. Hyodo, S. Noda, Multinuclear NMR Studies on the Thermal Stability of SAPO-34, Journal of Catalysis, 143 (1993) 430-436.

[37] G. Busca, V. Lorenzelli, V.S. Escribano, R. Guidetti, FT-113 study of the surface properties of the spinels NiAl2O4 and $CoAl_2O_4$ in relation to those of transitional aluminas, Journal of Catalysis, 131 (1991) 167-177.

[38] G. Busca, V. Lorenzelli, G. Ramis, R.J. Willey, Surface sites on spinel-type and corundum-type metal oxide powders, Langmuir, 9 (1993) 1492-1499.

[39] E.A. Eilertsen, B. Arstad, S. Svelle, K.P. Lillerud, Single parameter synthesis of high silica CHA zeolites from fluoride media, Microporous Mesoporous Materials., 153 (2012) 94-99.

[40] E. Gianotti, V. Dellarocca, E.C. Oliveira, S. Coluccia, H.O. Pastore, L. Marchese, Acidity of mesoporous aluminophosphates and silicas MCM-41. A combined FTIR and UV-Vis-NIR study, Study in Surface Science and Catalysis, Elsevier, 2002, pp. 1419-1426.

[41] S. Bordiga, L. Regli, D. Cocina, C. Lamberti, M. Bjørgen, K.P. Lillerud, Assessing the acidity of high silica chabazite H-SSZ-13 by FTIR using CO as molecular probe: Comparison with H-SAPO-34, Journal of Physical Chemistry B, 109 (2005) 2779-2784.

[42] F. Bleken, M. Bjørgen, L. Palumbo, S. Bordiga, S. Svelle, K.P. Lillerud, U. Olsbye, The effect of acid strength on the conversion of methanol to olefins over acidic microporous catalysts with the CHA topology, Topics in Catalysis, 52 (2009) 218-228.

[43] T.V.W. Janssens, A new approach to the modeling of deactivation in the conversion of methanol on zeolite catalysts, Journal of Catalysis, 264 (2009) 130-137.

[44] D. Chen, H.P. Rebo, K. Moljord, A. Holmen, Influence of Coke Deposition on Selectivity in Zeolite Catalysis, Industrial & Engineering Chemical Research, 36 (1997) 3473-3479.

[45] U. Sedran, A. Mahay, H.I. De Lasa, Modelling methanol conversion to hydrocarbons: revision and testing of a simple kinetic model, Chemical Engineering Science, 45 (1990) 1161-1165.

[46] D. Chen, H.P. Rebo, K. Moljord, A. Holmen, The role of coke deposition in the conversion of methanol to olefins over SAPO-34, Study in Surface Science and Catalysis, 111 (1997) 159-166.

[47] D. Chen, H.P. Rebo, K. Moljord, A. Holmen, Methanol Conversion to Light Olefins over SAPO-34 - Sorption, Diffusion, and Catalytic Reactions, Industrial & Engineering Chemistry Research, 38 (1999) 4241-4249.

[48] J.M. Smith, H.C. Van Ness, M.M. Abbott, Introduction to chemical engineering thermodynamics, 7th ed., McGraw-Hill, Boston, 2005.

[49] R.A. Alberty, C.A. Gehrig, Standard chemical thermodynamic properties of alkene isomer groups, Journal of Physical Chemistry 14 (1985) 803-820.

[50] S. Svelle, L. Sommer, K. Barbera, P.N.R. Vennestrøm, U. Olsbye, K.P. Lillerud, S. Bordiga, Y.H. Pan, P. Beato, How defects and crystal morphology control the effects of desilication, Catalysis Today, 168 (2011) 38-47.

[51] P. Sazama, B. Wichterlova, J. Dedecek, Z. Tvaruzkova, Z. Musilova, L. Palumbo, S. Sklenak, O. Gonsiorova, FTIR and 27Al MAS NMR analysis of the effect of framework Al- and Si-defects in micro- and micro-mesoporous H-ZSM-5 on conversion of methanol to hydrocarbons, Microporous Mesoporous Materials, 143 (2011) 87-96.

[52] D. Chen, A. Grønvold, K. Moljord, A. Holmen, Methanol Conversion to Light Olefins over SAPO-34: Reaction Network and Deactivation Kinetics, Industrial & Engineering Chemistry Research, 46 (2006) 4116-4123.

[53] I.M. Dahl, H. Mostad, D. Akporiaye, R. Wendelbo, Structural and chemical influences on the MTO reaction: a comparison of chabazite and SAPO-34 as MTO catalysts, Microporous Mesoporous Materials, 29 (1999) 185-190.

[54] P. Barger, Methanol to olefins (MTO) and beyond, in: M. Guisnet, J.P. Gilson (Eds.) Zeolites for Cleaner Technologies (Catalytic Science Series Vol. 3), Imperial College Press, London, 2002, pp. 239-260.

[55] B.P.C. Hereijgers, F. Bleken, M.H. Nilsen, S. Svelle, K.P. Lillerud, M. Bjørgen, B.M. Weckhuysen, U. Olsbye, Product shape selectivity dominates the Methanol-to-Olefins (MTO) reaction over H-SAPO-34 catalysts, Journal of Catalysis, 264 (2009) 77-87.

[56] W. Song, H. Fu, J.F. Haw, Supramolecular Origins of Product Selectivity for Methanol-to-Olefin Catalysis on HSAPO-34, Journal of American Chemical Society, 123 (2001) 4749-4754.

[57] B. Arstad, J.B. Nicholas, J.F. Haw, Theoretical Study of the Methylbenzene Side-Chain Hydrocarbon Pool Mechanism in Methanol to Olefin Catalysis, Journal of American Chemical Society, 126 (2004) 2991-3001.

[58] H. Zhou, Y. Wang, F. Wei, D. Wang, Z. Wang, Kinetics of the reactions of the light alkenes over SAPO-34, Applied Catalysis A: General, 348 (2008) 135-141.

[59] D. Chen, K. Moljord, A. Holmen, A methanol to olefins review: Diffusion, coke formation and deactivation on SAPO type catalysts, Microporous Mesoporous Materials, 164 (2012) 239-250.

[60] C.M. Wang, Y.D. Wang, Z.K. Xie, Insights into the reaction mechanism of methanol-to-olefins conversion in HSAPO-34 from first principles: Are olefins themselves the dominating hydrocarbon pool species? Journal of Catalysis, 301 (2013) 8-19.

[61] C.M. Wang, Y.D. Wang, Z.K. Xie, Z.P. Liu, Methanol to olefin conversion on hsapo-34 zeolite from periodic density functional theory calculations: A complete cycle of side chain hydrocarbon pool mechanism, Journal of Physical Chemistry C, 113 (2009) 4584-4591.

[62] K. Hemelsoet, J. Van der Mynsbrugge, K. De Wispelaere, M. Waroquier, V. Van Speybroeck, Unraveling the Reaction Mechanisms Governing Methanol-to-Olefins Catalysis by Theory and Experiment, ChemPhysChem, 14 (2013) 1526-45.

[63] M. Westgård Erichsen, S. Svelle, U. Olsbye, The influence of catalyst acid strength on the methanol to hydrocarbons (MTH) reaction, Catalysis Today 215 (2013) 216-223.

[64] S.J. Kim, H.G. Jang, J.K. Lee, H.K. Min, S.B. Hong, G. Seo, Direct observation of hexamethylbenzenium radical cations generated during zeolite methanol-to-olefin catalysis: An ESR study, Chemical Communication, 47 (2011) 9498-9500.

# 4. Conversion of methanol to olefins: Stabilization of nanosized SAPO-34 by hydrothermal treatment

# 4.1.Introduction

Nowadays, the high industrial demand for ethylene and propylene has renewed the interest on the reaction of methanol to olefins (MTO). In fact, more than 20 units are expected to operate in China in the next 2-3 years with an overall olefin capacity of more than 11 million Ton/year [1]. The feed methanol is obtained from reaction of synthesis gas on appropriate catalysts, being the synthesis gas obtained by gasification of coal or biomass and by steam-reforming of natural gas. The increasing amount of gas reserves due to the upcoming of shale gas have led to cheaper methane [2] and are expected to affect the market of methanol, renewing the interest for the MTO process [3]. If propylene is desired the catalyst used is based on high silica ZSM-5 (MTP process), which has a lifetime of 650 h in between the regeneration steps [4]. Another possibility is to use a catalyst based on silicoaluminophosphate SAPO-34 that can yield different C2=/C3= ratios depending on reaction conditions [5-7]. However, the latter catalyst has a much shorter lifetime than ZSM-5 due to the extension of coking reactions inside the cages of the CHA structure, and a continuous catalyst regeneration process is required. In fact, since the mechanism of the MTO reaction in the CHA structure was established by Haw and coworker on a hydrocarbon pool formed by alkylated aromatics[8], the faster deactivation is explained due to the growth of these aromatics that cannot diffuse trough the 8MR windows of the structure forming coke therefore blocking the access to the rest of the structure. Therefore, lifetime of the catalyst depends greatly on the degree of the utilization of the catalyst crystal. Lifetime of SAPO-34 can be extended by using mesoporous SAPO-34 [9-13], by decreasing the size of the crystal [14-19] or by including metal oxides in the catalyst composition [20]. Smaller crystallites of SAPO-34 were achieved recently by heating the synthesis gel in a microwave apparatus [21, 22]. In this way, crystallites of 20nm sizes were obtained, and the resultant SAPO-34 presented much longer lifetimes than standard SAPO-34 samples. However, we showed recently [22] that due to the small size of crystallites and the high external surface area, the material was very sensitive to hydrolysis by moisture at room conditions and suffered complete hydrolysis after months of storage. This behavior was already reported in the literature for more conventional SAPO-34 samples [23-26]. Briend et al. [23] related the lack of long-term stability to

the presence of silicon islands, favored by the use of morpholine as template. Other authors [24, 27] showed that the structural deterioration can be prevented if after removing the template the acid sites are covered with ammonia.

In the present work we started from the hypothesis that it could be possible to increase the stability of SAPO-34 samples by performing a controlled hydrolysis of a part of the silicon, in an analogous way as it occurs with high aluminum zeolites that can be stabilized by controlled partial dealumination [28]. Therefore, we will present here the effect of the hydrothermal treatment at different temperatures on the long-term stability of nano and standard SAPO-34 materials. We will show how by an appropriate steaming temperature, nano-SAPO-34 becomes stabilized towards moisture. In addition, we will show that hydrothermal stability tests for SAPO-34, which are normally performed at very high temperatures (800°C) [1, 12, 30], should also include stability tests at reaction temperatures close to the reaction temperature used for MTO, to better ascertain the viability of this type of catalyst for the mentioned catalytic process.

# 4.2. Experimental

## 4.2.1. Synthesis of materials

Nano-SAPO-34 and standard SAPO-34 were obtained as the description in Chapter 3. Hydrothermal treatments have been done in a small laboratory muffle in which catalyst have been placed in small planar crucibles pelletized at 0.2-0.4 mm of size and water have been introduced by means of a quart tube filled with quartz beads at a flow of 2 ml min$^{-1}$.

## 4.2.2. Characterization

The characterization measurements are carried out in the same way as described in the Chapter 3.

## 4.2.3.Catalytic experiments

The catalysts were tested in the same conditions as we have shown in the Chapter 3. All characterization and catalytic results of hydrothermally treated samples will be compared with those obtained previously with the parent nano and standard-SAPO-34 samples as shown in the Chapter 3.

# 4.3.Results and discussion

## 4.3.1.Crystallinity and acidity of SAPO-34 samples
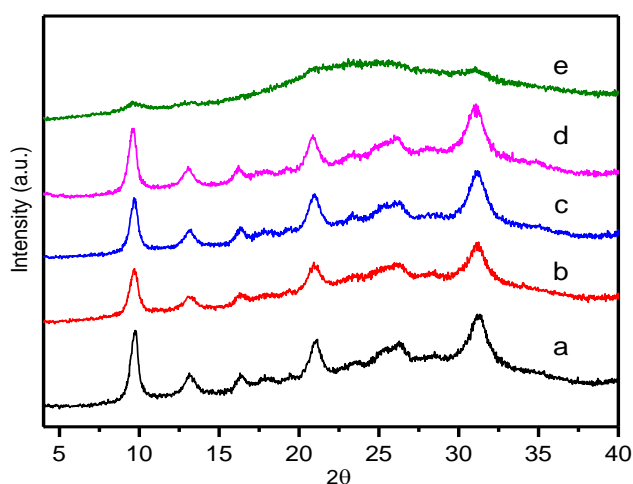


Fig 4.1 XRD patterns of nano-SAPO-34 (a) as calcined, and after steaming at (b) 700°C, (c) 600°C, (d) 550°C, (e) 400°C.
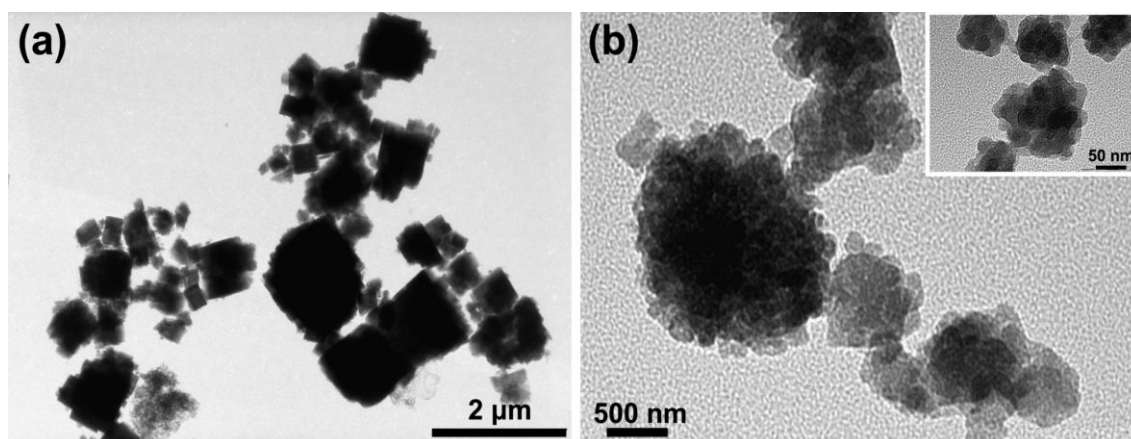


Fig 4.2 TEM images of a) standard and b) nano-SAPO-34.
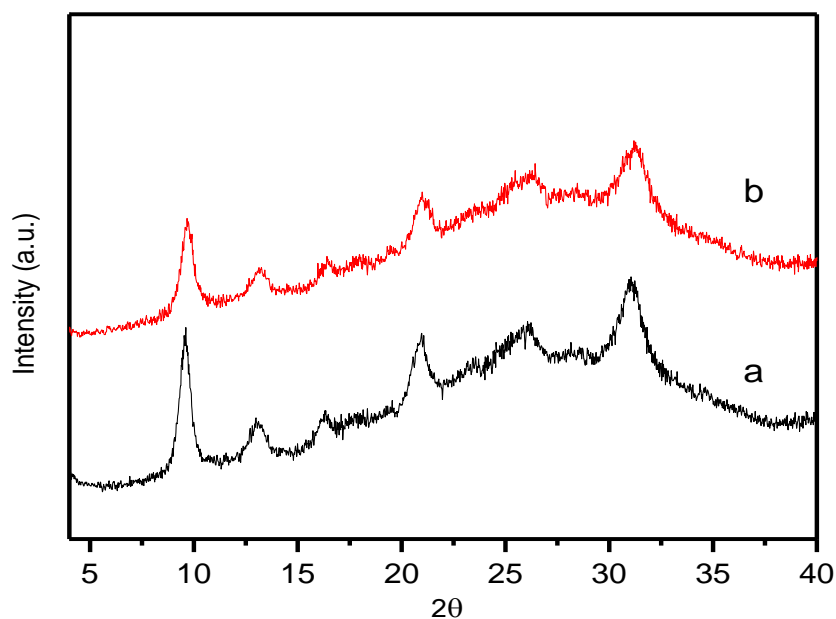
Fig 4.3 XRD patterns of nano-SAPO-34 steamed at 700°C after contact with moisture for (a) 1day (b) 67 days.

The XRD patterns of the calcined parent nano-SAPO-34 and steamed at different temperatures are shown in Fig 4.1 . The broad shape and low intensity of the XRD of the parent material is characteristic of the small size of the crystals [22], which is around 20 nm (see Fig 4.2). After steaming at temperatures of 550°C and 600°C, the diffraction patterns are still similar to that of nano-SAPO-34 suggesting that the structure of these samples is maintained. At 700°C a slight decrease in the intensity of the peaks is observed. However, the sample steamed at 400°C presents amorphous XRD pattern. In agreement with the XRD results, adsorption of nitrogen (Table 4.1) shows that the nano-SAPO-34 steamed at 400°C loses the microporosity while those steamed at higher temperatures preserve most of the textural properties with an optimum in microporosity for the sample steamed at 600°C. Even more important is the observation that for samples steamed at T≥550°C and exposed to moisture during days at room temperature, their crystallinity and micropore volume are preserved (Table 4.1and Fig 4.3), while non steamed template-free nano-SAPO-34 is negatively affected when exposed to moisture at room temperature. On the other hand, standard-SAPO-34 with larger cubic crystallites of around 500 nm is much less affected by steaming, with a smaller decrease in the BET surface after steaming at low (400) and high (700°C) temperatures.

Table 4.1 Textural properties of nano-SAPO-34 and standard-SAPO-34 samples fresh and steamed at different temperatures after days of exposure to moisture.

| Sample | Steaming temperature (°C) | Days with moisture at r.t. | BET $(m^2g^{-1})$ | t-plot $S_{ext}$ $(m^2/g)$ | $V_{micro}$ $(cm^3/g)$ | $V_{meso}$ $(cm^3/g)$ | Acidity (mmol $NH_3$/ g) |
|---|---|---|---|---|---|---|---|
| Nano-SAPO-34 | fresh | 1 | 646 | 231 | 0.20 | 0.21 | 1.03 |
| | fresh | 14 | 616 | 224 | 0.19 | 0.20 | 0.86 |
| | fresh | 42 | 561 | 223 | 0.18 | 0.20 | 0.56 |
| | fresh | 107 | 536 | 223 | 0.15 | 0.20 | - |
| | 400 | 1 | 120 | 57 | 0.03 | 0.15 | 0.43 |
| | 550 | 1 | 534 | 177 | 0.17 | 0.21 | 0.74 |
| | 550 | 7 | 534 | 176 | 0.18 | 0.21 | - |
| | 550 | 14 | 538 | 179 | 0.18 | 0.21 | - |
| | 600 | 1 | 575 | 172 | 0.20 | 0.20 | 0.77 |
| | 600 | 12 | 574 | 173 | 0.20 | 0.20 | - |
| | 600 | 23 | 581 | 180 | 0.20 | 0.21 | - |
| | 700 | 1 | 490 | 143 | 0.17 | 0.18 | 0.43 |
| | 700 | 50 | 488 | 160 | 0.16 | 0.19 | - |
| | 700 | 65 | 491 | 144 | 0.17 | 0.19 | - |
| Standard-SAPO-34 | fresh | 5 | 460 | 63 | 0.19 | 0.11 | 1.01 |
| | fresh | 29 | 463 | 62 | 0.19 | 0.11 | 0.97 |
| | fresh | 44 | 463 | 64 | 0.19 | 0.11 | 0.95 |
| | 400 | 1 | 432 | 41 | 0.19 | 0.10 | 0.83 |
| | 700 | 1 | 443 | 40 | 0.20 | 0.10 | 0.73 |
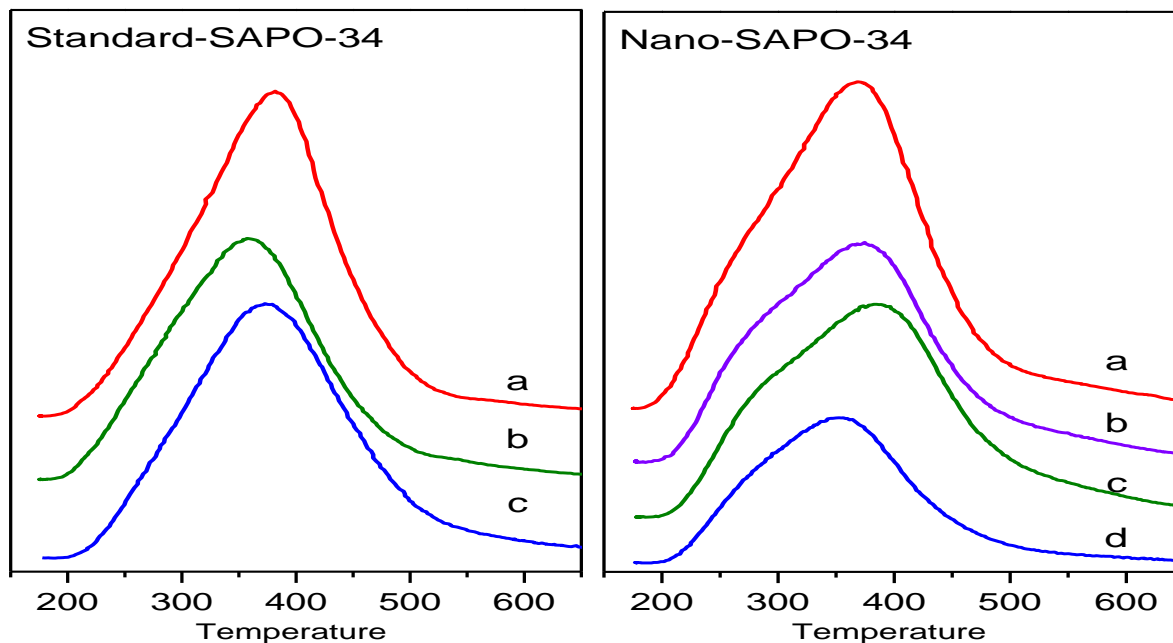
Fig 4.4 NH$_3$-TPD curves of standard-SAPO-34 (a) fresh, (b) steamed at 400ºC, (c) steamed at 700ºC; and nano-SAPO-34 (a) fresh, and steamed at (b) 550, (c) 600 and (d) 700ºC.

When the acidity of the samples was measured by TPD of ammonia (Table 4.1 and Fig 4.4) the results indicate that, in general, steaming reduces the acidity of the samples when compared to the parent sample. This decrease is stronger in the case of the steaming at 700ºC, while the samples steamed at 550 and 600°C present very similar acidity. When comparing the shape of the TPD desorption curves, it can be seen that all samples present a main component with a maximum in the range from 314 to 381°C, and a shoulder ca. 230°C (Fig 4.4). The peak at higher temperature of desorption corresponds mainly to Brönsted acidity and the differences in the temperature of the maxima are better related to the amount of acid sites than to differences in acidity strength. The shoulder at low temperatures corresponds to physisorption of ammonia and not to adsorption on catalytically active sites [31]. From the amounts of adsorbed ammonia given in Table 4.1, it can be seen that the decrease in acidity is proportionally larger than the decrease in micropore volume when increasing steaming temperatures (see Fig 4.5). The results suggest that the hydrolysis of the acid sites when steaming do not necessarily imply a loss of crystallinity, i.e., a partial collapse of the structure but, as it occurs during a controlled steam dealumination process for high Al content zeolites in which silicon is reinserted in the framework, in the case of SAPO-34 can occur a migration of

phosphorus to fill up some of the T-sites left by silicon. Then, we will investigate now by solid NMR the physicochemical transformations occurring in SAPO-34 upon steaming.
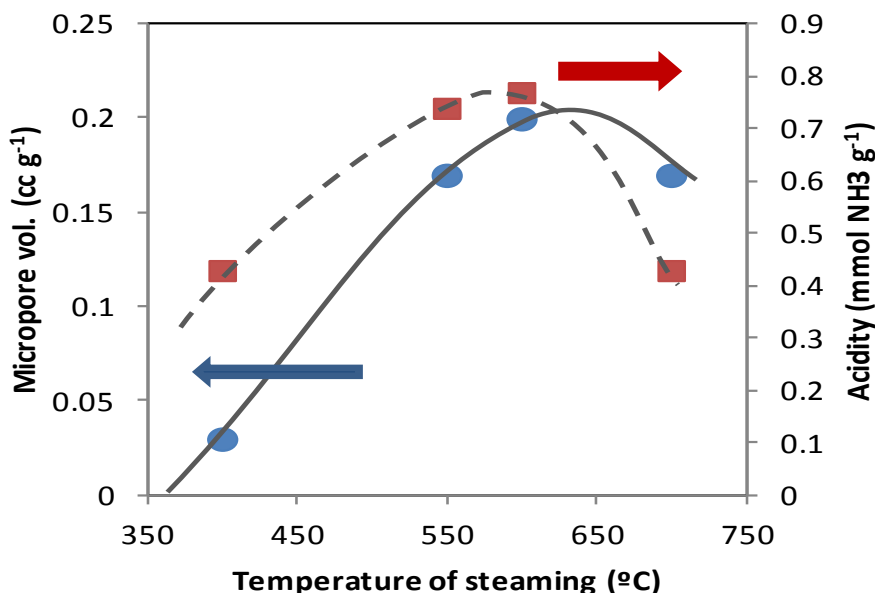


Fig 4.5 Micropore volume (circles) and acidity (squares) of nano-SAPO-34 samples steamed at different temperatures.

## 4.3.2.Solid NMR characterization
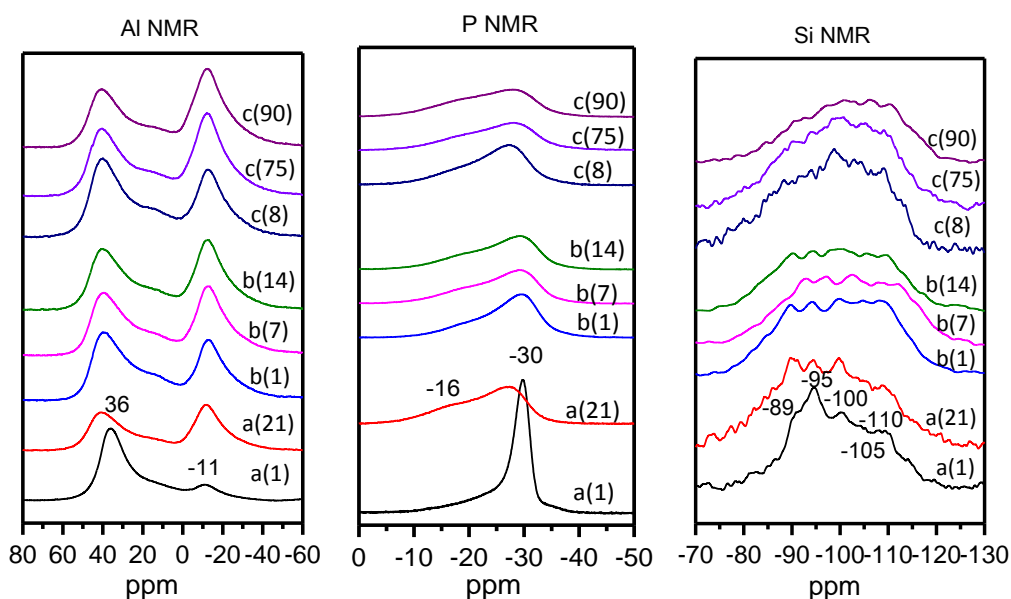


Fig 4.6 $^{27}Al$, $^{31}P$ and $^{29}Si$ MAS NMR of nano-SAPO-34 samples (a) fresh and steamed at (b) 600 or (c) 700°C followed by exposure to moisture at room temperature for (days).

Table 4.2 Distribution of silicon species by deconvolution of different $^{29}$Si MAS NMR signal of samples of nano-SAPO-34 fresh and steamed at 600 or 700°C followed by exposure to moisture (days) at room temperature. Standard error of distribution values < 1%

| Silicon species | ppm | Fresh | Fresh (23d) | St-700 (8d) | St-700 (75d) | St-700 (90d) | St-600 (1d) | St-600 (7d) | St-600 (21d) |
|---|---|---|---|---|---|---|---|---|---|
| Defects | -78, -85 | 5.1 | 14.3 | 13.9 | 11.5 | 7.9 | 7.4 | 3.5 | 1.5 |
| Si4Al | -89 | 16.3 | 18.7 | 12.2 | 12.9 | 12.8 | 16.1 | 9.4 | 8.5 |
| Si3Al1Si | -95 | 25.6 | 17.2 | 14.6 | 15.2 | 14.9 | 16.9 | 16.2 | 16.7 |
| Si2Al2Si | -100 | 18.9 | 18.8 | 19.8 | 19.7 | 17.0 | 17.7 | 16.6 | 16.8 |
| Si1Al3Si | -105 | 13.7 | 13.6 | 16.9 | 17.3 | 16.8 | 15.9 | 18.4 | 19.3 |
| Si4Si | -110 | 20.4 | 17.4 | 22.6 | 23.4 | 30.6 | 26.1 | 35.9 | 37.2 |
| Si in silicon islands | -100 to -110 | 53 | 49.8 | 59.3 | 60.4 | 64.4 | 59.7 | 70.9 | 73.3 |

The $^{27}$Al MAS NMR spectra of nano-SAPO-34 given in Fig 4.6 show an intense peak at 36 ppm and other two signals at -11 and 14 ppm for calcined nano-SAPO-34, that correspond to tetrahedrally coordinated aluminum in local structures of Al(PO)$_4$, and octa and pentacoordinated aluminum, respectively. After exposing the calcined sample to moisture at room temperature at increasing times, the octahedral Al signal at -14 ppm continuously increases, indicating hydration of the Al(PO)$_4$ species [25, 29]. Meanwhile, the signal of tetrahedral aluminum is shifted to 41 ppm, due to the distortion of the structure by interaction with water [31]. The $^{27}$Al MAS NMR spectra of nano-SAPO-34 sample steamed at 700ºC presents band intensities which are independent of the time of exposure and only a slight increase of octahedral aluminum is observed, indicating an increasing hydration effect with time.

The hydration effect is also evidenced through the $^{31}$P NMR spectra. Nano-SAPO-34 exhibits an asymmetrical signal at -30 ppm corresponding to tetrahedral P(OAl)$_4$. After 21 days of hydration, another signal at -16 ppm appears, which can be attributed to P(OAl)$_x$(H$_2$O)$_y$ formed by P atoms coordinated with water [25, 27, 32]. After steaming the fresh nano-SAPO-34 sample at 700°C, the shoulder at -16 ppm appears, and slightly increases after long contact with moisture. This result

correlates well with the increase in the signal of Al NMR at -14 ppm assigned to the hydration of the $Al(PO)_4$ species.

The $^{29}Si$ MAS NMR spectra give further information, and clear differences are observed with the hydrated-parent and steamed samples (Fig 4.6 and Table 4.2). The different silicon species of nano-SAPO-34 have been described elsewhere [22]. This sample shows a large amount of silicon in silicon islands, Si3Al, Si2Al, Si1Al and Si0Al, which corresponds to the -95,-100, -,105 and -110 ppm bands respectively, and isolated silicon which is related to the band at -89 ppm. The deconvolution of the spectra is shown in Table 4.2. The fresh nano-SAPO-34 sample was shown to hydrolyze in contact with moisture by transforming silicon at the edge of the silicon islands (-95 ppm) into defective sites at -78,-85 ppm [22]. As we will see later this has an effect in activity, selectivity and deactivation of the catalyst during the reaction of methanol to olefins. However, when the fresh calcined sample is steamed, the population of isolated silicon Si4Al decreases which is in agreement with the reduction in acidity shown by TPD of ammonia. At the same time, the signals corresponding to silicon within silicon islands, especially Si0Al at -110 ppm, increases together with a reduction of silicon on the edge (Si3Al at -95) with no raise in defects (-78 to -85 ppm). In addition, the distribution of silicon species is not importantly affected when the steamed samples are contacted with moisture at room temperature. The above described effects are qualitatively similar for the sample steamed at 600 and 700°C, being the decrease of isolated silicon Si4Al species higher for the sample steamed at 700°C.

The results obtained here are in line with those previously reported for SAPO-34 and other SAPO's [33-35], in the sense that when they were thermally treated at high temperatures in the absence of added steam, part of silicon migrates to silicon islands while phosphorus healed the framework vacancies with no formation of defects. However, we have seen clear differences in the population of the different Si species and an impact on stability when the samples were steamed. The question then is what is the effect of steaming on the framework composition and its implication on stability to moisture, acidity, activity and selectivity for MTO.

Wilson and Barger [7, 36] studied the effect of hydrothermal treatment on the activity and selectivity of SAPO-34 and they observed no degradation of the structure and a longer lifetime. Recently, Aramburo et al. [26] reported no difference

with the purely thermally treated samples [33-35], i.e., a reduction in acidity with migration of silicon species to silicon islands. However, in  an earlier contribution Park et al. [37] showed that SAPO-34 thermally treated at 750°C loses more crystallinity after reaction with water than the fresh sample indicating that only thermal treatment does not stabilize SAPO-34 samples. If our original hypothesis on the positive effect of water on the mobility of silicon and phosphorus through the framework of SAPO-34, in a similar way as it occurs with aluminum and silicon during ultrastabilization without generation of defects in zeolites, was possible in SAPO-34, a controlled steaming of the SAPO should stabilize towards the negative effect of moisture at room conditions on crystallinity. In this case, steam at high temperatures should facilitate the formation of larger silicon islands together with an easier reallocation of phosphorus occupying the vacancies left by silicon. This hypothesis is supported by a smaller amount of silicon species on the edge of the silicon islands found in steamed samples, as deduced from silicon NMR with an increase in the signals of silicon islands upon steaming. Theoretical calculations on the role of steaming on clusters of isomorphous zeolites SSZ-13 and SAPO-34 [38] also to support our hypothesis on the effect of steaming on SAPO-34 stability.

In summary, we can say that steaming produces a decrease of isolated Si species and its migration to silicon islands which grow in size, as suggested by the decrease of silicon species at the edge of silicon islands. The effect of steaming on lowering the amount of Si at the border of Si islands can explain the lower extension of hydrolysis in the steamed samples upon exposure to moisture at room temperature. This, in turn, would be responsible for the higher stability of the steamed samples.

## 4.3.3. Catalytic activity

### 4.3.3.1. Influence of stabilization on catalyst activity and lifetime

The activity of calcined and steamed nano-SAPO-34 is shown in Fig 4.7. The experiments were performed at WHSV=7h$^{-1}$ and 400°C of reaction temperature. Nano-SAPO-34 samples steamed at 550, 600 and 700°C present a lifetime close to fresh nano-SAPO-34, though clear differences appear in the slope or the time at which catalyst deactivation starts to be observed. Here we have fitted the

experimental data to the kinetic model developed by Janssens [39]. This model is able to separate the contribution of activity (K) from the deactivation rate (a) on ZSM-5 and was also successfully applied to SAPO-34 [22]. By doing that, the effect of steaming temperature is clearly visible. Indeed, the results in Table 4.3 indicate that activity (K) decreases when increasing the steaming temperature and that decrease correlates well with the decrease of acidity measured by TPD of ammonia. On the other hand, the rate of deactivation, which is also a measure of the catalyst half lifetime, is maintained despite the decrease of overall acidity due to steaming. In the case of the sample steamed at 550°C even halflifetime ($t_{0,5}$) showed a small increase after 7 days of hydration, indicating that at steaming temperatures lower than 600°C the material is not fully stabilized. Therefore, steaming decreases the activity of the catalyst while deactivation rate does not increase.
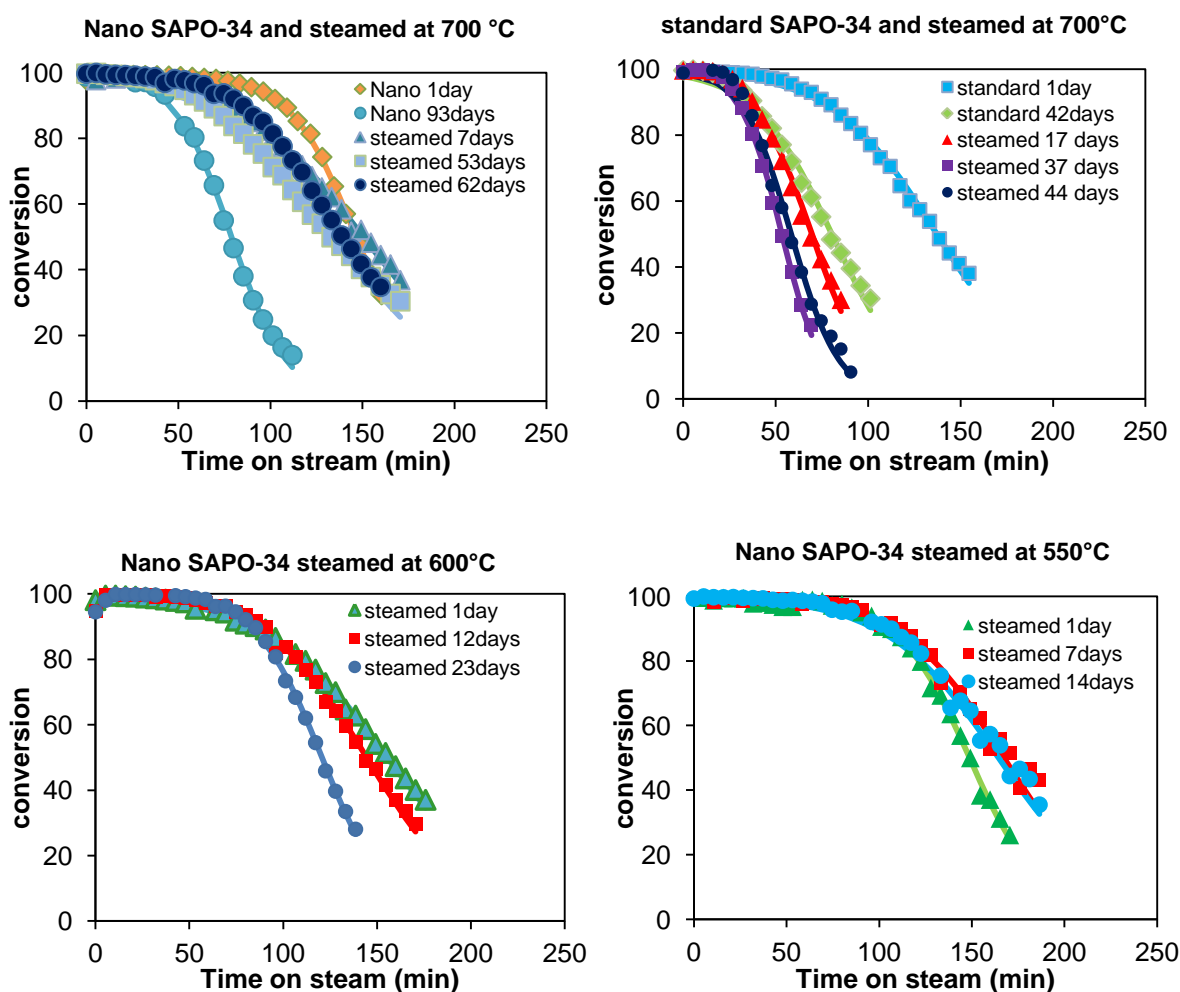


Fig 4.7 Conversion of methanol at 400°C and WHSV= 7 $h^{-1}$ on nano-SAPO-34 and standard-SAPO-34 samples fresh, after steaming at different temperatures and subsequent exposure to moisture. Lines correspond to the fitting following Janssens's kinetic model.

Table 4.3 Kinetic parameters, half lifetime ($t_{0.5}$), breakthrough time ($t_{0.98}$), and methanol conversion capacity of nano and standard-SAPO-34 samples obtained by fitting of Janssen's kinetic model.

| Sample | Days of exposure to moisture | k (mol/gh) | a (g/mmol) | $t_{0.5}$ (min) | $t_{0.98}$ (min) | Methanol conversion capacity ($g_{metanol}/g_{catalyst}$) |
|---|---|---|---|---|---|---|
| Nano SAPO-34 | 1 | 9.98 | 5.6 | 147 | 76.7 | 15.9 |
| | 28 | 6.82 | 3.6 | 231 | 70.0 | 25.1 |
| Nano SAPO-34 St. 700ºC | 7 | 5.51 | 5.5 | 149 | 20.4 | 16.2 |
| | 53 | 5.47 | 6.3 | 131 | 17.2 | 14.2 |
| | 62 | 6.86 | 5.9 | 138 | 42.3 | 15.0 |
| Nano SAPO-34 St. 600ºC | 1 | 5.94 | 5.3 | 155 | 31.1 | 16.9 |
| | 12 | 7.00 | 5.8 | 142 | 45.7 | 15.4 |
| | 22 | 8.85 | 6.8 | 120 | 55.5 | 13.0 |
| Nano SAPO-34 St. 550ºC | 1 | 9.08 | 5.5 | 149 | 71.2 | 16.2 |
| | 7 | 7.70 | 4.9 | 167 | 63.8 | 18.1 |
| | 14 | 7.23 | 4.9 | 166 | 56.9 | 18.1 |

However, the most important observation is that the samples steamed at temperatures ≥550°C present a similar activity and lifetime after days, and even months, of contact with moisture at room temperature. This result would be consistent with the preservation of micropore volume and acidity of steamed samples observed upon exposure to moisture for long periods of time. The long-term stability must be related to the decrease of silicon at the edge of silicon islands due to both, migration of silicon and merging of small to larger islands in which the contribution of edges is less important. In addition, the decrease of Si species at the edge (Si3Al) is also responsible for the longer lifetime of the remaining acid sites since those sites have been considered strongly acid [40-42] and thus, more prone to deactivation by coking.

When the micropore volume of steamed samples of nano-SAPO-34 was plotted versus the temperature of steaming, it appears that an optimum steaming temperature may exist between 600 and 700°C. In fact, at lower steaming temperatures samples are hydrolyzed as shown by BET measurements, while at

higher temperatures the decrease in acidity produced is larger with the correspondent loss of activity observed (Fig 4.5).

Finally, a sample of nano-SAPO-34 which was only thermally treated in air at 700°C was also tested when fresh and after being in contact with moisture at increasing times. It can be clearly seen in Fig 4.8 that despite the high initial lifetime of the fresh thermally treated sample, this strongly decreases when contacted with moisture. This result is in clear contrast what it occurs with the samples steamed at T≥550°C that retain their microporosity, acidity and activity upon exposure to moisture.
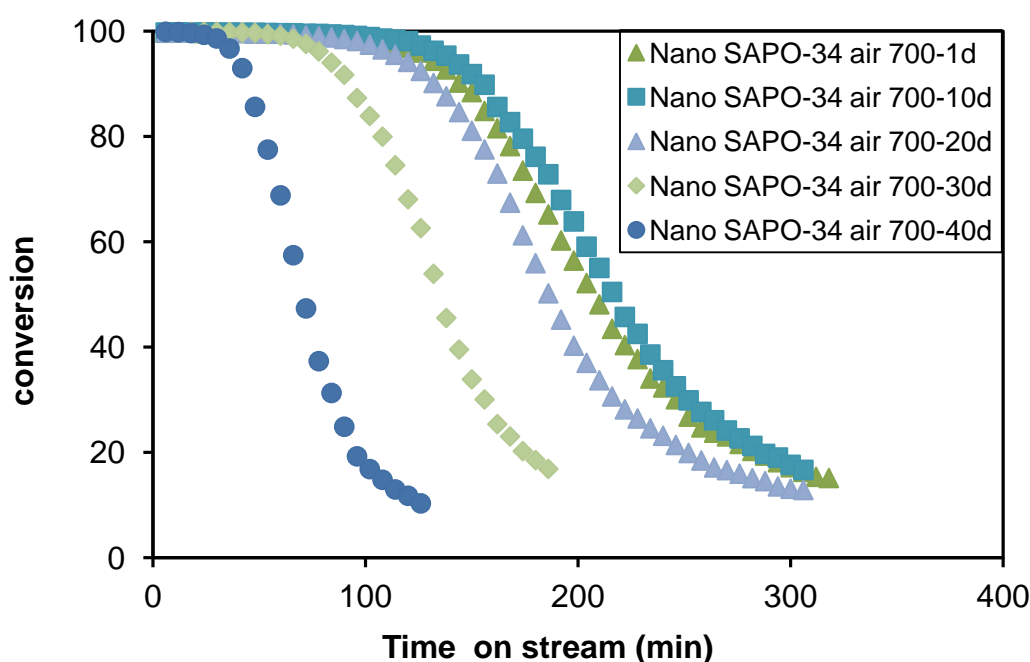


Fig 4.8 Conversion of methanol at 400°C and WHSV= 7 h$^{-1}$ on nano-SAPO-34 thermally treated in air at 700ºC for 5h fresh and after contact with moisture at room temperature up to 40 days.

## 4.3.3.2.Influence of stabilization on catalyst selectivity

Selectivity at constant conversion of the steamed samples is shown in Fig 4.9. Notice that in the case of MTO it is mandatory to compare the selectivities at the same level of conversion. By doing that, the effect of thermodynamic equilibrium among olefins at high methanol conversion, can be isolated from the true selectivity of the hydrocarbon pool in SAPO-34. In fact, it was shown recently [22] that as the hydrocarbon pool forms through the catalytic bed, its selectivity is modified by further secondary reaction on the fresh portion of the catalyst, approaching thermodynamic

equilibrium and masking therefore the selectivity obtained. It is also important to show that while conversion decreases, selectivity is constant being that a clear indication of a "non selective deactivation".
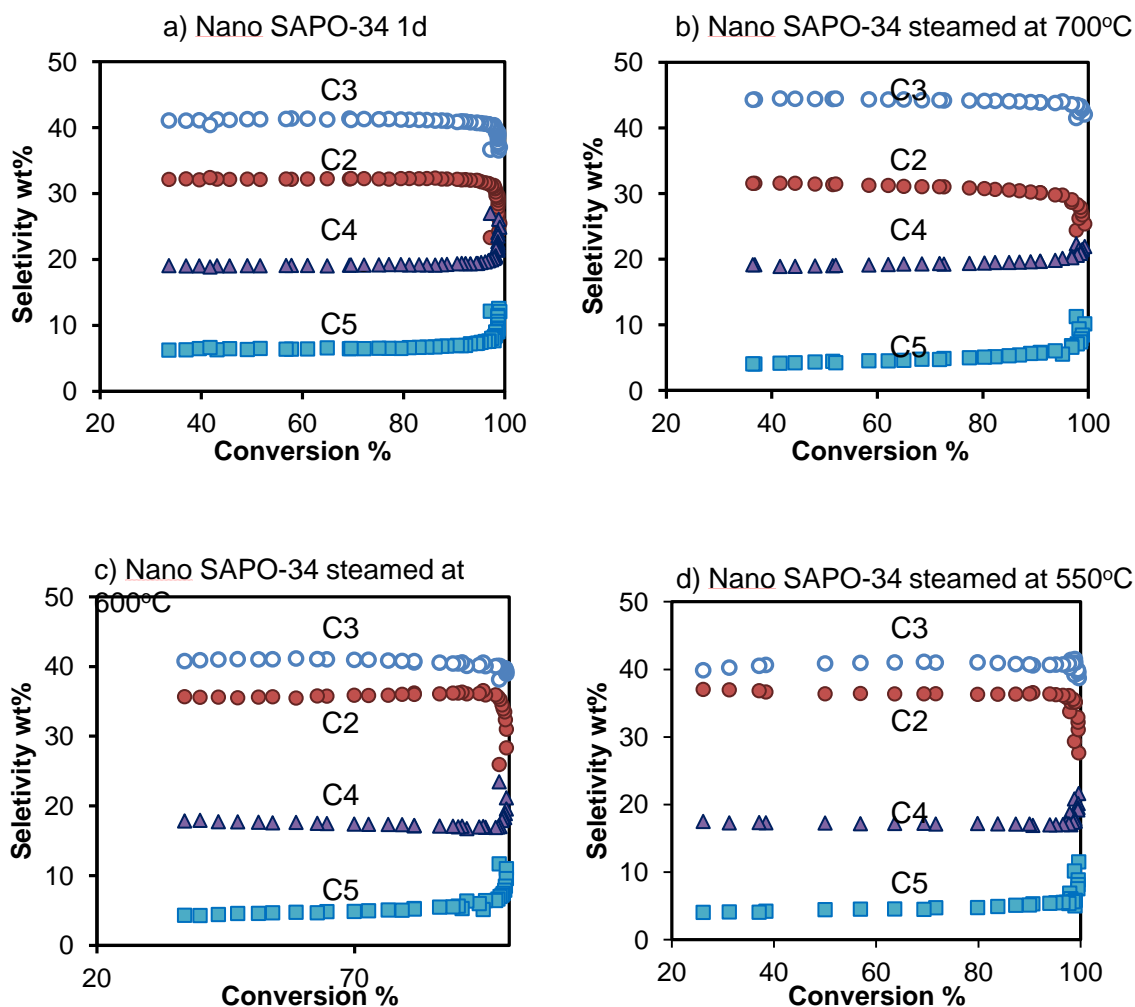


Fig 4.9 Selectivities to C2, C3, C4 and C5+ hydrocarbons in the conversion of methanol   on nano-SAPO-34   fresh and steamed at 550, 600 and 700°C.

When comparing different selectivities of steamed samples at constant conversion it can be seen that $C_2^=/C_3^=$ ratio decreases after steaming when compared with calcined nano-SAPO-34, being the decrease more marked at 700°C of steaming temperature (Fig 4.10). More specifically, the results show an effective decrease of the selectivity to ethylene, while the distribution among the other olefins is not affected. This effect on the selectivity of ethylene must be related to the decrease in the strength of the acid sites due to the formation of larger silicon islands and the consequent decrease in the density of silicon species located at the edge,

when compared with the calcined parent sample, as it is supported by $^{29}$Si NMR results (Table 4.2).

## C2/C3 (mol/mol)
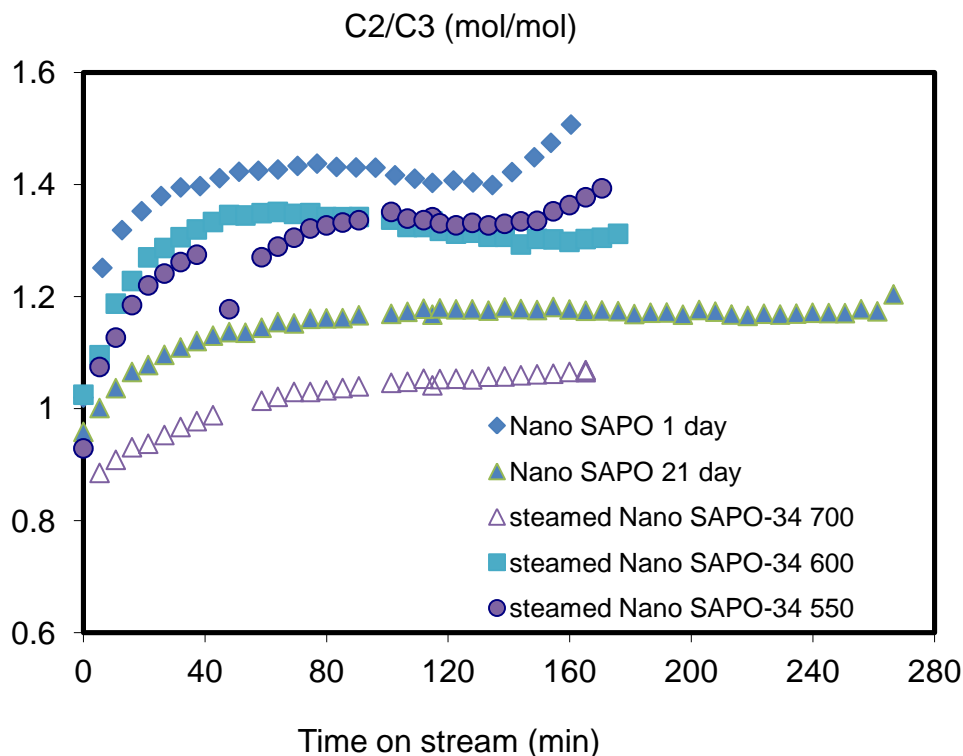


Fig 4.10 C2/C3 ratio of products in the conversion of methanol at 400ºC and WHSV = 7 h$^{-1}$ on nano-SAPO-34 fresh and after steaming at 550, 600 and 700°C.

Previously, when the parent nano-SAPO-34 (20 nm) was compared with a standard SAPO-34 of similar total acidity and much larger crystal size (500nm), nano-SAPO-34 presented much higher $C_2^=/C_3^=$ ratio [18], indicating that this ratio is not controlled by a faster diffusion of ethylene vs. propylene [5, 43, 44] but it would support the fact that with a higher acid strength, the olefin selectivity is produced through aromatic intermediates by the side-chain methylation mechanism [45]. If this is so, then a SAPO-34 with higher acid strength should yield more ethene since the formation from a hexa or tetramethylbenzene reaction center is less energetically favoured [46]. Recently when comparing the selectivities of isomorphous SAPO-5 to SSZ-24 for MTH, it has been proposed the key reaction steps of the alkene and arene cycles can display a different sensitivity to acid strength [47]. If in the case of SAPO-34, only the arene cycle participates in the mechanism, it is logical to think that one bottleneck of the mechanism is the final elimination of the olefin from the

arene, and that propene elimination should be more favored than ethene. In addition, there is also the possibility that both cycles, alkene and arenes participate in SAPO-34, even in this case, as occurs for SAPO-5 a lower acidity strength could drive the mechanism to a higher contribution of the alkene cycle, in which ethene yield is not produced by oligomerization-cracking at the relatively low temperatures of MTO. In our case, after steaming of nano-SAPO-34, the $C_2^=/C_3^=$ ratio also decreases when compared with the parent sample, in line with a decrease in the distribution of silicon species at the edge of silicon islands.

We can conclude from the experimental data that selectivity is governed by silicon distribution, (which has been modified by steaming) and not by shape selectivity effects, due to preferential diffusion of ethene or deactivation by coke.

## 4.3.3.3. Methodology suggested for performing SAPO-34 stability tests

In addition, the results presented in this contribution help to define which are the best conditions to perform a SAPO-34 stability test that simulates a long period of a working catalyst with many cycles of reactions and regeneration, both in the presence of water. This has been done for other petrochemical process using zeolites in the catalyst inventory as it is the case of Fluid Catalytic Cracking. In this case, steaming at temperatures of 750°C or higher and high partial pressures of water are used for simulating an equilibrium catalyst. However, this kind of hydrothermal stability test does not seem suitable for SAPO-34 since the mechanism of dealumination for zeolites is different from the desilication on silicoaluminophosphates [38]. In fact, while steaming at high temperature generates wide dealumination in ZSM-5 crystals with severe loss of acidity [48-50], in the case of standard SAPO-34, both, textural and acidity properties are preserved (see Table 1 and ref. [26]). Moreover, if the SAPO-34 sample presents high mesoporosity, as it is the case of the nano-SAPO-34 sample, steaming at 400°C strongly affects the stability. Our results indicate that SAPO-34 samples, especially if they are of hierarchical nature, should be submitted to hydrothermal stability test at low temperature, similar to the reaction temperature of methanol to olefins in order to evaluate their properties as potential MTO catalyst. Then, if required, they can be stabilized by steaming at 600-700°C.

# 4.4.Conclusions

Nano-SAPO-34 has been stabilized towards contact with moisture by steaming at T≥550ºC. The stabilization effect is attributed to the migration of silicon to larger silicon islands in which the overall contribution of Si species on the edge of silicon islands has been reduced. The role of steam at high temperature is to facilitate the migration of silicon while the vacancies are healed by phosphorus. In the absence of steam, thermally treated nano-SAPO-34 is not stabilized and its lifetime decreases after contact with moisture. At low temperature of steaming the structure of nano-SAPO-34 collapses due to the hydrolysis of Si-O-Al bonds. Suitable hydrothermal stability tests for nanosized or mesoporous SAPO-34 samples should include steaming at temperatures close to the temperature of the reaction of methanol and, if required, stabilization by steaming at T≥550°C should be performed.

# References

[1] Z. Liu, Y. Wei, P. Tian, L. Xu, Methanol to olefin: from fundamental to commercialization, 17th International Zeolite Conference, Moscow, 2013.

[2] Annual Energy Outlook 2012 with Projections to 2035, in, U.S. Energy Information Administration, 2012.

[3] M. Stöcker, Methanol to Olefins (MTO) and Methanol to Gasoline (MTG), in: Zeolites and Catalysis, Wiley-VCH Verlag GmbH & Co. KGaA, 2010, pp. 687-711.

[4] H. Koempel, W. Liebner, Lurgi's Methanol To Propylene (MTP) Report on a successful commercialisation, Study in Surface Science and Catalysis, Elsevier, 2007, pp. 261-267.

[5] P. Barger, Methanol to olefins (MTO) and beyond, in: M. Guisnet, J.P. Gilson (Eds.) Zeolites for Cleaner Technologies (Catalytic Science Series Vol. 3), Imperial College Press, London, 2002, pp. 239-260.

[6] S. Kvisle, H.R. Nilsen, T. Fuglerud, A. Gronvold, B.V. Vora, P.R. Pujado, P.T. Barger, J.M. Andersen, Methanol to olefins: state of the art and perspectives, Erdöl, Erdgas, Kohle, 118 (2002) 361-365.

[7] S. Wilson, P. Barger, The characteristics of SAPO-34 which influence the conversion of methanol to light olefins, Microporous Mesoporous Materials, 29 (1999) 117-126.

[8] J.F. Haw, D.M. Marcus, Well-defined (supra)molecular structures in zeolite methanol-to-olefin catalysis, Topics in Catalysis, 34 (2005) 41-48.

[9] S.T. Yang, J.Y. Kim, H.J. Chae, M. Kim, S.Y. Jeong, W.S. Ahn, Microwave synthesis of mesoporous SAPO-34 with a hierarchical pore structure, Materials Research Bulletin, 47 (2012) 3888-3892.

[10] Y. Cui, Q. Zhang, J. He, Y. Wang, F. Wei, Pore-structure-mediated hierarchical SAPO-34: Facile synthesis, tunable nanostructure, and catalysis applications for the conversion of dimethyl ether into olefins, Particuology, 11 (2013) 468-474.

[11] H. Yang, Z. Liu, H. Gao, Z. Xie, Synthesis and catalytic performances of hierarchical SAPO-34 monolith, Journal of Materials Chemistry, 20 (2010) 3227-3231.

[12] J. Zhu, Y. Cui, Y. Wang, F. Wei, Direct synthesis of hierarchical zeolite from a natural layered material, Chemical communications (Cambridge, England), (2009) 3282-3284.

[13] F. Schmidt, S. Paasch, E. Brunner, S. Kaskel, Carbon templated SAPO-34 with improved adsorption kinetics and catalytic performance in the MTO-reaction, Microporous Mesoporous Materials, 164 (2012) 214-221.

[14] S. Lin, J. Li, R.P. Sharma, J. Yu, R. Xu, Fabrication of SAPO-34 crystals with different morphologies by microwave heating, Topics in Catalysis., 53 (2010) 1304-1310.

[15] Y. Hirota, K. Murata, S. Tanaka, N. Nishiyama, Y. Egashira, K. Ueyama, Dry gel conversion synthesis of SAPO-34 nanocrystals, Materials Chemistry and Physics, 123 (2010) 507-509.

[16] T. Álvaro-Muñoz, C. Márquez-Álvarez, E. Sastre, Enhanced stability in the methanol-to-olefins process shown by SAPO-34 catalysts synthesized in biphasic medium, Catalysis Today, 215 (2013) 208-215.

[17] T. Álvaro-Muñoz, C. Márquez-Álvarez, E. Sastre, Use of different templates on SAPO-34 synthesis: Effect on the acidity and catalytic activity in the MTO reaction, Catalysis Today, 179 (2012) 27-34.

[18] W. Pengfei, Y. Dexing, H. Jie, X. Jing'an, L. Guanzhong, Synthesis of SAPO-34 with small and tunable crystallite size by two-step hydrothermal crystallization and its catalytic performance for MTO reaction, Catalysis Today, 212 (2013).

[19] M. Yang, P. Tian, C. Wang, Y. Yuan, Y. Yang, S. Xu, Y. He, Z. Liu, A top-down approach to prepare silicoaluminophosphate molecular sieve nanocrystals with improved catalytic activity, Chemical communications (Cambridge, England), (2014).

[20] S.C. Fung, D. Levin, J. Santiesteban, N.P. Coute, Conversion of oxygenates into olefins using a metal oxide-containing zeolitic molecular sieve catalyst, in, Exxonmobil Chemical Patents Inc., USA . 2006, pp. 12 pp.

[21] G. Yang, Y. Wei, S. Xu, J. Chen, J. Li, Z. Liu, J. Yu, R. Xu, Nanosize-Enhanced Lifetime of SAPO-34 Catalysts in Methanol-to-Olefin Reactions, The Journal of Physical Chemistry C, 117 (2013) 8214-8222.

[22] Z. Li, J. Martinez-Triguero, P. Concepcion, J. Yu, A. Corma, Methanol to olefins: activity and stability of nanosized SAPO-34 molecular sieves and control of selectivity by silicon distribution, Physical Chemistry Chemical Physics, 15 (2013) 14670-14680.

[23] M. Briend, R. Vomscheid, M.J. Peltre, P.P. Man, D. Barthomeuf, Influence of the Choice of the Template on the Short- and Long-Term Stability of SAPO-34 Zeolite, J.Phys.Chem., 99 (1995) 8270-8276.

[24] F.D.P. Mees, L.R.M. Martens, M.J.G. Janssen, A.A. Verberckmoes, E.F. Vansant, Improvement of the hydrothermal stability of SAPO-34, Chemical Communication, 9 (2003) 44-45.

[25] A. Buchholz, W. Wang, A. Arnold, M. Hunger, Successive steps of hydration and dehydration of silicoaluminophosphates H-SAPO-34 and H-SAPO-37 investigated by in situ CF MAS NMR spectroscopy, Microporous Mesoporous Materials, 57 (2003) 157-168.

[26] L.R. Aramburo, J. Ruiz-Martínez, L. Sommer, B. Arstad, R. Buitrago-Sierra, A. Sepúlveda-Escribano, H.W. Zandbergen, U. Olsbye, F.M.F. de Groot, B.M. Weckhuysen, X-Ray Imaging of SAPO-34 Molecular Sieves at the Nanoscale: Influence of Steaming on the Methanol-to-Hydrocarbons Reaction, ChemCatChem, 5 (2013) 1386-1394.

[27] A. Buchholz, W. Wang, M. Xu, A. Arnold, M. Hunger, Sequential Steps of Ammoniation of the Microporous Silicoaluminophosphates H-SAPO-34 and H-SAPO-37 Investigated by In Situ CF MAS NMR Spectroscopy, Journal of Physical Chemistry B, 108 (2004) 3107-3113.

[28] J. Klinowski, J.M. Thomas, C.A. Fyfe, G.C. Gobbi, Monitoring of structural changes accompanying ultrastabilization of faujasitic zeolite catalysts, Nature, 296 (1982) 533-536.

[29] G. Liu, P. Tian, Y. Zhang, J. Li, L. Xu, S. Meng, Z. Liu, Synthesis of SAPO-34 templated by diethylamine: Crystallization process and Si distribution in the crystals, Microporous Mesoporous Materials, 114 (2008) 416-423.

[30] Q. Zhu, J.N. Kondo, T. Tatsumi, S. Inagaki, R. Ohnuma, Y. Kubota, Y. Shimodaira, H. Kobayashi, K. Domen, A Comparative Study of Methanol to Olefin over CHA and MTF Zeolites, Journal of Physical Chemistry C, 111 (2007).

[31] C.S. Blackwell, R.L. Patton, Solid-state NMR of silicoaluminophosphate molecular sieves and aluminophosphate materials, The Journal of Physical Chemistry, 92 (1988) 3965-3970.

[32] Y. Watanabe, A. Koiwai, H. Takeuchi, S.A. Hyodo, S. Noda, Multinuclear NMR Studies on the Thermal Stability of SAPO-34, Journal of Catalysis, 143 (1993) 430-436.

[33] A. Buchholz, W. Wang, M. Xu, A. Arnold, M. Hunger, Thermal stability and dehydroxylation of brønsted acid sites in silicoaluminophosphates H-SAPO-11, H-SAPO-18, H-SAPO-31, and H-SAPO-34 investigated by multi-nuclear solid-state NMR spectroscopy, Microporous Mesoporous Materials, 56 (2002) 267-278.

[34] M.J. Peltre, P.P. Man, M. Briend, M. Derewinski, D. Barthomeuf, Changes upon heating of the distribution of Al, P and Si atoms in the SAPO-37 molecular sieve, Catalysis Letters, 16 (1992).

[35] D. Miroslav, P. Marie Jeanne, B. Marguerite, B. Denise, P.M. Pascal, Solid-state transformation of SAPO-37 molecular sieve above 1100 K, Journal of Chemical Society, Faraday Transaction, 89 (1993).

[36] P.T. Barger, D.A. Lesch, Hydrothermal stability of SAPO-34 in the methanol-to-olefins process, Arabian Journal for Science and Engineering, 21 (1996) 263-272.

[37] Y.-K. Park, S.-W. Baek, S.-K. Ihm, Effect of reaction conditions and catalytic properties on methanol conversion over SAPO-34, Journal of Industrial and Engineering Chemistry (Seoul, Repub. Korea), 7 (2001) 167-172.

[38] T. Fjermestad, S. Svelle, O. Swang, Mechanistic Comparison of the Dealumination in SSZ-13 and the Desilication in SAPO-34, The Journal of Physical Chemistry C, 117 (2013).

[39] T.V.W. Janssens, A new approach to the modeling of deactivation in the conversion of methanol on zeolite catalysts, Journal of Catalysis, 264 (2009) 130-137.

[40] G.A.V. Martins, G. Berlier, S. Coluccia, H.O. Pastore, G.B. Superti, G. Gatti, L. Marchese, Revisiting the nature of the acidity in chabazite-related silicoaluminophosphates: Combined FTIR and29Si MAS NMR study, Journal of Physical Chemistry C, 111 (2007) 330-339.

[41] G. Sastre, D.W. Lewis, C. Richard, A. Catlow, Modeling of silicon substitution in SAPO-5 and SAPO-34 molecular sieves, Journal of PhysicalvChemistry B, 101 (1997) 5249-5262.

[42] D. Barthomeuf, Topological model for the compared acidity of SAPOs and SiAl zeolites, Zeolites, 14 (1994) 394-401.

[43] I.M. Dahl, H. Mostad, D. Akporiaye, R. Wendelbo, Structural and chemical influences on the MTO reaction: a comparison of chabazite and SAPO-34 as MTO catalysts, Microporous Mesoporous Materials, 29 (1999) 185-190.

[44] B.P.C. Hereijgers, F. Bleken, M.H. Nilsen, S. Svelle, K.P. Lillerud, M. Bjørgen, B.M. Weckhuysen, U. Olsbye, Product shape selectivity dominates the Methanol-to-Olefins (MTO) reaction over H-SAPO-34 catalysts, Journal of Catalysis, 264 (2009) 77-87.

[45] K. Hemelsoet, J. Van der Mynsbrugge, K. De Wispelaere, M. Waroquier, V. Van Speybroeck, Unraveling the Reaction Mechanisms Governing Methanol-to-Olefins Catalysis by Theory and Experiment, ChemPhysChem, 14 (2013) 1526-1545.

[46] B. Arstad, J.B. Nicholas, J.F. Haw, Theoretical Study of the Methylbenzene Side-Chain Hydrocarbon Pool Mechanism in Methanol to Olefin Catalysis, Journal of American Chemical Society, 126 (2004) 2991-3001.

[47] M. Westgård Erichsen, S. Svelle, U. Olsbye, The influence of catalyst acid strength on the methanol to hydrocarbons (MTH) reaction, Catalysis Today 215 (2013) 216-223.

[48] T. Blasco, A. Corma, J. Martineztriguero, Hydrothermal stabilization of ZSM-5 catalytic-cracking additives by phosphorus addition, Journal of Catalysis, 237 (2006) 267-277. [

[49] G. Caeiro, P. Magnoux, J.M. Lopes, F.R. Ribeiro, S.M.C. Menezes, A.F. Costa, H.S. Cerqueira, Stabilization effect of phosphorus on steamed H-MFI zeolites, Applied Catalysis A: General, 314 (2006).

[50] M.T.A. Sami, M. Brahim, A.P. Evgeny, C.M.M.M. Pieter, J.M.H. Emiel, Influence of steaming on the acidity and the methanol conversion reaction of HZSM-5 zeolite, Journal of Catalysis, 307 (2013) 194-203.

# 5. Synthesis of nano-SSZ-13 and the application in the reaction of methanol to olefins

# 5.1.Introduction

Methanol to olefins (MTO) is an important reaction for obtaining ethylene and propylene which are principal chemicals for the polymer industry, especially with the development of shale gas and the price decrease of natural gas. Currently, the most widely used materials for MTO are zeolites ZSM-5(10 member-ring) and SAPO-34 (8 member-ring).  ZSM-5 offers the versatility to be used to yield propylene (MTP) or aromatics (MTG) depending on the reaction conditions and the Si/Al ratio of the catalyst [1-3]. SAPO-34 due to the size of its channels that hinder the diffusion of aromatics yields mainly ethylene and propylene. However the diffusion limitations for reactants and products and the formation of coke deposits in the cages, results in faster deactivation and low catalyst utilization. This is common for most industry processes catalyzed by zeolites such as cracking, isomerization, alkylation and so on [4, 5].

To overcome the diffusion problems, several approaches have been proposed such as to reduce the crystallite size of the catalyst with the purpose of increasing the external surface area and shortening the diffusion path length or by the generation of mesoporosity in the microporous zeolites. In this way, the generation of hierarchical zeolite can be obtained by direct synthesis or by post-treatment methods. Hierarchical zeolites present advantages such as enabling the formation of molecules larger than the micropores and offering  mesoporous channels for fast diffusion and mass transport to avoid the coke deposition on the catalytic sites to improve catalyst lifetime and reactant conversions [6].  Following this, much effort has been taken on the synthesis of nano sheet ZSM-5[7, 8] and meso-ZSM-5 by desilication [5, 9-12] or by soft or hard templating [13, 14] and other surfactants [6, 13, 15]. In the case of SAPO-34, its performance has been improved by developing mesopores [16-20] and by synthesizing crystals of smaller size [21-28].

The use of dual templates which contains small organic struture directing agent for the formation of micropores and large organic surfactants molecular for developing mesopores as a strategy to prepare meso-MFI has been proposed by the earlier researchers[29-34]. The large molecular surfactant hexadecyl trimethyl ammonium bromide (CTAB) firstly used to prepare MCM-41 has been employed to the synthesis of hierarchical zeolites [35-37] in the dual template method. It has been

shown that the zeolite precusor contains primary units of zeolite seeds, nanocyrstals, nano particles and subnanocrystals which assembly and grow to zeolite crystal by feeding later in the crystallization. With the addition of CTAB, the the process of zeolite crystalization is delayed and the formation the mesopoures phase is accelerated and controlled by kinetic priority [35, 36].

SSZ-13 the aluminosilicate homologue of SAPO-34 with CHA topology [38, 39] has offered a alternative for MTO. Due to its higher acidity strength, the reaction of methanol to olefins starts at lower low temperature or with a high flow rate, which could save energy and smooth the reactor design [40, 41]. However, also due to the higher acidity strength, SSZ-13 presents similar or even faster deactivation that SAPO-34. In order to improve the pore acessibility and diffusion to reduce the deactivation, Olsbye and co-authors have tried to modified H-SSZ-13 by alkaline treatment to form mesopores in the catalyst. However, the success was very limited and lifetime of the material was not improved [42]. In contrast, the catalyst performance of SSZ-13 was enhanced after neutron irradiation that induced structural defects [43]. Recently, Hensen et al. have applied a co-template way to the synthesis of SSZ-13, showing an increased mesoporosity and lifetime for SSZ-13 [34]. In this work, we have prepared nano-SSZ-13 by direct or one-pot synthesis strategy by the addition of hexadecyl trimethyl ammonium bromide (CTAB) into the zeolite precursor. A similar method has been also used in the synthesis of heriarchical ZSM-5 by Zhu et al.[44]. We have studied the catalyst performance in methanol to olefins compared with the conventional SSZ-13, and the stability by steaming treatment. Moreover, we will show how the reduced size of the crystallites affects selectivity, acidity, deactivation and lifetime.

# 5.2.Experimental

## 5.2.1.Catalyst synthesis

Conventional SSZ-13 was synthesized with the gel composition as follows: $0.1Na_2O:1SiO_2:0.025Al_2O_3:0.2TMAdOH:44H_2O$.N,N,N-trimethyl-1-adamantanammonium hydroxide (TMAdOH) was firstly mixed with NaOH and deionized water at room temperature until it was dissolved completely. Then, TMAdOH solution was added, with the following addition of $SiO_2$ (Aerosil) as the silica source. Finally, $Al_2O_3$ was

dissolved into the solution mentioned above. The resulting gel was stirred at room temperature for 1 hour to obtain a homogeneous gel, which was then transferred into a Teflon-lined steel autoclave and kept statically in oven at 160°C for 6 days. The product was separated by filtration, washed with deionized water and dried at 100°C. The catalyst was calcined at 580°C to removal the template air. H-SSZ-13 was obtained by ion exchange of calcined sample with 2.5M $NH_4Cl$ solution (80°C and liquid to solid ratio of 10) for 2 hours and then calcined at 500 °C for three hours in air.

Nano-SSZ-13 was synthesized with same procedure and gel composition as SSZ-13 with the difference of the addition of CTAB (hexadecyl trimethyl ammonium bromide) after the resulting gel was left in oven at 160°C for 1day. After CTAB was mixed completely with the solution, the resulted gel was then transferred into the Telfon-line steel autoclave again and heated in oven at the same temperature for 9 days. The product was recovered by filtration, washed with deionized water, dried, calcined at 580°C, and followed by the ion exchange with $NH_4Cl$ solution and calcinations at 500°C.

## 5.2.2. Characterization

The characterizations are carried out in the same way as described in the Chapter 3.

## 5.2.3. Catalytic experiments

The test conditions of the catalyst in this chapter are almost the same as we have shown in Chapter 3, but  methanol was introduced by saturating $N_2$ (30mL/min) through a bubble hold at -17°C, being the space velocity WHSV=0.8 $h^{-1}$. After reaction, the catalyst was regenerated at 540°C in 80ml of air for 3h and the reaction was repeated again. Conversion and selectivities were calculated in carbon basis being methanol and dimethylether considered as feed.

# 5.3. Results and discussion

## 5.3.1. Characterization
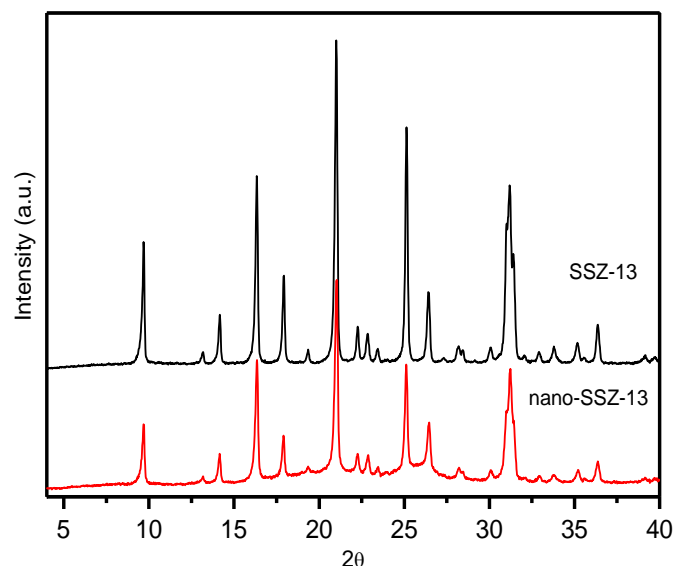


Fig 5.1 The XRD patterns of the synthesized standard SSZ-13 and nano-SSZ-13.

The XRD patterns of the synthesized standard SSZ-13 and nano-SSZ-13 are shown in Fig 5.1 after template removal by calcination. The nano-SSZ-13 shows same peaks position and shapes as the standard SSZ-13 typical of CHA topology type structure. However, the intensity of the nano-SSZ is lower, which is assigned to partial loss of micropore volume and also to a decrease in the size of the crystal.

The Fig 5.2 shows the SEM and TEM images of the standard SSZ-13 and the nano-SSZ-13. The standard SSZ-13 presents highly overlapped growth and irregular crystal with the size in the range of 1.5-2.5µm, while the nano-SSZ-13 shows different morphology with aggregates of nanoscale size as sheets in the range of 150-500 nm. The TEM images confirm that with the addition of surfactant the size of the crystallites of nano-SSZ-13 is much smaller than standard SSZ-13 and presents interparticle mesoporosity.
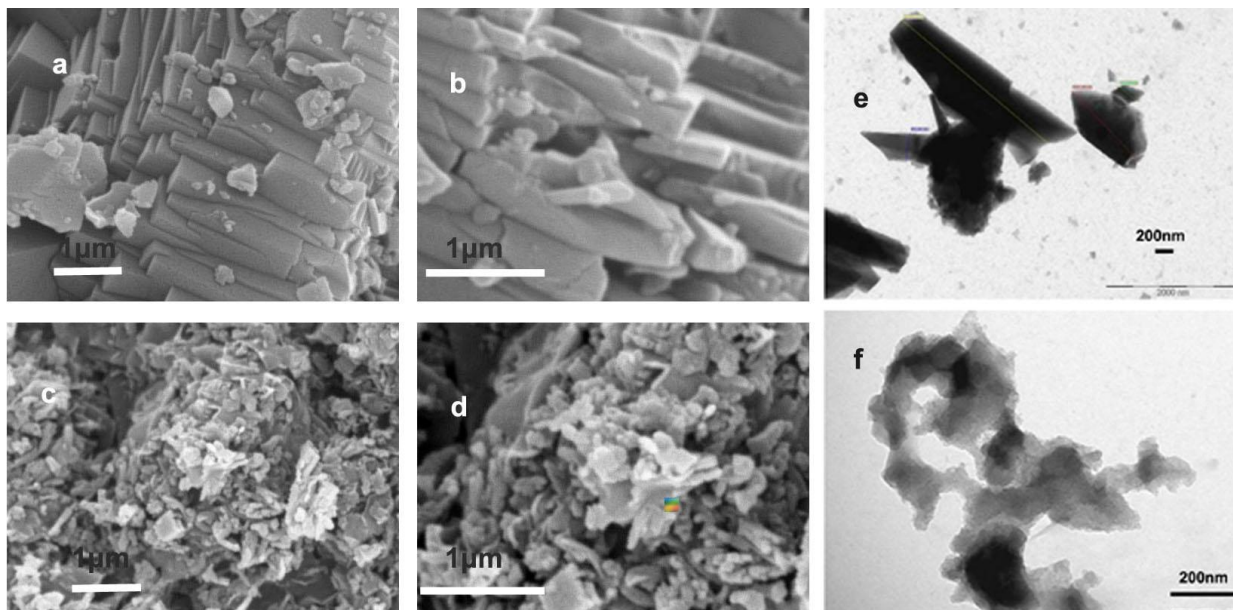
Fig 5.2 SEM images of the standard SSZ-13,a,b) nano SSZ-13, c, d) and TEM images of Standard SSZ-13 e) nano SSZ-13,f).
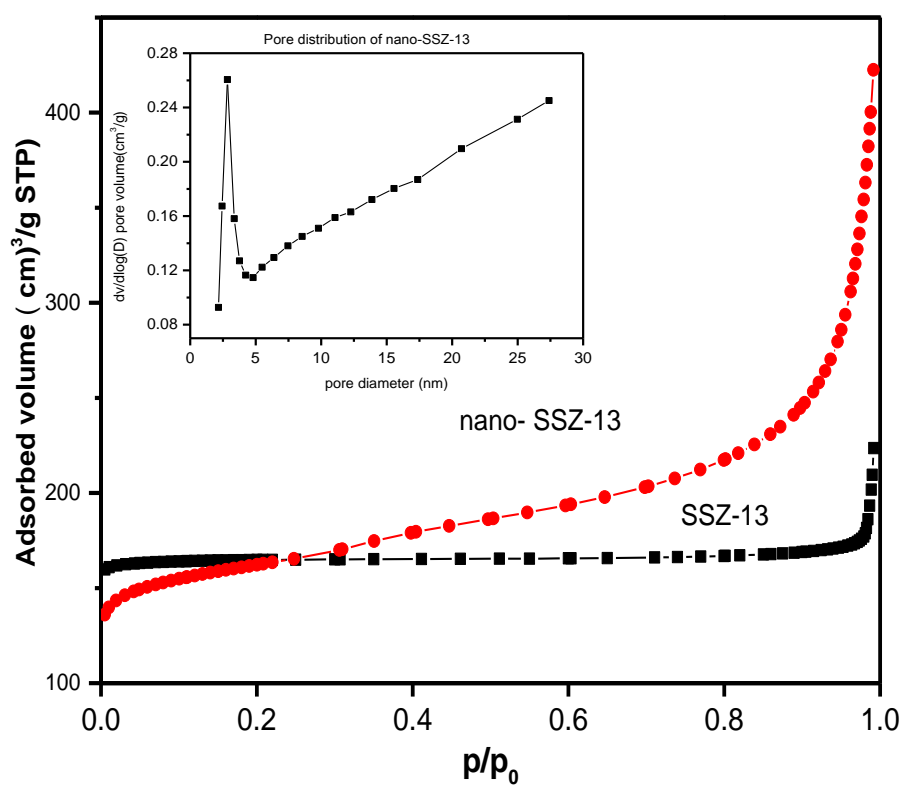


Fig 5.3 $N_2$ adsorption isotherms of nano and standard SSZ-13, and pre size distribution of nano-SSZ-13.

Table 5.1 The textural properties of the SSZ-13 and nano SSZ-13.

| SAMPLE | Si/Al | SDA | T (°C) | t (d) | BET (m²/g) | $A_{micro}$ (m²/g) | $A_{Ext}$ (m²/g) | $V_{micro}$ (cm³/g) | $V_{meso}$ (cm³/g) |
|---|---|---|---|---|---|---|---|---|---|
| SSZ-13 | 15.3 | TMAdOH | 160 | 6 | 520 | 517 | 3 | 0.253 | 0.093 |
| nano-SSZ-13 | 17 | TMAdOH+CTABr | 160 | 1+9 | 530 | 401 | 129 | 0.204 | 0.446 |

More information can be obtained from the $N_2$ adsorption isotherms showed in Fig 5.3 and the textural properties of the samples summarized in Table 5.1. Fig 5.3 shows the SSZ-13 synthesized in the traditional way exhibit a type I isotherm due to the microporosity, however the nano-SSZ-13 presents characteristic isotherm of type IV with the initial stage of steep uptake due to the micropore and another sharp inflection at P/P0 =0.8-1.0 which is assigned to condensation in the interparticles. The final uptake at high pressure agrees with an interparticle mesoporosity due to the small nanocrystals of nano-SSZ-13. Pore size distribution (PSD) of nano-SSZ-13 presents a narrow peak at 3nm typical of mesoporous materials. The isotherm is very similar to that obtained with nano-SAPO-34 with crystal size of 20 nm and shown in chapter 3.

Both samples show similar BET surface areas though the nano-SSZ-13 sample shows a little larger value than the standard one. However, the former sample presents extremely high external surface area (129 m²/g) compared with the standard SSZ-13 (3 m²/g) as the consequence of appearance of smaller crystallites. In addition, nano-SSZ-13 shows much larger mesopore volume compared with the standard SSZ-13, which is consistent with the result in Table 5.1The high external surface of nano-SSZ-13 will offer increased accessibility, and will have a strong impact on the catalytic performance in the reaction of methanol to olefins.
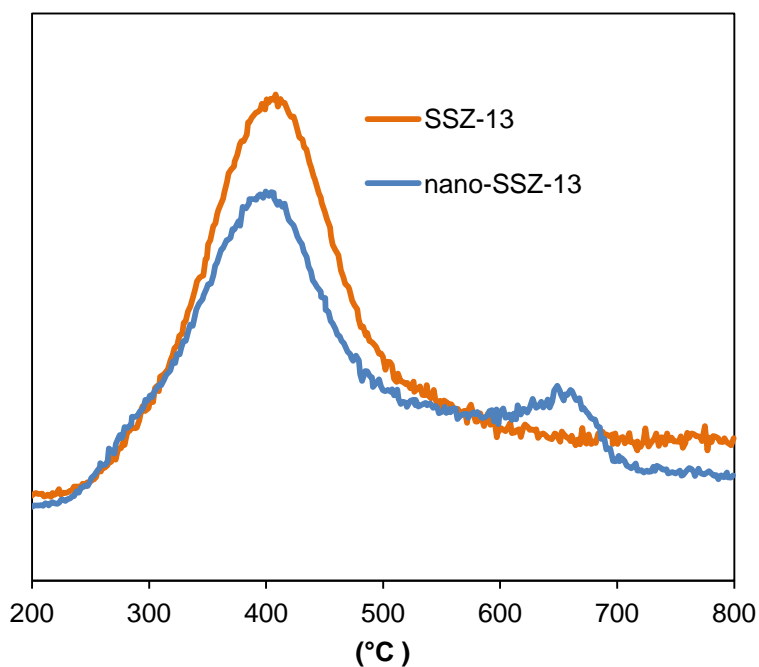
Fig 5.4 NH$_3$-TPD curves of standard and nano-SSZ-13.

Acidity of samples measured by adsorption of ammonia is shown in Fig 5.4. When comparing the shape of desorption (Fig 5.4) all samples present a main component with a maximum in the range from 337 to 407°C, and a shoulder at 280°C. The peak at 407°C of desorption corresponds mainly to Brönsted acidity. The lower intensity of the nano-SSZ-13 corresponds to lower amount of acid sites comparing with standard SSZ-13, that agrees with its lower aluminum content. The shoulder at 280°C for nano-SSZ-13 assigned to sites of weak acidity and must be attributed mainly to external silanols or Lewis acidity of extra-framework. This peak is intentionally suppressed due to the temperature of adsorption of ammonia done at 175°C. The shoulder at 657°C corresponds to interference with water due to dehydroxylation at high temperature.
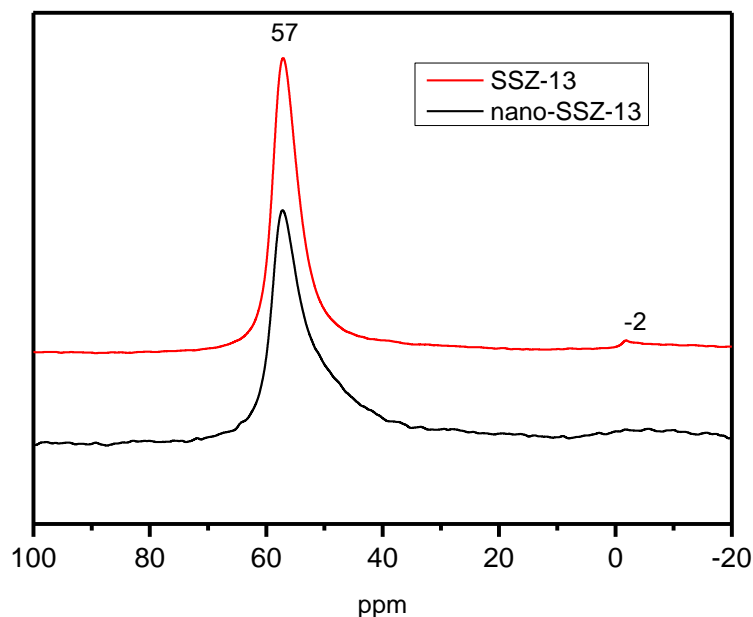
Fig 5.5 ^{27}Al NMR of the standard and nano-SSZ-13.

The ^{27}Al NMR MAS spectra of all samples are shown in Fig 5.5. All spectra present a dominant signal at 57 ppm characteristic of tetracoordinated framework aluminum and a low intensity one at around -2 ppm due to the presence of octahedral extra-framework aluminum. The signal at 57 of nano-ssz-13 is more asymmetrical and also presents a small broad band of octahedral aluminum close to 0 ppm that is sharper for standard SSZ-13.

Information about the structural defects and different Si coordination is given in the ^{29}Si NMR spectra Fig 5.6. The samples show resonances at -112, -106 and -99 corresponding to Si(4Si), Si(3Si 1Al), Si(2Si 2Al) and other signal at -102 that has been assigned to Si-OH(defects) [45]. The presence of mesoporosity in nano-SSZ-13 is reflected in a decrease in the -106 signal while the signal at -102 ppm due to structural defects increases comparing to the standard SSZ-13(shown in Table 5.2).
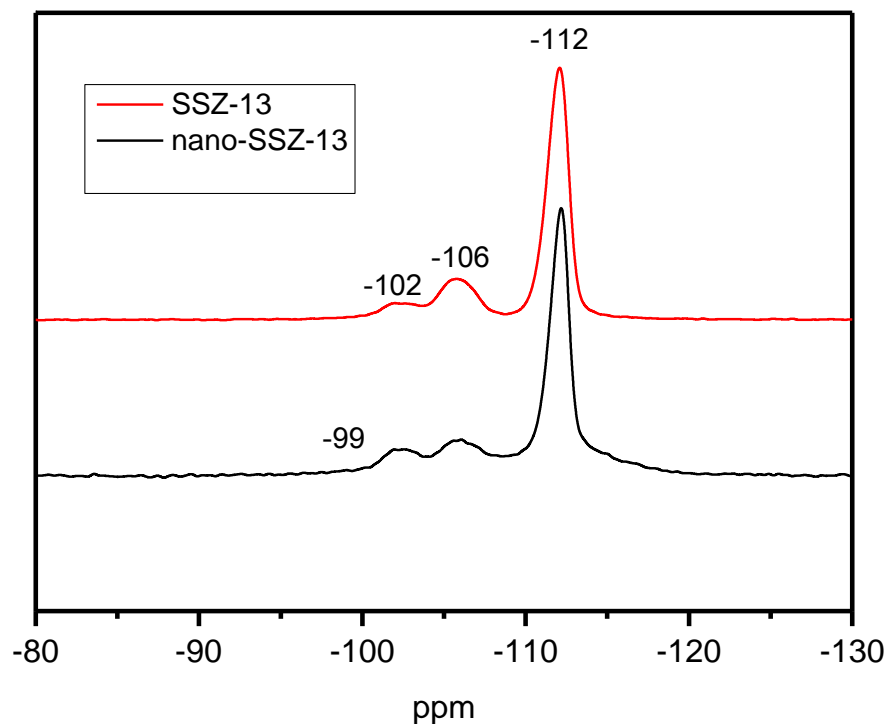
Fig 5.6 ^{29}Si NMR of the standard and nano-SSZ-13.

Table 5.2 Si/Al ratio from ^{29}Si NMR deconvonlusion and acidity measured by $NH_3$ temperature at 175 °C.

| Sample | Si/Al | Si-OH defects (wt%) | $NH_3$(mmol/g) |
|---|---|---|---|
| SSZ-13 | 16.5 | 5.6 | 0.66 |
| nano-SSZ-13 | 17.5 | 8.2 | 0.43 |

## 5.3.2. Catalytic performance

The activity of the samples in the reaction of methanol to olefins at WHSV=0.8 h^{-1} and 350 °C is shown in Fig 5.7. These reaction conditions have been used recently by Wu et al. [46] for testing mesoporous SSZ-13 samples obtained by adding mesoporogen agents to the synthesis gel and hence, the results obtained with nano-SSZ-13 can be compared with those mesoporous SSZ-13 samples. As it can be seen, all samples show initial 100% conversion from the beginning after the induction period, then, after the time of breakthrough the conversion decreases with the time on stream due to acidity loss and coke deposition. It is important to note that

nano-SSZ-13 shows much longer lifetime than the standard SSZ-13 in agreement with the presence of intercrystalline mesoporosity which improves the diffusion rate and decreases the negative effect of coke in the channels. In the case of standard SSZ-13 conversion decreases to 50% at 310 min, while for nano-SSZ-13 50% conversion is obtained at 760 min, which states its higher lifetime
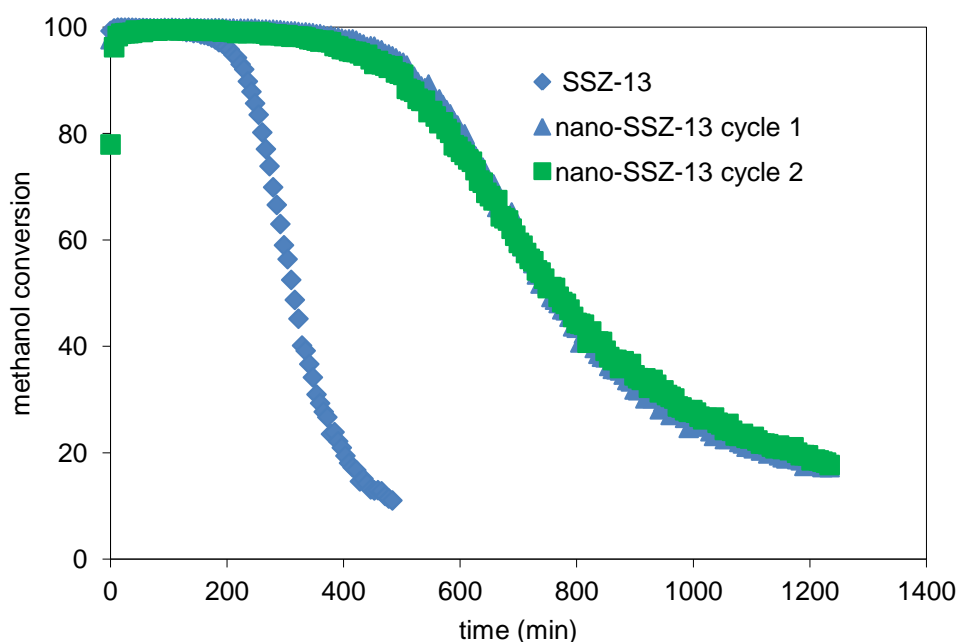


Fig 5.7 Conversion of methanol at 350°C and WHSV=0.8 h$^{-1}$ on conventional SSZ-13 and nano-SSZ-13.

Table 5.3 K and a values of the SSZ-13 and nano-SSZ-13 from the Janssens' model [47]

| Sample | K (mol/g$_{cat}$ h) | a (g/mol) | t0.5(min) | t0.98(min) | R (gmeoh/gcat) |
|---|---|---|---|---|---|
| SSZ-13 | 10.05 | 0.00260 | 314 | 165.8 | 4.2 |
| nano-SSZ-13 | 6.52 | 0.00104 | 783 | 212.3 | 10.4 |

The conversion values have been fitted to kinetic model proposed by Janssen [47] to describe the activity of ZSM-5 in the conversion of methanol with two parameter: K for contribution of activity and a for the deactivation rate, which also have been applied to SAPO-34 in Chapter 3 and 4. As shown in the Table 5.3 , both kinetic parameter "K" and "a" of SSZ-13 are two times larger than those of nano-SSZ-13. Following the terminology used by Janssens, SSZ-13 presents then high activity (K) and fast deactivation (a), while nano-SSZ-13 shows low activity and slow deactivation. These results of the fitting agree with the fact that nano-SSZ-13

possesses lower number of acid sites as determined by $NH_3$-TPD (lower K value) while its higher external surface facilitates diffusion of reactants and products, being less affected by coking ( lower a value, slow deactivation).

The deactivated nano-SSZ-13 was restored by oxidation of the coke by in air at 540°C for 3h. The catalyst was applied to reaction-oxidation for several cycles, and the performance was similar.

Yields to different products are compared at constant conversion in Fig 5.8. In this way the true selectivity of the hydrocarbon pool is isolated from the thermodynamic equilibrium as shown before in the case of SAPO-34. It is important to notice that different yields do not depend on conversion during the deactivation of the catalyst and therefore, the deactivation is again "non-selective". As a consequence, the yields to different products are not controlled by diffusion during deactivation.
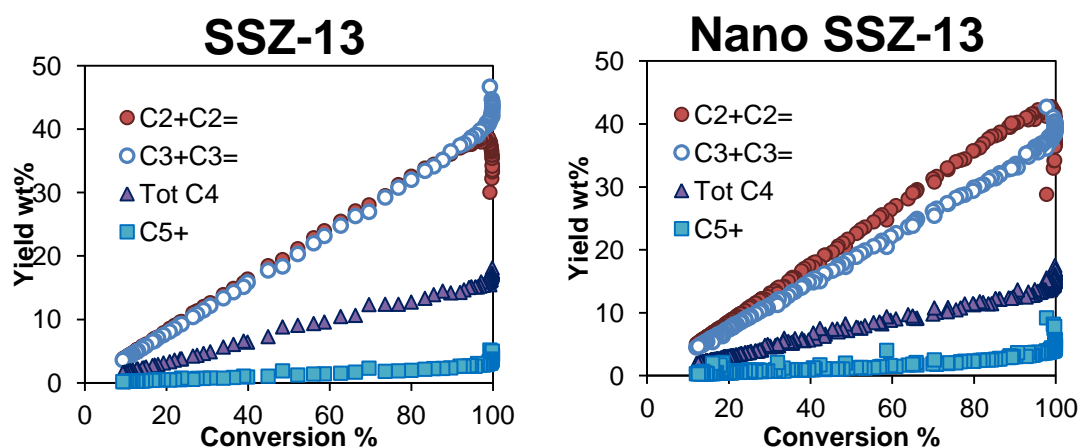


Fig 5.8 Yields to C2, C3, C4 and C5+ hydrocarbons in the conversion of standard and nano-SSZ-13 at 350°C and WHSV=0.8 h$^{-1}$.
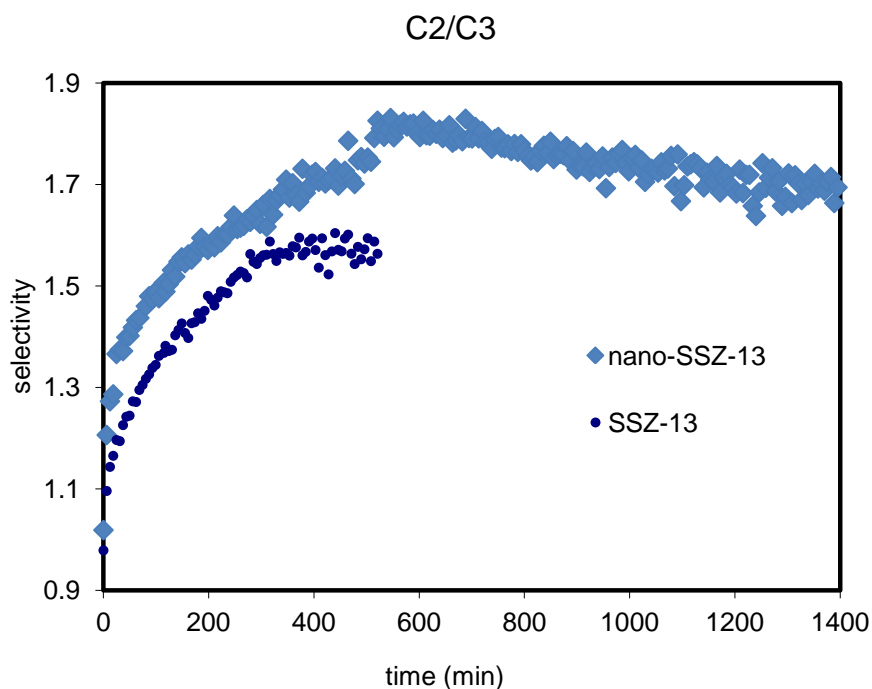
Fig 5.9 The C2/C3 ratio of the standard and nano-SSZ-13 samples in conversion of methanol at 350°C and WHSV=0.8 h$^{-1}$.

When comparing selectivities at constant conversion it can be seen that C2/C3 ratio increased in the nano-SSZ-13 comparing with the SSZ-13(Fig 5.9). More specifically, the results have shown an effective increase in the selectivity to ethylene (Fig 5.10), while the distribution among the other olefins is not affected. The different behavior of C2 for nano and standard SSZ-13, while C3, C4 and C5 are very similar, points out the existence of a dual cycle for the yield of products, in the same way that occurs for ZSM-5[48]. The two mechanisms, the olefin cycle and the aromatics cycle yield different distribution of products. The aromatic cycle mainly produce ethylene while the olefin cycle yields C3 to C5 olefins by methylation-cracking of an adsorbed olefin. It is so, the higher selectivity to ethylene of nano-SSZ-13 should be related to a higher contribution of the aromatics cycle.
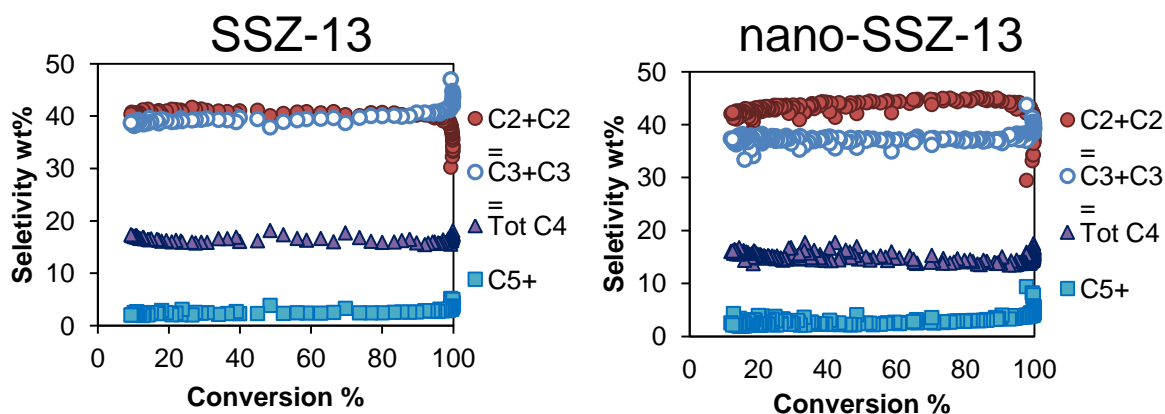
## SSZ-13

## nano-SSZ-13

Fig 5.10 Selectivities to C2, C3, C4 and C5+ hydrocarbons in the conversion of methanol on standard and nano- SSZ-13.

## Hydrogen transfer
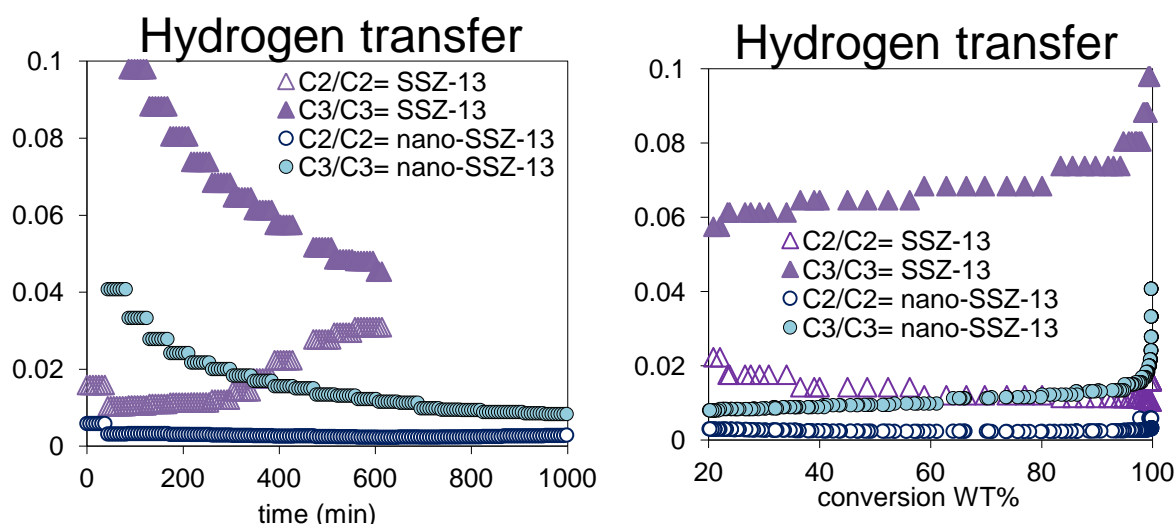
## Hydrogen transfer

Fig 5.11 The hydrogen transfer index of the samples in the conversion of methanol.

Hydrogen transfer index (HTI, C3/C3$^=$ C2/C2$^=$) is been shown in the Fig 5.11 , which clearly shows that nano-SSZ-13 present higher amount of hydrogen transfer reactions comparing to nano-SSZ-13. Since hydrogen transfer is closely related to the formation of coke it follows that SSZ-13 should deactivate faster that is in agreement with the results obtained in the reaction of methanol. Moreover, the higher hydrogen transfer and the faster deactivation of SSZ-13 could explain a lower contribution of the aromatic cycle in the dual cycle concept of the reaction. In this way, the aromatics that form part of the hydrocarbon pool in SSZ-13 are more prone to grow and develop coke by successive methylation, cyclization and hydrogen transfer, becoming deactivated. On the contrary, in the case of nano-SSZ-13, the

aromatic cycle, once formed, suffers slower deactivation contributing more than in the case of SSZ-13.

# 5.4.Conclusion

We have demonstrated that the nanosized SSZ-13 zeolite can be obtained from one-pot synthesis procedure by with the addition of surfactant to conventional synthesis precursor. The hierarchical materials exhibit much longer lifetime than the standard SSZ-13. This is mainly due to the presence of intercrystalline mesoporosity, which facilitates a more efficient use of the catalyst. A higher C2/C3 ratio was found in the nano-SSZ-13, which can be explained due to a lower contribution of hydrogen transfer reaction leading to lower deactivation of the aromatics-based hydrocarbon pool.

# References

[1] P.L. Benito, A.G. Gayubo, A.T. Aguayo, M. Olazar, J. Bilbao, Effect of Si/Al ratio and of acidity of H-ZSM5 zeolites on the primary products of methanol to gasoline conversion, Journal of Chemical Technology & Biotechnology, 66 (1996) 183-191.

[2] A.T. Aguayo, A.G. Gayubo, M. Castilla, J.M. Arandes, M. Olazar, J. Bilbao, MTG Process in a Fixed-Bed Reactor. Operation and Simulation of a Pseudoadiabatic Experimental Unit, Industrial & Engineering Chemistry Research, 40 (2001) 6087-6098.

[3] H.A. Zaidi, K.K. Pant, Catalytic conversion of methanol to gasoline range hydrocarbons, Catalysis Today, 96 (2004) 155-160.

[4] A. Taguchi, F. Schüth, Ordered mesoporous materials in catalysis, Microporous and Mesoporous Materials, 77 (2005) 1-45.

[5] J. Perez-Ramirez, C.H. Christensen, K. Egeblad, C.H. Christensen, J.C. Groen, Hierarchical zeolites: enhanced utilisation of microporous crystals in catalysis by advances in materials design, Chemical Society reviews, 37 (2008) 2530-2542.

[6] K. Moller, T. Bein, Mesoporosity--a new dimension for zeolites, Chemical Society reviews, 42 (2013) 3689-3707.

[7] M. Firoozi, M. Baghalha, M. Asadi, The effect of micro and nano particle sizes of H-ZSM-5 on the selectivity of MTP reaction, Catalysis Communications, 10 (2009) 1582-1585.

[8] K. Na, M. Choi, R. Ryoo, Recent advances in the synthesis of hierarchically nanoporous zeolites, Microporous and Mesoporous Materials, 166 (2013) 3-19.

[9] J.C. Groen, L.A.A. Peffer, J.A. Moulijn, J. Pérez-Ramírez, Mesoporosity development in ZSM-5 zeolite upon optimized desilication conditions in alkaline medium, Colloids and Surfaces A: Physicochemical and Engineering Aspects, 241 (2004) 53-58.

[10] J.C. Groen, W. Zhu, S. Brouwer, S.J. Huynink, F. Kapteijn, J.A. Moulijn, J. Pérez-Ramírez, Direct Demonstration of Enhanced Diffusion in Mesoporous ZSM-5 Zeolite Obtained via Controlled Desilication, Journal of the American Chemical Society, 129 (2006) 355-360.

[11] B. Gil, Ł. Mokrzycki, B. Sulikowski, Z. Olejniczak, S. Walas, Desilication of ZSM-5 and ZSM-12 zeolites: Impact on textural, acidic and catalytic properties, Catalysis Today, 152 (2010) 24-32.

[12] M. Bjørgen, F. Joensen, M. Spangsberg Holm, U. Olsbye, K.-P. Lillerud, S. Svelle, Methanol to gasoline over zeolite H-ZSM-5: Improved catalyst performance by treatment with NaOH, Applied Catalysis A: General, 345 (2008) 43-50.

[13] V.N. Shetti, J. Kim, R. Srivastava, M. Choi, R. Ryoo, Assessment of the mesopore wall catalytic activities of MFI zeolite with mesoporous/microporous hierarchical structures, Journal of Catalysis, 254 (2008) 296-303.

[14] L.-H. Chen, X.-Y. Li, J.C. Rooke, Y.-H. Zhang, X.-Y. Yang, Y. Tang, F.-S. Xiao, B.-L. Su, Hierarchically structured zeolites: synthesis, mass transport properties and applications, Journal of Materials Chemistry, 22 (2012) 17381.

[15] K. Egeblad, C.H. Christensen, M. Kustova, C.H. Christensen, Templating Mesoporous Zeolites†, Chemistry of Materials, 20 (2008) 946-960.

[16] S.T. Yang, J.Y. Kim, H.J. Chae, M. Kim, S.Y. Jeong, W.S. Ahn, Microwave synthesis of mesoporous SAPO-34 with a hierarchical pore structure, Materials Research Bulletin, 47 (2012) 3888-3892.

[17] Y. Cui, Q. Zhang, J. He, Y. Wang, F. Wei, Pore-structure-mediated hierarchical SAPO-34: Facile synthesis, tunable nanostructure, and catalysis applications for the conversion of dimethyl ether into olefins, Particuology, 11 (2013) 468-474.

[18] H. Yang, Z. Liu, H. Gao, Z. Xie, Synthesis and catalytic performances of hierarchical SAPO-34 monolith, Journal of Materials Chemistry, 20 (2010) 3227-3231.

[19] J. Zhu, Y. Cui, Y. Wang, F. Wei, Direct synthesis of hierarchical zeolite from a natural layered material, Chemical Communications, (2009) 3282-3284.

[20] F. Schmidt, S. Paasch, E. Brunner, S. Kaskel, Carbon templated SAPO-34 with improved adsorption kinetics and catalytic performance in the MTO-reaction, Microporous and Mesoporous Materials, 164 (2012) 214-221.

[21] S. Lin, J. Li, R.P. Sharma, J. Yu, R. Xu, Fabrication of SAPO-34 crystals with different morphologies by microwave heating, Topics in Catalysis, 53 (2010) 1304-1310.

[22] Y. Hirota, K. Murata, S. Tanaka, N. Nishiyama, Y. Egashira, K. Ueyama, Dry gel conversion synthesis of SAPO-34 nanocrystals, Materials Chemistry and Physics, 123 (2010) 507-509.

[23] T. Álvaro-Muñoz, C. Márquez-Álvarez, E. Sastre, Effect of silicon content on the catalytic behavior of chabazite type silicoaluminophosphate in the transformation of methanol to short chain olefins, Catalysis Today, 213 (2013) 219-225.

[24] T. Álvaro-Muñoz, C. Márquez-Álvarez, E. Sastre, Use of different templates on SAPO-34 synthesis: Effect on the acidity and catalytic activity in the MTO reaction, Catalysis Today, 179 (2012) 27-34.

[25] W. Pengfei, Y. Dexing, H. Jie, X. Jing'an, L. Guanzhong, Synthesis of SAPO-34 with small and tunable crystallite size by two-step hydrothermal crystallization and its catalytic performance for MTO reaction, Catalysis Today, 212 (2013).

[26] M. Yang, P. Tian, C. Wang, Y. Yuan, Y. Yang, S. Xu, Y. He, Z. Liu, A top-down approach to prepare silicoaluminophosphate molecular sieve nanocrystals with improved catalytic activity, Chemical communications (Cambridge, England), (2014).

[27] G. Yang, Y. Wei, S. Xu, J. Chen, J. Li, Z. Liu, J. Yu, R. Xu, Nanosize-Enhanced Lifetime of SAPO-34 Catalysts in Methanol-to-Olefin Reactions, The Journal of Physical Chemistry C, 117 (2013) 8214-8222.

[28] Z. Li, J. Martinez-Triguero, P. Concepcion, J. Yu, A. Corma, Methanol to olefins: activity and stability of nanosized SAPO-34 molecular sieves and control of selectivity by silicon distribution, Physical Chemistry Chemical Physics, 15 (2013) 14670-14680.

[29] L. Emdadi, Y. Wu, G. Zhu, C.-C. Chang, W. Fan, T. Pham, R.F. Lobo, D. Liu, Dual Template Synthesis of Meso- and Microporous MFI Zeolite Nanosheet

Assemblies with Tailored Activity in Catalytic Reactions, Chemistry of Materials, 26 (2014) 1345-1355.

[30] A. Karlsson, M. Stöcker, R. Schmidt, Composites of micro- and mesoporous materials: simultaneous syntheses of MFI/MCM-41 like phases by a mixed template approach, Microporous and Mesoporous Materials, 27 (1999) 181-192.

[31] J. Pérez-Pariente, R. García, L. Gómez-Hortigüela, A.B. Pinar, Co-Templates in Synthesis of Zeolites, in: Zeolites and Catalysis, Wiley-VCH Verlag GmbH & Co. KGaA, 2010, pp. 107-129.

[32] S.J. Weigel, J.-C. Gabriel, E.G. Puebla, A.M. Bravo, N.J. Henson, L.M. Bull, A.K. Cheetham, Structure-Directing Effects in Zeolite Synthesis: A Single-Crystal X-ray Diffraction, 29Si MAS NMR, and Computational Study of the Competitive Formation of Siliceous Ferrierite and Dodecasil-3C (ZSM-39), Journal of the American Chemical Society, 118 (1996) 2427-2435.

[33] R. García, L. Gómez-Hortigüela, I. Díaz, E. Sastre, J. Pérez-Pariente, Synthesis of Materials Containing Ferrierite Layers Using Quinuclidine and 1-Benzyl-1-methylpyrrolidine as Structure-Directing Agents. An Experimental and Computational Study†, Chemistry of Materials, 20 (2008) 1099-1107.

[34] L. Wu, V. Degirmenci, P.C.M.M. Magusin, B.M. Szyja, E.J.M. Hensen, Dual template synthesis of a highly mesoporous SSZ-13 zeolite with improved stability in the methanol-to-olefins reaction, Chemical communications, 48 (2012) 9492-9494.

[35] Y. Liu, W. Zhang, T.J. Pinnavaia, Steam-Stable MSU-S Aluminosilicate Mesostructures Assembled from Zeolite ZSM-5 and Zeolite Beta Seeds, Angewandte Chemie International Edition, 40 (2001) 1255-1258.

[36] K.S. Triantafyllidis, E.F. Iliopoulou, E.V. Antonakou, A.A. Lappas, H. Wang, T.J. Pinnavaia, Hydrothermally stable mesoporous aluminosilicates (MSU-S) assembled from zeolite seeds as catalysts for biomass pyrolysis, Microporous and Mesoporous Materials, 99 (2007) 132-139.

[37] D. Pan, P. Yuan, L. Zhao, N. Liu, L. Zhou, G. Wei, J. Zhang, Y. Ling, Y. Fan, B. Wei, H. Liu, C. Yu, X. Bao, New Understanding and Simple Approach to Synthesize Highly Hydrothermally Stable and Ordered Mesoporous Materials, Chemistry of Materials, 21 (2009) 5413-5425.

[38] L.T. Yuen, S.I. Zones, T.V. Harris, E.J. Gallegos, A. Auroux, Product selectivity in methanol to hydrocarbon conversion for isostructural compositions of AFI and CHA molecular sieves, Microporous Materials, 2 (1994) 105-117.

[39] F. Bleken, M. Bjørgen, L. Palumbo, S. Bordiga, S. Svelle, K.P. Lillerud, U. Olsbye, The effect of acid strength on the conversion of methanol to olefins over acidic microporous catalysts with the CHA topology, Topics in Catalysis, 52 (2009) 218-228.

[40] S. Bordiga, L. Regli, D. Cocina, C. Lamberti, M. Bjorgen, K.P. Lillerud, Assessing the acidity of high silica chabazite H-SSZ-13 by FTIR using CO as molecular probe: Comparison with H-SAPO-34, The journal of physical chemistry. B, 109 (2005) 2779-2784.

[41] F. Bleken, M. Bjørgen, L. Palumbo, S. Bordiga, S. Svelle, K.-P. Lillerud, U. Olsbye, The Effect of Acid Strength on the Conversion of Methanol to Olefins Over Acidic Microporous Catalysts with the CHA Topology, Topics in Catalysis, 52 (2009) 218-228.

[42] L. Sommer, D. Mores, S. Svelle, M. Stöcker, B.M. Weckhuysen, U. Olsbye, Mesopore formation in zeolite H-SSZ-13 by desilication with NaOH, Microporous and Mesoporous Materials, 132 (2010) 384-394.

[43] L. Sommer, A. Krivokapić, S. Svelle, K.P. Lillerud, M. Stöcker, U. Olsbye, Enhanced Catalyst Performance of Zeolite SSZ-13 in the Methanol to Olefin Reaction after Neutron Irradiation, The Journal of Physical Chemistry C, 115 (2011) 6521-6530.

[44] Y. Zhu, Z. Hua, J. Zhou, L. Wang, J. Zhao, Y. Gong, W. Wu, M. Ruan, J. Shi, Hierarchical mesoporous zeolites: direct self-assembly synthesis in a conventional surfactant solution by kinetic control over the zeolite seed formation, Chemistry, 17 (2011) 14618-14627.

[45] J. Barras, J. Klinowski, D. W. McComb, ^{27}Al and ^{29}Si Solid-state NMR studies of dealuminated Mordenite. Journal of Chemical Society, Faraday Transactions, 90 (1994) 3719–3723.

[46] L. Wu, V. Degirmenci, P.C.M.M. Magusin, N.J.H.G.M. Lousberg, E.J.M. Hensen, Mesoporous SSZ-13 zeolite prepared by a dual-template method with improved performance in the methanol-to-olefins reaction, Journal of Catalysis, 298 (2013) 27-40.

[47] T.V.W. Janssens, A new approach to the modeling of deactivation in the conversion of methanol on zeolite catalysts, Journal of Catalysis, 264 (2009) 130-137.

[48] M. Bjørgen, S. Svelle, F. Joensen, J. Nerlov, S. Kolboe, F. Bonino, L. Palumbo, S. Bordiga, U. Olsbye, Conversion of methanol to hydrocarbons over zeolite H-ZSM-5: On the origin of the olefinic species, Journal of Catalysis, 249 (2007) 195-207.

# 6. Desilication of ZSM-5 by the treatment of NaOH and NaOH/TPAOH solution and the application in methanol to olefins

# 6.1.Introduction

Due to the increasing demand of ethylene and propylene, methanol which is a possible alternative to crude oil as it can be transformed into olefins (methanol to olefins) and hydrocarbons (methanol to hydrocarbons), has attracted great interest both from industry and academy, especially with the new development of processes to obtain methanol from natural gas, biomass, and other carbon-rich feedstocks[1-4]. The reaction of methanol to hydrocarbons was first discovered by the Chang and Silvestri in 1977[5] and the first commercial MTG plant using ZSM-5 as the catalyst was built in New Zealand, but shut down later due to the oil price negative fluctuations [6]. Haldor Topsøe also has developed the Topsøe Integrated Gasoline Synthesis (TIGAS) process, which also applies ZSM-5 as the catalyst and starts from synthesis gas as reactant [7]. However, the only currently commercial process is Lurgi's MTP (methanol to propylene), in which by using a small high Si/Al ZSM-5-based catalyst manufactured by Süd-Chemie (now Clariant) the yield of aromatics is decreased increasing therefore the yield to propylene. Two plants are working in China [8].

Zeolites are a microporous materials with unique channels and cages, composed by the connection of $TO_4$ (T=Si, Al) tetrahedral in a three dimensional array, with Brønsted acid sites located in the channels. ZSM-5 is a 10 member-rings medium size zeolite formed by two 10-membered rings intersected channels by one straight channels(5.1 Å x 5.5 Å) and another zigzag one(5.3 Å X 5.6 Å) [9]. The dimensions of the channels control the selectivity of the reactions. However, the microporosity also hinder the diffusion of reactant and products and limits the performance of zeolites[10].

Decreasing the crystal size of the zeolites offers other way to overcome the diffusion limitations. Catalytic performance has been improved by decreasing crystal size which for ZSM-5[11,12], zeolite beta[13], zeolite Y[14], mordenite[10] and SAPO-34[8,15]. With a smaller crystal size, the catalyst presents higher external surface and shorter diffusion paths, which is even more important for the reaction of bulky molecules [16].

An effective route also proposed to overcome the diffusion limitations is the combination of micropores with meso/macroporous in the same particle, which

contains properties of the zeolitic micropores with high accessibility and meso/macropores with improved diffusion rate [10, 16]. In this respect, hierarchical zeolites have been obtained, such as ZSM-5, Silicalite-1, BEA, LTA, TS-1 and so on [16]. To date, the approaches to prepare hierarchical zeolites can be classified into one indirect synthesis by using soft or hard templates or the addition of surfactant in the synthesis system way [16, 17], and the post-synthesis ways such as acid and base etching, steaming, delamination, desilication or steaming [16-18]. From these post-synthesis methods desilication procedures have been reported to develop mesoporous ZSM-5 by means of removal of Si in alkaline solutions such as NaOH, $Na_2CO_3$, TPAOH or TBAOH[19]. The performance of desilicated mesoporous H-ZSM-5 has been investigated in the reaction of methanol to gasoline and it has been reported an increased lifetime and methanol conversion capacity until deactivation of the catalyst [20, 21].

In this chapter we will investigate the effect of different desilication methods on two high silica ZSM-5 samples, and on the catalytic behavior in the reaction methanol to olefins. In addition we will study the effect of desilication treatment on the hydrothermal stability of the samples and its effect in the reaction of methanol to olefins. The use of TPAOH mixed with NaOH solution will be used to treat the ZSM-5 samples and the mesopore sizes and their interconnection to the micropores will be compared with the mesoporosity obtained with the samples desilicated in NaOH alone.

# 6.2. Experimental

## 6.2.1. Catalyst preparation

The parent samples ZSM-5 were obtained from Zeolyst International named as CBV8020 (Si/Al=40, defined as ZL) and CBV28014 (Si/Al=140, defined as ZH). The desilication process was carried out in the following conditions: The calcined ZSM-5 samples were suspended in 0.2 [M] NaOH solutions (AT) at 85°C 90mins, or 0.2[M] NaOH+0.1 [M] TPAOH solutions (MT) at 65°C 30min. Then, the desilicated samples were washed with Milli-Q water until neutral pH and filtrated, followed with 3 times ion exchange in 2.5[M] $NH_4Cl$(N) solution for 2 hours or in 0.075[M] Oxalic acid solution (H) at 80°C for 4hours. Then, the samples were dried at 100°C for 3h and

calcined at 500°C for 5h. The steaming treatment was carried out in 700°C for 5h with 100% steaming. This steaming treatment has been designed as "deactivation test" to simulate long-term working of ZSM-5 at reactions condition of methanol to olefins at 450°C in the presence of water and after many cycles of reaction-regeneration. The definition of the desilicated samples is detailed in Table 6.1.

Table 6.1 The definition of the parents and desilicated samples

| Sample | Definition | Basic solution | | Ion exchange | |
|---|---|---|---|---|---|
| | | 0.2[M]NaOH | 0.2[M]NaOH+TPAOH | NH$_4$Cl | Oxalic acid solution |
| CBV8020(Si/Al=40) | Z$_L$ –AT-N | + | | + | |
| | Z$_L$ –AT-H | + | | | + |
| | Z$_L$ –MT-N | | + | + | |
| | Z$_L$ –MT-H | | + | | + |
| | Z$_L$ –0.5[M] | treated in 0.5[M] NaOH solution | | | + |
| CBV28014(Si/Al=140) | Z$_H$-AT-N | + | | + | |
| | Z$_H$-AT-H | + | | | + |
| | ZH-MT-N | | + | + | + |
| | Z$_H$-MT-H | | + | | |

## 6.2.2. Characterization

The characterization has been carried out in the same way as we have shown in Chapter 3.

## 6.2.3. Catalytic experiments

The reaction procedure has been performed as described in Chapter 3, but the catalysts were tested at higher space velocity WHSV=12 h$^{-1}$ and at higher temperature (450°C) more typical of the reaction of methanol to olefins on high silica ZSM-5. The catalyst was calcined in a nitrogen flow of 80 ml/min for 1 h at 540°C firstly, and then the temperature was cooled to reaction conditions (450°C). Analysis of products was done each 35 min with two online gas chromatographs with FID detectors. First in a Varian 3400CX with a 50m PONA capillary column, from 37°C to 250°C with a rate of 7°C /min, and after condensation of water in a second gas chromatograph HP 3890 with a 50m Al$_2$O$_3$-Plot capillary column from 60°C to 220°C

with a rate of 20°C /min. Conversion and selectivities were calculated in carbon basis being methanol and dimethylether considered as feed.

# 6.3.Results and discussion

## 6.3.1.Characterization
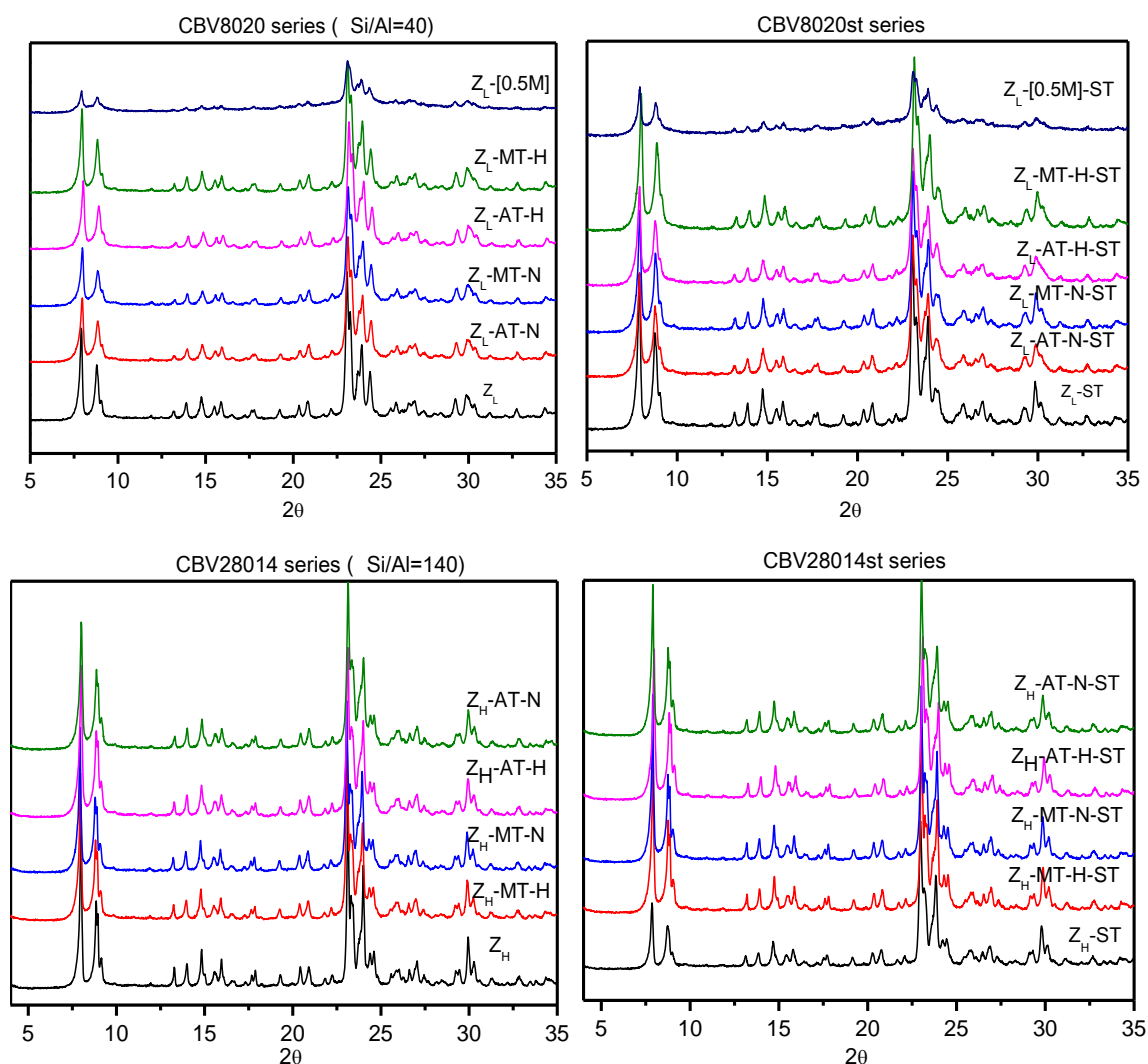


Fig 6.1 XRD patterns of the parents, desilicated samples and steamed ZSM-5 samples.

XRD patterns of the parent, treated with NaOH or NaOH/TPAOH solution and steamed ZSM-5 samples are shown in Fig 6.1. The samples treated by alkali or mix alkali solution show similar diffraction patterns as their parent ZSM-5 samples despite the difference in the Si/Al ratios, which indicates the maintenance of the MFI

structure after the treatments. It is worth to note that the partial destruction of sample treated with high concentration NaOH(0.5[M]) solution is observed, which shows lower intensity compared with lower differences for the other desilicated samples treated with lower concentration of NaOH solution. Another finding that needs to be noted is that the crystalline structures are still retained even when samples are submitted to steaming for 5 hours at 700°C, which suggests the high hydrothermal stability of the structure of these desilicated samples. Relative crystallinity values have been calculated based on the characteristic peaks from the range 22.5 to 25° as shown in Table 6.2. The results confirm the preservation of the crystalline structure after desilication provided that the increase of mesoporosity is moderate. For higher mesoporosity as in the case of sample $Z_L$ –0.5[M], the crystallinity decreases along with a decrease in micropore volumes. The high crystallinity of desilicated samples may be explained because of the defects that are modified when treated in the alkaline solutions[22]. Also, Groen reported that the Al removed from the zeolite structure in alkaline solution are reinserted into the framework [23]. Similar result was also obtained from Sadowska[24]. After steaming, there is a small loss of crystallinity for all parent and desilicated samples. In the case of low Si/Al ratio sample, the loss of microporosity is higher than the decrease of crystallinity, indicating that there could be a partial plugging by extra-framework aluminum that does not occur for the high Si/Al sample. It is interesting to note that for the high Si/Al SAM-5 sample, the desilicated samples preserve more crystallinity after steaming than the parent sample.

$N_2$ desorption measurements have been used to measure the textural properties of the treated samples as the results summarized in Table 6.2. When the Si/Al=40 sample was treated by desilication procedures, the BET surfaces and mesopore volumes have improved to 412-467 $m^2$/g (389 $m^2$/g for parent ZSM-5) and 0.19-0.33 $cm^3$/g( 0,09 $cm^3$/g for parent ZSM-5) respectively depending on different treatment conditions, along with a decrease of micropore volumes. The main reason for higher BET surfaces of the treated samples are due to the formation of mesopore in the desilication process, which also result in the increase values for the external surfaces (from 46 $m^2$/g for the parent ZSM-5 to 102-188 $m^2$/g for the desilication samples).

Table 6.2 Chemical and textural properties of the parents and the desilicated ZSM-5 samples.

| Samples | ICP(Si/Al) | BET (m2/g) | t-plot $S_{ext}$ ( $m^2$/g) | $V_{micro}$ ($cm^3$/g) | $V_{meso}$ ($cm^3$/g) | crystallinity(%) |
|---|---|---|---|---|---|---|
| $Z_L$(Si/Al=40) | 40 | 389 | 46.1 | 0.17 | 0.091 | 100 |
| $Z_L$ –AT-N | 51.7 | 447 | 159 | 0.14 | 0.22 | 98.7 |
| $Z_L$ –MT-N | 21.2 | 468 | 188 | 0.14 | 0.19 | 99.2 |
| $Z_L$ –AT-H | 27.5 | 436 | 145 | 0.14 | 0.22 | 100 |
| $Z_L$ –MT-H | 28.1 | 418 | 102 | 0.15 | 0.12 | 96.4 |
| $Z_L$ – [0.5M] | 31.1 | 413 | 178 | 0.11 | 0.34 | 55.2 |
| $Z_H$(Si/Al=140) | 140 | 377 | 43.4 | 0.16 | 0.072 | 100 |
| $Z_H$-MT-H | 100 | 400 | 82.9 | 0.16 | 0.19 | 97.7 |
| $Z_H$-MT-N | 81.6 | 394 | 84.0 | 0.16 | 0.18 | 98.1 |
| $Z_H$-AT-H | 105 | 405 | 69.0 | 0.17 | 0.21 | 100 |
| $Z_H$-AT-N | 79.9 | 397 | 70.7 | 0.16 | 0.21 | 100 |

| Samples | BET ($m^2$/g) | t-plot $S_{ext}$ ($m^2$/g) | $V_{micro}$ ($cm^3$/g) | $V_{meso}$ ($cm^3$/g) | crystallinity |
|---|---|---|---|---|---|
| $Z_L$-ST | 364 | 53.3 | 0.15 | 0.11 | 94.2 |
| $Z_L$ –AT-N-ST | 378 | 145 | 0.12 | 0.26 | 80.4 |
| $Z_L$ –MT-N-ST | 370 | 118 | 0.18 | 0.17 | 87.3 |
| $Z_L$ –AT-H-ST | 404 | 205 | 0.099 | 0.24 | 82.1 |
| $Z_L$ –MT-H-ST | 386 | 136 | 0.126 | 0.25 | 97.1 |
| $Z_L$ – [0.5M]-ST | 315 | 159 | 0.075 | 0.32 | 50.7 |
| $Z_H$-ST | 366 | 38.8 | 0.16 | 0.070 | 78.8 |
| $Z_H$-MT-H-ST | 367 | 82.0 | 0.15 | 0.20 | 94.1 |
| $Z_H$-MT-N-ST | 371 | 82.1 | 0.15 | 0.20 | 90.7 |
| $Z_H$-AT-H-ST | 371 | 62.6 | 0.16 | 0.20 | 90.7 |
| $Z_H$-AT-N-ST | 362 | 72.3 | 0.15 | 0.21 | 87.1 |

However, from the results shown above, they indicate that the effects of NaOH and NaOH/TPAOH in the desilication processes are not the same way. On the one hand, in the mix alkaline solution treatment condition, the samples show smaller mesopore volumes when compared with NaOH method treatment on the same conditions, due of the aid of TPA$^+$ cations, which protected the attack of OH$^-$ on the ZSM-5 structure in desilication process[24, 25]. On the other hand, after alkali treatment, oxalic acid is much more effective than $NH_4Cl$ for removing alumina debris (lower Si/Al ratios) by acid wash in the micropore mouth [17]. The sample treated

with the highest concentration of NaOH shows the largest mesopore volumes and a significant loss in micropore volume indicating partial destruction, which is consistent to the XRD results for the lower crystallinity.

Similar effects of increasing of BET and external surfaces have been found on the treated Si/Al =140 ZSM-5 samples, which are attributed to the formation of mesopores after desilication process.

When the desilicated samples were treated by steaming, the BET surfaces have shown a slight decrease due to the partial destruction of the micropore volumes while mesopore volumes are maintained, which indicates that the desilicated samples are not sensitive to water attack on the zeolite structures. When comparing the micropore volumes of the two series of samples, those coming from Si/Al=40 lose more micropore volumes after steaming, indicating that dealumination has occurred partially plugging the micropores while the samples of high Si/Al ratio are less affected due to its lower original amount of aluminum.
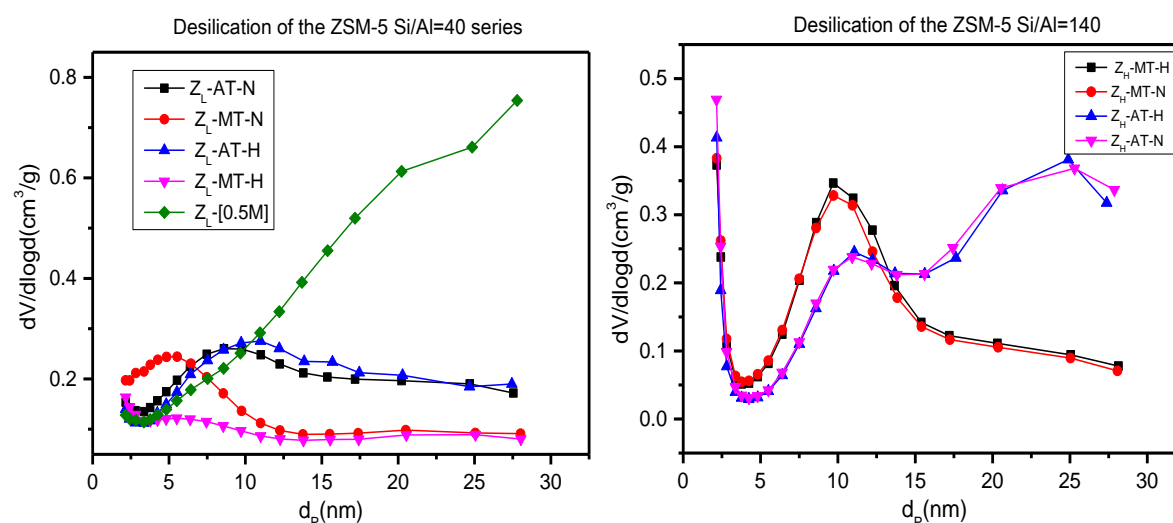


Fig 6.2 Pore distributions of the desilicated ZSM-5 samples of low and high Si/Al ratios calculation from the $N_2$ adsorption-desorption.

BJH model has been used to calculate the pore distribution of the desilicated samples as show in Fig 6.2 The Si/Al=40 ZSM-5 samples treated by NaOH/TAPOH present narrower mesopore diameter distribution at about 5nm, however when the same parent sample treated in NaOH solution shows much larger diameter distribution at about 10nm, but when the high concentration of NaOH solution(0.5[M]),

the mesopore diameters of the interpartical are about 20nm. The mesopore diameters of treated Si/Al =140 ZSM-5 samples are about 10nm and 15nm respectively for treated in NaOH/TPAOH and NaOH solutions. It is worth noticing that the formation of interpartical pore whose diameters that are at about 25nm for the ZSM-5 Si/Al after the treatment in NaOH solution. The different pore sizes of the treated different Si/Al ratios is consistent with the previous report that wider pores were formed in higher Si/Al ratios ZSM-5 [24].

The addition of TPAOH to NaOH not only has resulted in an effect on pore volumes but also to different pore diameters (from the Table 6.2 and Fig 6.2). When the Si/Al ratio increased for the ZSM-5 (from 40 to 140), it leads to the formation of interparticle pores. From previous studies by Perez-Ramirez and other authors [22, 25], both the Al extracted from zeolite structure in the desilication process and amine cations from amine hydroxide can play as an important effect in the formation of mesopore which were called the pore-directing agents[26]. They demonstrate that Al and amine cations can protect from the OH- attack on the zeolites surface towards dissolution of the structure. Several results [26] have reported the formation of larger pores with the presence of Al content and smaller pores in the case of addition of amine hydroxide into NaOH solution. As reported from Sadowska[28], the practical absence of aluminum in the framework brought amine hydroxide to play the dominant role in the formation of pore formation, with narrower pores into the structure.
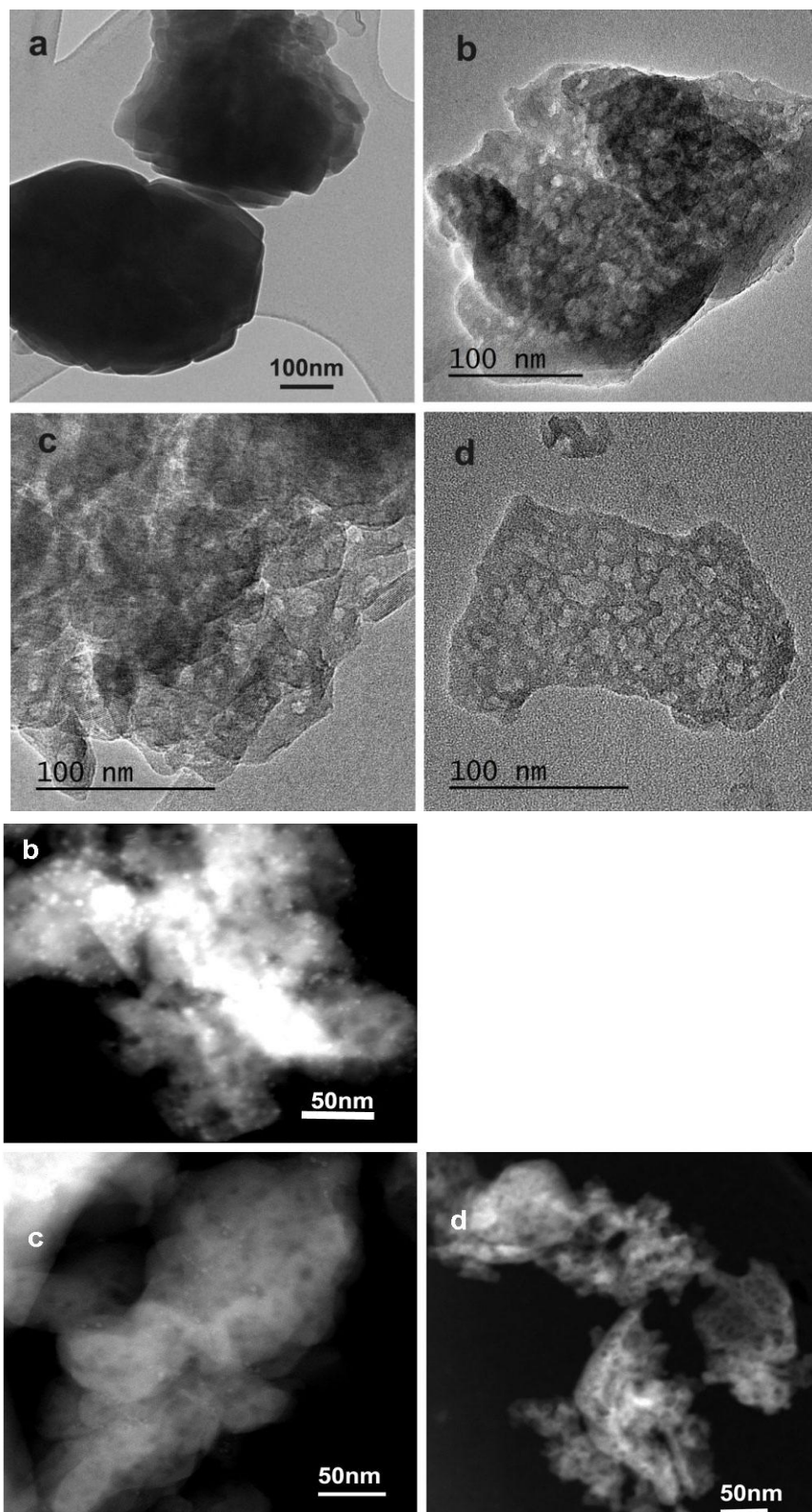
Fig 6.3 TEM images of the parent sample a) $Z_L$ and representative desilicated samples b) $Z_L$-AT-H c) $Z_L$-MT-H d) $Z_L$-[0.5M] obtained in bright and dark field.
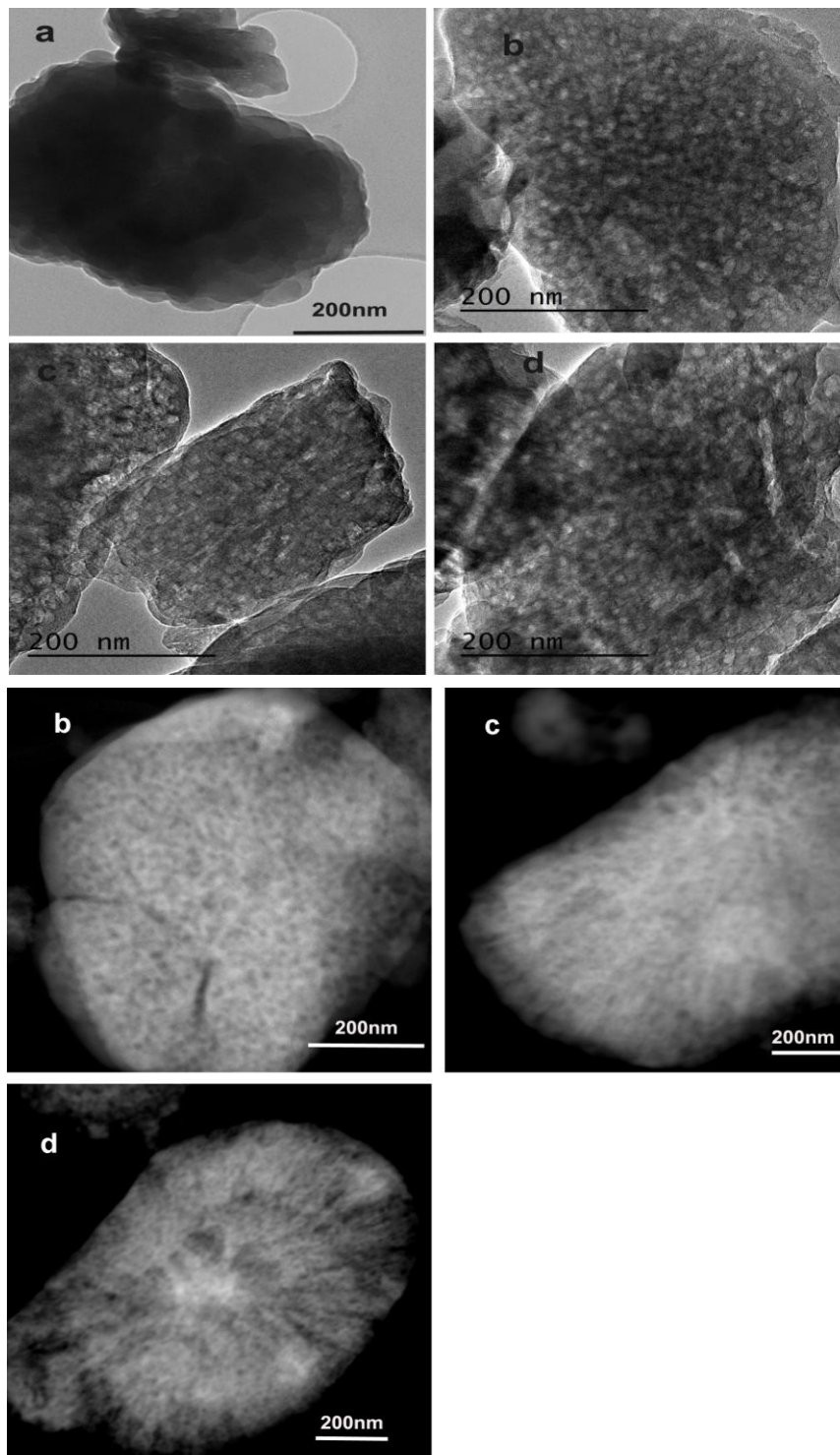
Fig 6.4 TEM images of the parent sample a) $Z_H$ and representative desilicated samples b) $Z_H$-MT-H c) $Z_H$-AT-N d) $Z_H$-AT-H obtained in bright and dark fields.

TEM images of the representative desilicated samples are shown in Fig 6.3, Fig 6.4. Both parent ZSM-5 with different Si/Al ratios present a crystal size in the range 400-600nm with a sphere like shape and no mesopores. After desilication treatment,

the morphology of the desilicated samples is totally different comparing with the parent samples. In fact, the external surface of the desilicated zeolite samples become rough and rugged with the appearance of nanoscale open holes and the particle turns to be crack sheet-shape according to the attack by the OH$^-$ ions. Furthermore, the open holes randomly distributed on the surface with the penetration into bulk crystal as illustrated in the TEM images, means that the interior crystal has been affected by the desilication process. In fact, from the images taken in the dark field, it can be easily seen the connection of the mesopores with the micropores. The open mesopore holes present on the surface accelerate the transfer of reactants or products to and from the active sites in the zeolite micro-channels, which improve the performance of the samples in the reaction of methanol to olefins. The samples with the higher concentration NaOH solution(0.5[M]) treated show much larger holes in the bulk of zeolite crystal with partial collapse structure as can be seen in the figure, which is a consistent result with the XRD and $N_2$ adsorption and desorption measurement.

In the dark field analysis of high resolution transmission electron microscopy, small particles of silica have been found on the crystal surface, which may be due to the deposition of silica from the desilication process.
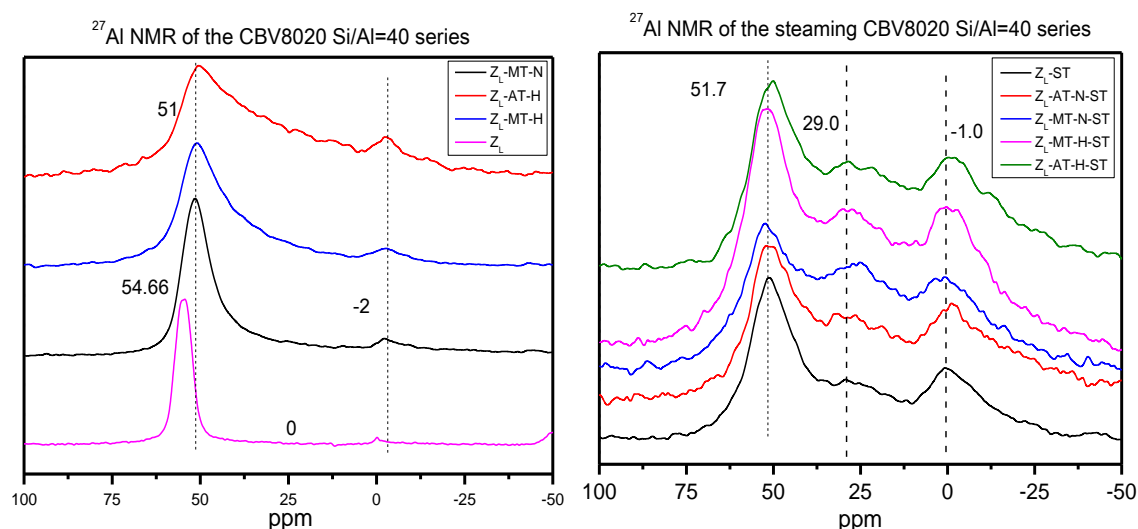


Fig 6.5 The $^{27}$Al NMR of the parent, desilicated and steamed samples $Z_L$ (ZSM-5 Si/Al=40) series.

$^{27}$Al MAS NMR (Fig 6.5) has been applied to characterize the coordination of Al atoms in the zeolite structure. The peaks at 51.6ppm and -2.5ppm are assigned to framework tetrahedral coordination Al atoms and octahedral coordination extra-framework aluminum respectively. In the desilication process, the extraction of

silicon was accompanied by the broken bond of Si-O-Al, even though the Si-O-Si bonds are fragile to suffer hydrolysis and dissolution without the neighboring Al atom conditions [23,29]. In this case, the appearance of signal at -2.5ppm of the desilicated samples indicates the presence of extra-framework aluminum atoms after desilication process treated by alkaline solution, accompanied with the four-coordination framework aluminum atoms transfer to six-coordination extra-framework ones[30]. The peaks of tetrahedral Al of the desilicated samples turn broader when compared with parent one due to the framework disturbance, which suggests higher heterogeneity of the Al environment [19]. After steaming, the peaks of extra-framework Al atoms increase due to the Al removal in the desilication process.

Table 6.3 Pyridine adsorption of parent and desilicated ZSM-5 samples at different temperatures.

| Sample | | 150 | 250 (mmol/g) | 350 | Sample | | 150 | 250 (mmol/g) | 350 |
|---|---|---|---|---|---|---|---|---|---|
| $Z_L$ | $C_B$ | 0.203 | 0.193 | 0.159 | $Z_H$ | $C_B$ | 0.0838 | 0.0749 | 0.0660 |
| | $C_L$ | 0.0194 | 0.0137 | 0.0114 | | $C_L$ | 0.00456 | 0.00342 | 0.00171 |
| $Z_L$–AT-N | $C_B$ | 0.262 | 0.213 | 0.192 | $Z_H$-MT-H | $C_B$ | 0.0353 | 0.0342 | 0.0245 |
| | $C_L$ | 0.0496 | 0.0410 | 0.0393 | | $C_L$ | 0.0216 | 0.0165 | 0.0152 |
| $Z_L$–MT-N | $C_B$ | 0.207 | 0.184 | 0.161 | $Z_H$-MT-N | $C_B$ | 0.0308 | 0.0279 | 0.0188 |
| | $C_L$ | 0.0542 | 0.0507 | 0.0496 | | $C_L$ | 0.0467 | 0.04318 | 0.0343 |
| $Z_L$–AT-H | $C_B$ | 0.264 | 0.213 | 0.180 | $Z_H$-AT-H | $C_B$ | 0.0353 | 0.0291 | 0.0217 |
| | $C_L$ | 0.0239 | 0.0205 | 0.0160 | | $C_L$ | 0.0229 | 0.0127 | 0.00762 |
| $Z_L$–MT-H | $C_B$ | 0.207 | 0.187 | 0.142 | $Z_H$-AT-N | $C_B$ | 0.0296 | 0.0262 | 0.0182 |
| | $C_L$ | 0.0228 | 0.0182 | 0.0165 | | $C_L$ | 0.0356 | 0.0292 | 0.0114 |
| $Z_L$– [0.5M] | $C_B$ | 0.0524 | 0.0445 | 0.0291 | | | | | |
| | $C_L$ | 0.0546 | 0.0508 | 0.0343 | | | | | |

| Sample | | 150 | 250 (mmol/g) | 350 | Samples | | 150 | 250 (mmol/g) | 350 |
|---|---|---|---|---|---|---|---|---|---|
| $Z_L$-ST | $C_B$ | 0.0262 | 0.00969 | 0.00285 | $Z_H$-ST | $C_B$ | 0.00057 | 0.0006 | 0.0006 |
| | $C_L$ | 0.0965 | 0.0673 | 0.0368 | | $C_L$ | 0.0152 | 0.0127 | 0.0102 |
| $Z_L$-AT-N-ST | $C_B$ | 0.0229 | 0.0152 | 0.00381 | $Z_H$-MT-H-ST | $C_B$ | 0.0546 | 0.0457 | 0.0330 |
| | $C_L$ | 0.0234 | 0.0217 | 0.00684 | | $C_L$ | 0.0216 | 0.0178 | 0.0064 |
| $Z_L$-MT-N-ST | $C_B$ | 0.0241 | 0.0140 | 0.00508 | $Z_H$-MT-N-ST | $C_B$ | 0.00741 | 0.0063 | 0.0034 |
| | $C_L$ | 0.0342 | 0.0257 | 0.0148 | | $C_L$ | 0.0152 | 0.0114 | 0.0064 |
| $Z_L$-AT-H-ST | $C_B$ | 0.0318 | 0.0191 | 0.00635 | $Z_H$-AT-H-ST | $C_B$ | 0.0148 | 0.0063 | 0.0023 |
| | $C_L$ | 0.0257 | 0.0245 | 0.0154 | | $C_L$ | 0.0521 | 0.0267 | 0.0178 |
| $Z_L$-MT-H-ST | $C_B$ | 0.0254 | 0.0165 | 0.00635 | $Z_H$-AT-N-ST | $C_B$ | 0.0108 | 0.0063 | 0.0034 |
| | $C_L$ | 0.0410 | 0.0257 | 0.0171 | | $C_L$ | 0.0165 | 0.0102 | 0.0051 |
| $Z_L$-[0.5M]-ST | $C_B$ | 0.00969 | 0.00855 | 0.00171 | | | | | |
| | $C_L$ | 0.0406 | 0.0267 | 0.0191 | | | | | |

Pyridine chemisorption and infrared spectroscopic measurements have been used to identify Brønsted (BAS) and Lewis acid sites(LAS) of the parent ZSM-5 and their treated samples, with a summary in the Table 6.3 at three different temperatures of desorption: 150 250 and 350°C [31-33]. Firstly, the amount of BAS for the series Si/Al=40 ZSM-5, is very similar despite differences in Si/Al bulk ratio measured by ICP analysis, especially for the samples with ionic exchange with $NH_4Cl$. Therefore, the treatment with oxalic acid is more efficient for removing extra-framework alumina. In the case of the high Si/Al ZSM-5, the desilication treatment seems to have decreased the BAS acidity. The acidity strength can be measured by comparing the BAS retained after desorption of pyridine at higher temperatures. For the Si/Al=40 ZSM-5 and series treated samples, the parent sample BAS retain 78% (decrease from 0.2032 to 0.1588) compared with the 73, 78 and 68% maintenance of the treated by alkaline solution when the temperature increases from 150 to 350°C which is consistent with the results from Sadowaska on the lower acid strength of the sites of the desilicated samples[19]. Conversely, the sample treated at high concentration NaOH solution has lost 75% acidity, indicating that despite the high mesoporosity acidity has been severely affected. For the Si/Al=140 ZSM-5 series treated samples, BAS concentration decreases along with the increase in LAS concentration when compared with the parent samples.

In summary, from the characterization performed it can be said that desilication procedures create open mesopores that are narrower in the case of high Si/Al ZSM-5 and also when TPAOH is added to the NaOH solution. The acidity strength is lowered. In addition, mesoporosity is preserved after hydrothermal treatment.

## 6.3.2. Catalytic performance
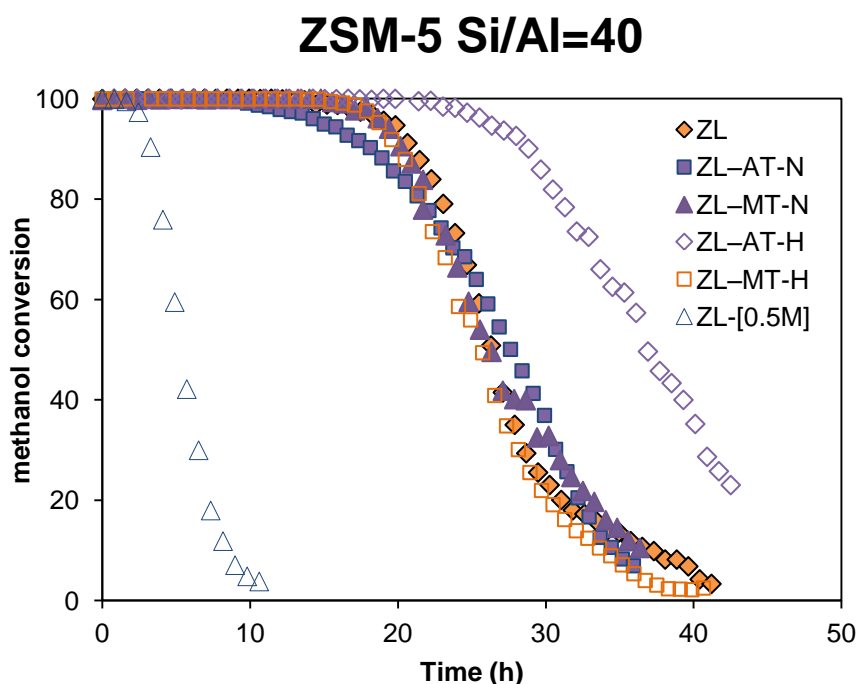
### ZSM-5 Si/Al=40



Fig 6.6 Conversion of Methanol at 450°C and WHSV=12h$^{-1}$ on ZSM-5 Si/Al=40 $Z_L$ and desilicated samples.

The catalytic performance of the parent ZSM-5 and the desilicated samples in methanol to hydrocarbons reactions at 450°C temperature with a WHSV=12h$^{-1}$ are shown in Fig 6.6. Spatial velocity is much higher than industrial conditions with the objective to obtain a curve of deactivation in a short period of time. Industrial lifetimes for high Si/Al ratio ZSM-5 are around 1000h and are not practical from a laboratory point of view. On the contrary, for the steamed samples it is not possible to obtain a curve of deactivation in a short period time since deactivation by coking is very slow due to the decreased acidity. In this case conversions (that are constants in time after the induction period) are compared at different contact times obtaining a S-shaped curve also used in the literature for comparing catalyst in MTH [34]. The lifetime was defined as the time for methanol conversion 50% and the product selectivity are mainly olefins, C6-C10 (aromatics) and some other naphthenes and paraffins.

From the curves of time on stream, all the Si/Al=40 ZSM-5 and their desilicated samples shows initial 100% conversion at first. However, it is clearly shown that not

all the desilicated samples present higher lifetime compared with the parent sample. The sample $Z_L$–0.5[M] with high mesoporosity and low micropore volume presents the shortest lifetime, while the sample $Z_L$-AT-H shows the highest. The rest of the samples despite their increased mesoporosity does not improve lifetime of the parent Si/Al=40 ZSM-5. It appears that the improvement of lifetime for $Z_L$-AT-H should be assigned to the combination of improved mesoporosity, preserved microporosity and acidity. All of these, increase diffusion rates and prevents micropore blocking by coke delaying therefore deactivation. In this way, the oxalic acid treatment is beneficial for removing the amorphous formed by disordered alumina in the micropore mouth in the desilication process[17], which improves the accessibility of the reactant to the reaction centers and the diffusion of the product to leave the acid sites.
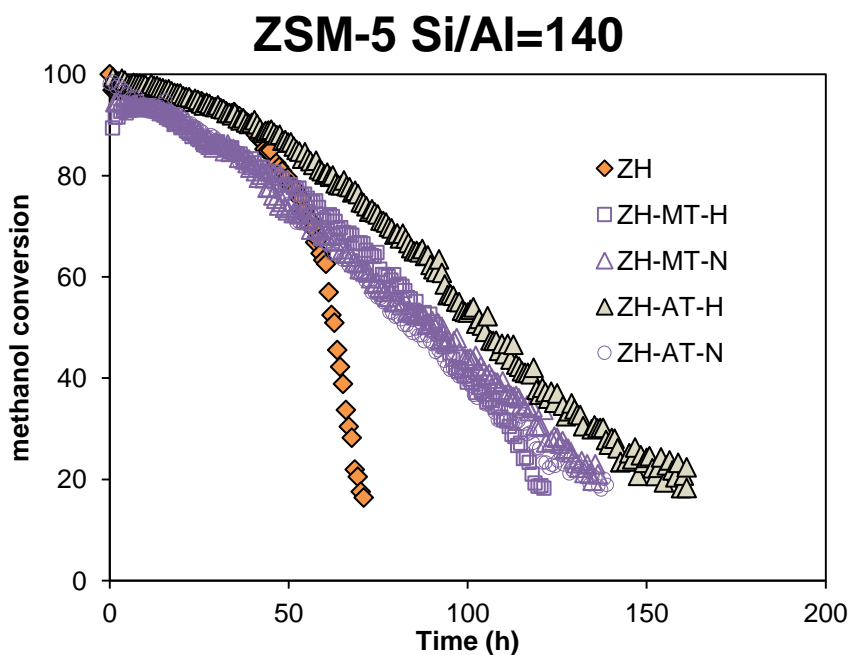


Fig 6.7 Conversion of Methanol at 450ºC and WHSV=12h$^{-1}$ on ZSM-5 Si/Al=140 $Z_H$ and desilicated samples.

For the Si/Al=140 ZSM-5 samples, the initial stage conversions are not fully 100% because of the lower acidity as shown in Table 6.3, However, lifetime until 50% conversion is much longer than for the series of Si/Al=40. This is due to the different mechanism of the hydrocarbon pool for these samples as we will comment later, in which high Si/Al ZSM-5 converts methanol following the olefin cycle instead of the aromatic one. This, together with the lower density of acid sites decrease the amount of bimolecular reactions as cyclization and hydrogen transfer that further lead to

coke. When comparing the activity of the samples it can be appreciated that the slope of deactivation is slower for the desilicated samples comparing with the parent sample from which deactivation is much faster. This leads to higher lifetime for all the desilicated samples, and this is much notorious for the sample $Z_H$-AT-H while, for example the sample $Z_H$-AT-N present lower increase in lifetime. Both samples have similar mesoporosity and micropore volume, while $Z_H$-AT-H has preserved more Brönsted acidity after the desilication treatment. It could be argued that the increased lifetime is due to lower acidity comparing to the parent sample, however the acidity of the parent sample is already so low that higher Si/Al ratio, though may delay coking and deactivation, does not present activity enough as we will show later for the steamed samples. In addition, for the high Si/Al ZSM-5, the desilication treatments with TPAOH/NaOH, though making a more controlled size of mesoporous did not show an improved effect on lifetime comparing with NaOH alone.

Table 6.4 Conversion of Methanol at 450ºC but different space velocities on steamed parent and desilicated samples ZSM-5 Si/Al=40 $Z_L$, Si/Al=140 $Z_H$ samples.

| | WHSV($h^{-1}$) | | | | WHSV($h^{-1}$) | | |
|---|---|---|---|---|---|---|---|
| sample | 12 | 2.5 | 1 | | 12 | 2.5 | 1 |
| $Z_L$ | 100 | - | 100 | $Z_H$ | 97 | - | 99 |
| $Z_L$-ST | 0.60 | 57 | 92 | $Z_H$-ST | 0.16 | 0.32 | 20 |
| $Z_L$ –AT-N-ST | 0.29 | 0.79 | 62 | $Z_H$-MT-H-ST | 0.20 | 0.60 | 1.8 |
| $Z_L$ –MT-N-ST | 0.68 | 58 | 64 | $Z_H$-MT-N-ST | 0.20 | 1.82 | 72 |
| $Z_L$ –AT-H-ST | 0 | 1.6 | 63 | $Z_H$-AT-H-ST | 0.21 | 17 | 64 |
| $Z_L$ –MT-H-ST | 0.70 | 50 | 90 | $Z_H$-AT-N-ST | 0.26 | 0.28 | 17 |
| $Z_L$ – [0.5M]-ST | 0.17 | 0.54 | 18 | | | | |

An important question is how desilicated samples behave after many cycles of reaction-regeneration. This parameter could be of great economic impact for the profitability of the plant, since the cost of the catalyst is important. As commented before, a reversible deactivation occurs after each cycle due to the dealumination of the structure and the loss of acidity that the operators can compensate by increasing the severity of the reactor up to a certain limit, beyond this limit the catalyst is discarded. Submitting the samples to steaming at 700°C for 5h an accelerated deactivation can be obtained and the activity of the samples can be compared (Table 6.4). Due to the lower acidity, activity is much lower and deactivation takes place at times too long for laboratory tests. Therefore, the steamed samples have been

compared by their conversion values at different spatial velocities from 12, to 1h$^{-1}$. For the series of Si/Al=40, steamed desilicated samples present in general lower activity than the steamed parent sample. While for the series Si/Al=140, it appears that some steamed desilicated samples present higher activity than the parent one. Since the textural parameters are preserved during steaming, the differences should be due to different dealumination sensitivity of parent and desilicated samples. How to improve this stability for the parent and desilicated samples is a matter of next chapter.
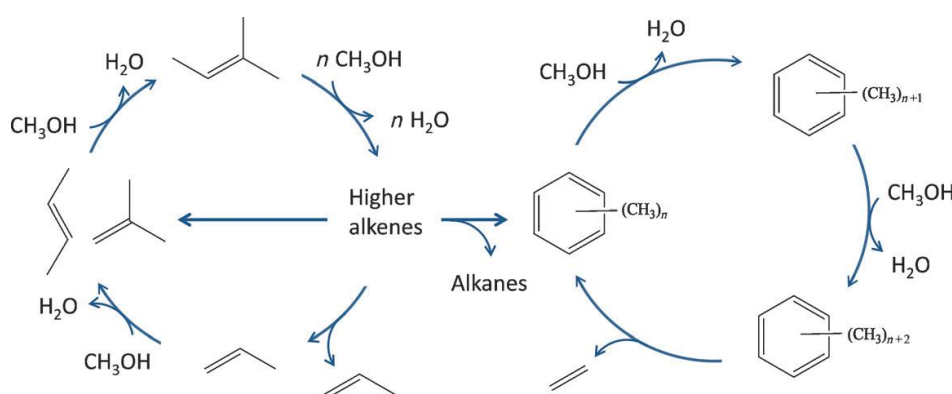


Scheme 6.1 Suggested dual-cycle concept for the conversion of methanol over H-ZSM-5 [2]

In order to reveal the different behaviors in the methanol to hydrocarbons reactions of the parent and desilicated samples, the differnt mechanism of formation of ethylene and propylene will be discussed firstly. According to the known dual-cycle mechanism shown in the Scheme 6.1 for methanol to olefins in ZSM-5, two cycles of reactions run simultaneously and interact: aromatics and olefins are continuously formed in the aromatics-based cycle, while in other cycle olefins are also formed by methylation-cracking and they interact by the hydrogen transfer reactions [2]. The mechanism elucidates that the formation of ethylene is due to the contribution of aromatics-based hydrocarbon pool route, while propylene and higher alkenes are formed by methylation or interconversions and cracking [7, 35].

## C2/C3
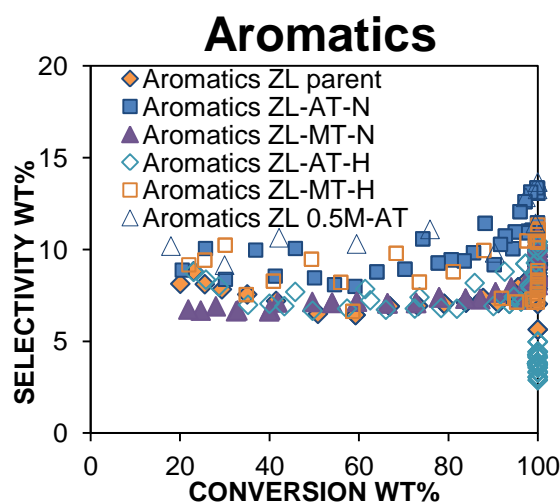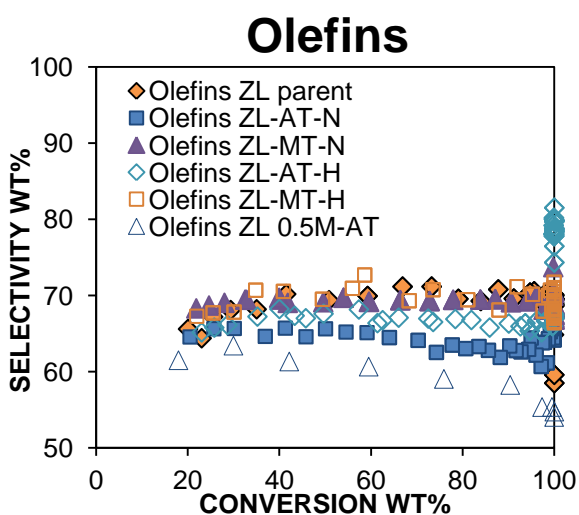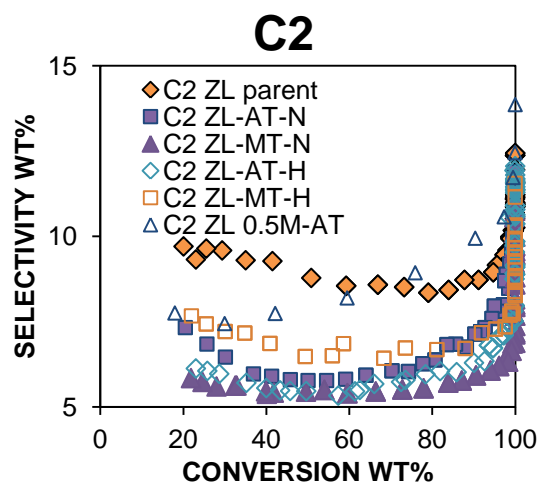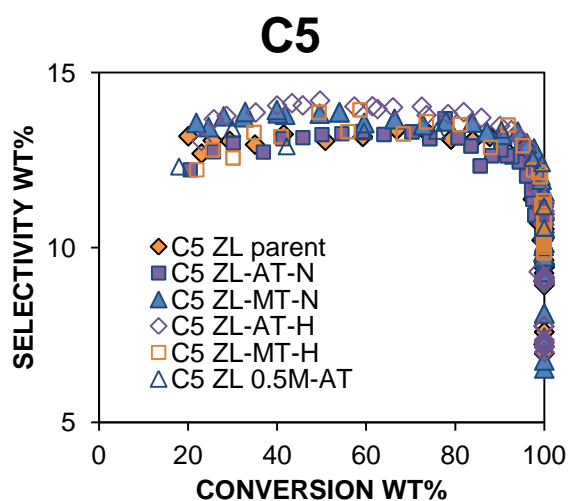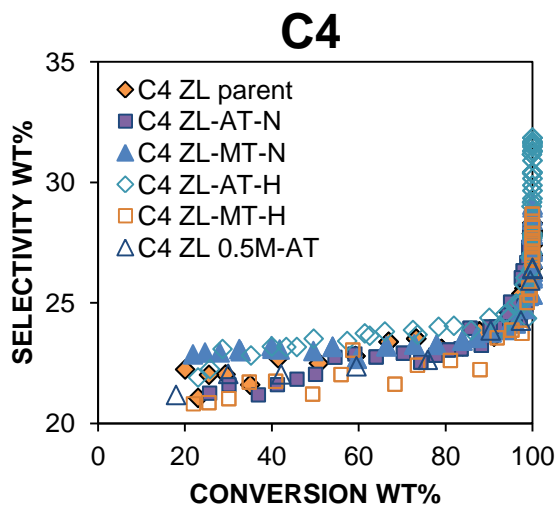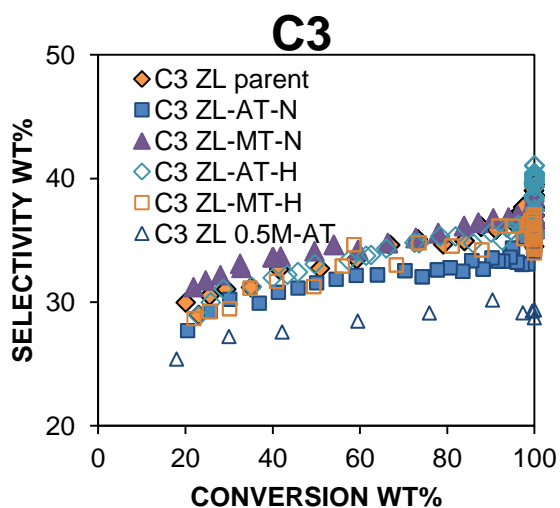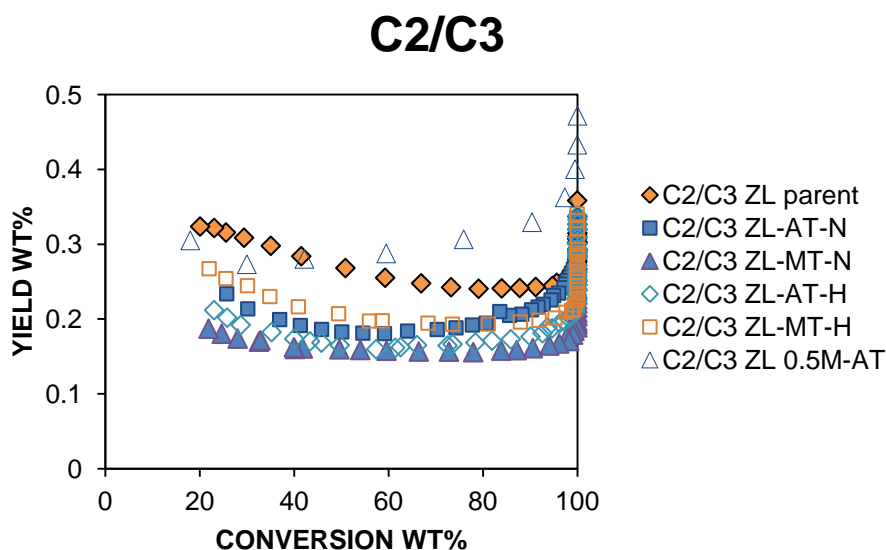


Fig 6.8 Product distributions of the desilicated ZSM-5 Si/Al =40 $Z_L$ samples at 450°C and WHSV=12h$^{-1}$.

The main product selectivity versus conversion of these samples at the identical condition in the methanol to hydrocarbons reactions have been summarized in the Fig 6.8. It has been well known that the acidity plays an important role in the activity and coke formation. For the Si/Al =40 ZSM-5 series, C3 C4 C5 and C2 are the main products, plus $CH_4$ and C6+, products. It is notable to show that the selectivity curves of the three products C3 C4 and C5 at conversion lower than 100% are independent on conversion in the parent and desilicated samples, which is consistent with the work done by Olsbye that product distribution in the methanol conversion is mainly independent of deactivation [36], and similar situation has been found in other reaction in which ZSM-5 used as the catalyst [37]. At conversions close to 100%, it occurs as shown before for SAPO-34, interconversion between products on fresh catalyst drives the olefin selectivity to equilibrium. Therefore, the true selectivity of the hydrocarbon pool on ZSM-5 is shown at intermediate conversions lower than 100%.

When comparing the different selectivities between parent and desilicated samples, there are changes in selectivities. The parent sample Si/Al=40 ZSM-5 exhibits the highest selectivity of the C2, and the samples $Z_L$-MT-N showed the lowest C2 selectivity. The difference in the product selectivities are assigned to the difference in the mechanism. The formation of mesopores in the ZSM-5 seems not to have effect on the C3, C4, C5 selectivities, which also reveal that product selectivity

in this reaction is not controlled by diffusion. The larger differences are shown on C2 selectivity. In general, the mesoporous samples show lower selectivity to C2. However, it is important to notice that this decrease is not accompanied by a lower selectivity to aromatics. Therefore, the presence of mesoporosity developed by desilication does not seem to change the relative contribution of both cycles, olefins and aromatics. Then, the different selectivity to ethylene for desilicated samples could be explained by a lower acid strength. This lower strength should favour the elimination of propylene vs. ethylene in the final step of dealkylation in the aromatic cycle. In addition, same reasoning should be applied to the C2/C3 ratio in the way that a lower ratio for the desilicated samples should be attributed to a lower acid strength more than to a change in the contribution of each cycle of the hydrocarbon pool. The sample $Z_L$ 0.5M-AT with decreased microporosity, presents an anomalous behaviour with high selectivity to ethylene and low yield to olefins (high hydrogen transfer reactions) that should be linked with its fast deactivation comparing with the rest of the samples. Hence, as said before, an optimum desilication treatment should balance meso and microporosity.
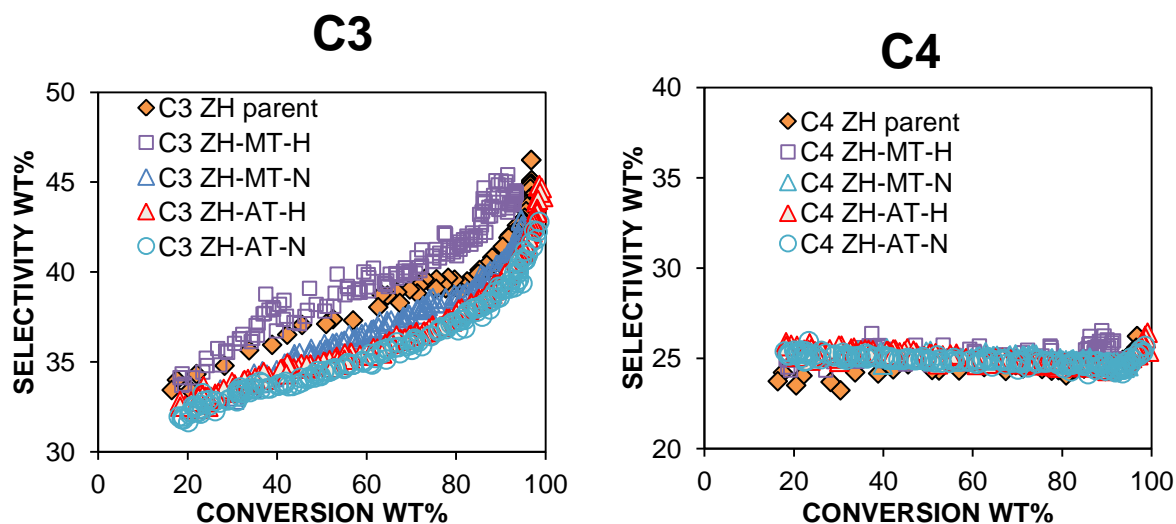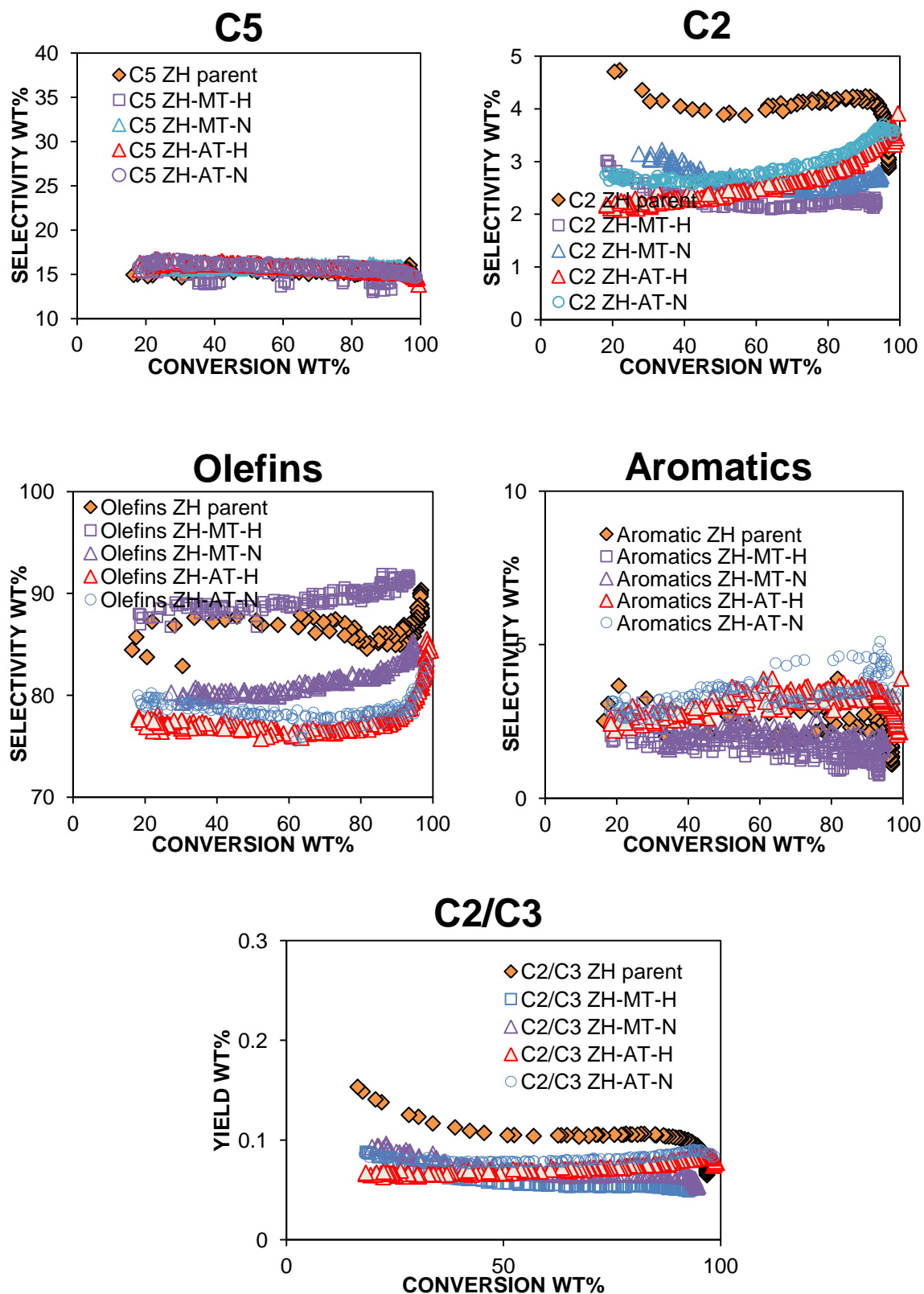
Fig 6.9 Product distribution of the desilicated samples of the Si/Al =140 $Z_H$ at 450°C and WHSV=12h$^{-1}$.

For the Si/Al=140 ZSM-5 series, it is clear that the low Al content that results in lower total acidity causes a change in the mechanism of the reaction, with a lower contribution of the aromatic cycle. In fact comparing with the parent Si/Al=40, the sample Si/Al=140 presents lower selectivity of both characteristic products of the aromatic cycle: aromatics and ethylene.

When comparing the selectivities, the desilicated samples show even lower selectivities to ethylene and also aromatics at least for the samples treated with oxalic acid, while the selectivities to butylenes and pentenes are almost unchanged, which suggests that the contribution of the aromatic cycle is further decreased. However, the reduction in total acidity of the desilicated samples could also be responsible of this results. Recently, the propylene selectivity has been shown to improve with lower Brønsted acid density [38-41]. Moreover, the lower C2/C3 ratios also suggest that the olefin cycle governs the selectivity of the desilicated samples. However, the samples with final ionic exchange yield more aromatics than the samples washed with oxalic acid. The increasing of aromatics in the desilicated samples with ionic exchange may be due to the higher Lewis acidity (see Table 6.3) due to extra-framework aluminum comparing with the samples washed with acid.

# 6.4. Conclusions

Mesopores are formed by desilication process carried out with NaOH and NaOH/TPAOH solutions in both ZSM-5 Si/Al=40 and 140 samples. Wider mesopores were found in the samples treated by NaOH compared with NaOH/TPAOH, and also it was found desilication process was much more effective on the high Si/Al ratio ZSM-5(140). Due to the formation of mesopores the desilicated samples exhibit larger BET and external surface areas, and these mesopores are well connected to the micropores. In the reaction of methanol to olefins, the desilicated samples of ZSM-5 Si/Al=140 present longer lifetime compared with their parent samples. In addition, it also suggests that the reaction mechanism is different for ZSM-5 Si/Al=40 and 140 samples, in which the aromatic mechanism is more dominant for the ZSM-5 Si/Al=40 while the alkene mechanism predominates for ZSM-5 Si/Al=140.

# References

[1] Y.-K. Park, C. Lee, N. Kang, W. Choi, S. Choi, S. Oh, D. Park, Catalytic Cracking of Lower-Valued Hydrocarbons for Producing Light Olefins, Catalysis Surveys from Asia, 14 (2010) 75-84.

[2] U. Olsbye, S. Svelle, M. Bjorgen, P. Beato, T.V. Janssens, F. Joensen, S. Bordiga, K.P. Lillerud, Conversion of methanol to hydrocarbons: how zeolite cavity and pore size controls product selectivity, Angewandte Chemie, 51 (2012) 5810-5831.

[3] S. Ilias, A. Bhan, Mechanism of the Catalytic Conversion of Methanol to Hydrocarbons, ACS Catalysis, 3 (2013) 18-31.

[4] D. Chen, K. Moljord, A. Holmen, A methanol to olefins review: Diffusion, coke formation and deactivation on SAPO type catalysts, Microporous Mesoporous Materials, 164 (2012) 239-250.

[5] C.D. Chang, A.J. Silvestri, The conversion of methanol and other O-compounds to hydrocarbons over zeolite catalysts, Journal of Catalysis, 47 (1977) 249-259.

[6] J. Cobb, New Zealand Synfuel: The Story of the World's First Natural Gas to Gasoline Plant, New Zealand Synthetic Fuels Corporation, (1985).

[7] M. Bjorgen, S. Svelle, F. Joensen, J. Nerlov, S. Kolboe, F. Bonino, L. Palumbo, S. Bordiga, U. Olsbye, Conversion of methanol to hydrocarbons over zeolite H-ZSM-5: On the origin of the olefinic species, Journal of Catalysis, 249 (2007) 195-207.

[8] Z. Li, J. Martinez-Triguero, P. Concepcion, J. Yu, A. Corma, Methanol to olefins: activity and stability of nanosized SAPO-34 molecular sieves and control of selectivity by silicon distribution, Physical Chemistry Chemical Physics, 15 (2013) 14670-14680.

[9] C. Baerlocher, L.B. McCusker, D.H. Olson, MFI - Pnma, in: C. Baerlocher, L.B. McCusker, D.H. Olson (Eds.) Atlas of Zeolite Framework Types (Sixth Edition), Elsevier Science B.V., Amsterdam, 2007, pp. 212-213.

[10] S. van Donk, A.H. Janssen, J.H. Bitter, K.P. de Jong, Generation, Characterization, and Impact of Mesopores in Zeolite Catalysts, Catalysis Reviews, 45 (2003) 297-319.

[11] M. Firoozi, M. Baghalha, M. Asadi, The effect of micro and nano particle sizes of H-ZSM-5 on the selectivity of MTP reaction, Catalysis Communication, 10 (2009) 1582-1585.

[12] K. Na, M. Choi, R. Ryoo, Recent advances in the synthesis of hierarchically nanoporous zeolites, Microporous Mesoporous Materials, 166 (2013) 3-19.

[13] G. Bellussi, G. Pazzuconi, C. Perego, G. Girotti, G. Terzoni, Liquid-Phase Alkylation of Benzene with Light Olefins Catalyzed by β-Zeolites, Journal of Catalysis, 157 (1995) 227-234.

[14] G. Tonetto, J. Atias, H. de Lasa, FCC catalysts with different zeolite crystallite sizes: acidity, structural properties and reactivity, Applied Catalysis A: General, 270 (2004) 9-25.

[15] S. Lin, J. Li, R.P. Sharma, J. Yu, R. Xu, Fabrication of SAPO-34 crystals with different morphologies by microwave heating, Topics in Catalysis, 53 (2010) 1304-1310.

[16] L.-H. Chen, X.-Y. Li, J.C. Rooke, Y.-H. Zhang, X.-Y. Yang, Y. Tang, F.-S. Xiao, B.-L. Su, Hierarchically structured zeolites: synthesis, mass transport properties and applications, Journal of Materials Chemistry, 22 (2012) 17381.

[17] K. Moller, T. Bein, Mesoporosity--a new dimension for zeolites, Chemical Society Reviews, 42 (2013) 3689-3707.

[18] V. Valtchev, G. Majano, S. Mintova, J. Perez-Ramirez, Tailored crystalline microporous materials by post-synthesis modification, Chemical Society Reviews, 42 (2013) 263-290.

[19] K. Sadowska, A. Wach, Z. Olejniczak, P. Kuśtrowski, J. Datka, Hierarchic zeolites: Zeolite ZSM-5 desilicated with NaOH and NaOH/tetrabutylamine hydroxide, Microporous and Mesoporous Materials, 167 (2013) 82-88.

[20] M. Bjørgen, F. Joensen, M. Spangsberg Holm, U. Olsbye, K.-P. Lillerud, S. Svelle, Methanol to gasoline over zeolite H-ZSM-5: Improved catalyst performance by treatment with NaOH, Applied Catalysis A: General, 345 (2008) 43-50.

[21] S. Fathi, M. Sohrabi, C. Falamaki, Improvement of HZSM-5 performance by alkaline treatments: Comparative catalytic study in the MTG reactions, Fuel, 116 (2014) 529-537.

[22] G.T. Kokotailo, A.C. Rohrman, Method for purifying zeolitic material, in, Google US Patents 4,703,025, 1987.

[23] J.C. Groen, L.A.A. Peffer, J.A. Moulijn, J. Pérez-Ramírez, Mechanism of Hierarchical Porosity Development in MFI Zeolites by Desilication: The Role of

Aluminium as a Pore-Directing Agent, Chemistry – A European Journal, 11 (2005) 4983-4994.

[24] J.C. Groen, J.A. Moulijn, J. P?rez-Ram?rez, Desilication: on the controlled generation of mesoporosity in MFI zeolites, Journal of Materials Chemistry, 16 (2006) 2121.

[25] J. Pérez-Ramírez, D. Verboekend, A. Bonilla, S. Abelló, Zeolite Catalysts with Tunable Hierarchy Factor by Pore-Growth Moderators, Advanced Functional Materials, 19 (2009) 3972-3979.

[26] D. Verboekend, J. Perez-Ramirez, Desilication mechanism revisited: highly mesoporous all-silica zeolites enabled through pore-directing agents, Chemistry, 17 (2011) 1137-1147.

[27] S. Abelló, A. Bonilla, J. Pérez-Ramírez, Mesoporous ZSM-5 zeolite catalysts prepared by desilication with organic hydroxides and comparison with NaOH leaching, Applied Catalysis A: General, 364 (2009) 191-198.

[28] K. Sadowska, K. Góra-Marek, M. Drozdek, P. Kuśtrowski, J. Datka, J. Martinez Triguero, F. Rey, Desilication of highly siliceous zeolite ZSM-5 with NaOH and NaOH/tetrabutylamine hydroxide, Microporous and Mesoporous Materials, 168 (2013) 195-205.

[29] T. Sano a, Y. Nakajima a, Z.B. Wang a, Y. Kawakami a, K. Soga a, A. Iwasaki b, Effect of framework aluminum on the dissolution process of SM-5 zeolite crystal, Microporous Materials, 12 (1997) 71-77.

[30] C. Mei, P. Wen, Z. Liu, H. Liu, Y. Wang, W. Yang, Z. Xie, W. Hua, Z. Gao, Selective production of propylene from methanol: Mesoporosity development in high silica HZSM-5, Journal of Catalysis, 258 (2008) 243-249.

[31] E. Parry, An infrared study of pyridine adsorbed on acidic solids. Characterization of surface acidity, Journal of Catalysis, 2 (1963) 371-379.

[32] K.P. Nan-Yu Topsøe, Eric G. Derouane, Infrared and temperature-programmed desorption study of the acidic properties of ZSM-5-type zeolites, Journal of Catalysis, 70 (1981) 41-52.

[33] C. Emeis, Determination of Integrated Molar Extinction Coefficients for Infrared Absorption Bands of Pyridine Adsorbed on Solid Acid Catalysts, Journal of Catalysis, 141 (1993) 347-354.

[34] M. Derewinski, P. Sarv, X. Sun, S. Müller, A.C. van Veen, J.A. Lercher, Reversibility of the Modification of HZSM-5 with Phosphate Anions, The Journal of Physical Chemistry C, 118 (2014) 6122-6131.

[35] S. Svelle, F. Joensen, J. Nerlov, U. Olsbye, K.P. Lillerud, S. Kolboe, M. Bjorgen, Conversion of methanol into hydrocarbons over zeolite H-ZSM-5: ethene formation is mechanistically separated from the formation of higher alkenes, Journal of the American Chemical Society, 128 (2006) 14770-14771.

[36] F.L. Bleken, T.V.W. Janssens, S. Svelle, U. Olsbye, Product yield in methanol conversion over ZSM-5 is predominantly independent of coke content, Microporous and Mesoporous Materials, 164 (2012) 190-198.

[37] D. Chen, H.P. Rebo, K. Moljord, A. Holmen, Influence of Coke Deposition on Selectivity in Zeolite Catalysis, Industrial & Engineering Chemistry Research, 36 (1997) 3473-3479.

[38] C.D. Chang, C.T.W. Chu, R.F. Socha, Methanol conversion to olefins over ZSM-5: I. Effect of temperature and zeolite $SiO_2Al_2O_3$, Journal of Catalysis, 86 (1984) 289-296.

[39] C.T.W. Chu, C.D. Chang, Methanol conversion to olefins over ZSM-5: II. Olefin distribution, Journal of Catalysis, 86 (1984) 297-300.

[40] F.L. Bleken, S. Chavan, U. Olsbye, M. Boltz, F. Ocampo, B. Louis, Conversion of methanol into light olefins over ZSM-5 zeolite: Strategy to enhance propene selectivity, Applied Catalysis A: General, 447–448 (2012) 178-185.

[41] J.W. Park, S.J. Kim, M. Seo, S.Y. Kim, Y. Sugi, G. Seo, Product selectivity and catalytic deactivation of MOR zeolites with different acid site densities in methanol-to-olefin (MTO) reactions, Applied Catalysis A: General, 349 (2008) 76-85.

# 7. Hydrothermal stabilization of mesoporous high Si/Al ZSM-5 by phosphorus addition and its effect on the activity of methanol to olefins

# 7.1.Introduction

The conversion of methanol, an alternative for the increasing demand for the light olefins, mainly ethylene and propylene, has attracted the interest of researchers especially with the new technologies developed for the transformation of natural gas, biomass, and other carbon-rich feedstocks into methanol [1-4]. SAPO-34 and ZSM-5 are the main zeolites applied in these reactions, whereas SAPO-34 exhibits high selectivities of ethylene and propylene, ZSM-5 presents a broader product distribution including olefins, aromatics, paraffins, naphthenes and so on. However, the solutions to obtain more light olefins especially in the propylene product have been proposed by means of the increasing Si/Al ratios ZSM-5 [5-6]. The introduction of phosphorus to modify ZSM-5 is also one of the ways to improve the propylene selectivity and reduce the aromatics product in the expense of the decrease of acidity [6-9], and with the washing of hot water, additional Brønsted acidity can be recovered [10, 11]. Since it was firstly reported, the phosphorus modification has been applied to different reactions such as fluid catalytic cracking , toluene alkylation, also the methanol to hydrocarbons included [11]. The introduction of phosphorus also plays an important role in enhancement the hydrothermal stability of the ZSM-5, as it was first reported by Lischke et al. [10], and confirmed by the other scientists [12-16].

However, there is still a debate about the mechanism of the introduction phosphorus, along with the unclearly agreement about the interaction of the phosphorus with the zeolitic structure.  Many mechanisms have been proposed such as the direct connection of phosphorus and the zeolite frameworks, framework interactions or the formation of tetrahydroxyphosphonium ions [10, 12, 13, 17-22] which have been summary by Lercher and shown in Scheme 7.1[11].
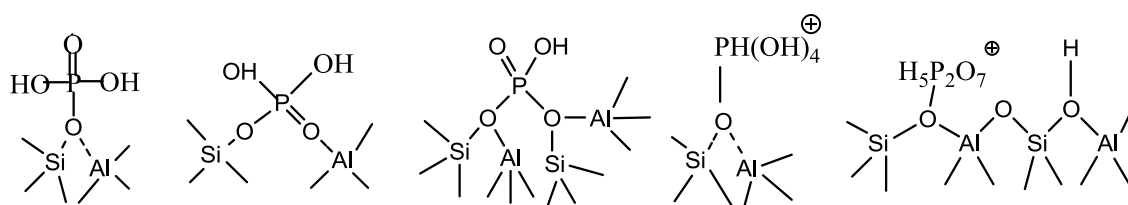


Scheme 7.1 Different models on the interaction between the phosphorus and the ZSM-5 framework [11].

In this chapter, we have prepared phosphorus modified ZSM-5 samples starting from high Si/Al ZSM-5 and also pretreated with basic/acid solution for the development of mesoporosity and we have investigated the effect in the acidity and their performance in the methanol to hydrocarbons reactions The properties and catalytic performance of the phosphorus modified sample were also tested after steaming. Finally, we will discuss about the mechanism of the phosphorus introduction and the interaction of the phosphorus and the zeolites, in order to better understand the phosphorus effect.

# 7.2. Experimental

## 7.2.1. Catalyst preparation

The parent ZSM-5 were obtained from Zeolyst International named as CBV28014 (Si/Al=140, parent samples defined as $Z_H$) as we mentioned in the Chapter 6. The desilication process selected was [0.2M]-NaOH and washing in acid oxalic solution and the procedure was described in the Chapter 6. The desilicated samples were then impregnated in rotavapour at 80°C with a $NH_4H_2PO_4$ (Solid/Liquid ratio of 10) solution until evaporation followed by calcination at 500°C for 5 hours. The samples fabricated in this procedure are defined as Z-S-x% P, where x means the weight amount of the introduction phosphorus. An alternative way to prepare the phosphorus modified sample is directly to impregnate the parent samples into the $NH_4H_2PO_4$ solution followed by calcination at 500°C for 5 hours. The sample obtained from this method was defined as Z-x% P, where x the weight percent of phosphorus.

The steaming process was carried out at 700°C for 5 hours as we have mentioned in the Chapter 6, and steamed sample was addition with "st" when compared with their parent samples.

## 7.2.2. Characterization

All the measurements here are referenced as described in the Chapter 3.

## 7.2.3.Catalytic experiments

The conditions of the catalytic test are similar as described in Chapter 6, but the amount of catalysts tested in the reaction in this chapter is 25mg with WHSV=24h$^{-1}$ with the objective to limit lifetime to less than one week for all the catalysts. The steamed P-modified catalysts are tested at different contact times with 0.50mg of catalyst by varing the flow of nitrogen in the bubbler of methanol at 25°C. Conversion and selectivities were calculated in carbon basis being methanol and dimethylether considered as feed.

# 7.3.Results and discussions

## 7.3.1.Characterization
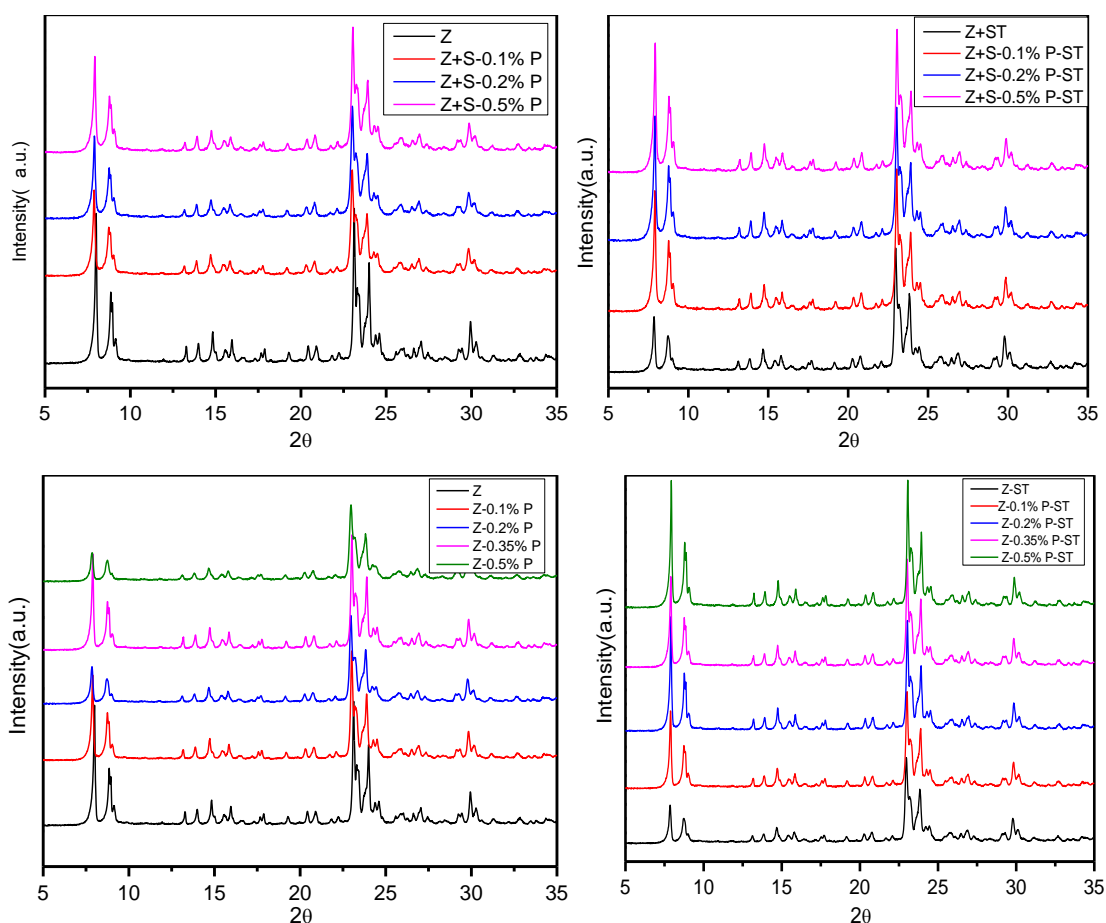


Fig 7.1 XRD patterns of the parent, P-modified and steamed ZSM-5 samples.

X-Ray diffraction patterns of the parent ZSM-5 treated in alkaline solution and with phosphorus and the direct introduction of phosphorus to the parent ZSM-5, are shown in Fig 7.1 fresh and after steaming at 700°C for 5 hours. The parent samples modified by phosphorus(Z+%P), the parent samples treated by alkali solution and phosphorus(Z+S+%P) show similar diffraction patterns as their parent ZSM-5 samples, which means the MFI structures have been maintained without much changes after the treatment and modification. However, crystallinity loses are still found when comparing with parent samples as listed in Table 7.1, which shows the relative crystallinity value of the samples calculated based on the characteristic peaks the range from 22.5 to 25°. The desilication process resulted in the formation of structural defects, which makes the treated samples present relative lower crystallinity compared with the parent samples. This can be also found in the following measurements of $^{27}$Al MAS NMR spectra and TEM images. The crystallinity loss for the direct introduction of phosphorus is possibly because of slight dealumination of the parent samples. Meanwhile, the MFI structure still remained even when the samples suffered hydrothermal treatment as shown in the Fig 7.1. The steamed samples lose crystallinity due to the steam treatment.

Table 7.1 Chemical and textural properties of the parent and P-modified ZSM-5 samples.

| Samples | ICP (Si/Al) | Lifetime (h) | BET ($m^2$/g) | t-plot $S_{ext}$ ($m^2$/g) | $V_{micro}$ ($cm^3$/g) | $V_{meso}$ ($cm^3$/g) | Crystallinity |
|---|---|---|---|---|---|---|---|
| Z (Si/Al=140) | 140 | 27 | 377 | 43.4 | 0.16 | 0.07200 | 100 |
| Z-S- 0.1% P | 103.4 | 70.5 | 414 | 70.5 | 0.17 | 0.20 | 92 |
| Z-S- 0.2% P | 103.6 | 83.1 | 406 | 67.2 | 0.17 | 0.20 | 87 |
| Z-S- 0.5% P | 107.8 | - | 409 | 66.3 | 0.17 | 0.19 | 95 |
| Z-0.1% P | 120.3 | 16.81 | 379 | 39.4 | 0.16 | 0.063 | 89 |
| Z-0.2% P | 87.6 | 13.9 | 380 | 37.9 | 0.16 | 0.061 | 79 |
| Z-0.35% P | 119.0 | - | 379 | 36.6 | 0.16 | 0.061 | 94 |
| Z-0.5% P | 100.5 | - | 368 | 32.4 | 0.16 | 0.060 | 88 |

The textural properties of parent and the treated samples have been measured by N2 adsorption measurements and the results summarized in Table 7.1. BET areas and mesopore volumes increase after desilication process as shown in previous chapter, with the preservation of the micropore volumes. When the desilication+phosphourus treated samples are compared with the parent one, the

micropore volumes are preserved due to the removal of extra-framework Al atoms in the channel by the acid treatments. The presence of mesopore in the desilication+ phosphorus samples is proved by the pore distribution calculated on the BJH model as shown in Fig 7.2, It reveals that the pore diameter is about 12.5nm which is in the range of the mesopore size. The direct introduction of phosphorus samples on the parent sample has no important effect in the textural properties surface areas. Only a small decrease in BET and external surface is seen after the addition of the highest amount of phosphorus. When the samples are submitted to hydrothermal treatment, the desilication+phosphorus modified samples still keep their higher BET and external surface areas, and maintain the larger mesopore volumes Table 7.2 which suggest that the addition of P induces high hydrothermal stability that could be an important property for methanol to olefins reaction provided that framework aluminum is stabilized by the addition of phosphorus. Even the direct introduction of phosphorus samples also show better stability than the parent sample with no P, that presents lower BET, external surface areas micro/meso pores, and crystallinity after steaming than the P-containing samples. It offers another proof that the introduction of phosphorus enhances the hydrothermal stabilization of the structure.

Table 7.2 Textural properties of the parent and phosphorus treated ZSM-5 samples after steaming treatments.

| Samples | BET $(m^2/g)$ | t-plot $S_{ext}$ $(m^2/g)$ | $V_{micro}$ $(cm^3/g)$ | $V_{meso}$ $(cm^3/g)$ | Crystallinity |
|---|---|---|---|---|---|
| Z-ST (Si/Al=140) | 366 | 38.8 | 0.16 | 0.070 | 78 |
| Z-S- 0.1% P- ST | 369 | 69.2 | 0.16 | 0.21 | 88 |
| Z-S- 0.2% P- ST | 398 | 65.0 | 0.17 | 0.20 | 91 |
| Z-S- 0.5% P- ST | 403 | 64.1 | 0.17 | 0.20 | 93 |
| Z - 0.1% P- ST | 371 | 32.9 | 0.16 | 0.058 | 85 |
| Z - 0.2% P- ST | 377 | 31.8 | 0.17 | 0.054 | 92 |
| Z - 0.35% P- ST | 384 | 32.6 | 0.16 | 0.051 | 91 |
| Z - 0.5% P-ST | 383 | 27.5 | 0.17 | 0.045 | 98 |
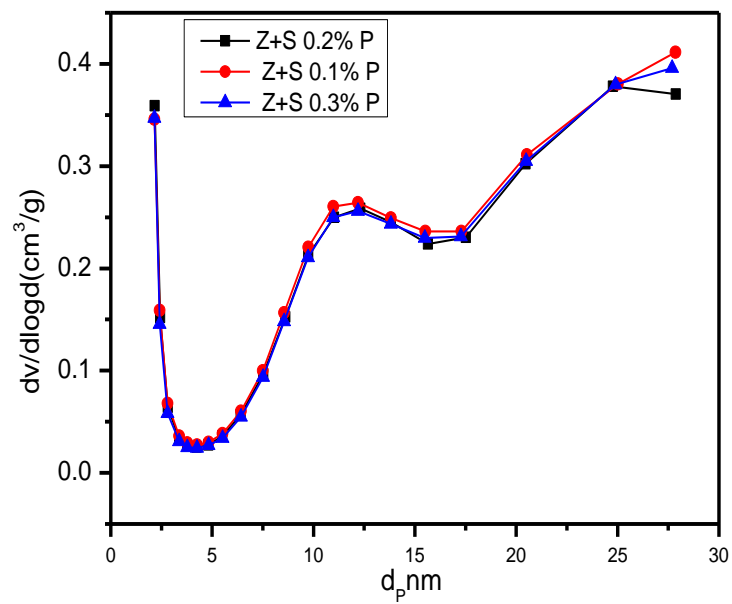
Fig 7.2 The pore distribution of the desilication + phosphorus ZSM-5 samples.
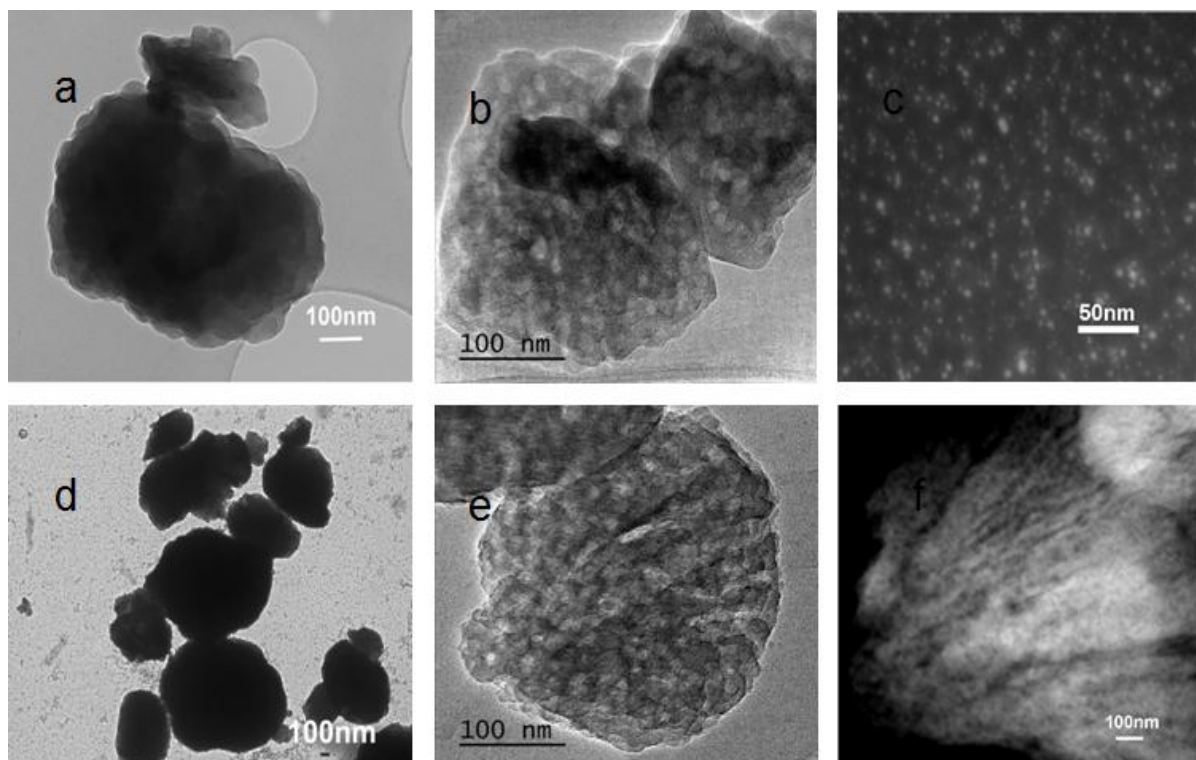


Fig 7.3 TEM images of the parent a) Z and treated samples b) Z+S-0.1% P d) Z -0.1% P e) Z+S-0.5% P in bright field and c) Z+S-0.1% P f) Z+S-0.5% P in dark field.

TEM images of the parent samples in the bright and dark field of samples are shown in Fig 7.3. It is worth noting that there are no mesopores in parent ZSM-5 before and after P-addition, in which the crystal size are about the range of 400-600nm. However, mesopores in the range 10-15nm appear in the desilication+phosphorus samples sheet with crystal size about 200-400nm as shown in the Fig 7.3, which are due to the basic attack. The external surface of the desilication+phosphorus samples turns to be rough with the presence of open holes, as well as the crystal becomes cracked due to the attack with OH⁻ ions. What is important is that the random distributions of the open holes are perfectly connected through the zeolite crystals, which could be illustrated by means the dark filed images. These results are consistent with the XRD and $N_2$ adsorption and desorption measurements.
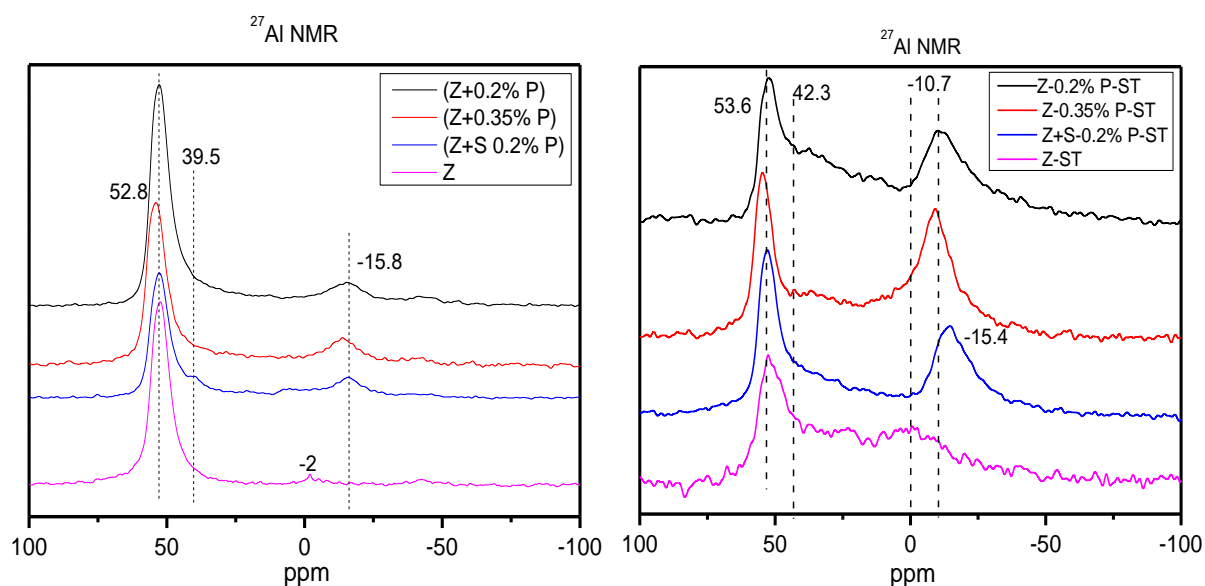


Fig 7.4 $^{27}$Al MAS NMR spectra of the parent and P-modified samples and their steamed samples.

$^{27}$Al MAS NMR spectra of the parent samples, desilication + phosphorus treated samples, and direct introduction of phosphorus samples are shown in Fig 7.4, as well as the steamed treatment samples. The main peak at 52.8 ppm is assigned to tetrahedral framework aluminum, along with the weak peak around 0 ppm which suggests octahedral extra-framework aluminum species respectively [13]. The introduction of phosphorus leads to the loss of the peak at -2ppm and the emergence of the new peaks at 39.5 ppm and -15.8 ppm which are corresponding

to distorted tetrahedral aluminum located framework or extra-framework which are connected with phosphorus species and aluminum attached to the terminal polyphosphate group[13,23]. However, the signals of the framework Al would decrease when these samples are steamed, along with the emergence of new peaks 30-42.3ppm, which are difficult to identify because of the peaks overlapping especial in the one-dimensional ^{27}Al NMR spectrum, even though some previous reports expounded the assignment of these peaks may be the formation of distinct types of aluminum phosphate [12] or distorted tetrahedral coordination framework aluminum species [8]. The resonance of 42.3ppm is ascribed to P interacting with Al tetrahedrally [13].
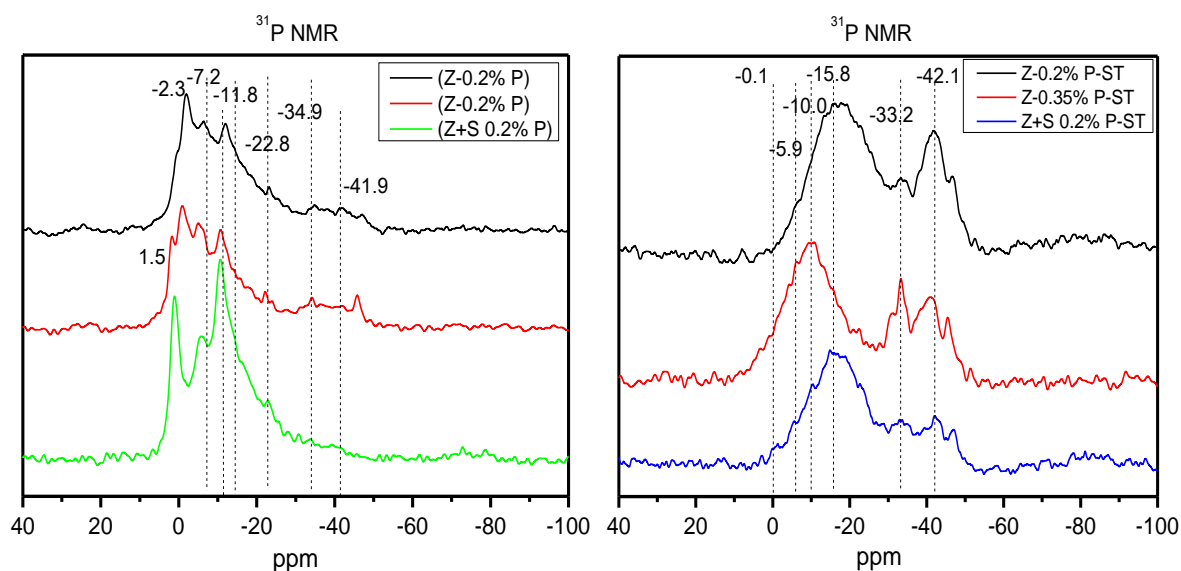


Fig 7.5 ^{31}P NMR of the parent and P-modified samples and their steamed samples.

The ^{31}P NMR of the P-modified samples is illustrated in Fig 7.5. A weak signal can be detected at 1.5ppm, which is attributed to phosphorus without connection to the framework aluminum [21, 22, 24]. The intense peak at -7.2 ppm is attributed to phosphorus in  polyphosphoric or pyrophosphorus acid  or terminal groups which are located in short-chain polyphosphates [10, 24-26] species and two broad resonances at -11.8,-34.9 ppm which correspond to middle groups of short-chain pyrophosphates or polyphosphates[25], or amorphous aluminum phosphate[27]. The signal at -41.9 ppm is associated to the P species in $P_4O_6$ [8, 10, 13], along with the signals in the range -30- -41.9ppm which are attributed to the formation of $(SiO)_xAl(OP)_{4-x}$ or to aluminum phosphate[13], these results are consistent with ^{27}Al NMR we discussed previously. After steaming, the signal at -7.2 shifts and decrease,

while the signal at -11.8 shifts to -15.8 and increases, while the signals at -34.9 and -41.9ppm increases, which suggests that more condensed phosphorus species are formed [13].

Table 7.3 The acidity properties of the parent and P-modified ZSM-5 samples.

| Samples | | 150 | 250 (mmol/g) | 350 | Samples | | 150 | 250 (mmol/g) | 350 |
|---|---|---|---|---|---|---|---|---|---|
| Z | $C_B$ | 0.08382 | 0.0749 | 0.0660 | Z-ST | $C_B$ | 0.00057 | 0.00057 | 0.000570 |
| | $C_L$ | 0.00456 | 0.00342 | 0.00171 | | $C_L$ | 0.0152 | 0.0127 | 0.0102 |
| Z-S-0.1% P | $C_B$ | 0.0686 | 0.0546 | 0.0521 | Z-S-0.1% P -ST | $C_B$ | 0.0203 | 0.00889 | 0.00635 |
| | $C_L$ | 0.0108 | 0.00456 | 0.00342 | | $C_L$ | 0.00570 | 0.00342 | 0.00228 |
| Z-S-0.2% P | $C_B$ | 0.0432 | 0.0305 | 0.0241 | Z-S-0.2% P-ST | $C_B$ | 0.0394 | 0.0203 | 0.0191 |
| | $C_L$ | 0.00399 | 0.00171 | 0.00057 | | $C_L$ | 0.00741 | 0.00342 | 0.00228 |
| Z-S-0.5% P | $C_B$ | 0.0813 | 0.0572 | 0.0521 | Z-S-0.5% P -ST | $C_B$ | 0.0292 | 0.0114 | 0.0102 |
| | $C_L$ | 0.00684 | 0.00228 | 0.00228 | | $C_L$ | 0.00399 | 0.00114 | 0.000570 |
| Z-0.1% P | $C_B$ | 0.0864 | 0.0737 | 0.0394 | Z-0.1% P-ST | $C_B$ | 0.0152 | 0.00889 | 0.00762 |
| | $C_L$ | 0.00456 | 0.00171 | 0.00057 | | $C_L$ | 0.00741 | 0.00570 | 0.00285 |
| Z-0.2% P | $C_B$ | 0.0724 | 0.0559 | 0.0330 | Z-0.2% P-ST | $C_B$ | 0.0229 | 0.0203 | 0.0114 |
| | $C_L$ | 0.00456 | 0.00114 | 0.00057 | | $C_L$ | 0.00798 | 0.00456 | 0.00342 |
| Z-0.35% P | $C_B$ | 0.0711 | 0.0445 | 0.0203 | Z-0.35% P-ST | $C_B$ | 0.0876 | 0.0635 | 0.0470 |
| | $C_L$ | 0.00456 | 0.00285 | 0.00171 | | $C_L$ | 0.0108 | 0.00912 | 0.00741 |
| Z-0.5% P | $C_B$ | 0.0495 | 0.0318 | 0.0216 | Z-0.5% P-ST | $C_B$ | 0.0343 | 0.0241 | 0.0102 |
| | $C_L$ | 0.00399 | 0.00228 | 0.00171 | | $C_L$ | 0.00456 | 0.00171 | 0.00114 |

The acid properties of the parent ZSM-5, the direct introduction of phosphorus samples, desilication+phosphorus samples and the steamed samples have been measured by pyridine adsorption and are summarized in the Table 7.3. The results reveal that the acidity of the direct introduction of phosphorus on the parent sample decreases after addition of phosphorus, and the reduction is proportional with the amount of phosphorus. As shown in Table 7.3, the strongest acidity loss occurs at the largest addition phosphorus samples, as have been reported in the previous studies [11, 13, 23].   On the contrary, for the desilicated samples, increasing amounts of P also increases the acidity. This increase should be attributed to the formation of aluminum phosphate that removes the remaining extra-framework aluminum produced by the desilication treatment and that may occupy cationic positions. In fact, the introduction of P also decreases Lewis acidity.  After steaming, the parent sample loses most of its Brönsted acidity, along with the slight increase of Lewis acidity which due to the adsorption of pyridine of the emergence of new weak Lewis acid site [11, 23]. And the two series of samples retain more acidity than the parent sample after steaming. Both series present an optimum amount of P at 0.2-0.35wt% of P that corresponds to a P/Al ratio of around 0.5 and agrees with other reports done with ZSM-5 of lower Si/Al ratio [13].

In summary, the addition of phosphorus result in minor differences in the MFI structure, for both parent and desilicated samples. However acidity is affected by phosphorus, decreasing in the case of the parent ZSM-5 and increasing for the desilicated samples. After steaming both series preserves more acidity and textural properties than the parent ZSM-5 with an optimum in the amount of P that should have consequences in the catalytic activity as we will show below.

## 7.3.2. Catalytic performance
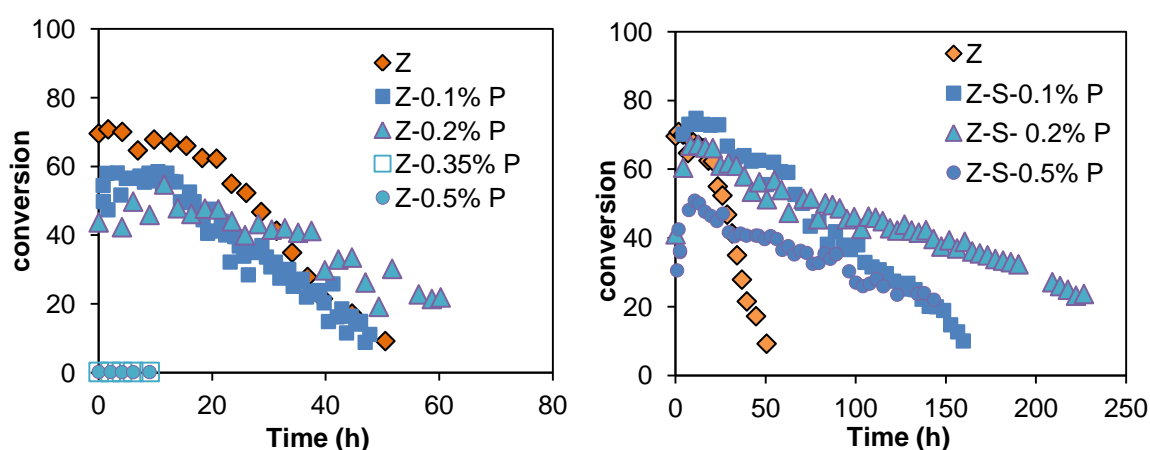


Fig 7.6 Conversion of methanol on the parent and P-modified samples at 450ºC and WHSV=24h$^{-1}$.

The catalytic properties of the parent samples and, both series of phosphorus modified samples in the methanol to hydrocarbons reactions are shown in the Fig 7.6 The reactions were carried out at WHSV=24h$^{-1}$ and 450 ºC of reaction temperature and the lifetime of the samples is defined to the conversion at 50%. It is worth to note that the desilicated samples show longer lifetime than the parent sample due to their mesoporosity, and after the addition of P they present an optimum in the amount of phosphorus at 0.2 wt%. When the addition of phosphorus is higher, the maximum value, the activity of the P modified samples show lower performance in the methanol to olefins reaction.

On the contrary, for the parent sample, the direct introduction of phosphorus at any percentage causes the decrease in initial activity and also lifetime. As it has

been said before, the addition of phosphorus to parent ZSM-5 leads to the loss in acidity as was observed from pyridine adsorption measurements. However this reduction in acidity does not mean an increase in lifetime. Since it does not occur for the mesoporous samples, this lower lifetime of the P-parent ZSM-5 could be attributed to an increase in diffusional resistances due to phosphorus in the channels and also pore mouths than nitrogen adsorption barely can measure.
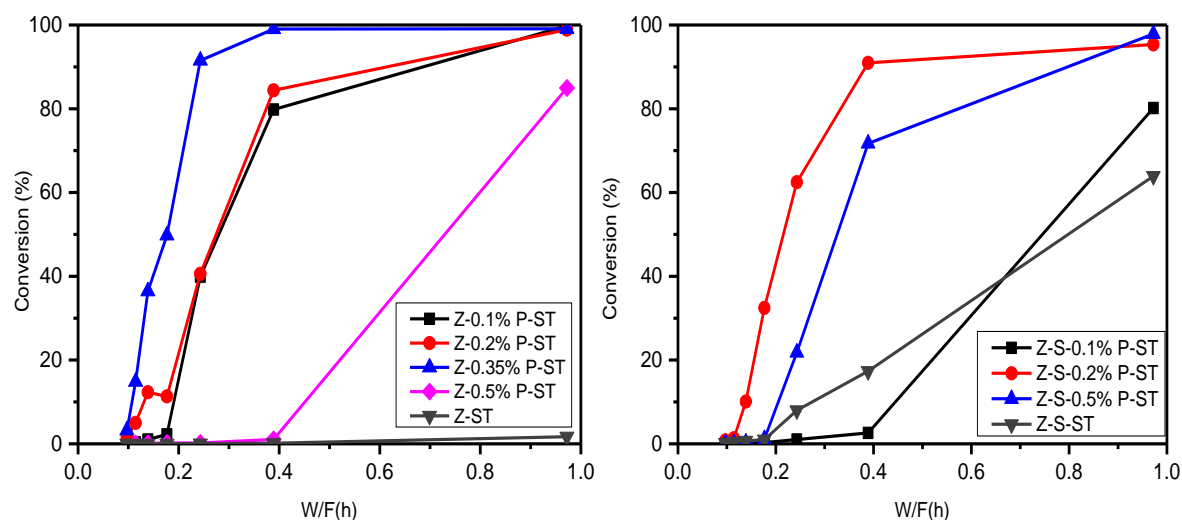


Fig 7.7 The catalytic performance of the steamed parent and P-modified ZSM-5 samples at 450ºC and WHSV=12h$^{-1}$.
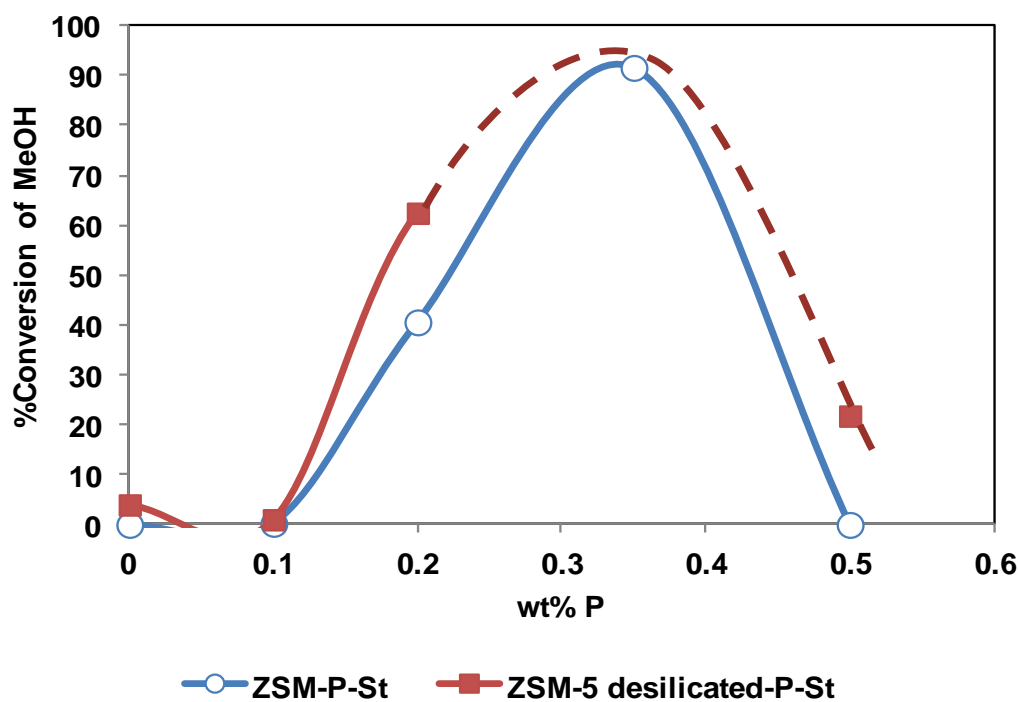


Fig 7.8 Conversion of methanol at 450ºC W/F=0.21h on ZSM-5 and desilicated ZSM-5 after P addition and steaming at 700ºC

The catalytic properties of the steamed samples are shown in the Fig 7.7. The activity after steaming at 700ºC is a good measure of the activity that would remain after many cycles of reaction-regeneration at real reaction conditions in the presence of water. As done in last chapter, activity is reduced after steaming and lifetime is too long for to be measured at laboratory conditions due to the decreased acidity that delays coking reactions. Therefore, conversions after induction period are compared at different spatial velocities in Fig 7.7. It can be seen that after steaming, steamed desilication+0.2% phosphorus samples exhibits the highest activity in this reaction. And in the direct introduction of phosphorus on the parent ZSM-5, the 0.35% addition of phosphorus sample shows the best performance in the reaction (Fig 7.8). Therefore, both series present an optimum amount of P around 0.2-0.35 in which the activity is preserved after steaming in line with acidity measurements, and around P/Al molar ratio of 0.5 as reported for other ZSM-5 of lower Si/Al ratios for catalytic cracking [13].

## 7.3.2.1.The influence of phosphorus addition in the product selectivities

In the methanol to hydrocarbons reactions, ethylene and propylene derive from different mechanism in the dual-cycle mechanism. Ethylene comes from the aromatics route and propylene and other light olefins come from the olefin route [28]. The contribution of each mechanism depends on the acid density, that strongly affects the ethylene/propylene ratio [29].

Selectivity at constant conversion of the desilication+phosphorus treated samples is shown in Fig 7.9. It is notable to observe that desilication+phosphorus treated samples have more selectives of  C3, C4, C5 than the parent ZSM-5 samples, and the selectivities of these products increase with the amount of phosphorus, which can be explained in the low acidity condition, the products from olefins is  dominant, which is consistent with the report by Bao [8]. This result is also proved by selectivity to olefins as shown in the Fig 7.9. However, the C2 selectivity shown a distinguished decrease compared with the parent samples, the selectivity of C2 decrease with the increasing of the introduction amount of phosphorus, due to the low conversion of aromatic route in the low conditions [28,29], which also be certify by the selectivity to aromatics as shown in Fig 7.9 All our results also prove the correct of the model proposed by Bjorgen [28].

## C3



## C4



## C5



## C2
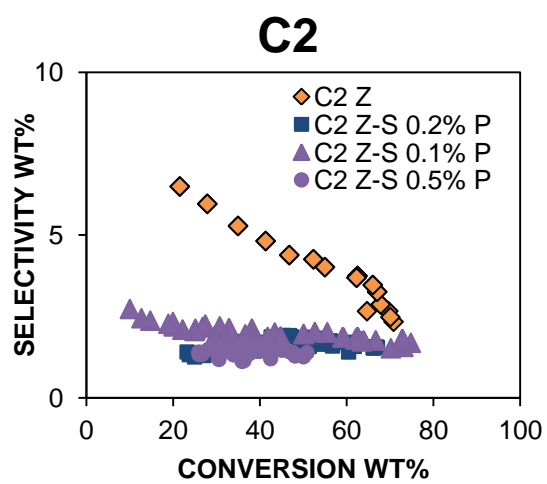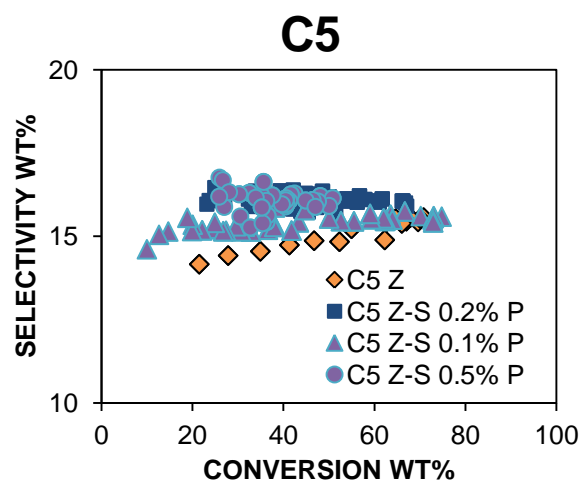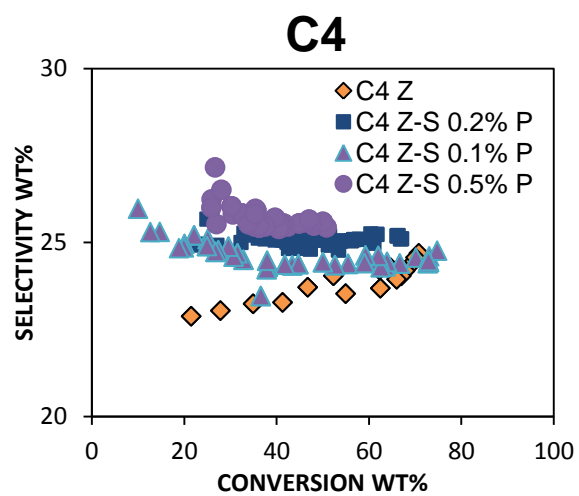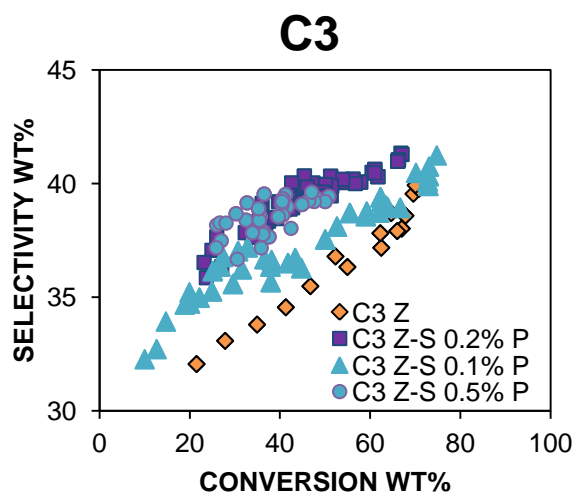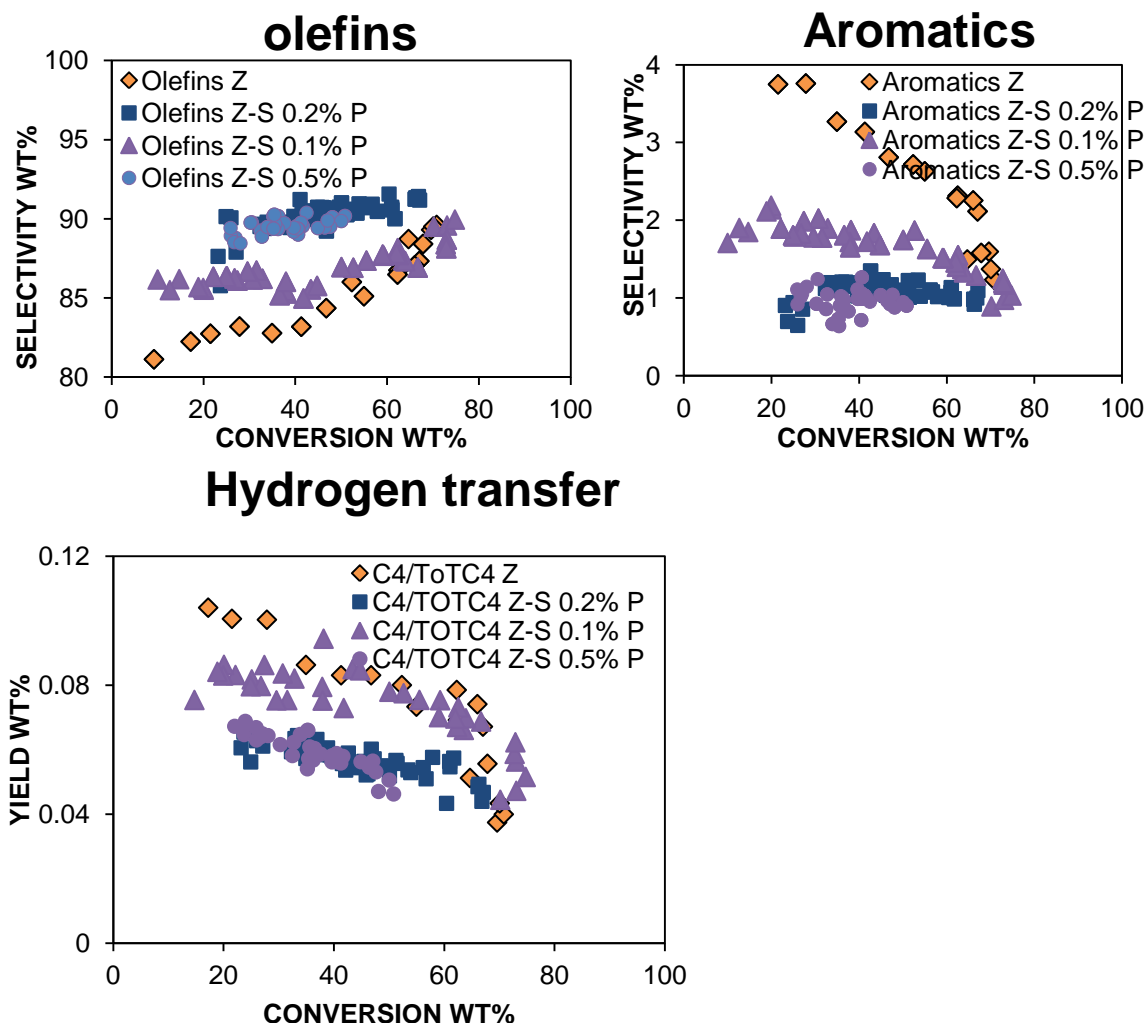
Fig 7.9 The selectivity of the main products of the P-modified ZSM-5 in the conversion of methanol at 450ºC and WHSV=24h$^{-1}$.

## 7.3.2.2.A model for P interaction on ZSM-5

Lastly, several contributions have tried to explain the stabilization effect of phosphorus on ZSM-5 and its effect on activity and selectivity of the reaction of methanol. Derewinski et al. [11] showed that phosphorus interacted with aluminum creating octahedral and Al tetrahedral distorted Al-O-P, being aluminum mainly into the framework due to its reversibility by washing with water. On the other hand, van der Bij et al. [30] attributed the stabilization effect of phosphorus to the formation of local silicoaluminophosphates interfaces (the distorted tetrahedral Al). However none of these models clearly explain why there is an optimum in the amount of P at P/Al=0.5 and why acidity is preserved against steaming by the presence of phosphorus.
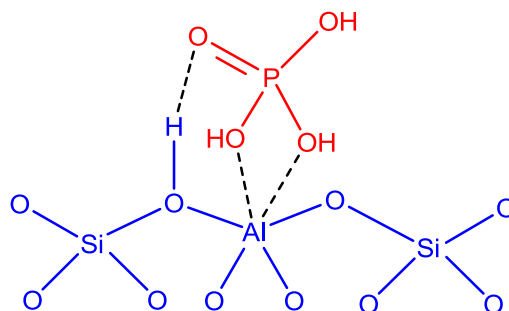
Scheme 7.2 Hypothetical model on the interaction between the phosphorus and the ZSM-5 framework.

From the results presented in this chapter we have seen that the interaction of phosphorus affects acidity with higher reduction than expected from Al and P NMR. In fact, medium and strong acidity decreases more than 50 wt% for the sample 0.35 wt% P-ZSM-5 while the amount of aluminum in octahedral and distorted tetrahedral is much less than 50%, and the P-NMR indicates that most of phosphorus remains as polyphosphoric acid on the surface. In agreement with the model proposed by Blasco et al. [13] it is consistent with a decrease in  acidity due to the protonation of P=O  groups while framework aluminum interacts with oxygen from P-OH or P-O-P groups presenting a penta or octahedral coordination if the interaction is with one or two groups. This interaction is preferential with P=O groups. The preservation of the acidity after steaming should be attributed to the acid sites not affected by phosphorus that could be stabilized by the vicinity of compensated framework aluminums. It could be argued this argument taking into account that the amount of aluminum for these samples is very low. However, the addition of phosphorus also decreases hydrogen transfer in C4 fraction and the aromatic yields to a half, and the reactions leading to those products also needs the proximity of  acid sites and hence, of framework aluminums. This indicates that even for high Si/Al ZSM-5 framework aluminums are close enough to feel stabilization effects on each other.

## 7.4.Conclusions

We have investigated the phosphorus modified samples obtained by two different approaches such as desilication+phosphorus way and the direct introduction of phosphorus. They have shown different physical properties and performance in the methanol to olefins reactions, in which the

desilication+phosphorus treated samples exhibit a maximum lifetime when the addition of phosphorus is 0.2% in weight. This sample retained much more activity after steaming treatment when compared with other samples, which indicated the better hydrothermal stability due to the introduction of phosphorus. These results suggest the amount of the phosphorus introduce have a maximum amount value, if the amount of phosphorus larger than this value, the modified sample will lost the acidity and activity with the increasing of phosphorus.

The introduced phosphorus samples still present large BET surface and retained micropore, which indicates the impregnated phosphorus do not block the zeolite micropores and channels, that will be helpful to understand the interaction of the phosphorus and zeolite frameworks.

# References

[1] Y.-K. Park, C. Lee, N. Kang, W. Choi, S. Choi, S. Oh, D. Park, Catalytic Cracking of Lower-Valued Hydrocarbons for Producing Light Olefins, Catalysis Surveys from Asia, 14 (2010) 75-84.

[2] U. Olsbye, S. Svelle, M. Bjorgen, P. Beato, T.V. Janssens, F. Joensen, S. Bordiga, K.P. Lillerud, Conversion of methanol to hydrocarbons: how zeolite cavity and pore size controls product selectivity, Angewandte Chemie, 51 (2012) 5810-5831.

[3] S. Ilias, A. Bhan, Mechanism of the Catalytic Conversion of Methanol to Hydrocarbons, ACS Catalysis, 3 (2013) 18-31.

[4] D. Chen, K. Moljord, A. Holmen, A methanol to olefins review: Diffusion, coke formation and deactivation on SAPO type catalysts, Microporous Mesoporous Materials, 164 (2012) 239-250.

[5] C. Mei, P. Wen, Z. Liu, H. Liu, Y. Wang, W. Yang, Z. Xie, W. Hua, Z. Gao, Selective production of propylene from methanol: Mesoporosity development in high silica HZSM-5, Journal of Catalysis, 258 (2008) 243-249.

[6] J. Liu, C. Zhang, Z. Shen, W. Hua, Y. Tang, W. Shen, Y. Yue, H. Xu, Methanol to propylene: Effect of phosphorus on a high silica HZSM-5 catalyst, Catalysis Communications, 10 (2009) 1506-1509.

[7] H.E. van der Bij, B.M. Weckhuysen, Local silico-aluminophosphate interfaces within phosphated H-ZSM-5 zeolites, Physical Chemistry Chemical Physics, 16 (2014) 9892-9903.

[8] P. Li, W. Zhang, X. Han, X. Bao, Conversion of Methanol to Hydrocarbons over Phosphorus-modified ZSM-5/ZSM-11 Intergrowth Zeolites, Catalysis Letters, 134 (2010) 124-130.

[9] J.C. Védrine, A. Auroux, P. Dejaifve, V. Ducarme, H. Hoser, S. Zhou, Catalytic and physical properties of phosphorus-modified ZSM-5 zeolite, Journal of Catalysis, 73 (1982) 147-160.

[10] G. Lischke, R. Eckelt, H.G. Jerschkewitz, B. Parlitz, E. Schreier, W. Storek, B. Zibrowius, G. Öhlmann, Spectroscopic and physicochemical characterization of P-Modified H-ZSM-5, Journal of Catalysis, 132 (1991) 229-243.

[11] M. Derewinski, P. Sarv, X. Sun, S. Müller, A.C. van Veen, J.A. Lercher, Reversibility of the Modification of HZSM-5 with Phosphate Anions, The Journal of Physical Chemistry C, 118 (2014) 6122-6131.

[12] J. Zhuang, D. Ma, G. Yang, Z. Yan, X. Liu, X. Liu, X. Han, X. Bao, P. Xie, Z. Liu, Solid-state MAS NMR studies on the hydrothermal stability of the zeolite catalysts for residual oil selective catalytic cracking, Journal of Catalysis, 228 (2004) 234-242.

[13] T. Blasco, A. Corma, J. Martineztriguero, Hydrothermal stabilization of ZSM-5 catalytic-cracking additives by phosphorus addition, Journal of Catalysis, 237 (2006) 267-277.

[14] G. Zhao, J. Teng, Z. Xie, W. Jin, W. Yang, Q. Chen, Y. Tang, Effect of phosphorus on HZSM-5 catalyst for C4-olefin cracking reactions to produce propylene, Journal of Catalysis, 248 (2007) 29-37.

[15] D. Liu, W.C. Choi, C.W. Lee, N.Y. Kang, Y.J. Lee, C.-H. Shin, Y.K. Park, Steaming and washing effect of P/HZSM-5 in catalytic cracking of naphtha, Catalysis Today, 164 (2011) 154-157.

[16] H.E. van der Bij, L.R. Aramburo, B. Arstad, J.J. Dynes, J. Wang, B.M. Weckhuysen, Phosphatation of Zeolite H-ZSM-5: A Combined Microscopy and Spectroscopy Study, ChemPhysChem, 15 (2014) 283-292.

[17] J.A. Lercher, G. Rumplmayr, Controlled decrease of acid strength by orthophosphoric acid on ZSM5, Applied Catalysis, 25 (1986) 215-222.

[18] W.W. Kaeding, S.A. Butter, Production of chemicals from methanol: I. Low molecular weight olefins, Journal of Catalysis, 61 (1980) 155-164.

[19] M. Göhlich, W. Reschetilowski, S. Paasch, Spectroscopic study of phosphorus modified H-ZSM-5, Microporous and Mesoporous Materials, 142 (2011) 178-183.

[20] N. Xue, X. Chen, L. Nie, X. Guo, W. Ding, Y. Chen, M. Gu, Z. Xie, Understanding the enhancement of catalytic performance for olefin cracking: Hydrothermally stable acids in P/HZSM-5, Journal of Catalysis, 248 (2007) 20-28.

[21] G. Seo, R. Ryoo, 31P, 27Al, and 129Xe NMR study of phosphorus-impregnated HZSM-5 zeolite catalysts, Journal of Catalysis, 124 (1990) 224-230.

[22] K. Damodaran, J.W. Wiench, S.M. Cabral de Menezes, Y.L. Lam, J. Trebosc, J.P. Amoureux, M. Pruski, Modification of H-ZSM-5 zeolites with phosphorus. 2. Interaction between phosphorus and aluminum studied by solid-state NMR spectroscopy, Microporous and Mesoporous Materials, 95 (2006) 296-305.

[23] K. Ramesh, C. Jie, Y.-F. Han, A. Borgna, Synthesis, Characterization, and Catalytic Activity of Phosphorus Modified H-ZSM-5 Catalysts in Selective Ethanol Dehydration, Industrial & Engineering Chemistry Research, 49 (2010) 4080-4090.

[24] J. Caro, M. Bülow, M. Derewinski, J. Haber, M. Hunger, J. Kärger, H. Pfeifer, W. Storek, B. Zibrowius, NMR and IR studies of zeolite H-ZSM-5 modified with orthophosphoric acid, Journal of Catalysis, 124 (1990) 367-375.

[25] T.M. Duncan, D.C. Douglas, On the 31P chemical shift anisotropy in condensed phosphates, Chemical Physics, 87 (1984) 339-349.

[26] A.R. Grimmer, U. Haubenreisser, High-field static and MAS31P NMR: Chemical shift tensors of polycrystalline potassium phosphates P2O5·xK2O (O ≤x ≤ 3), Chemical Physics Letters, 99 (1983) 487-490.

[27] P.M. Bautista, J.M. Campelo, A. Garcia, D. Luna, J.M. Marinas, A.A. Romero, A1P04-A12O3 catalysts with low alumina content: I. Structural and textural characterization of catalysts obtained with aqueous ammonia, Applied Catalysis A: General, 96 (1993) 175-199.

[28] M. Bjorgen, S. Svelle, F. Joensen, J. Nerlov, S. Kolboe, F. Bonino, L. Palumbo, S. Bordiga, U. Olsbye, Conversion of methanol to hydrocarbons over zeolite H-ZSM-5: On the origin of the olefinic species, Journal of Catalysis, 249 (2007) 195-207.

[29] J.W. Park, S.J. Kim, M. Seo, S.Y. Kim, Y. Sugi, G. Seo, Product selectivity and catalytic deactivation of MOR zeolites with different acid site densities in methanol-to-olefin (MTO) reactions, Applied Catalysis A: General, 349 (2008) 76-85.

[30] H.E. Van Der Bij, B.M. Weckhuysen, Local silico-aluminophosphate interfaces within phosphated H-ZSM-5 zeolites, Physical Chemistry Chemical Physics, 16 (2014) 9892-9903.

# 8. Conclusions

**1.** The nano sized sample of SAPO-34 synthesized by microwave heating present much higher lifetime than standard-SAPO-34 synthesized by conventional hydrothermal method for the reaction of methanol to olefins. A "transition-state selectivity effect" in which higher amount distribution of products is affected by different acid properties of the catalyst and not by an "easier diffusion" has been proposed on the base of the changes of C2/C3 ratios. In addition, the initial olefin distribution is strongly affected by thermodynamic distribution among the two olefins, decreasing the yield of ethylene, which is produced above the equilibrium by the aromatics-based hydrocarbon pool mechanism.

**2.** Nano-SAPO-34 has been stabilized towards contact with moisture by steaming at T≥550°C. The stabilization effect is attributed to the migration of silicon to larger silicon islands in which the overall contribution of Si species on the edge of silicon islands has been reduced. Suitable hydrothermal stability tests for nanosized or mesoporous SAPO-34 samples should include steaming at temperatures close to the temperature of the reaction of methanol and, if required, stabilization by steaming at T≥550ºC should be performed.

**3.** The nanosized SSZ-13 zeolites obtained from one-pot synthesis procedure by with the addition of surfactant to conventional synthesis precursor exhibit much longer lifetime than the standard SSZ-13. Due to the formation of intercrystalline mesoporosity, the nano-SSZ-13 material presents high diffusion rate and low coke deposition rate. A higher C2/C3 ratio was found in the nano SSZ-13, which could be explained due to a lower contribution of hydrogen transfer reactions leading to lower deactivation of the aromatics-based hydrocarbon pool.

**4.** Mesopores are formed by desilication process carried out with NaOH and NaOH/TPAOH solutions in both ZSM-5 Si/Al=40 and 140 samples. Due to the formation of mesopores, the desilicated samples exhibit larger BET, external surface areas, and these mesopores are well connected to the micropores. In the reaction of methanol to olefins, the desilicated samples of ZSM-5 Si/Al=140 present longer lifetime compared with its parent sample. In addition, it also suggests that the reaction mechanisms are different for ZSM-5 Si/Al=40 and 140 samples, in which the aromatic mechanism is more dominant for the ZSM-5 Si/Al=40 while the alkenes mechanism predominates for the ZSM-5 Si/Al=140.

**5.** We have investigated the phosphorous modified samples obtained by two different approaches such as desilicaiton+phosphorous way and the direct introduction of phosphorous way. They have shown different physical properties and performance in the methanol to olefins reactions, in which the desilication+phosphorous treated samples exhibit a maximum lifetime when the addition of phosphorous is 0.2% in weight. This sample retained much more activity after steaming treatment when compared with other samples, which indicated the better hydrothermal stability due to the introduce of phosphorous. These results suggest the amount of the phosphorous introduce have a optimum value, if the amount of phosphorous larger than this value, the modified sample will lost the acidity and activity with the increasing of phosphorous.

The introduced phosphorous samples still present large BET surface and retained micropores, which indicates the impregnated phosphorous do not block the zeolite micropores and channels, that will be helpful to understand the interaction of the phosphorous and zeolite frameworks.

# Index of Figures

# Index of Schemes

# Index of Tables

# Acknowledgements